BIOGENIC METAL SULFIDE NANOPARTICLES FROM WASTEWATER AND THEIR POTENTIAL APPLICATIONS

A Thesis

Submitted in partial fulfillment of the requirement for the award of the degree of

DOCTOR OF PHYLOSOPHY

By

Manoj Kumar

Department of Biosciences and Bioengineering

Indian Institute of Technology Guwahati

Guwahati-781039, Assam, India

March 2022

Dedicated to My Parents

Indian Institute of Technology Guwahati

Department of Biosciences and Bioengineering

Declaration

I, hereby declare that the content embodied in this thesis entitled **"Biogenic metal sulfide nanoparticles from wastewater and their potential applications"** is the result of investigation carried out by me at the Department of Biosciences and Bioengineering, Indian Institute of Technology Guwahati, Guwahati, India, under the supervision of **Prof. Kannan Pakshirajan.**

In keeping with the general practice of reporting scientific observations, due acknowledgement have been made wherever the work described is based on the findings of other investigators.

Date: **Manoj Kumar**

Place: IIT Guwahati

Indian Institute of Technology Guwahati

Department of Biosciences and Bioengineering

Certificate

It is certify that the work described in this thesis entitled **"Biogenic metal sulfide nanoparticles from wastewater and their potential applications"** by **Manoj Kumar** for the award of degree of Doctor of Philosophy is an authentic record of the results obtained from the research work carried out under my supervision in the Department of Biosciences and Bioengineering, Indian Institute of Technology Guwahati, Guwahati, India, and this work has not been submitted either in whole or in part elsewhere for a degree.

Date:

Place: IIT Guwahati

(Signature of thesis supervisor)

Prof. Kannan Pakshirajan

Professor

Department of Biosciences and Bioengineering

Indian Institute of Technology Guwahati

Guwahati-781039, Assam, India.

ACKNOWLEDGEMENTS

First of all, I would like to thank my parents and almighty God for giving me the strength and knowledge to perform this task.

I express my sincere gratitude to my supervisor Prof. Kannan Pakshirajan, Department of Biosciences and Bioengineering, for his encouragement, support, and constant supervision of the progress of my research. His scientific suggestions and constructive valuable comments on the research were critical to completing this work.

I express my gratitude to my Doctoral committee, Prof. Gurvinder Kaur Saini, Prof. A. B. Kunnumakkara, and Prof. Chandan Das, for their precious suggestions and comments for this work.

I extend my gratitude to the Department of Biosciences and Bioengineering, Centre for the Environment, Department of Chemical Engineering, Department of Physics and Central Instrumentation Facility, IIT Guwahati for providing technical and instrumental support to this work. I also take this opportunity to thank all the non-teaching staff and teaching assistants who helped in different instrumentation. I would gratefully acknowledge the fellowship provided to me by the Institute during all these years and the Council of Scientific and Industrial Research, Government of India for funding this work.

I am grateful to Prof. G. Pugazhenthi, sir, Department of Chemical Engineering, for providing me space and time to perform membrane

work. Without his guidance and support, this work would not have been completed successfully.

I am grateful to all my former and current lab mates Dr. Vibha Sinha, Dr. Gopi Kiran, Dr. Arindam Sinharoy, Dr. Lalit Goswami, Dr. M. M. Tejas Namboodiri, Dr. Tanushree Paul, Dr. Arvind Kumar Sakya, Dr. Arul Manikanda, Dr. Arun Sakthivel, Surjith Ramasamy, Dipak Kumar Kanaujiya, Sudeshna Saikia, Bharat Bhusan Negi, Ajay Kumar P V, Moumita Nandi and Selvanayaki S. for their help and support during my research work. I would like to thank Dr. Arindam Sinharoy for introducing me to the field of sulfate reduction and wastewater treatment. Special thanks to Dr. M. Gopi Kiran for clearing my research queries and helping me throughout my Ph.D. journey. This section is incomplete without acknowledging my friends Shubhank Sherekar, Simons Dhara, Mayur Kedare, Vishnu Kumar, Suraj Kumar Panda, and Allampalli Satya Sai Pavan for their support and encouragement.

Finally, I would like to express my deepest gratitude to my family members for their continuous support and blessings. Thanks to my parents for supporting me in chasing my dreams. Without your constant support, love, and sacrifice, this would not have been possible.

March 2022 *Manoj Kumar*

IIT Guwahati

Abstract

Metal containing wastewater such as acid mine drainage (AMD) has severe effects on the environment if discharged without proper treatment. On the other hand, such wastewater can serve as an excellent source for recovering the metals. This is mainly important because the naturally found metal ores are depleting due to ever increasing demand of metals for different application. Hence, alternative sources of metals is of atmost important. To fulfill the requirement, treatment of heavy metal-containing wastewater for both removal and recovery is an interesting option. Characterization of AMD shows it has a low pH and high concentration of sulfate and heavy metals including cadmium, copper, iron, nickel, lead, zinc. However, presence of one or more metals depends on the location and source of AMD.

Biological method for heavy metal removal by sulfate reducing bacteria is well-known. However, less focus has been given to the recovery of metals. Biological sulfide precipitation has many advantages over the conventional chemical hydroxide and carbonate precipitation processes, e.g., (1) no use of harmful chemicals (2) low amount of secondary sludge generation (3) cost-effective. During biological sulfide precipitation, a highly insoluble metal sulfide precipitate is formed under anaerobic conditions by sulfate-reducing bacteria (SRB). SRB utilizes sulfate present in such waste streams to produce different sulfide species (S_2^-, HS^-, H_2S) and the sulfide produced reacts with metals to form metal sulfide precipitate in the system. Such metal sulfide precipitate can be recovered from the system for metal extraction. Recovery of metal nanoparticles from wastewater by sulfide precipitation is interesting option from economic and environmental perspectives.

The current thesis demonstrated successful removal and recovery of different heavy metals in the form of nanoparticles from simulated wastewater by anaerobic biomass containing SRB. Initially, anaerobic biomass from three different sources were screened on the basis of their metal removal and sulfate reduction efficiencies. At low metal loading conditions, the biomass obtained from a laboratory scale anaerobic rotating biological contactor (An-RBC) reactor treating metallic wastewater showed a maximum metal removal (95 ± .50%), sulfate reduction (90 ± 1.56%) and COD removal (80 ± .88%); however, the values decreased at a high metal concentration for all the biomass. The major mechanism of metal sulfide formation involved the binding of metals to sulfide produced outside the cell surface due to sulfate reduction. The metal bioprecipitates formed external to the bacterial cell surface showed easy recovery for potential application.

Further, heavy metal removal and recovery from synthetic wastewater containing Cd^{2+}, $Cu^{2+,}$ Fe^{3+}, Ni^{2+}, Pb^{2+} and Zn^{2+} was investigated using two continuously operated sulfidogenic anaerobic inverse fluidized bed reactors (referred as R1 and R2) supplied with influent of pH 7.0 and 3.0, respectively. IFBR with influent pH 7.0 (R1) performed better than R2 with influent pH 3.0 in terms of metal recovery from wastewater. Maximum recovery of Cu was obtained followed by that of Pb and Cd. The overall order of the metal recovery was Cu > Pb > Cd > Zn > Ni > Fe. This study proved that IFBR has the potential not only to treat heavy metal laden acidic wastewater but also the ability to recover heavy metals in the form of nanoparticles.

In order to purify the copper sulfide nanoparticles (CuS NPs) obtained from synthetic wastewater by biological sulfate reduction, an indigenous low-cost ceramic membrane was used. Pretreatment using probe sonication was found effective for an efficient purification of the nanoparticles by releasing the CuS NPs from contaminating impurities. Microfiltration using the ceramic membrane showed 92% purification efficiency of the CuS NPs with a flux of 77×10^{-4} m^3/m^2s. Excellent characteristics of the CuS NPs in terms of crystallinity, size, shape and purity established its potential industrial application. Porosity (40%), pore size distribution, water permeability (3.758×10^{-6} m/skPa), resistance against acidic and alkaline solution as well as low-cost ($160/$m^2$) of the indigenously prepared ceramic membrane further established its potential application for large-scale purification of CuS NPs and for other industrial use.

A novel adsorbent based on biogenic metal sulfide nanoparticles (MeSNPs) from sulfate rich metallic wastewater was evaluated for treating dye-containing wastewater. The MeSNPs showed a very high capacity to adsorb the azo dyes Direct Red 80 (DR 80) and Mordant Blue 9 (MB 9) from aqueous solution even at their high initial concentration and within a short contact time. More than 99% removal efficiency of both the dyes was achieved by using MeSNPs at the following optimum conditions: 200 mg dosage, pH 2, 6 min contact time, and 100 mg/L initial dye concentration. Mechanism of dye sorption onto MeSNPs was shown to involve electrostatic interaction between the dyes and the adsorbent. Dynamic adsorption of the dyes was studied using a fixed-bed column with the MeSNPs as a function of liquid flow rates. The results showed an increase in breakthrough time with a decline in the flow rates for both DR 80 and MB 9 and the breakthrough behavior was explained using Thomas, Clark, and Yoon-Nelson models.

To check the application potential, biogenic CuS NPs from synthetic wastewater were synthesized and evaluated as a catalyst in click reaction to produce triazoles. The optimum condition for triazole formation was 0.1 mole% CuNPs, water as a solvent, 12 h reaction time. The best triazole yield (94%) was obtained in a reaction between azidobenzene and propargyl chloride. The catalyst was characterized using different techniques such as FESEM, FETEM, XRD, TGA, EDX which revealed its potential industrial applications. Recycle and reuse of the spent PVA-SA-CuNPs catalyst in the study for upto five cycle resulted in a slight decrease in triazole yield with every subsequent run.

The toxicity analysis as induced oxidative stress in *R. opacus* PD 630 due to biogenic PbS NPs and CdS NPs was studied. A dose-dependent increase in PbS NPs and CdS NPs uptake by the bacterium was observed upto a maximum of 16.4 and 15.6 mg/(g cell), corresponding to 98% and 95% uptake. A dose-dependent increase in intracellular levels of hydroxyl radicals (˙OH) were also observed. Besides, increase in TAG accumulation by *R. opacus* PD 630 due to oxidative stress induced by biogenic/chemical PbS NPs and CdS NPs was observed. Hence, this study shows that both biogenic and chemical metal sulfide nanoparticles exert almost similar effect on the industrially relevant bacteria.

Contents

List of Figures

List of Tables

Abbreviations

AMD: Acid mine drainage

APF: p–aminophenyl fluorescein

APHA: American public health association

BET: Brunauer–Emmett–Teller

COD: Chemical oxygen demand

DR 80: Direct Red 80

EDX: Energy dispersive X-ray

EPS: Exopolysaccharide

FBR: Fluidized bed reactor

FESEM: Field emission scanning electron microscopy

FETEM: Field emission transmission electron microscopy

FTIR: Fourier transform infrared spectroscopy

H_2S: Hydrogen sulfide

HRT: Hydraulic retention time

IEP: Isoelectric point

IFBR: Inverse fluidized bed reactor

MB 9: Mordant Blue 9

MF: Microfiltration

MP-AES: Microwave plasma atomic emission spectroscopy

$^{\bullet}OH$: Hydroxyl radical

PTFE: Polytetrafluoroethylene

PVA: Polyvinyl alcohol

SAED: Selected area diffraction

SRB: Sulfate reducing bacteria

TAG: Triacylglycerol

TGA: Thermogravimetric analysis

VFA: Volatile fatty acid

XRD: X-ray diffraction

Notations

A: Effective membrane area (m^2)

C_0: Initial dye concentration (mg/L)

Ce: Equilibrium dye concentration (mg/L)

F: flow rate (mL/h)

n: Freundlich constant

N_{AB}: Saturation concentration (g/L)

^oC: Degree centigrade

$q_{e(exp)}$: Dye sorption capacity of the column

g/L: gram/liter

h: Hour

k_1: Pseudo-first order rate constant (1/min)

k_2: Pseudo-second order rate constant (g/mg/min)

k_{AB}: Kinetic constant (mL/mg/min)

K_L: Langmuir adsorption constant (L/mg)

k_s: Sips equilibrium constant (L/mg)

k_{YN}: Yoon-Nelson rate constant (L/min)

l: Pore length of the membrane (m)

L_h: Water permeability of the membrane ($m^3/m^2/skPa$)

mg/L: milligram per liter

min: Minute

mL/min: milliliter per minute

m_{total}: Total quantity of dye

q_e: Adsorption capacity at equilibrium (mg/g)

q_e: Amount of dye adsorbed (mg/g)

q_t: Adsorption capacity at time *t* (mg/g)

r: Clark model constants (1/min)

R^2: Coefficient of determination

rpm: Rotation per minute

u: Linear velocity of liquid flow inside the column (cm/min)

v/v: volume/volume

V: Total volume of the membrane

w/v: weight/volume

W: Amount of adsorbent used in the column (g)

z: Bed height (cm)

ΔP: Applied pressure across membrane (kPa)

Greek letters

ε: Porosity of the membrane (%)

$\rho_{w:}$ Density of water (Kg/m^3)

μ: Viscosity of water (sPa)

τ: Tortuosity factor

Chapter 1

Introduction

1.1 Introduction

Increasing demand of metals in industrial sectors has led to the depletion of metal and mineral resources. Metallic wastewater from industrial activities such as mining, metallurgy, galvanization of iron products, electroplating, and alloy manufacturing can serve as a potential source for recovering valuable metals. Low pH, low COD and high concentration of heavy metals categorize the metallic wastewater (Johnson and Hallberg 2005; Cotoras et al., 2017; Kiran et al., 2017). These metals (e.g. cadmium, lead, copper etc.) are toxic in nature and non-biodegradable, but can be transformed into less toxic insoluble form (Kiran et al., 2017). If discharged into the environment without proper treatment, potentially toxic metal containing wastewater may pose many adverse effects on the environment as well as on human health, such as respiratory problems, diarrhea, stomatitis, paralysis, vomiting, depression, and pneumonia (Verma et al., 2013). Therefore, the treatment of heavy metal containing wastewater is necessary prior to its release into the environment.

Metallic wastewaters rich in sulfate and low in pH, e.g. acid mine drainage (AMD) are usually treated by chemical precipitation with sodium hydroxide because of its following advantages: i) easy operation, ii) requirement of low-cost chemicals and iii) simple process control (Fu and Wang et al., 2011). On the other hand, it suffers from certain limitations including i) production of unstable metal hydroxides, ii) difficulty with recovery of metals and iii) secondary sludge disposal problem (Johnson et al., 2000; Esposito et al., 2006). Ion exchange, electrolysis and reverse osmosis are among the other processes used to treat heavy metal containing wastewater, but these are not commonly used due to one or more drawbacks, such as requirement of high capital investment, secondary sludge disposal problems and need for further treatment (Aziz et al., 2008; Fu and Wang et al., 2011). Hence, recent research is focused towards biological sulfate reduction

for both removal and recovery of valuable metals using sulfate reducing bacteria (SRB). In this technique, sulfate is first reduced to sulfide by the action of SRB; sulfide then reacts with metals and forms insoluble metal sulfide precipitates.

Sulfide precipitation by SRB is advantageous over the conventional methods due to the following reasons: (i) formation of insoluble salts even in low pH (2.5-3.0) condition (Villa-Gomez et al., 2013); (ii) selective metal recovery is possible as metals differ by their solubility product with sulfide (Sampaio et al., 2009); (iii) high settling rate, excellent thickening and dewaterability characteristics (Djedidi et al., 2009) and (iv) low capital investment.

Under anaerobic environment, SRB consume SO_4^{2-} as the terminal electron acceptor by oxidizing simple organic compounds and, as a result, it produces sulfide which then reacts with dissolved metals present in the wastewater and forms highly insoluble metal sulfide precipitate. Metal sulfide formation can be described as represented in Eq. (1.1) and (1.2), and the solution pH increases due to alkalinity produced during the process (Eq. 1.3)

$$2CH_2O + SO_4^{2-} \rightarrow H_2S + 2HCO_3^- \quad (1.1)$$

Where CH_2O is organic matter (electron donor)

$$H_2S + M^{2+} \rightarrow MS + 2H^+ \quad (1.2)$$

Where M^{2+} is metal, e.g. Cd^{2+}, Mn^{2+}, Pb^{2+}, Cu^{2+}, etc.

$$HCO_3^- + H^+ \rightarrow CO_2(g) + H_2O \quad (1.3)$$

Thus biological sulfate reduction for metal removal from wastewater is attractive for recovering the metals in the form of nanosized (10-50 nm) insoluble metal sulfide precipitates. Nanoparticles are usually characterized by small size, high reactivity, and large specific surface area, and metal

sulfide nanoparticles find many applications in various fields. For example, Shamraiz et al. (2016) used copper sulfide nanoparticles for degradation of dyes, and Gong et al. (2016) used iron sulfide nanoparticles for the removal of other heavy metals from wastewater. Therefore, recovery of metal nanoparticles from wastewater by sulfide precipitation is both attractive from economic and environmental perspectives. Synthesis of metal nanopowders by sulfate reduction process is a new topic of research and has not been widely reported since earlier studies were focused on sulfate reduction and metal removal. It has been recognized recently that recovery of valuable metals such as Zn, Cu, Cd, Ni, etc. from wastewater can be achieved in nano-size range by precipitation as metal sulfide using SRB.

Tabak (2003) and Gallegos-Garcia (2009) studied different configurations of sulfidogenic bioreactors for metal removal including single and multi-stage systems. In a single-stage reactor system, both sulfate reduction and metal precipitation are carried out in a single bioreactor unit (Kaksonen et al., 2003), whereas in a multi-stage system sulfide generation and metal precipitation units are separated (Bhagat et al., 2004; Sierra-Alvarez et al., 2006). Among the different reactor configurations, fluidized bed and gas lift reactors are known for efficient recovery of heavy metals from wastewater. Although, the concept of sulfate reduction and metal removal by sulfide precipitation is not new, the recovery of heavy metals using a single stage bioreactor system is quite recent and not widely reported.

Hence, there is a need to develop a suitable bioprocess for sulfate reduction and metal removal which can also be efficiently used to recover heavy metals from wastewater. The recovered metals in the form of nanoparticles need some further processing before its application in different fields. For purification, there is need to apply cost effective method such as microfiltration using ceramic membrane. Also, the application potential of the recovered nanopowders need to be investigated.

1.2 Aim and objectives

This study was aimed at developing an efficient bioprocess for removal and recovery of metals from metallic wastewater in the form of nanopowders and its potential applications.

To achieve this aim, the following investigations were carried out:

i. Screening of anaerobic biomass collected from different sources for heavy metal removal and recovery under sulfate reducing condition

ii. Performance evaluation of sulfidogenic inverse fluidized bed reactor system for heavy metal removal and recovery

iii. Purification of biologically synthesized copper sulfide nanoparticles by low-cost ceramic membrane

iv. Preparation, characterization and application of biometal nanopowders from metallic wastewater for azo dye removal from aqueous solution

v. Biological synthesis of copper catalyst for click reaction from metallic wastewater

vi. Induced oxidative stress of PbS NPs and CdS NPs in the oleaginous bacteria *Rhodococcus opacus*

1.3 Organization of thesis

The present work is divided into nine chapters. The first chapter presents the general introduction, aim, and objectives of the work. Chapter 2 presents the available literature on heavy metal removal and recovery, different reactor combinations used for heavy metal recovery, the effect of different process parameters on heavy metal recovery, and the application of recovered metal nanopowders in various fields, etc. In Chapter 3, screening of anaerobic biomass capable of sulfate reduction and heavy metal removal, heavy metal recovery, and characterization of recovered nanopowders are reported. Chapter 4 describes the performance evaluation of the inverse fluidized bed (IFB) bioreactor for simultaneous heavy metal removal and recovery. The effect of different process parameters is also discussed in this chapter. Chapter 5 reports the fabrication of a low-cost ceramic

membrane to purify biologically synthesized copper sulfide nanoparticles. Preparation, characterization, and application of biometal nanopowders from metallic wastewater for azo dye removal from aqueous solution are reported in Chapter 6. Chapter 7 describes the application of biologically recovered copper sulfide nanoparticles for click reaction. In Chapter 8, induced oxidative stress of lead and cadmium sulfide nanoparticles in the oleaginous *Rhodococcus opacus* by. Chapter 9 provides a summary and appropriate conclusions based on the previous chapters. This chapter also includes some recommendations for future research in this area.

Chapter 2

Literature Review

2.1 Heavy metals

Metals are naturally occurring elements with relatively high density and atomic weights. Due to wide application of heavy metals in different fields along with depletion of natural sources of metal ores, there is an increasing demand for metals around the world (Villa-Gomez et al., 2011). On the other hand, their extensive use has raised concerns over their effects on human health and the environment. Some heavy metals, such as iron, cobalt, zinc, etc., are considered essential nutrients at trace quantities, whereas other heavy metals, such as cadmium, mercury, and lead, are highly toxic even at very low amount (Kieu et al., 2011). Therefore, removal and recovery of heavy metals from wastewater is important from both environment and industrial perspectives.

2.1.1 Sources of metals in environment

Metals are naturally occurring elements present throughout the earth's crust. Anthropogenic activities such as mining, industrial production, and agricultural use of metals and metal-containing compounds can lead to human exposure and environmental contamination. Heavy metal pollution can also occur through metal corrosion, atmospheric deposition, soil erosion of metal ions, leaching of heavy metals, sediment re-suspension, etc. (Kieu et al., 2011) from water resources to soil and groundwater. Heavy metal contamination also occurs through natural phenomena such as weathering and volcanic eruptions. Some industrial sources of heavy metal pollution include electroplating, metal processing in refineries, coal burning in power plants, petroleum combustion, nuclear power stations and high tension lines, plastics, textiles, microelectronics, wood preservation, and paper processing plants, etc. Electroplating and coal burning power plants generate significant amount of wastewater containing various heavy metal such as copper, cadmium, lead, nickel, zinc, chromium etc. (Kiran et al., 2017). The wood

preservation industry use chromated copper arsenate wood treatment which produces copper and arsenic containing wastewater; pigment industry produces wastes containing cadmium sulfide; petroleum refinery generates conversion catalyst contaminated with nickel and chromium; textile industry uses color pigments for textile dyes which generates waste containing heavy metals such as lead, cadmium, copper and chromium. Table 2.1 presents different anthropogenic and natural sources of heavy metals in the environment.

Table 2.1 Anthropogenic and natural sources of metal in environment

Anthropogenic sources	**Metals found**	**Reference**
Pesticides and Fertilizers	Cadmium, lead, copper, zinc, cobalt, arsenic etc.	Hariprasad et al., 2013
Biosolids (municipal sewage sludge)	Cadmium, copper, lead, nickel, zinc etc.	Smith et al., 2009
Industries such as paints, pigment, steel plant, varnishes, thermal power plant, pulp and paper, tannery, distillery, rayon, cotton textiles, rubber, galvanization of iron products and mining industries	Copper, cadmium, lead, nickel, zinc, chromium, iron, cobalt etc.	Kieu et al., 2011 Kiran et al., 2017
Metal mining & milling process	Cadmium, copper, iron, nickel, lead, zinc, chromium, aluminium etc.	Johnson et al., 2003
Natural sources		
Seepage from rocks into water	Lead, iron, nickel, copper, lead etc.	Akcil et al., 2006
Volcanic activity	Arsenic, mercury, etc	Verma et al., 2013
Forest fire	Nickel, manganese and cobalt etc.	Verma et al., 2013

2.1.2 Environmental effects of metal containing wastewater

Metal containing wastewater generated from various industries generally has a high concentration of heavy metals. Due to high metal concentration, it causes severe toxic effects on the aquatic environment. The presence of iron precipitate increases the turbidity of water streams, limits oxygen diffusion, and reduces light penetration (Johnson et al., 2000). It also affects water quality in agriculture, industries, and recreational purposes. It further affects humans and can cause reduced mental and central nervous function, kidney and liver failure, lungs problem, blood composition damage, etc.

Long-term exposure may result in physical, muscular, and neurological disorders that mimic Alzheimer's disease, Parkinson's disease, muscular dystrophy, and multiple sclerosis. Allergies are not uncommon, and repeated long-term contact with some metals or their compounds may even cause cancer (International Occupational Safety and Health Centre 1999). Table 2.2 presents the permissible limit of different heavy metals in drinking water.

Table 2.2 Permissible limits of metals in drinking water (mg/L)

Parameter (mg/L)	Indian standard institution	Central pollution control board (India)	World health organization
Iron	0.3	1.0	0.1
Copper	0.05	1.5	1.0
Zinc	5.0	15.0	5.0
Cadmium	0.01	No Relaxation	0.005
Lead	0.10	No Relaxation	0.05
Manganese	0.10	NA (Not available)	0.40
Nickel	0.02	NA	NA

2.2 Metal removal

2.2.1 Metal removal by Physico-chemical process

Metal containing wastewaters such as AMD is usually treated by chemical precipitation because of its following advantages: i) process simplicity, ii) requirement of low-cost chemicals, and iii) easy process control (Villa-Gomez et al., 2011). However, some major limitations of the method are i) production of unstable metal hydroxides, ii) recovery of metals is difficult, and iii) sludge disposal problem (Esposito et al., 2006). Ion exchange, electrolysis, and reverse osmosis are among the other processes used to treat heavy metal containing wastewater, but these are not commonly used because of one or more drawbacks such as the requirement of high capital investment, sludge disposal problems, and requirement of further treatment (Aziz et al., 2008; Fu and Wang et al., 2011). To overcome such limitations of conventional methods, research is currently diverted towards biological sulfate reduction methods using sulfate reducing bacteria (SRB).

2.2.2 Metal removal by biological sulfate reduction

Biological sulfate reduction by SRB is a well-known method for metal sulfide precipitation from wastewater, especially when sulfate is present along with heavy metals in wastewater, e.g., AMD. Biological sulfide precipitation requires an electron donor and essential nutrients for the growth of SRB.

SRB can be divided into two groups, first is heterotrophic anaerobes, which use organic compounds, and the other is autotrophic anaerobes, which use H_2 as an electron donor and CO_2 as carbon source, capable of reducing sulfate to sulfide by a dissimilatory, bioenergetic metabolism (Nagpal et al., 2000). SRB are prokaryotes, which are ubiquitous in water and sediments because

of their ability to utilize a wide range of substrates and capability to survive in extreme conditions (Schwartz 1985). For sulfate reduction using SRB, the following conditions are needed, an anaerobic environment (redox potential < –200 mV), pH > 5.0, presence of organic substrate, presence of appropriate sulfur species (as sulfate) to be reduced (Gibert et al., 2002).

Some SRBs (such as *Desulfobacter*, *Desulfococcus*, *Desulfosarcina*, *Desulfonema*, and *Desulfobacterium*) can oxidize carbon sources into CO_2. Some SRBs (such as *Desulfovibrio*, *Desulfomonas*, *Desulfobulbus*, and *Termodesulfobacterium*) oxidize the carbon source incompletely to acetate, CO_2, and H_2. Some SRBs, such as *Desulfotomaculum* species, utilize acetate as the sole carbon source for sulfate reduction.

In biological sulfate reduction, SRB use SO_4^{2-} as terminal electron acceptor and convert it into different sulfide forms (H_2S, HS^-, S^{2-}) as respiratory products. These sulfide products are responsible for metal precipitation as they combine with different metals and form insoluble metal sulfide precipitate in the system. Bioreactors for sulfate reduction can be grouped depending upon whether the biomass is suspended or in attached form. Different types of bioreactors have been studied for sulfate reduction and each of these reactor types has some merits and demerits, which are presented in Table 2.3. For simultaneous reduction of sulfate and heavy metals, down flow fluidized bed reactor, also called inverse fluidized bed reactor, is advantageous over other reactors in terms of ease of metal recovery (Villa-Gomez et al., 2011; Sinharoy et al., 2019; Negi et al., 2020).

Table 2.3 Merits and demerits of different bioreactor configurations studied for metal removal by biological sulfate reduction (Papirio et al., 2013; Kiran et al., 2017)

Bioreactor type	Merits	Demerits	References
Continuous stirred tank reactor (CSTR)	Consistent and reliable performance	High solid retention time (SRT) results in a large reactor volume; biomass washout	Barnes et al., 1991; Lens et al., 2002
Gas lift reactor (GLR)	High mass transfer efficiency, very good mixing	High pressure needed to pump gas inside the reactor	Dijkman et al., 1999; Lens et al., 2002
Packed bed reactor (PBR)	High SRT result in lower reactor volume than CSTR; can be operated in up-flow or down-flow mode	Clogging; requirement of high pressure for pumping the flow	Anderson et al., 1990; Jong and Parry et al., 2003; Zaluski et al., 2003; Kolmert and Johnson et al., 2001
Membrane bioreactor (MBR)	No need of sedimentation basin; high biomass retention results in high substrate degradation rate; avoids direct contact between metals and SRB	High manufacturing cost to overcome the trans-membrane pressure; requires periodic backwash of the membrane	Tabak and Govind et al., 2003; Mack et al., 2004; Vallero et al., 2005; Manconi and Lens, 2009

Up-flow anaerobic sludge blanket (UASB)	No clogging; good biomass settling capacity; no requirement of support material	Biomass washout; high susceptibility to influent characteristics	Lettinga et al., 1980; Speece et al., 1983; Omil et al., 1996; Vallero et al., 2003
Bubble column reactor (BCR)	Good mixing; applicable for turbid medium and shear sensitive cells	Not available (NA)	NA
Fluidized bed reactor (FBR)	No channeling or clogging, good biomass retention; high biomass activity and treatment efficiency is high	Energy needed to be spent for carrier fluidization; shear force can lead to detachment of biomass; less volume available for biomass compared to the UASB reactor due to the inert biomass carrier	Speece et al., 1983; Yoda et al.,1989; Anderson et al., 1990; Melin et al., 1997; Marin et al., 1999
Anaerobic filter reactor (AFR)	Low shear force; sludge retention time is more than that for CSTR; H_2S stripping is effective in downflow mode	Channeling of flow; large pressure gradients	Speece et al., 1983; Anderson et al., 1990; Barnes et al., 1991

Anaerobic digester (AD)	Excellent biomass holding capacity as compared with the CSTR	Biomass disintegrates into flocks and sludge	Speece et al., 1983
Anaerobic hybrid reactor (AHR)	Less vulnerable to clogging compared with the AFR; sludge removal easier than in the AFR; biomass retention better than in the UASB	Not available	Steed et al., 2000
Anaerobic baffled reactor (ABR)	High sludge retention time; reduced costs due to no biomass carrier; good tolerance for shocks of hydraulic and organic loading	Not available	Speece et al., 1983; Barber and Stuckey et al., 2000

2.2.2.1 Single stage reactor systems for metal removal

Simultaneous removal of sulfate and metals can be achieved in a single bioreactor unit as shown in Fig. 2.1. Villa-Gomez et al. (2011) used single-stage IFB reactor unit for heavy metal removal from wastewater and achieved high removal of Cd (96.5%), Cu (99.1%), Pb (92.4%) and Zn (91.3%) at 5 mg/L inlet concentration and at pH 7.0 and COD/sulfate ratio of 1. Similar results of more than 99% removal efficiency of Fe, Zn and Cd was obtained by Gallegos-Garcia et al. (2009) in a single unit system treating metallic wastewater at pH 5.0. Another example of the single-system approach is a full-scale plant at the Budelco zinc refinery in Budel-Dorplein, Netherlands, that remediates metal-containing groundwater (Dvorak et al., 1992; Kaksonen et al., 2007).

Different bioreactor types have been explored for simultaneous sulfate reduction and metal precipitation in the last few years; only some of these have been applied for sulfate reduction and metal precipitation in a single stage (Table 2.4). Single-stage metal sulfide precipitation process is cost effective in comparison with two-stage systems but it has some limitations in treating wastewater with low pH and high concentration of heavy metals. To overcome the limitations of handling low pH wastewater, single unit systems are added with alkaline material to generate additional alkalinity. In some other cases, two or more bioreactors are used in series to increase the efficiency of sulfate reduction and metal removal.

Biological treatment using SRB often increases the pH of the wastewater by producing alkalinity during the treatment process, and because of which low pH of the influent waste stream does not affect the biological activity of the SRBs. Kaksonen et al. (2004) successfully reported the sulfate reduction in wastewater at low pH of 3.8. However, for simultaneous sulfate reduction and metal removal in a single-stage bioreactor system, the lowest influent pH of 5.0 has been reported (Sahikaya and Gungor et al., 2010).

The main drawback with single-stage system is inhibitory effect of metals on SRB due to direct contact between SRB and heavy metals. Depending on the sludge characteristics, SRB is capable of actively metabolizing in removing a large amount of heavy metals. It has been shown that in a single-stage system, biofilms are highly tolerant to heavy metals upon short-term exposure, but when exposed for a long time SRB activity is completely inhibited (Teitzel et al., 2003).

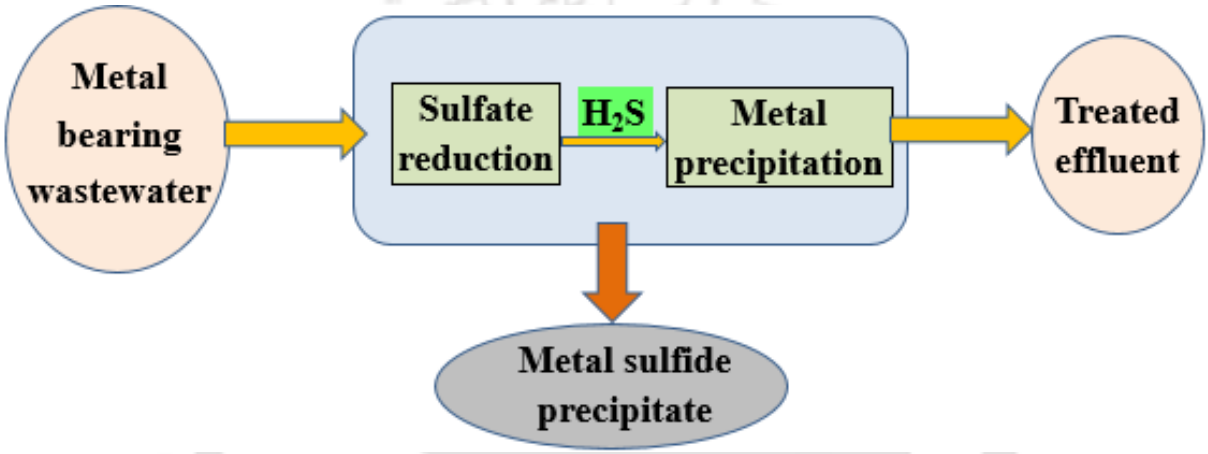

Fig. 2.1 Schematic showing single-stage treatment system for sulfate reduction and metal precipitation.

Metal recovery is another major drawback of single-stage system since metal sulfide can precipitate in the biomass itself. Although metals can be recovered from the metal sulfide containing sludge, this implies biomass loss (Tabak et al., 2003). Table 2.4 summarizes the data on different bioreactors used for treating sulfate rich metallic wastewater in a single-stage system along with electron donor used, values of COD/sulfate ratio and HRT followed, sulfate and metal removal efficiencies observed in these studies. As shown in Table 2.4, different carbon sources have been examined for sulfate reduction and metal removal in various bioreactor configuration, and lactate is the most preferred carbon source due to its high negative Gibb's free energy change. Kaksonen et al. (2003) achieved >99% removal efficiency of Zn and Fe using fluidized bed reactor

at very low influent pH (≤ 3.0), which proved SRB can grow and heavy metal removal is possible at acidic pH. Villa-Gomez et al. (2011) tested different COD/SO_4^{2-} of 1 and 5 using two similar inverse fluidized bed reactors with different influent pH (7 and 3), and observed that the metal removal efficiency in both the reactors did not vary much (Table 2.4).

2.2.2.2 Two-stage or multi stage system for metal removal

In a two-stage system, sulfate reduction to sulfide and subsequent metal precipitation due to the sulfides formed in the previous step are separated as depicted in Fig. 2.2. A major advantage of this two-stage system is that it avoids direct contact between the biomass and metals, thereby overcoming the toxic effect of metals on biomass due to high acidity and metal concentration (Johnson and Hallberg 2005).

A two-stage treatment system was first evaluated by Rowley et al. (1997) for treating AMD by which sulfate reduction in a sulfigdogenic bioreactor was carried out followed by metal precipitation in a separate unit. The authors achieved very high removal efficiency (>99%) of all the metals such as copper, cadmium and zinc. In another work by Tabak et al. (2003), more than 99% removal of copper and zinc from AMD was obtained using a four-step precipitation process. In the last decade, this technique has been evaluated for removing Cu and Zn from wastewaters (Foucher et al., 2001; Al-Tarazi et al., 2005; Gramp et al., 2006; Esposito et al., 2006). Selective metal recovery is also possible by controlling the pH and sulfide concentration (Sampaio et al., 2009), which finds several applications in different industries (Grootscholten et al., 2008).

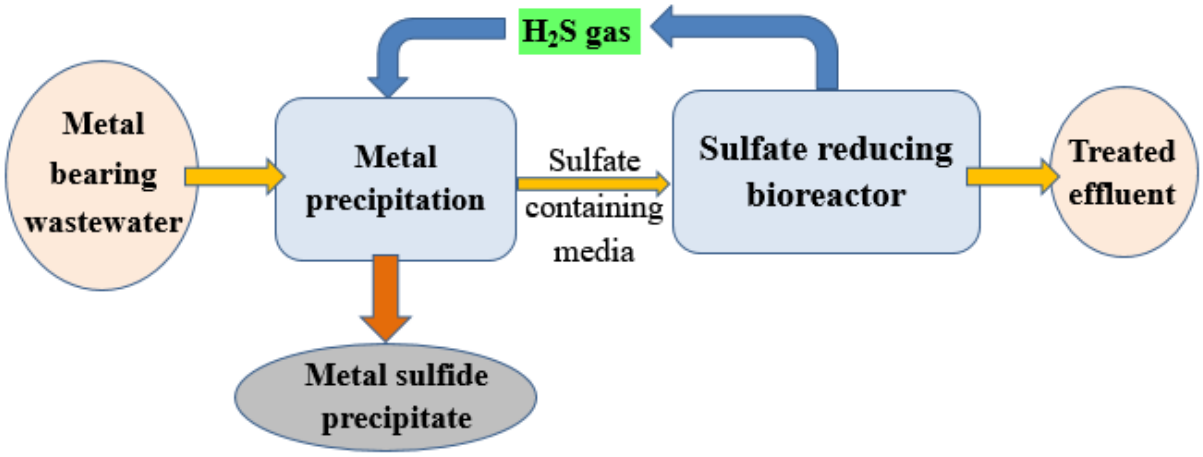

Fig. 2.2 Schematic showing two-stage system for treating heavy metal containing wastewater by sulfate reduction.

Table 2.4 Performance of different sulfidogenic bioreactors studied based on different carbon sources for sulfate reduction and heavy metal precipitation by SRB

Carbon source	HRT (h)	T (°C)	Influent pH	COD/SO_4^{2-} ratio	COD removal (%)	Sulfate removal (%)	Metal	Metal removal (%)	References
Upflow anaerobic sludge blanket reactor (UASB)									
Stillage from distilleries	18	25	7.0	Not Available (NA)	NA	93.75	Cd Zn	>99 >99	Goncalves et al., 2007
Sodium lactate	NA		7.5-8.5	2	NA	50	Pb	85-95	Hoa et al., 2007
Sodium lactate	6	30	7.0	0.5	~100	27-95	Se	>95	Lenz et al., 2008
Ethanol	4	NA	NA	NA	NA	79	Zn Cd Co Cu	>99 >99 >99 >99	Barnes et al., 1991
Ethanol	96	30	7.0	1.5	NA	>91	Pb	>99	Velasco et al., 2008
Lactate	16	35	3.0	0.66	>98	NA	Zn Fe	>99 >99	Kaksonen et al., 2003
Ethanol	24	30	4.5	1.28	90.5-85.8	NA	Cu Zn Ni	100 99.5 99.6	Sierra-Alvarez et al., 2006
Inverse fluidized bed reactor (IFBR)									
Lactate	24	27	7.0	NA	90	NA	Se	98	Arindam et al., 2019
Lactate	9	30	7.0	5	27	76	Cu Zn Pb Cd	~98.4 ~96.5 ~96 ~97.9	Villa-Gomez et al., 2011
Lactate	9	30	7.0	1	68	17	Cu Zn Pb	~99.9 ~98.6 ~99.2	Villa-Gomez et al., 2011

							Cd	~99.7	
Lactate	24	35	4.0	1.25	55-95	40-88	Zn Cu	>99 >99	Sahinkaya and Gungor et al., 2010
Lactate and Ethanol	24	18-26	5-6	0.8	~50	41	Fe Zn Cd	>98 >98 >99	Gallegos-Garcia et al., 2009
Fluidized bed reactor (FBR)									
Lactate and yeast extract	4	NA	NA	NA	NA	73.8	Cd	99.8	Ma and Hua et al., 1997
Ethanol	6.5	35	3-3.2	0.72	NA	76	Zn Fe	>98 >98	Kaksonen et al. 2004
Lactate	16	35	2.5	0.66	>98	NA	Zn Fe	>99 >99	Kaksonen et al., 2003
Molasses	6.8	30-31	5.2	NA	99	91	Ni U Cu Cd Zn As Pb	93 66.7 93.3 60 76.7 95 90	Somlev and Banov et al., 1998
Lactate or ethanol	24	65	7.8	NA	NA	~50	Fe	>99	Sahinkaya et al., 2007
Lactate	12	35	5.0	0.85	87-95	60-86	Zn Cu	>99 >99	Sahinkaya and Gungor et al., 2010
Ethanol	12 and 24	35	2.7-4.3	0.85	80	90	Al Cu Ni Pb Zn Mn	99.9 99.9 99.9 99.9 99.9 94	Sahinkaya et al., 2010
Anaerobic filter reactor (AFR)									
Acetic acid	202	30	7.5	0.7	>95	NA	Fe Zn Mn	>99 >99 >97	Steed et al. (2000)

							Cu Cd As Pb	>99 >99 >99 >99	
Cow manure, Saw dust, cheese whey	115-190		6.5	NA	NA	80-98	Fe Mn Zn Cu Cd As	84 40 99.7 99 99 89	Drury et al., 1999
Cow manure	50-100		NA	NA	NA	70	Zn Mn Cd	96-99 71-91 95-99	Farmer et al., 1995
Gas lift reactor (GLR)									
Lactate syrup	98.4	24-30	2.3	NA	NA	NA	Fe Cu Zn Al MN	>99 >99 >99 >99 >91	Hammack et al., 1994
CO_2	24.2	NA	NA	NA	NA	90	Zn	99	Bijmans et al., 2019
Upflow anaerobic packed bed reactor (UAPBR)									
Acid washed mushroom compost	12		4.5	1.9	NA	NA	Ni	>99	Hammack and Edenborn et al., 1992
Lactate	16.2	25	4.5	2	NA	NA	Cu Zn Ni As Fe Mg Al	>97.5 >97.5 >97.5 >77.5 >82 0 0	Jong and Parry et al., 2003
Compost	480	25	6.8	NA	NA	NA	Fe Zn Mn	<80 >99 <1	Chang et al., 2000

							Cu	>99	
Cow manure	96	20-23.5	2.6-2.9	NA	NA	NA	Mg Fe Zn Mn Al Cu Cd	>99 >99 >99 >94 >99 >99 >99	La et al., 2003
Lactate	16.16	25	4.5	NA	NA	NA	Cu Zn Ni Fe As Al Mg	>97.5 >97.5 >97.5 >82 >77.5 NA NA	Jong et al., 2003
Anaerobic baffled reactor (ABR)									
Ethanol	-	35	7.0	0.67	85	40-65	Cu Zn	100 83-98	Sahinkaya et al., 2009
Upflow anaerobic membrane bioreactor (UAMBR)									
Lactate	24	25	3.0	0.67	NA	84	Fe Cu Mn	86.2 99.9 52.6	Bai et al., 2013
Bubble column reactor (BCR)									
N_2-H_2S	NA	NA	7.1	NA	NA	NA	Ni Co	>90 >90	Lewis et al., 2006
Packed bed reactor (PBR)									
H_2S	NA	25	6.6	2	NA	NA	Fe Cu Zn Al	91.3 96.1 79 99	Jimenez-Rodriguez et al., 2009
Anaerobic packed bed reactor (APR)									
Lactate	NA	30	7.0	0.67	92.8	85	Cu Cd Ni Fe Pb	>70 60 >70 >70 >70	Kiran et al., 2015

							Zn	>70	
Anaerobic biological contactor reactor (An-RBC)									
Lactate	48	25	7.0	0.67	68-82	53-77	Cu Cd Ni Fe Pb Zn	97 90 >77 >77 >77 >77	Kiran et al., 2017
Upflow biofilm sulfidogenic bioreactor (UBSB)									
Glycerol	47	NA	3.6	NA	NA	NA	Cu Zn	>99 >99	Ňancucheo et al., 2012
Glycerol	47	NA	2.2	NA	NA	NA	Cu Zn	>99 8.0	Ňancucheo et al., 2012

*NA = Not available

2.3 Metal recovery by biological sulfate reduction

Metals are non-renewable resources and its recovery from heavy metal containing wastewater such as AMD is important from ecological as well as economical points of view. Metal recovery can be achieved by using any of the reactors presented in Table 2.5. For selective metal removal by precipitatation, pH and sulfide concentration are the most important factors; and for metal recovery, a multistage system in which sulfate reduction is separated from metal precipitation proves helpful. For instance, Tabak et al. (2003) reported that Fe, Zn Cu, Al can be precipitated separately in a four-stage system using different concentrations of sulfide in the respective units. Similarly, Sampaio et al. (2009) reported 100% sequential precipitation of Cu and Fe at pH 2 and 3 using a CSTR. Thus, metal recovery can be achieved using either single or multistage system.

2.3.1 Metal recovery in a single-stage system

Heavy metal removal by sulfate reduction in single-stage system of different reactor configurations has been widely studied, but only a few studies have been carried out on recovery of metals from metallic wastewater. Gallegos-Garcia et al. (2009) reported 99.7%, 99.3%, 99.4% removal efficiencies of Fe, Zn and Cd, respectively, using IFBR operated at an influent pH 5. Recovery efficiency of more than 90% for Fe, Zn and Cd as metal sulfide was obtained.

The recovered metals were present as metal sulfides only; no metal hydroxides or carbonates were recognized. The study reported for the first time the feasibility to recover metal sulfides separated from the biomass using a single stage reactor system (Gallegos-Garcia et al., 2009). IFBR is found to be highly effective as heavy metal containing wastewater reacts immediately with the produced sulfide which causes precipitation of the metals at the bottom of the reactor for an easy separation and recovery. For metal recovery, the metal sulfide precipitate obtained is first dried in an oven at

105 ºC followed by incineration at 550 ºC for 1 h to remove all the volatile composites. The total ash obtained is then used for calculating the fixed solid balance.

In another study, Villa-Gomez et al. (2011) reported less than 50% recovery of Cu, Zn, Pb, Cd using an IFB reactor, which was less compared with the results reported by Gallegos-Garcia et al. (2009). This difference could be attributed to the different SRB species used by Gallegos-Garcia et al. (2009) in their study. Another reason could be due to the method employed for metal recovery by Gallegos-Garcia et al. (2009) assuming that the total suspended solids (TSS) concentrations equal the metal sulfide composition (Kaksonen et al., 2003; Gallegos-Garcia et al., 2009). On the other contrary, Villa-Gomez et al. (2011) showed that in addition to the metal precipitates, salts present in the mineral medium as well contributed to the total suspended solids, which slightly increased the actual metal recovery value. Therefore, in order to exclude the salts present in the TSS for calculating the metal recovery value, Villa-Gomez et al. (2011) acidified the recovered solids before analysis of the metals present. Thereby resulting in accurate determination of metal recovery efficiency in the study.

Bijmans et al. (2008) studied selective recovery of nickel from nickel and iron containing solution by sulfate reduction at low pH (5.0) using a single-stage gas lift bioreactor. The results showed selective removal of nickel (>83 %) as nickel sulfide (NiS). At pH 5.5, the metal recovery obtained was more than 99.9%; however, iron removal and recovery as FeS could not be achieved at this pH value. Hence, controlling the bioreactor pH allows selective metal precipitation from wastewater.

Although by controlling the pH, selective recovery of different heavy metals can be achieved using a single-stage system, SRB are inhibited even at a slightly acidic pH (<5) due to increase in toxic

effect of sulfide and acetate at low pH. Copper can be precipitated as CuS even at an extremely low pH (≤1) whereas zinc does not precipitate as ZnS until pH 1.3 (Sahinkaya et al., 2009).

Although single-stage bioreactor system for selective heavy metal removal at low pH has several advantages such as low-operation cost, simple process design, homogeneous distribution of sulfide inside the bioreactor, etc. it is difficult to operate sulfidogenic bioreactor at low pH (<4). Hence, it is necessary to separate biological sulfide reduction step from metal precipitation to achieve both SRB activity (pH 7.0–8.0) and selective metal precipitation (pH 1.0 -7.0). Table 3 summarizes the results of metal removal as well as metal recovery efficiencies obtained using different single-stage bioreactor systems.

Table 2.5 Metal removal and metal recovery efficiency values obtained using different single-stage bioreactor systems

Reactor type	Metals	Metal removal (%)	Metal recovery (%)	References
Inverse fluidized bed reactor (IFBR)	Se	98.0	58.0	Sinharoy et al., 2019
Inverse fluidized bed reactor (IFBR)	Cu	99.9	41.1	Villa-Gomez et al., 2011
	Zn	98.6	44.2	
	Pb	99.2	60.3	
	Cd	99.7	47.4	
Inverse fluidized bed reactor (IFBR)	Fe	99.7	~90.0	Gallegos-Garcia et al., 2009
	Zn	99.3	~90.0	
	Cd	99.4	~90.0	
Gas lift reactor (GLR)	Ni	Not available (NA)	>99.9	Bijmans et al., 2008

2.3.2 Metal recovery in two-stage or multistage system

In order to avoid the afore-mentioned drawbacks with single-stage system for metal recovery, Tabak et al. (2003) used a two-stage system for selective, sequential precipitation (SSP) of metals, such as copper, zinc, aluminum, iron and manganese, as hydroxides and sulfides from Berkeley Pit AMD and followed additional processing of the recovered metals into marketable precipitates and pigments. The system involved a separate unit for sulfate reduction and metal precipitation; whereas the bioreactor was used to produce hydrogen sulfide in the first stage, the metal precipitation was carried out in a separate stage using the H_2S produced in the first stage.

The metal recovery percentage obtained using the SSP process was: 100% Zn (as sulfide), 99.8% Cu (as sulfide), 99.7% Al (as hydroxide), 97.1% Fe (as sulfide), 99.7% Cd (as sulfide), 99.1% Co (as sulfide), 97.1% Mn (as sulfide) and 47.8% Ni (as sulfide). The purity percentage of the different metal precipitates were: 92% copper sulfide, 81% ferric hydroxide, 97% zinc sulfide, 95% aluminum hydroxide and 75% manganese sulfide. Following the SSP treatment of the wastewater, Tabak et al. (2003) reported sulfate and sulfide concentrations below permissible limits and only calcium and magnesium were present in the effluent.

In another study on multi-stage system for recovery of Cu and Zn from AMD, Sahinkaya et al. (2009) utilized anaerobic baffled reactor (ABR) and the metals were precipitated separately based on their solubility product with gaseous sulfide produced in the first stage. The bioreactor was fed with ethanol (1340 mg/L) and sulfate (2000 mg/L) which yielded 65% sulfate reduction, 85% COD removal and 320 mg/L sulfide production values. Whereas Cu was precipitated separately using sulfide produced from ABR at low pH (<2) within 60 min, Zn did not precipitate at this pH. Following Cu removal, Zn recovery was achieved based on sulfide/Zn ratio with a Zn removal efficiency in the range 84-98%. Cu and Zn were precipitated as CuS and ZnS, respectively, with a

particle size in the range 10-50 µm. Table 2.6 presents the metal removal and recovery values with multi-stage bioreactor systems reported in the literature.

Table 2.6 Metal recovery using different multi-stage bioreactor systems

Reactor type	Metal	Metal removal (%)	Metal recovery (%)	References
Hollow fiber membrane bioreactor (MBR)	Al	Not available (NA)	99.8	Tabak et al., 2003
	Cd		99.7	
	Co		99.1	
	Cu		99.8	
	Fe		97.1	
	Mn		87.4	
	Ni		47.8	
	Zn		100.0	
Anaerobic baffled reactor (ABR)	Cu	84-98	NA	Sahinkaya et al., 2009
	Zn	100		

2.3.3 Single-stage vs multi-stage system

Table 2.7 compares the different parameters on metal sulfide precipitation using single-stage and multi-stage systems for the treatment of heavy metal containing wastewater by biological sulfate reduction.

Single-stage system is less labor intensive, quick, cost-effective and involves low operation as well as maintenance costs (Johnson et al., 2006; Villa-Gomez et al., 2011). Moreover, single-stage system has low area requirement, but the main advantage of multi-stage system is easy and selective metal recovery (Tabak et al., 2003).

Table 2.7 Comparison of advantages and disadvantages of single vs multi stage reactor systems

Parameter	Single stage system	Multistage system
Labor requirement	Low	High
Treatment area	Less	More
Metal recovery	Difficult	Easy
Cost	Low	High
Operation and maintenance expenditure	Low	High
Inhibitory effect on SRB	Low	High

2.4 Selection of sulfidogenic bioreactor for metal removal and recovery

Many different bioreactors have been reported for heavy metal removal but only a few have been evaluated for metal recovery purpose. The overall metal removal process involves metal precipitation followed by the accumulation of precipitate at the bottom of a reactor system. The metal bioprecipitate settled at the reactor bottom forms the basis for its recovery. However, most of the bioreactors designed for metal removal are not suitable for collecting the metal precipitate at the bottom for an easy recovery of the metals. Hence, single-stage bioreactors need to be modified for metal recovery, and one such example of a modified single-stage bioreactor system is inverse fluidized bed reactor (IFBR).

In FBR, growth of microbial community occurs on carrier support material within the reactor such that biomass is retained within the reactor. Moreover, in this bioreactor, liquid mixing and substrate transport is efficient due to upward movement of carrier support material by liquid upflow in the bioreactor (Gallegos-Garcia et al., 2009).

In FBR, the term fluidization is usually related to two or three-stage system wherein solid support are fluidized upward using any gas or liquid at high velocity against the gravity. Synthetic polymeric granules, silicate minerals and iron chips are some examples of carrier support used in FBR (Kaksonen et al., 2003). To achieve proper fluidization and high upflow velocity inside the FBR, not only influent but also effluent from the reactor is recycled from the top to bottom of the reactor. Advantages of FBR over other anaerobic reactors for metal removal are: (1) high removal efficiency (2) no risk of channeling or clogging (3) excellent biomass growth (4) low risk of shock load (5) good biomass retention (Kaksonen et al., 2006). In addition, FBR uses small carrier particles which allow sufficient microbial growth even with fluidization owing to large biofilm-liquid interfacial area, good mass transfer characteristics and high interfacial velocity. Schematic of a FBR system is depicted in Fig. 2.3.

In standard fluidization system, solid carrier support has higher specific density than the liquid inside. But in the case of downflow fluidized bed reactor, also knows as inverse fluidized bed reactor (IFBR), the carrier particles are less denser than liquid and expansion of bed happens downward as influent moves top to bottom (Karamanev and Nikolov et al., 1992). Inverse fluidization was invented in 1970 (Ibrahim et al., 1996) but it received less attention than standard fluidized bed reactors. The inverse fluidized bed reactors consist of floatable carrier particles which fluidize downwards, and following inoculation biofilm develops on the support material which remains on the top of the reactor during its operation (Fig. 2.3). Classical examples of carrier support used in IFBR are Kaldness-K1 (Arindam et al., 2019), polyethylene (Gallagos-Garcia et al., 2009; Villa-Gomez et al., 2011), cork (García-Calderón et al., 1998), polystyrene spheres (Nikolov and Karamanev 1987), and extendosphere (Buffiere et al., 2000; Arnaiz et al., 2003). Most of the earlier studies on hydrodynamics in IFBR employed non-biological particles with no

attached biofilm onto the carrier support (Chern et al., 1982; Fan et al., 1982; Ibrahim et al., 1996; Karamanev and Nikolov 1992a,b; Karamanev et al., 1992). The carrier support bed should facilitate a high biomass growth inside the bioreactor and also provide prolonged mean cell residence time without clogging problems (Shieh and Hsu 1996). But the main concern associated with the natural process of biofilm formation due to biomass accumulation is that it can enlarge the carrier particle diameter. It can also increase particle specific density because wet particle density with attached biofilm will be higher than the specific density of carrier particles devoid of any biofilm.

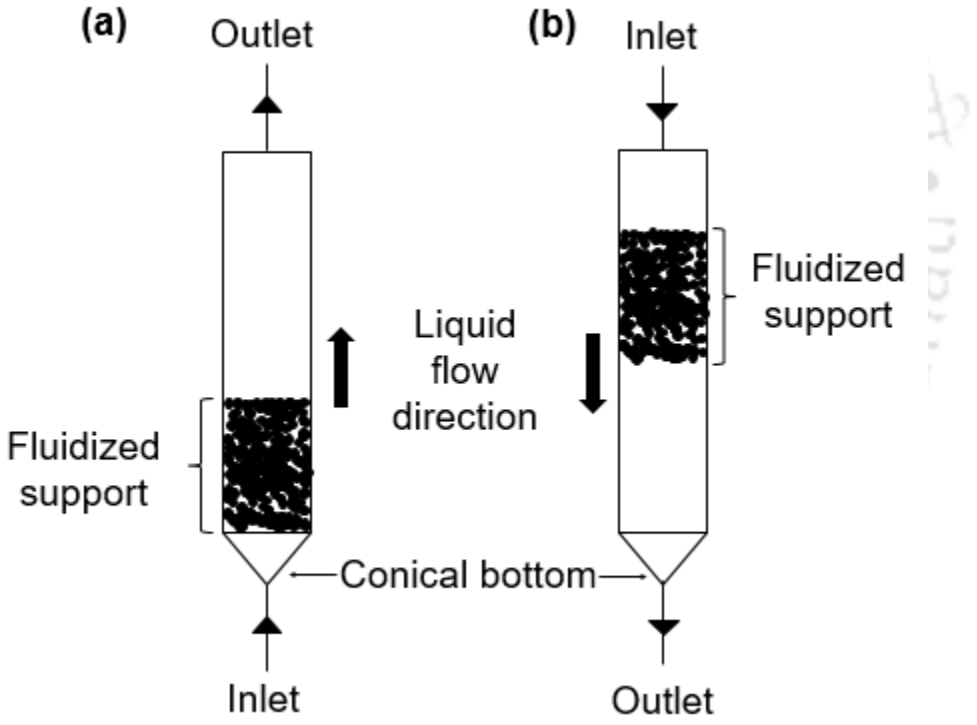

Fig. 2.3 Schematic of (a) up-flow and (b) inversed fluidized bed reactor (Kaksonen and Puhakka, 2007).

Many authors have evaluated different bioreactor configurations for metal precipitation. However, metal recovery was difficult because metals precipitates are usually associated with the biomass

which hampers their recovery. IFBR has been the most promising single-stage reactor configuration thus far for both metal removal and recovery. Villa Gomez et al. (2013) first investigated removal and recovery of heavy metals by sulfate reduction using IFBR. Support material with the biofilm remains at the top of the reactor and metal precipitate in the form of metal sulfide separated from the biomass and settled at the bottom. This unique feature is however uncommon in conventional high rate sulfidogenic reactors.

2.5 Effect of key factors on heavy metal removal and recovery in sulfidogenic bioreactors

2.5.1 Biomass composition

Microbial community in the biomass plays a vital role in the removal of sulfate and metal, thus affecting its recovery. Compared with single bacterial species, mixed microbial consortium offers several advantages such as: (1) no problem of contamination, (2) complete utilization of carbon source, (3) easy maintenance of culture condition, (4) robust performance. Hence, it is very important to select the finest consortium for achieving maximum heavy metal removal and recovery.

2.5.2 Reactor pH

pH is one of the most important factor affecting not only biological sulfate reduction for metal sulfide precipitation but also recovery of the metal precipitates. Different heavy metals precipitate at different pH as metal sulfides. As shown in the Eq. (2.1) and (2.2) the aqueous sulfide species (HS^- and S^{2-}) depend upon the solution pH. In acidic condition for metal removal, solubility of gaseous sulfide is very less, which lowers the available sulfide for metal precipitation (Villa-Gomez et al., 2011).

The thermodynamic equilibrium involved in metal sulfide precipitation can be expressed as follows:

$$H_2S \overset{Kp1}{\longleftrightarrow} HS^- + H^+ \qquad K_{p1} = \frac{[HS^-][H^+]}{[H_2S]} \qquad pK_1 = 6.99 \qquad (2.1)$$

$$HS^- \overset{Kp2}{\longleftrightarrow} S^{2-} + H^+ \qquad K_{p2} = \frac{[S^{2-}][H^+]}{[HS^-]} \qquad pK_2 = 17.4 \qquad (2.2)$$

$$M^{2+} + S^{2-} \leftrightarrow MS\,(s) \qquad (2.3)$$

$$M^{2+} + HS^- \leftrightarrow MS\,(s) + H^+ \qquad (2.4)$$

Where M^{2+} is any bivalent metal ion.

The solubility of different metals at a specific pH can lead to selective recovery of metals from solution containing a mixture of heavy metals (Bijmans et al., 2009; Sahinkaya et al., 2009; Tabak et al., 2003). The solubility constant (Ks) values of different metals sulfide (CuS, PbS, NiS, ZnS, FeS and CdS) are as follows: 6×10^{-36}, 8×10^{-28}, 3×10^{-19}, 2×10^{-25}, 6×10^{-18} and 8×10^{-28}, respectively. Table 2.8 shows pH values at which selective recovery of different metals as metal sulfide can be achieved.

Table 2.8 Effective pH for metal recovery by precipitation with hydrogen sulfide

Metal	pH	References
Fe	~6.0	Tabak et al., 2003; Sampaio et al., 2009
Cu	2.8 and 3.0	Foucher et al., 2001; Sampaio et al., 2009
Zn	5.5-6.0	Foucher et al., 2001; Sampaio et al., 2009
Ni	7.5-8.0	Samapaio et al., 2009
Cd	4.5-5.0	Gharabaghi et al., 2012
Pb	7.5-8.5	Hoa et al., 2007
Mn	9.4 and 10.3	Tabak et al., 2003

The low pH of metallic wastewaters such as AMD can limit the metal recovery efficiency in a single-stage system due to the following reasons: (1) inhibition of SRB activity, (2) inhibition of biomass growth and (3) low sulfate reduction efficiency. However, highly acidic wastewater (pH 2.5-3.0) is neutralized to pH 6-8 due to alkalinity produced by SRB in FBR (Kaksonen et al., 2003b). Djedidi et al. (2009) reported that metal sulfide precipitate formed at neutral pH exhibits better characteristics than the precipitates formed at a low pH, which are as follows: (1) good settling rate, (2) excellent solid-liquid separation, (3) high concentration of settleable solids and (4) agglomeration over crystallization. Villa-Gomez et al. (2014) observed similar results of increase in the precipitate amount from 5.1 to 9.4 mL/L due to an increase in the solution pH from 3 to 7.

2.5.3 Other influent parameters

In addition to solution pH, other influent parameters such as sulfate and metal concentrations, chemical oxygen demand (COD)/sulfate ratio have been shown to influence metal removal and recovery in sulfidogenic bioreactors. A high concentration of sulfate can adversely affect the SRB growth, whereas low sulfate concentration can promote methanogenic activity (Kiran et al., 2017). Visser et al. (1993) reported complete suppression of methanogen activity due to addition of sulfate in anaerobic granular sludge based reactor. High metal concentration also inhibits SRB activity, thereby affecting not only sulfate reduction efficiency but also metal removal and recovery efficiencies (Hao et al., 2000; Kiran et al., 2017).

Optimum COD/sulfate ratio is critical for interaction of SRB with sulfate and carbon source. The ideal theoretical value of COD/sulfate for complete removal of sulfate is 0.67. Hence, selecting a proper COD/sulfate ratio is key for the treatment of heavy metal and sulfate rich wastewater. Villa-Gomez et al. (2011) studied metal removal and recovery at two different COD/sulfate values of 5

and 1 using two identical sulfidogenic bioreactors. In both the bioreactors, the metal removal and recovery did not vary with COD/sulfate ratio. The metal removal efficiency was about 95% and the metal recovery efficiency was <50% for all the metals tested, e.g., Cu, Pb, Zn and Cd in both the bioreactors. Velasco et al. (2008) studied the effect of different COD/sulfate ratio between 1.5 and 2.5 on lead removal, and achieved >99% lead removal with COD/sulfate ratio of 1.5. In another study, Barbosa et al. (2014) obtained more than 90% removal of Ni, Cu and Mn with COD/sulfate ratio of 0.67, 1.0, 1.5 and 2.0, suggesting that enough sulfide was produced at all the ratio for an efficient removal of the metals.

2.5.4 Reactor design and operating conditions

Two main operational factors which affect the growth of SRB and its ability to tolerate metal toxicity are reactor pH and temperature. High temperature is advantageous as it is known to suppress the growth of methanogens.

High sulfide concentration is toxic to the growth of SRB, which consequently affects the metal removal and recovery efficiencies. At a high sulfate concentration, the presence of fine particles surrounding the SRB hinders the uptake of sulfate and other nutrients into the cell. Continuous stirring may affect the metal removal and recovery by affecting the SRB growth and rate of substrate uptake. Upflow liquid velocity reactors such as FBR and GLR are more vulnerable to biomass washout than down flow reactors such as IFBR.

Another factor that can affect the reactor performance is selection of suitable carbon source. Heavy metal containing wastewater has low amount of dissolved organic carbon, and therefore, requires addition of external organic carbon source for its treatment, increasing the overall cost of treatment (Gibert et al., 2004; Zagury et al., 2006). Choice of carbon source depends on different factors such as (i) cost of substrate used, (ii) substrate favorability for SRB, (iv) availability in sufficient

quantity, (v) pollution load in case of incomplete substrate degradation (Dries et al., 1998; Dijkman et al., 1999; Kiran et al., 2017).

SRB utilize low molecular weight compounds with simple structure as electron donor e.g. hydrogen, methanol, ethanol, lactate, glycerol and simple carbohydrates (glucose or sucrose). From Table 2.9, glycerol and lactate are the most favored carbon source for biological sulfate reduction owing to its high negative Gibb's free energy change and high energy biomass production. Bertolino et al. (2014) compared glycerol and lactate as the sole carbon source for sulfate reduction using fluidized bed reactors. Results obtained in the study showed that glycerol and lactate yielded the same sulfate reduction efficiency (~90%), suggesting that glycerol can serve as a low cost alternative to lactate (Bertolino et al., 2014). However, compared with the commonly used carbon sources (lactate and ethanol) for sulfate reduction, glycerol has not been explored much (Johnson et al., 2006; Bertolino et al., 2015).

Furthermore, a wide variety of SRB can utilize lactate as electron donor, and it produces bicarbonate, which helps in neutralizing the effluent acidity in a better way. On the other hand, drawbacks of using lactate are (i) more expensive than the alternative substrates, e.g. ethanol or acetate, (ii) it does not dissociate in acidic wastewater such as AMD and (iii) it can inhibit SRB activity (Kiran et al., 2017). Ethanol is the second most favorable carbon source for sulfide precipitation and it is easily available and cheaper than lactate (Kaksonen et al., 2004). Sulfate conversion efficiencies of more than 80% has been achieved in many previous studies. Ethanol is completely oxidized by *Desulfovibrio desulfuricans* and *Desulfobacter postgatei*. However, its utilization results in low biomass growth yield and acetate formation, which increases the acidity of the treated water.

Table 2.9 Values of Gibbs free energy change for sulfate reduction using different energy sources (Villa-Gomez et al., 2011, Bertolino et al., 2014)

Sulfate reduction with different carbon sources	ΔG^o (kJ/mol)
$4H_2 + SO_4^{2-} \rightarrow HS^- + 4H_2O$	-38.1
$Acetate + SO_4^{2-} \rightarrow 2HCO_3^- + HS^-$	-47.6
$Propionate + 3/4SO_4^{2-} \rightarrow Acetate + HCO_3^- + 3/4HS^- + 1/4H^+$	-37.7
$Butyrate + 1/2SO_4^{2-} \rightarrow 2Acetate + 1/2HS^- + 1/2H^+$	-27.8
$Lactate + 1/2SO_4^{2-} \rightarrow Acetate + HCO_3^- + 1/2HS^- + H^+$	-80.0
$Ethanol + 1/2SO_4^{2-} \rightarrow Acetate + HCO_3^- + 1/2HS^- + 1/2H^+ + H_2O$	-66.4
$Glycerol + 5/4SO_4^{2-} \rightarrow 1/2Acetate + 3/2H_2CO_3 + 1/2HCO_3^- + 5/4HS^- + 3/4OH^- + 1/4H_2O$	-424.5

2.6 Attached growth sulfidogenic bioreactors, bioprecipitate characterization and formation of metal sulfide nanoparticles

Wide range of industrial wastewater can be treated by sulfidogenic bioreactors for simultaneous removal of metal, sulfate and COD. Such reactors have advantages of easy sludge disposal and metal recovery (Gallegos-Garcia et al., 2009). The treatment efficiency and recovery capacity highly depend on the microbial composition of the biofilm in attached growth systems (Tekerlekopoulou et al., 2013). The biofilm is multipurpose and heterogeneous in nature. The biofilm enables sulfide production, metal sorption, mineral precipitation (Konhauser et al., 1993) and plays a key role in the formation of metal sulfide nanoparticles. Biofilm is usually composed of 25% bacteria and 75% extracellular polymeric substances (EPS) (Kiran et al., 2017). EPS forms gel type film and surround the bacteria and supporting material. The biofilm also comprise of different things such as bacteria cells, minerals and EPS (Flemming et al., 1995; van Hullebusch et al., 2003).

Under anaerobic condition in sulfidogenic bioreactors, biofilm on the support material mainly contains sulfate reducing bacteria. SRB structure typically consist of cytoplasm, murein, outer membrane and inner membrane. SRB is Gram negative bacteria and its outer membrane consists of lipopolysaccharides, lipids and protein. SRB secretes EPS in defense to toxicity produced by heavy metals or other toxic compounds. EPS mainly contains carbohydrates, proteins (protein with cations amino groups like ammonium and anions like phosphoryl, carboxyl groups) and enzymes (van Hullebusch et al., 2003; Kiran et al., 2017).

Yue et al. (2015) characterized EPS secreted by SRB called *D. desulfuricans* and reported the presence of polysaccharide, protein and nucleic acid as its major components. EPS also help in metal sequestration on the cell wall of the SRB by binding the freely suspended metal ions to the

anionic groups present on it. Vijayaraghavan et al. (2008) proposed two-step metal sulfide nanoparticle formation mechanism: (1) freely suspended metal ions bind to anionic groups present in EPS; (2) attached metal ions serve as nucleation site for more metals ions to get deposited. Therefore, SRBs cell wall act as nucleation site for metal aggregation and formation of metal sulfide nanoparticles. SRB use carbon source to reduce sulfate into sulfide as the respiratory product, and sulfide react with metals present on the cell wall of the bacteria or in the suspension to form metal sulfide nanoparticles (Kiran et al., 2015).

In another study, Murray et al. (2017) prepared biogenic zinc sulfide nanoparticles from AMD wastewater using batch serum bottles as well as in continuous sulfidogenic bioreactor operated at pH 4.0 with glycerol as the carbon source. Analysis of the ZnS nanoparticles using the TEM, XRD and particle size distribution confirmed that diameter of the ZnS nanoparticles was in the range 5-15 nm. Optical properties of the ZnS NPs revealed that it can be used as quantum dots (QDs). Such ZnS QDs have many applications in the field of optoelectronics as light emitting diodes and in solar photovoltaics (Smet et al., 2010; Murray et al., 2017). Spherical shaped zinc sulfide nanoparticles of size 2-5 nm in diameter were found synthesized in natural biofilm of sulfate reducing bacteria (Labrenz et al., 2000).

Weber et al. (2009) conducted microcosm experiments to examine the dynamics of freshwater floodplain soil contaminated with multi-metal such as Cd, Cu, Pb, Ni and Zn under a realistic sulfate-limited flooding regime. It was observed that CuS precipitate was the dominant sulfide formed in the flooded soil. Results suggested that Cd, Pb, Ni and Zn were also sequestered in sulfide precipitates and their sequestration pattern followed ascending order of solubility product of the respective metal sulfide.

2.7 Purification of metal sulfide bioprecipitate

In the biogenic sulfate reduction process, heavy metals can be removed as well as recovered as metal sulfide bioprecipitate. The metals present in metal sulfide bioprecipitates are in the nano-size range and can be efficiently recovered from the wastewater using an inverse fluidized bed reactor (IFBR) (Gallegos-Garcia et al., 2009; Villa-Gomez et al., 2011). However, metal sulfide nanoparticles are found attached to exopolysaccharide (EPS) secreted by SRB around the cell wall (Kiran et al., 2017). Hence, further processing of the bioprecipitate is required to extract the metal sulfide nanoparticles in pure form for its potential application in industries.

Conventional methods used to separate metal sulfide precipitate include solid-liquid separation, performed by gravitational clarifiers (thickeners) or filters, and SART (Sulfidization, Acidification, Recycling, and Thickening), which is another conventional method used in industries. These traditional processes have drawbacks such as large equipment size, high variability of the separation performance, complex operational conditions, and fine and colloidal particles remain in the suspension, promoting poor quality of clarified solutions. To overcome the limitations of conventional processes, membrane separation processes such as microfiltration (MF) and ultrafiltration (UF) using ceramic membranes are a valid alternative. Such techniques have many advantages like high yield, minimum separation steps, low working time, no need to use clarifying agents, easy cleaning and maintenance of equipment, and waste product reduction. In addition, membrane processes are characterized by their high efficiency, simple equipment, and low energy consumption.

Microfiltration based on membrane separation is an unexplored technique to purify metal sulfide nanoparticles from bioprecipitate (Suchecka et al., 2003; Monash et al., 2011). Mavrov et al.

(1998) used a microfiltration membrane to remove microorganisms from water for drinking water application, which resulted in a significant reduction in the microbial population. In another study, complete removal of *E. coli* was achieved by microfiltration using a polysulfone membrane (pore size 0.1 µm) (Karim et al., 2008). Lebleu et al. (2009) studied the removal efficiency of bacteria by polycarbonate microfiltration membranes. Similar reports on the separation of microbial biomass using polymeric membranes from aqueous solution can be found in the literature, but less attention has been given to the use of ceramic membranes, in particular, the purification of metal sulfide nanoparticles from contaminating biomass.

2.7.1 Conventional purification methods for metal sulfide precipitates

The metal sulfide precipitate can be clarified using the solid-liquid separation method. It has many advantages such as low solid content in treated solution, formation of concentrated slurry or cake, which needs to be further processed or disposed. The separation efficiency and quality of the treated solution should be high to minimize metal loss during the process, and it must satisfy the effluent discharge limit. Conventionally, solid-liquid separation is performed using gravitational clarifiers (thickeners) or filters (Estay et al., 2020). Lamella clarifiers are used as an alternative to gravitational clarifiers to overcome the complexity of metal sulfide precipitates. To improve the efficiency of solid-liquid separation, many studies are conducted to understand these metal sulfide precipitates with different characteristics (Chen et al., 2018; Gim-Krumm et al., 2019). Separation efficiency depends on operation conditions, solution chemistry, supersaturation control, and interaction of metal sulfide with water (Gim-Krumm et al., 2019; Wrighton-Araneda et al., 2019). On the other hand, metal sulfide precipitate is strongly influenced by the solution characteristics, especially particles with colloidal behavior. Some metal sulfides, such as copper sulfide, has high aggregation capacity, which increases its particles size in the system and improves its settling

efficiency (Quilaqueo et al., 2019). These findings reveal that fine and colloidal particles remain suspended, and has poor settling characterization in solid, liquid separation system.

To overcome the drawbacks of gravitational clarifiers, some studies have tried to transform the characteristics of suspension to enhance the settling performance. The following factors have been explored for different metals and systems, e.g., addition of other metal ions, addition of precipitates seeds to support better nucleation (Yan et al., 2017), use of calcium or magnesium ions to improve particle size and settling characteristics (Deng et al., 2020), and use of UV light irradiation during the precipitation process (Peng et al., 2019).

At an industrial level, the SART process is used for metal sulfide precipitation and solid-liquid separation. The SART technology uses conventional gravitational clarifiers to separate the suspension formed in the precipitation reactor. It also recirculates underflow to the reactor to increase the particle size of the precipitates (Estay et al., 2018). Clarification is the main challenging step in the SART technology for wider application (Breuer et al., 2015). The clarification performance is affected by the complex nature of precipitates, e.g. low settling velocity, and large equipment size (Estay et al., 2018).

2.7.2 Membrane based separation for purification of metal sulfide precipitates

Membrane separation techniques such as microfiltration (MF) and ultrafiltration (UF) are the most effective methods to overcome the limitations of conventional clarification process. The membrane process has many advantages, such as high yield, fewer processing steps, etc. In addition, they involve less working time, no use of clarifying agents, easy cleaning and maintenance of equipment, and reduction in waste byproducts (Estay et al., 2021). Also, membrane processes are characterized by their high efficiency, simple equipment, and low energy

consumption (Li et al., 2010). Microfiltration is used to filtrate particles ranging from 0.1 to 10 µm and operate at low-pressure conditions. Ultrafiltration operates at higher pressure (2-10 bar) and can separate molecules higher than the molecular weight of 1-1000 kDa (Cassano et al., 2014). The drawback associated with membrane filtration is the retention of some particles leading to their accumulation on the membrane surface, causing membrane fouling, which results in the reduction of permeate flux. The flow reduction causes loss in efficiency, increase operational costs, and demands maintenance (Saad et al., 2014).

2.7.2.1 Modes of operation in a membrane separation process

There are different operation modes in membrane processes. Fig. 2.4 represents the different modes of operation.

2.7.2.1.1 Dead-end filtration mode

This is the primary mode of membrane separation operation. The feed is forced to pass through the membrane using external pressure, and the filtered matter is accumulated on the top of the membrane surface. This mode of operation is called a batch process because filtered material accumulates on the membrane surface and clogs the pores, ultimately reducing the membrane efficiency and necessitates cleaning of the membrane surface. Nevertheless, dead-end filtration is a highly useful method for concentrating solids (Vasanth et al., 2011).

2.7.2.1.2 Cross-flow filtration mode

The technique is called "cross-flow" because the feed flow is perpendicular to the filtration flow direction. In this mode of operation, primarily tubular configuration of membranes is used. The high feed through the membrane surface act as a driving force to filter the feed, and a high flow rate creates high turbulent conditions. The higher pressure-driven feed flow restrains filtered

particles to retain on the surface of the membrane. The cross-flow mode is generally used for the feed having high filterable matter (Estay et al., 2021).

2.7.2.1.3 Hybrid-flow filtration mode

Hybrid-flow filtration mode combines both dead-end and cross-flow modes, and it consists of two phases: production and flushing. The production phase involves dead-end mode of operation, and the flushing phase consists of cross-flow mode. In flushing mode, both ends of the tubes are open, and the part of the feed that doesn't pass through the membrane is eliminated to clean the membrane surface. This type of filtration mode is generally used for feed with a high concentration of suspended matter.

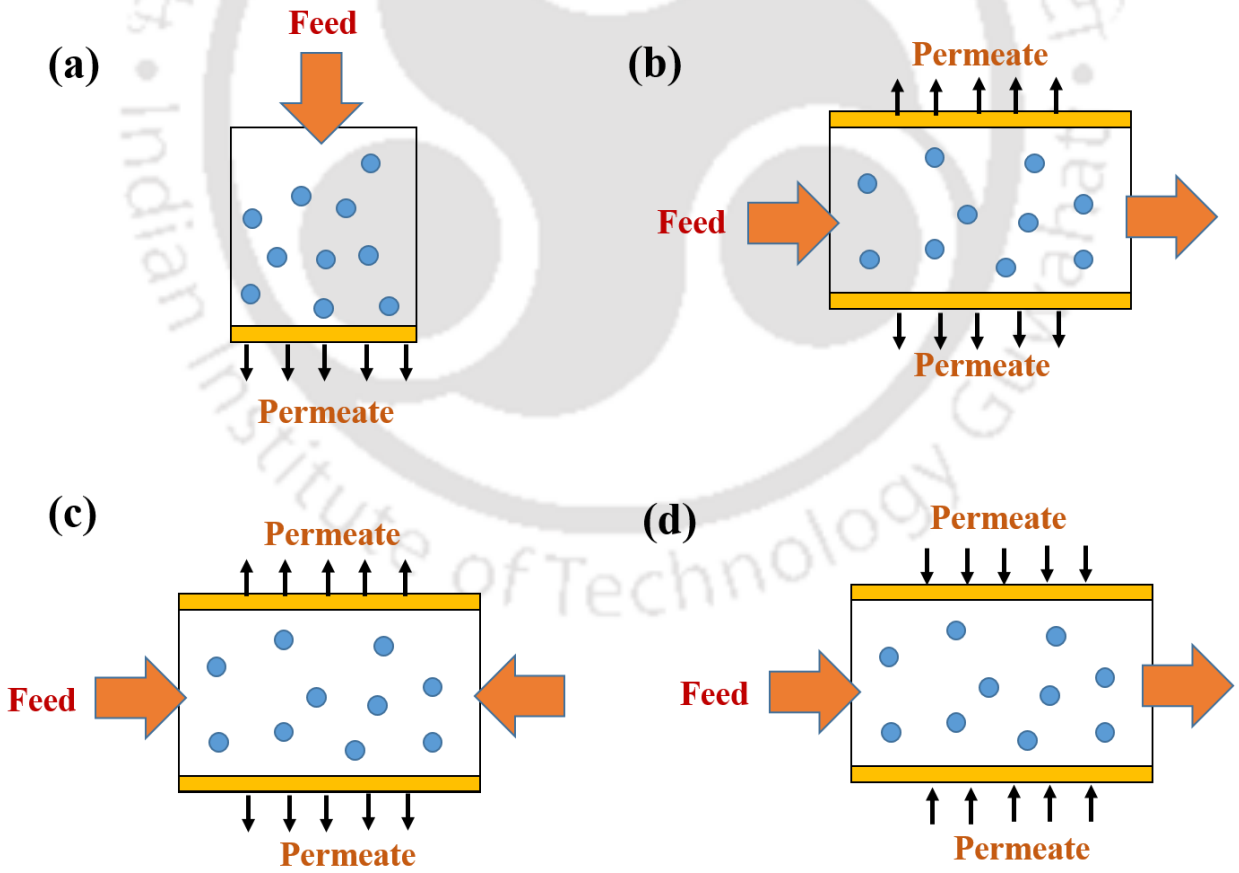

Fig. 2.4 Various modes of membrane separation operation (a) dead end (b) cross-flow (c-d) hybrid.

2.7.2.2 Membrane Modules

A membrane module is a way the membrane is incorporated into a filtration device for filtration. The following modules are commonly used in industries:

- Flat sheet modules
- Tubular modules
- Hollow fiber modules

These are the module design developed by manufacturers for various applications based on the type and characteristics of feed. The flat sheet membranes resemble filter paper. Similarly, tubular membrane resembles the single hollow tube of circular cross-section, in which the wall of the tube works as the membrane. Hollow fiber membranes also look like tubular membranes, but their diameter is very small compared to tubular membranes. The hollow fiber membranes have a typical diameter of 1 mm (Cui and Muralidhara 2010).

2.7.2.3 Membrane materials

The two most common membrane materials used to prepare symmetric membranes for industrial applications are polymeric and ceramic materials. The asymmetric membrane is prepared from symmetric polymeric and symmetric ceramic membrane material.

2.7.2.3.1 Polymeric membranes

Polymeric membranes have a thin film-like structure with a thickness of 10-100 μm. Various types of polymers are used to prepare the polymeric membrane, such as polyacrylonitrile (PAN), polyamide (PA), polyetherimide (PEI), cellulose acetate (CA), polypropylene (PP), polysulphone (PSU), etc. Table 2.10 presents advantages and disadvantages of polymeric membrane.

Table 2.10 Advantages and disadvantages of polymeric membrane

Advantages	Disadvantages
Different pore size ranges are available	Low life span
Low cost	Low solvent resistance
Easy to fabricate	Low corrosive resistance
Easy to scale up	Temperature sensitive

2.7.2.3.2 Ceramic membranes

Ceramic membranes are made from inorganic materials such as kaolin, alumina, zirconia, silica, titania, etc. The ceramic membrane provides good thermal, chemical, and mechanical stability. The pore diameter of commercially available ceramic membrane ranges from 10 nm to 10 μm, and thickness ranges from 2 to 5 mm depending on the type of application. Advantages and disadvantages of ceramic membrane are presented in Table 2.11.

Table 2.11 Advantages and disadvantages of ceramic membrane

Advantages	Disadvantages
High corrosive resistance	Brittle in nature
High temperature resistance	High cost
High solvent resistance	Most ceramic membranes are available in pore diameters within the MF and UF range (0.010 – 10 μm)
High life span	
High mechanical strength	

2.7.2.4 Polymer vs. Ceramic membranes

Comparing the advantages and disadvantages of polymeric and ceramic membranes, polymeric membrane seem to be more useful for lab-scale application. For industrial applications, cost and life span of the membrane are the two most important factors that need to be considered along with their efficiency. The life span of polymeric membranes varies from 12 to 18 months, and that of ceramic membranes is ten years (Mulder 1991). Therefore, life span of ceramic membranes are on the higher side if we consider their industrial application. Though the separation characteristics of ceramic membranes are similar to the polymeric membrane, they are not widely used in industries due to their higher costs. So the development of low-cost membranes with an increased life span is anticipated to drive the economic competitiveness of ceramic membranes in industries. The membrane filtration process has not been applied for filtration of metal sulfide precipitate formed by biogenic sulfate reduction despite the fact that the membrane filtration process has many advantages over conventional clarification processes.

From the detailed literature review, it is clear that the main focus has been given to treat heavy metal and sulfate-containing metallic wastewater and recovery of heavy metals in the nanopowder form employing IFBR. Although few literature reports are available for metal recovery using sulfidogenic reactors, the influence of specific process parameters such as influent with low pH, hydraulic retention time, low/high metal loading, etc., on metal recovery using IFBR has not been reported so far. Moreover, detailed characterization of metal bioprecipitates obtained from sulfidogenic reactors treating wastewaters for potential industrial application is limited. Also, purification of metal sulfide bioprecipitate recovered from IFBR using indigenous low-cost ceramic membrane has not been reported in the literature. Furthermore, application potential of metal sulfide nanoparticles recovered by sulfate reduction process need to be examined.

2.8 Applications of metal sulfide nanoparticles

Following removal and recovery of heavy metals as precipitate using sulfidogenic bioreactor, the precipitate mostly contains metal sulfide in nano-size range (Gallegos-Garcia et al., 2009). Table 2.10 summarizes the various application of metal sulfide nanoparticles in different fields along with synthesis methods and size of nanoparticles obtained.

2.8.1 Solar Cells

Metal sulfide nanoparticles find applications in solar systems because of its several distinguishing features such as: high extinction coefficient and a wider band gap. Copper sulfide nanoparticles (CuS NPs) are ideal for solar cell applications due to its absorbance peak in near infrared region and whole visible range, as revealed from UV-visible spectroscopy (Singh et al., 2015). Nickel sulfide nanoparticles (NiS NPs) were used in dye sensitized solar cells for its low cost and high efficiency of converting solar to electric power (Sarkar et al., 2018). Copper, zinc and tin sulfides nanoparticles forming thin films were investigated for solar cell modelling because of their unique morphological, structural and optical properties (Liu et al., 2014). Iron pyrite (FeS_2) nanoparticles can be used as a non-toxic photovoltaic material in the fabrication of efficient solar cell devices (Bi et al., 2011). Cadmium sulfide nanoparticles (CdS NPs) has also proved to be potential for solar cells due to its significant long-term stability in terms of greater resistance to oxygen degradation (Dowland et al., 2013). The dielectric studies using biologically synthesised lead sulfide thin films (PbS NPs) as reported by Sagadevan et al. (2014) prove their promising use in solar cell applications (Fig. 2.5).

Table 2.12 Application of metal sulfide nanoparticles in various fields

Metal Sulfide Nanoparticles (MeSNPs)	Synthesis Methods	Size and Shape	Applications	References
Iron (Fe)	Surfactant assisted hot-injection method (Chemical synthesis), High-energy milling (Mechanical method)	Cubic shape with good uniformity and size distribution ranging 60-200 nm	Photovoltaic devices, Labeling of biological materials, Transformer core materials, Environmental remediation and deactivation of radioactive heavy metals	Huber et al., 2005; Bi et al., 2011; Gong et al., 2016
Zinc (Zn)	Lewis acid-base reaction (Chemical synthesis), Thio-urea hydrolysis (Hydrothermal synthesis), Metal-organic framework strategy	Spherical crystals having average diameter of 5.5 nm	In vitro imaging, Light emitting diodes, Bioactive coatings, Fuel cells	Zhao et al., 2004; Jayalakshmi et al., 2006; Yu et al., 2013; Shakil et al., 2018
Copper (Cu)	Biological synthesis, Sonochemical synthesis using ultrasonicator, In-situ growth by solvothermal method, Microwave irradiation,	Different types-Spherical particles of average size 4 nm; Triangular plates of average size 12 nm; Distorted spherical to oval shape with slight	Dye degradation, Solar cells, Immuno-sensors, Drug-therapy, Agriculture, Lithium ion batteries, Wound dressings, Catalyst (Click reaction), Air filtration technology	Borkow et al., 2009; Liang et al., 2011; Zhao et al., 2012; Cai et al., 2014; Singh et al., 2015; Ibrahim et al., 2016; Sidhu et al., 2017

	Surfactant-based synthesis, Enzymatic treatment (Green synthetic method)	aggregations and size (8-14) nm.		
Cadmium (Cd)	Chemical precipitation method, Sonochemical method.	Varies from cubic to hexagonal crystalline structure with size ranging from 2.4 nm to 6.2 nm	Solar cells, Fluorescent probe, Water purification	El-Kemary et al., 2009; Dowland et al., 2013; Barman et al., 2016
Lead (Pb)	Chemical precipitation method, Ultrasonic irradiation.	Uniform nanowires of average diameter 40nm and length 5µ	Solar cells, Telecommunications	Karami et al., 2013; Sagadevan et al., 2014
Nickel (Ni)	Hydrothermal synthesis, Solvothermal method using domestic microwave oven.	Sphere like structure with average crystallite size of 22 nm	Dye-sensitized solar cells, Infrared detectors.	Sarkar et al., 2018; Nagaveena et al., 2013

2.8.2 Biomedical applications

Copper sulfide nanoparticles (CuS NPs) find several applications in biomedical field which includes detection of food borne pathogens, biomolecules (DNA), glucose, etc (Cai et al., 2014). These are extensively used as immunosensors, tools for *in vivo* molecular imaging, specific targeted drug therapy (Cai et al., 2014) and as an agent for photo-thermal ablation of cancer cells (Chen et al., 2010). Zinc sulfide nanoparticles (ZnS NPs) were reported to be widely acceptable for both *in vitro* imaging, and high resolution tumor-targeted imaging due to its biocompatibility (Yu et al., 2013). FeNPs proved to be highly potential in biomedical field including contrast intensification of magnetic resonance imaging, medical treatments like hyperthermia, and even labeling and magnetic separation of biological materials (Huber et al., 2005). Among different semiconductor nanoparticles, CdS NPs have been studied for quantitative determination of drug molecule contents as a fluorescent probe (El-Kemary et al., 2009).

2.8.3 Agriculture

In this recent era of continuous exploration of safe, eco-friendly techniques, CuS NPs are gaining attention for increasing wheat germination, improving tomato growth and quality. These nanoparticles were also used for evaluating antifungal activity against several phytopathogenic fungi (Sidhu et al., 2017).

2.8.4 Electronics

CuS NPs nanoparticles were found to be favorable as cathode materials for lithium ion batteries due to its high specific capacity (Zhao et al., 2012). As a conventional semiconducting phosphor material, ZnS NPs were extensively used in light emitting diodes, displays, di-electric filter, sensors and lasers (Jayalakshmi et al., 2006). Even ZnS NPs implanted in porous carbon matrices

has shown remarkable performance as an anode material in lithium ion batteries (Fu et al., 2015). FeS NPs were commercially applied in magnetic recording tapes, transformer core materials, etc. (Huber et al., 2005). CdS NPs has gained interest in manufacture of nanowires, nanospheres and nanobelts. NiS NPs find application as cathode materials for use in high energy batteries, infrared detectors, and designing of batteries (Nagaveena et al., 2013). Uses of PbS NPs in electronics include optical switches, telecommunications, photograph lasers, gas sensing agents in solid state sensors and also LED devices (Karami et al., 2013).

2.8.5 Bioactive coatings

ZnS NPs are used for coating multi walled carbon nanotubes (Zhao et al., 2004). CuS NPs were coated over cellulose films for imparting antibacterial activity against different bacterial sp. such as *S. aureus* and *E. coli* (Jia et al., 2012). CuS NPs are also effective as wound dressings and socks due to their biocidal properties (Borkow et al., 2009).

2.8.6 Catalytic Reactions

CuS NPs have been used as catalysts because of its low toxicity, affordability and regenerability (Rubilar et al., 2013). CuS NPs can be applied as an excellent catalyst in alkyne-azide cycloaddition “Click reaction” (Liang et al., 2011). CoS NPs also proved efficient as powerful catalyst for photoelectrochemical generation of hydrogen from water at neutral pH (Sun et al., 2013). ZnS and CdS nanoparticles combined with graphene forming nanohybrids were useful in photocatalytic reactions, including in water splitting, CO_2 reduction, textile wastewater degradation in presence of a photocatalyst (Thangavel et al., 2016). Iron-catalyzed sulphoxidation were also proved to be remarkably good under very simple reaction conditions in presence of aqueous H_2O_2 (Legros et al., 2004).

2.8.7 Environmental remediation

FeS NPs have been applied for environmental remediation of both groundwater and soil by reductive conversion of organic pollutants, and deactivation of radioactive heavy metals (Gong et al., 2016). CuS NPs were considered as antimicrobial compounds in air filtration technology to eliminate bio-aerosols through the process of ventilation (Ibrahim et al., 2016). CdS NPs in combination with zinc oxide proved to be efficient in water purification as they showed antimicrobial activity against water-borne pathogens (Barman et al., 2016). ZnS and Ag_2S bi-metallic nanoparticles have been successfully applied as cheap, renewable and interesting options to commercialized agents for decomposition of environmental pollutants (Abbasi et al., 2018).

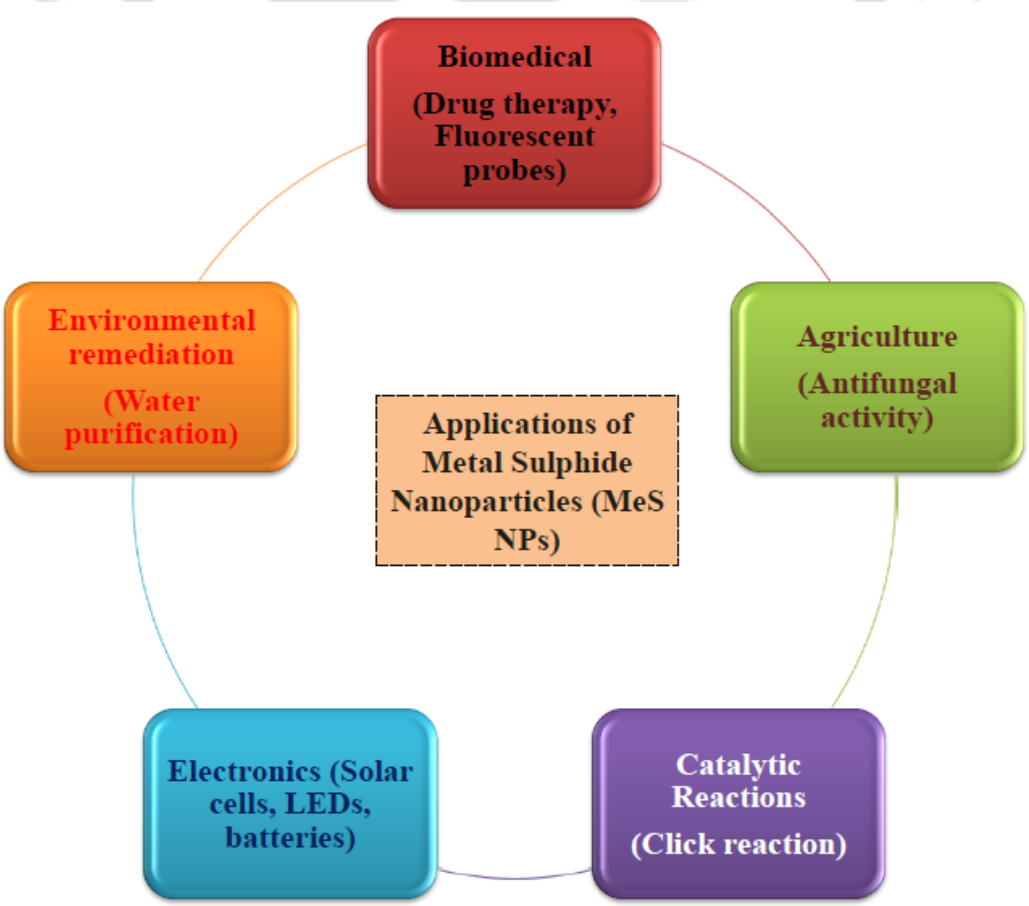

Fig. 2.5 Major application of MeS nanoparticles in various fields.

2.8.8 Fuel cells

The activity and stability of the most important cathodic reaction (O_2 reduction reaction) in fuel cells were improved by CoS NPs as reported by Bai et al. (2016). Similarly, ZnS NPs have several potential applications in fuel cells due to their excellent physical and chemical properties (Shakil et al., 2018).

Chapter 3

Screening of anaerobic biomass collected from different sources for heavy metal removal and recovery under sulfate reducing condition

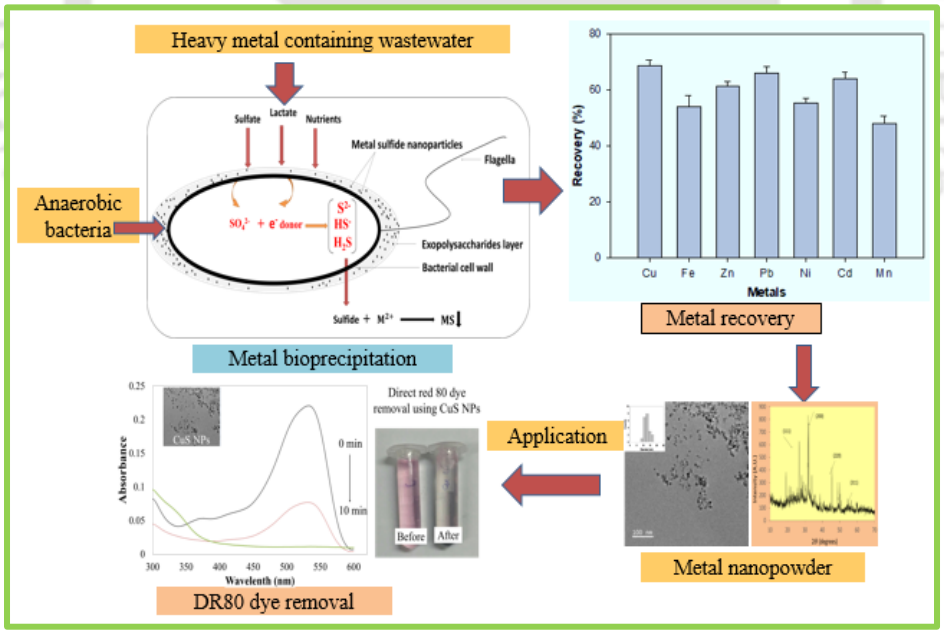

ABSTRACT

Biological sulfate reduction and heavy metal removal process is an emerging technique to recover heavy metals from wastewater. In this study, anaerobic biomass from three different sources were initially screened on the basis of their metal removal and sulfate reduction efficiencies. The effect of metal loading on the removal of sulfate and COD by sulfate reducing bacteria (SRB) present in the anaerobic biomass was further examined. At low metal loading conditions, the biomass obtained from a laboratory scale anaerobic rotating biological contactor (An-RBC) reactor treating metallic wastewater showed a maximum metal removal (95 ± .50%), sulfate reduction (90 ± 1.56%) and COD removal (80 ± .88%); however, the values decreased at a high metal concentration for all the biomass. Metals were then subsequently recovered in the form of nanopowder from bioprecipitates and the metal recovery efficiency was in the order Cu > Pb > Cd > Zn > Ni > Fe > Mn. Analysis of the bioprecipitates revealed the presence of metal sulfide, which was further confirmed by field emission scanning electron microscope (FESEM) and energy dispersive X-ray spectroscopy (EDX) analysis. Size, shape and crystallinity of the nanoparticles were confirmed by field emission transmission electron microscopy (FETEM) and X-ray diffractometer (XRD) which indicated its excellent potential for industrial reuse and application.

3.1 Introduction

Increasing demand of heavy metals in industrial sectors has led to the depletion of metal and mineral resources. To compensate for this loss, heavy metals need to be recovered from wastewater discharged from industries, particularly mining and metallurgy, which usually contains a high concentration of heavy metals (Kiran et al., 2018). Mine wastewater, commonly known as acid mine drainage (AMD), is characterized by its low pH, high sulfate and high metal content (Kieu et al., 2011; Kastyuchik et al., 2016; Kiran et al., 2017).

The most important factor which makes AMD an environmental threat is its ability to convert relatively inert ore into tremendous volumes of hazardous waste, extending its life and extreme difficulty in managing its flow (Johnson et al., 2005). Owing to the presence of toxic heavy metals, acid mine drainage (AMD) impact the environment due to ecological destruction of watersheds and heavy metal pollution of ground and surface water globally (Beyenal and Lewandowki et al., 2004; Kieu et al., 2011; Kiran et al., 2017). Hence, there is a need to not only treat heavy metal containing wastewater but also recovery of heavy metals before discharge into the environment.

Available physiochemical methods, including lime neutralization, adsorption, oxidation-reduction and chemical precipitation, to treat AMD and other metallic wastewater have one or more drawbacks, such as high cost, low removal efficiency, generation of high sludge volume, etc. (Kiran et al., 2015; Taseidifar et al., 2017). In this context, biological sulfate reduction using anaerobic sulfate reducing bacteria (SRB) is an effective method for both metal removal and recovery from wastewater. It is considered an effective alternative to conventional methods e.g. hydroxide precipitation due to its low capital cost and formation of highly insoluble salts (Kaksonen and Puhakka et al., 2007; Gallegos-Garcia et al., 2008).

Under anaerobic environment, SRB oxidize simple organic compounds by utilizing sulfate as an electron acceptor and generate sulfide and alkalinity. The biogenically produced sulfide is capable of reacting with dissolved metals to form highly insoluble metal sulfide precipitates since the solubility of the metal sulfides are generally very low.

Thus, there is an increased interest in the potential application of biological sulfate reduction as an alternative method for heavy metal removal and recovery from wastewater (Castillo et al., 2012; Sanchez-Andrea et al., 2014; Lefticariu et al., 2015). However, the potential use of SRB for synthesis of metal nanopowders through biogenic sulfate reduction has not been explored as most of the earlier studies are limited only to metal removal or sulfate reduction.

The problem with the sulfate reduction process for metal removal is the generation of insoluble metal precipitates, which may leach out and adversely affect the environment. However, metal recovery from such insoluble metal precipitate is an option. Moreover, metal recovery in the form of nanoparticles could serve as an incentive to industries that discharge heavy metal containing wastewater. Such metal nanoparticles have also shown to be toxic towards animals and other living organisms, thereby necessitating its recovery from wastewater. These nanoparticles are characterized by their small particle size, large specific surface area, and high surface reactivity, and hence, these metal nanoparticles find many applications in different areas. For example, nickel sulfide and copper sulfide nanoparticles can be used for dye degradation (Molla et al., 2016; Shamraiz et al., 2016) and iron sulfide nanoparticles can be used for the reduction of chlorinated organic compounds and heavy metal removal (Gong et al., 2016).

Hence, this study was aimed at screening of different anaerobic biomass with SRB for simultaneous removal and recovery of metals in the form of nanoparticles from heavy metal containing wastewater.

3.2 Materials and methods

3.2.1 Screening of anaerobic biomass for heavy metal removal and recovery

Anaerobic biomass collected from three different sources were screened for heavy metal removal and recovery as nanopowder from aqueous solution. These sources were: (1) large scale upflow anaerobic sludge blanket (UASB) reactor (located in Kavoor, Mangalore, Karnataka, India) treating sewage and wastewater from small scale industries, (2) a wastewater treatment plant (WWTP) situated in IIT Guwahati, Guwahati, Assam, India, and (3) a laboratory scale anaerobic rotating biological contactor (An-RBC) reactor treating heavy metal containing wastewater. The collected anaerobic biomass was stored at 4 °C in a refrigerator until further use.

For initial activation of microorganisms present in the biomass, 10% (v/v) of the respective anaerobic biomass from different sources was added to 1 L aspirator bottle containing modified Postgate media, which is commonly used for cultivating SRB, such as *Desulfovibrio* and *Desulfotomaculum* species. After purging with nitrogen, the bottles were incubated in an orbital shaker set at 30 °C and 150 rpm for one week. 60% (v/v) of sodium lactate was used as the carbon source and electron donor for culturing these biomass types. Sulfate was added as Na_2SO_4 at COD/SO_4^{2-} ratio of 0.67. The active biomass was subsequently tested for heavy metal removal and recovery experiments, as detailed later in the next section.

Composition of the modified Postgate medium for anaerobic growth of the biomass was as follows (g/L): ammonium chloride (1.0), potassium dihydrogen phosphate (0.5), sodium sulfate (1.47),

calcium chloride dihydrate (0.1), ascorbic acid (0.1), sodium citrate (0.3), ethylene diamine tetraacetic acid (0.3), ferrous sulfate heptahydrate (0.289), and yeast extract (1.0) (Postgate 1984). The pH of the media was adjusted to 7.0 using 2 N NaOH.

3.2.2 Heavy metal removal and recovery experiments

Batch experiments for heavy metal removal by sulfate reduction were performed using serum bottles of volume 120 mL each and sealed with polytetrafluoroethylene (PTFE) septum. The bottles were incubated in orbital shaker set at 30 °C and 150 rpm for five days. The bottles were purged with nitrogen gas prior to the experiment with 10% (v/v) biomass as the inoculum. Bottles containing biomass and carbon source but without any added metal served as the control in these batch experiments.

Individual metal stock solutions of Cu(II), Cd(II), Ni(II), Fe(II), Pb(II), Mn(II) and Zn(II) of 10,000 mg/L concentration each were prepared using copper chloride dihydrate, cadmium nitrate tetrahydrate, nickel chloride hexahydrate, iron chloride tetrahydrate, lead nitrate, manganese chloride tetrahydrate and zinc chloride, respectively. Serum bottles containing the Postgate medium as mentioned earlier were added with the individual metal-containing stock solution to obtain desired metal concentrations. Initial metal concentration in these experiments was chosen based on the composition of acid mine drainage from Makum Coalfield area located in North-East India (Equeenuddin et al., 2010). Table 3.1 provides the metal concentration tested in this study.

Table 3.1 Metal concentration tested in this study (pH 7.0)

S.No.	Metal	Concentration (mg/L)
1	Fe	50 - 150
2	Cu	5 - 15
3	Mn	5 - 15
4	Cd	1 - 5
5	Ni	1 - 5
6	Pb	1 - 5
7	Zn	1 - 5

Samples were taken at regular intervals during the experiments for analysis of mixed liquor volatile suspended solids (MLVSS), chemical oxygen demand (COD), pH, metal concentration, volatile fatty acid (VFA), sulfate and dissolve sulfide contents. All these batch experiments were conducted in triplicate and results reported are average of triplicate sample analysis. Among the biomass collected from different sources, it was found that the biomass obtained from An-RBC reactor was very efficient in terms of metal removal and sulfate reduction. Hence, metal sulfide precipitates obtained using this biomass type were subsequently used for recovering the metals present. The following equation was used to evaluate the metal recovery efficiency:

$$\text{Metal recovery efficiency (\%)} = \frac{M_b}{M_{total}} \times 100 \qquad (3.4)$$

Where M_b is metal (mg) recovered in the form of precipitates and M_{total} is the total metal (mg) added prior to the experiment.

3.2.3 Metal nanoparticle characterization

To verify potential application of metal nanopowders obtained in this study, its composition analysis and detailed characterization were carried out using techniques such as Fourier-transform infrared spectroscopy (FTIR), field emission scanning electron microscopes-energy dispersive X-ray (FESEM-EDX), field emission transmission electron microscopy (FETEM) and rotating anode X-ray diffractometer (XRD).

For FTIR analysis, control biomass and metal loaded biomass were centrifuged at 10,000 rpm for 10 min followed by washing of pellet obtained with distilled water. The samples were finally dried under vacuum for FTIR analysis (IR affinity-1S, Shimadzu, Japan). Samples treated similar to that for the FTIR analysis were used for FESEM-EDX (Zeiss, Sigma, Germany) analysis to check the morphology of the metal precipitates. In order to check the internal structure and morphology of the metal precipitates by FETEM analysis, control and metal loaded biomass was centrifuged thrice at 5,600×g for 10 min each followed by washing with distilled water after every run. The final pellet obtained was placed on copper grid and analyzed using EDS integrated FETEM (JOEL, JEM2100, Japan). Structural characterization of the samples were carried out by drying the sample at 120 °C and then grinding it to a powdered form, followed by analysis using a rotating anode based powder X-ray diffractometer (XRD) (Rigaku TTRAX III, 18 kW) with Cu K_α radiation ($\lambda = 0.1542$ nm).

3.2.4 Analytical methods

Biomass was estimated as mixed liquor volatile suspended solids (MLVSS) as per the method defined in the American Public Health Association (APHA, 2005). Sulfate concentration was determined using the standard barium chloride based turbidimetric method (APHA, 2005),

whereas COD in the samples was determined by the closed reflux method (APHA, 2005). Sulfide was measured based on a method described by Cord-Ruwisch (1985). Acetate was measured by high pressure liquid chromatography (Biorad, Shimadzu) after sample filtration through 0.45 µm nitrocellulose filter (Millipore). The HPLC was fitted with aminex hpx 87 h column and the mobile phase was 5 mmol H_2SO_4 at 0.6 mL/min flow rate.

Metal concentration in the samples was determined by atomic absorption spectroscopy (Varian, AA240, Netherlands) as per the APHA (2005) after passing the sample through 0.45 µm nitrocellulose filter (Millipore). To determine the metal recovery percentage in this study, the metal precipitates were first collected by withdrawing the liquid above and then the precipitates were acidified using 20% HNO_3 to ensure complete dissolution of the metal precipitates. The soluble metals were determined as mentioned earlier. All chemicals used in this study were of analytical grade (AR).

3.3 Results and discussion

3.3.1 Heavy metal removal

Fig. 3.1 shows the metal removal efficiency obtained using the three anaerobic biomass types at different low and high initial metal concentration. At a low initial metal concentration, more than 95% metal removal efficiency was achieved for all the metals, except with iron (90%), using the anaerobic biomass from An-RBC. Similar results were obtained using the anaerobic biomass obtained from UASBR after 120 h of incubation. The metal removal efficiency was less than 80% in case of WWTP biomass for all the metals.

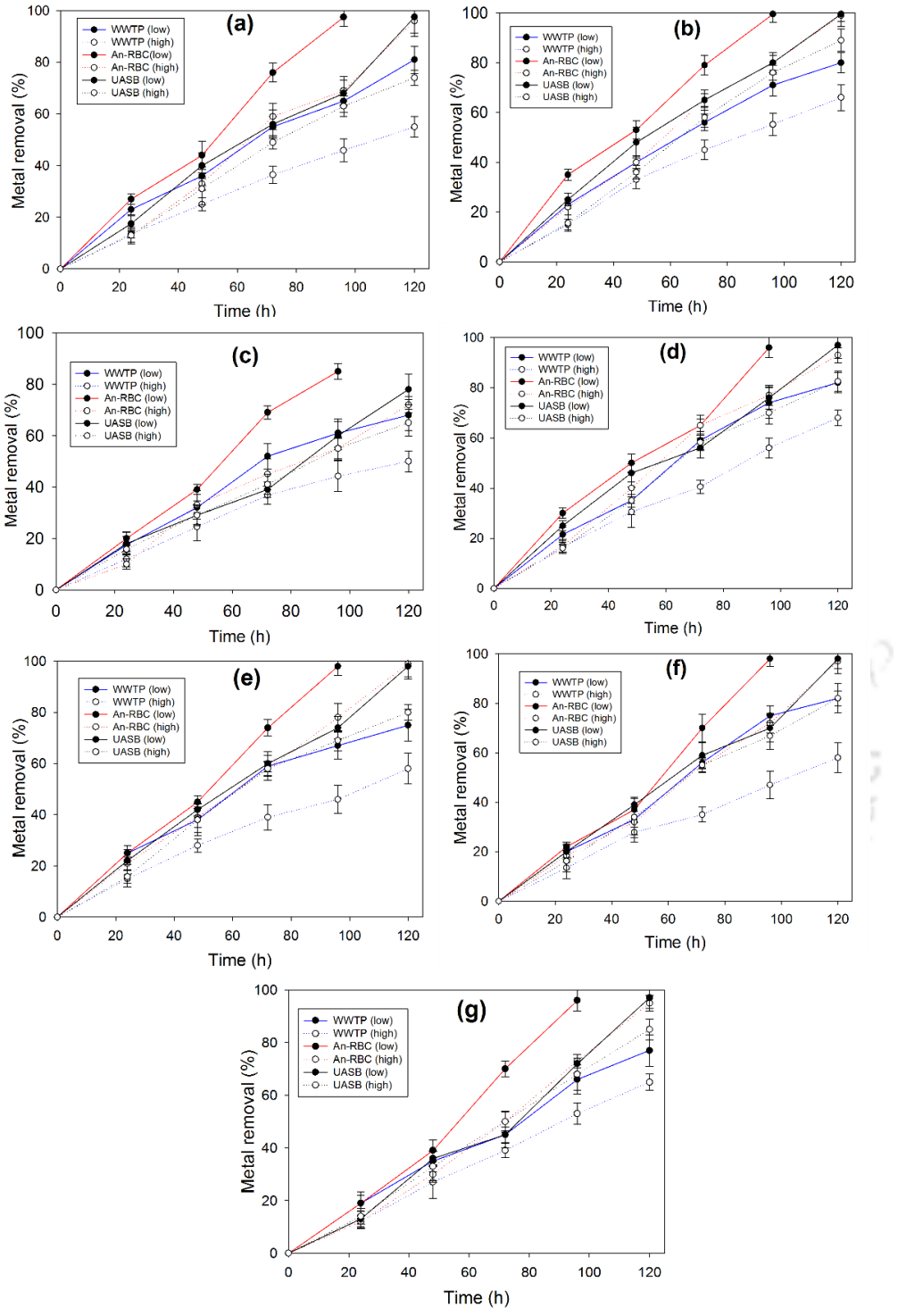

Fig. 3.1 Metal removal profile by anaerobic biomass from different sources at low (solid lines) and high (dotted lines) initial concentration of different metals (a) Cd, (b) Cu, (c) Fe, (d) Mn, (e) Ni, (f) Pb, (g) Zn.

These removal values were, however, lower at a high metal concentration for all the biomass types (Fig. 3.1). More than 92% metal removal efficiency was achieved for all the metals using An-RBC biomass, but in case of iron the value was slightly low (88%). UASBR biomass resulted in 80% removal with all the metals, except with cadmium and iron, in which case it was 75% and 69%, respectively. More than 60% removal of copper, manganese, lead and zinc was achieved using WWTP biomass, whereas the removal of cadmium, nickel and iron was only 55, 58 and 50%, respectively.

3.3.2 COD and sulfate removal

The results of sulfate reduction and COD removal by anaerobic biomass in the presence of different metals at a low initial concentration are depicted in Figs. 3.2 and 3.3, respectively. An-RBC and UASBR showed very high sulfate reduction efficiency (91% and 85%, respectively) with all the heavy metals, except with iron. On the other hand, sulfate reduction was low (55%) with WWTP biomass. However, at a high initial metal concentration, the sulfate removal efficiency reduced to 80%, 68% and 46% with An-RBC, UASBR and WWTP biomass, respectively (Fig. 3.2).

Fig. 3.3 depicts the COD removal in the presence of different metals at low and high initial metal concertations. At a low initial metal concentration, COD removal of more than 80% was achieved for all the metals using the An-RBC reactor biomass. Using the biomass from UASB reactor and WWTP, the COD removal was more than 70% at low concentrations of the metals, except for lead and cadmium and, the value for these two metals was slightly less than 70%. But, at a high initial metal concentration, the COD removal efficiencies slightly decreased (70%, 65% and 54% for An-RBC, WWTP and UASBR biomass, respectively) (Fig. 3.3).

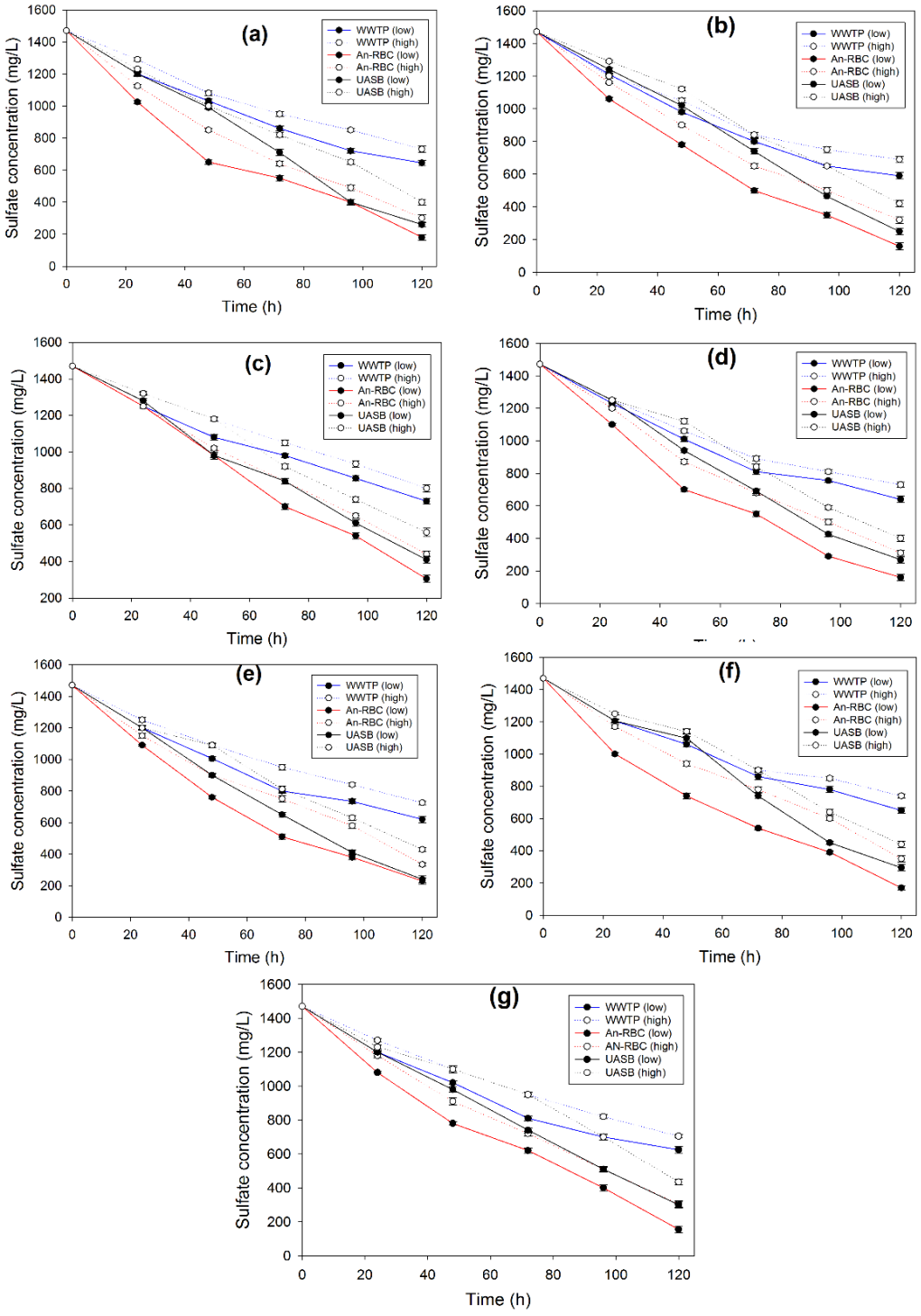

Fig. 3.2 Sulfate reduction profile by anaerobic biomass from different sources at low (solid lines) and high (dotted lines) initial concentration of different metals (a) Cd, (b) Cu, (c) Fe, (d) Mn, (e) Ni, (f) Pb, (g) Zn.

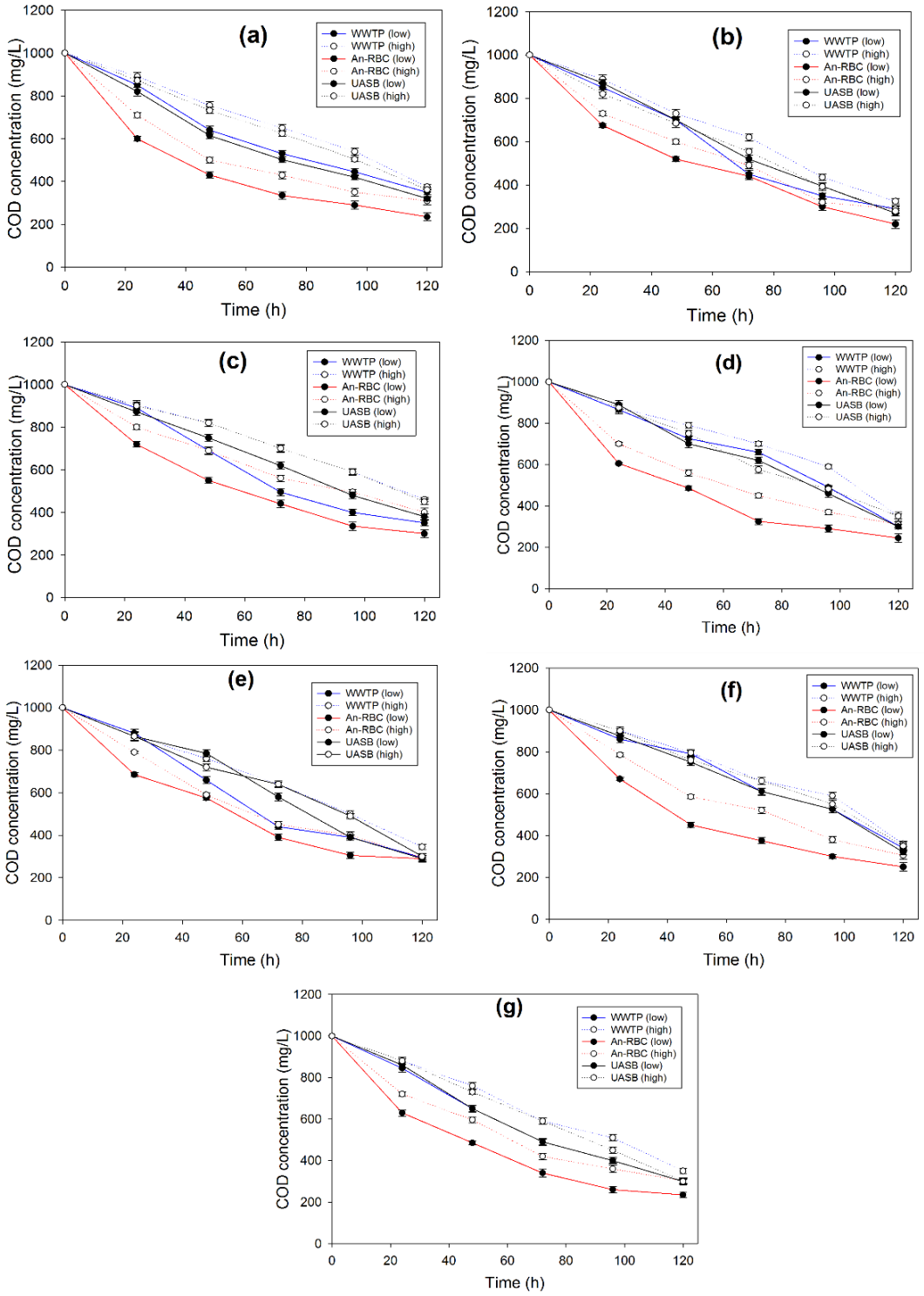

Fig. 3.3 COD removal profile by anaerobic biomass from different sources at low (solid lines) and high (dotted lines) initial concentration of different metals (a) Cd, (b) Cu, (c) Fe, (d) Mn, (e) Ni, (f) Pb, (g) Zn.

3.3.3 Heavy metal recovery

Metal removal efficiency using the An-RBC reactor biomass was almost 90% for all the metals tested, and, the metal precipitates obtained were further examined to recover the metals. The metal recovery percentage was calculated for low inlet metal concentration. It could be seen that the metal recovery from the precipitates was nearly 70% in the case of Cu and Pb. The value was slightly low in the case of the other metals. Fig. 3.4 shows the recovery efficiency of the different metals removed by sulfide precipitation using biomass collected from An-RBC reactor.

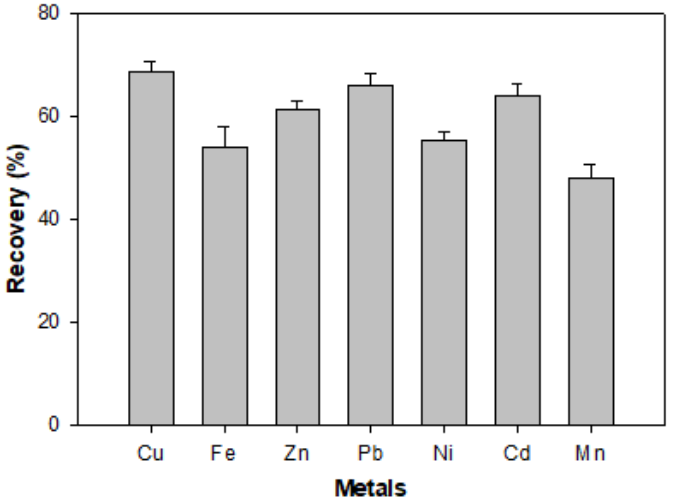

Fig. 3.4 Metal recovery percentage for different metals from bioprecipitates obtained using the An-RBC reactor biomass.

3.3.4 Sulfide and VFA production

Fig. 3.5 shows the dissolved sulfide concentration produced at the end of the experiments carried out in the presence of the different metals. At low metal concentration, a very high amount of 39.5 mg/L dissolved sulfide was produced in the presence of copper, but at a high initial metal concentration, the dissolved sulfide concentration was low (35.20 mg/L for copper). The high

amount of sulfide produced correlates well with the results of sulfate removal efficiency obtained in this study.

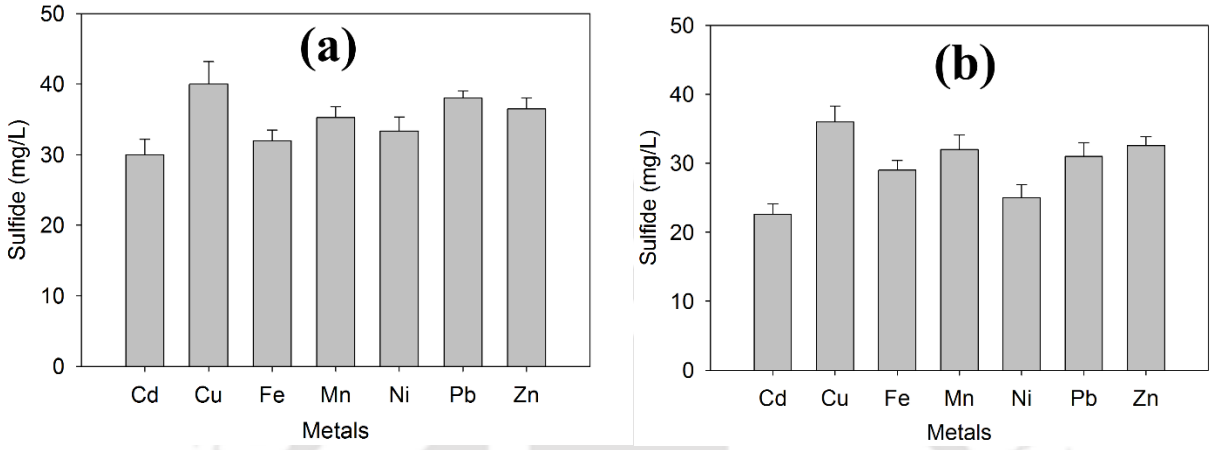

Fig. 3.5 Changes in sulfide concentration at (a) low and (b) high initial metal concentration.

Fig. 3.6 shows the concentration of volatile fatty acids (VFA) produced in the presence of different metals at low and high initial concentration.

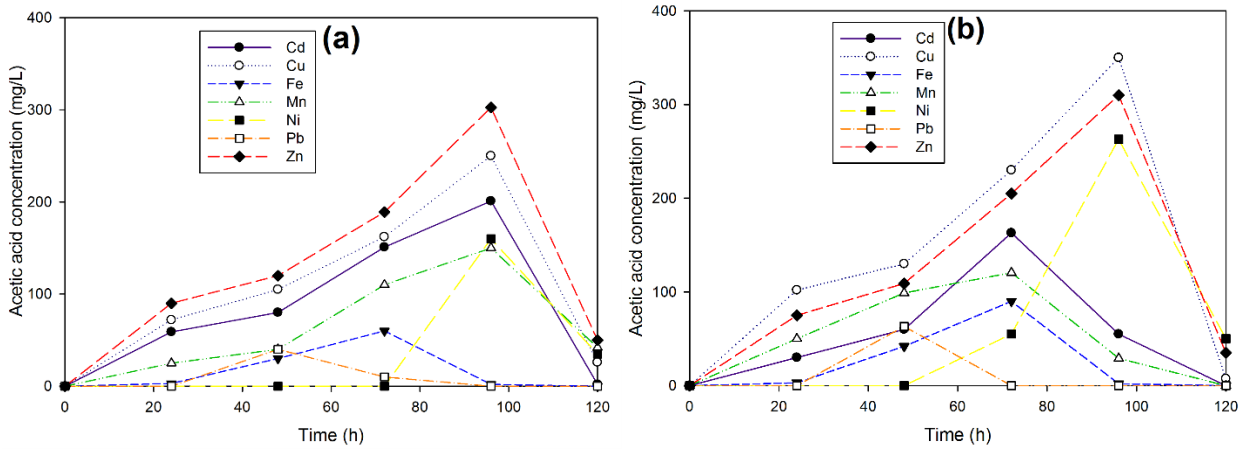

Fig. 3.6 Acetic acid production at (a) low and (b) high initial metal concentration.

At a low initial metal concentration, the maximum VFA produced as acetic acid was 302 mg/L with zinc as the heavy metal and the value was closely followed by that due to copper (250 mg/L),

cadmium (201.45 mg/L) and nickel (160.2 mg/L). However, with iron a very less amount (60 mg/L) of VFA was produced. At a high initial metal concentration, a maximum VFA production of 350 mg/L obtained in the case of copper, followed by that with zinc (310.5 mg/L) and nickel (215 mg/L).

3.3.5 Characterization of metal bioprecipitates

Metal bioprecipitates obtained using the An-RBC biomass, which yielded a maximum sulfate and metal removal efficiency, were further characterized by using different techniques. Fig. 3.7 shows FTIR spectra of the metal precipitates in the range 500 - 4000 cm^{-1} wave number, which reveals the different functional groups responsible for metal removal by sulfide precipitation. The broad band centered at 1100 cm^{-1} shows the presence of sulfate (Feio Maria et al., 2004; Kiran et al., 2015). A broad and deep band present in the range 3000 - 3700 cm^{-1} shows the presence of the hydroxyl group (-OH). Band stretching from 1600 to 1700 shows the presence of C=O carboxyl group. The band stretching from 1500 to 1580 cm^{-1} indicates the presence of the amide group (–NH) in the precipitate (Hongen et al., 2013; Kiran et al., 2018).

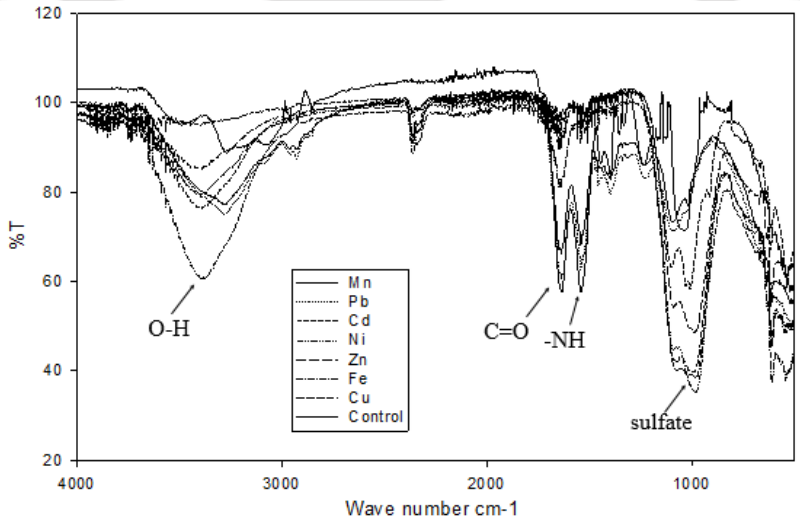

Fig. 3.7 FTIR spectra of An-RBC biomass with different heavy metals.

Fig. 3.8 shows FETEM images of the different metal nanoparticles obtained by using the An-RBC biomass, which shows a polycrystalline nature of these nanoparticles. The nanoparticles were of different size and shape depending on the heavy metals present.

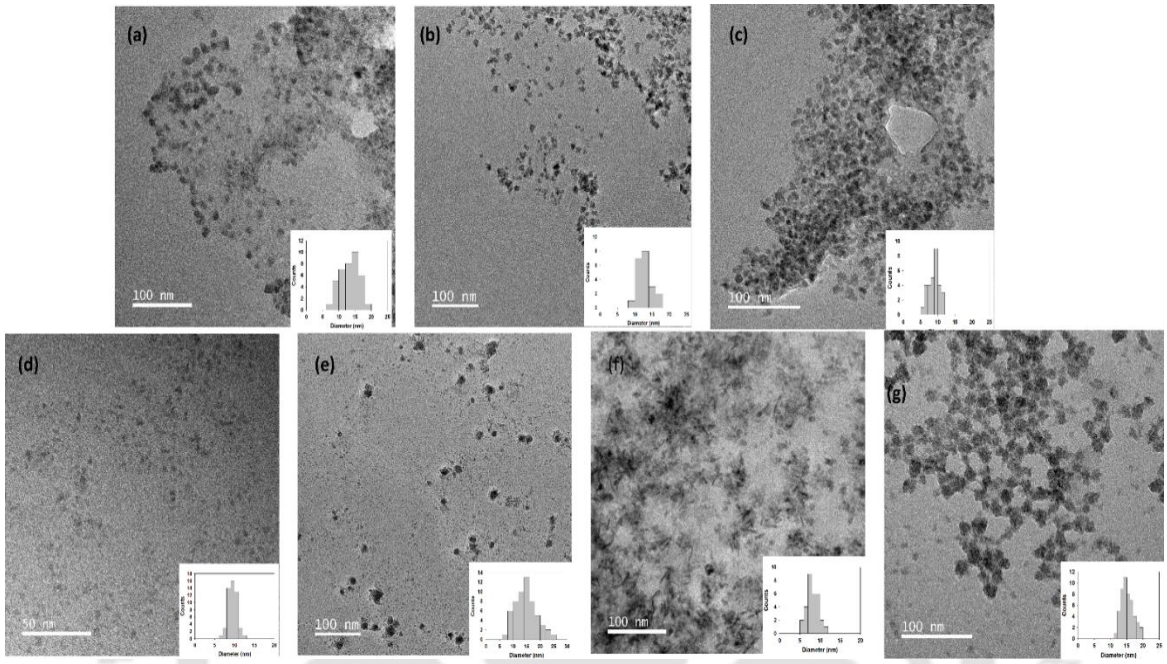

Fig. 3.8 FETEM images of the different metal bioprecipitates obtained in the study (a) cadmium, (b) copper, (c) iron, (d) manganese, (e) nickel, (f) lead, and (g) zinc. Particle size distribution is shown as insert to these figures.

Particle size distribution of the different nanoparticles revealed that CdS and CuS nanoparticles were 12-14 nm diameter; in the case of NiS and ZnS nanoparticles, their size was 15-17 nm, whereas for MnS it was in the range 9-11 nm. Similarly, the size of FeS and PbS nanoparticles was in the range 8-10 nm (Fig. 3.8).

Elemental composition and morphology of the metal bioprecipitates were further analyzed by using FESEM-EDX. The results shown in Fig. 3.9 revealed the presence of individual metals and sulfide, signifying that the nanoparticles were formed due to the formation of metal sulfides. All

these images also showed small peaks due to carbon, iron, oxygen, sodium, etc., which were present in the form of nutrients in the Postgate medium.

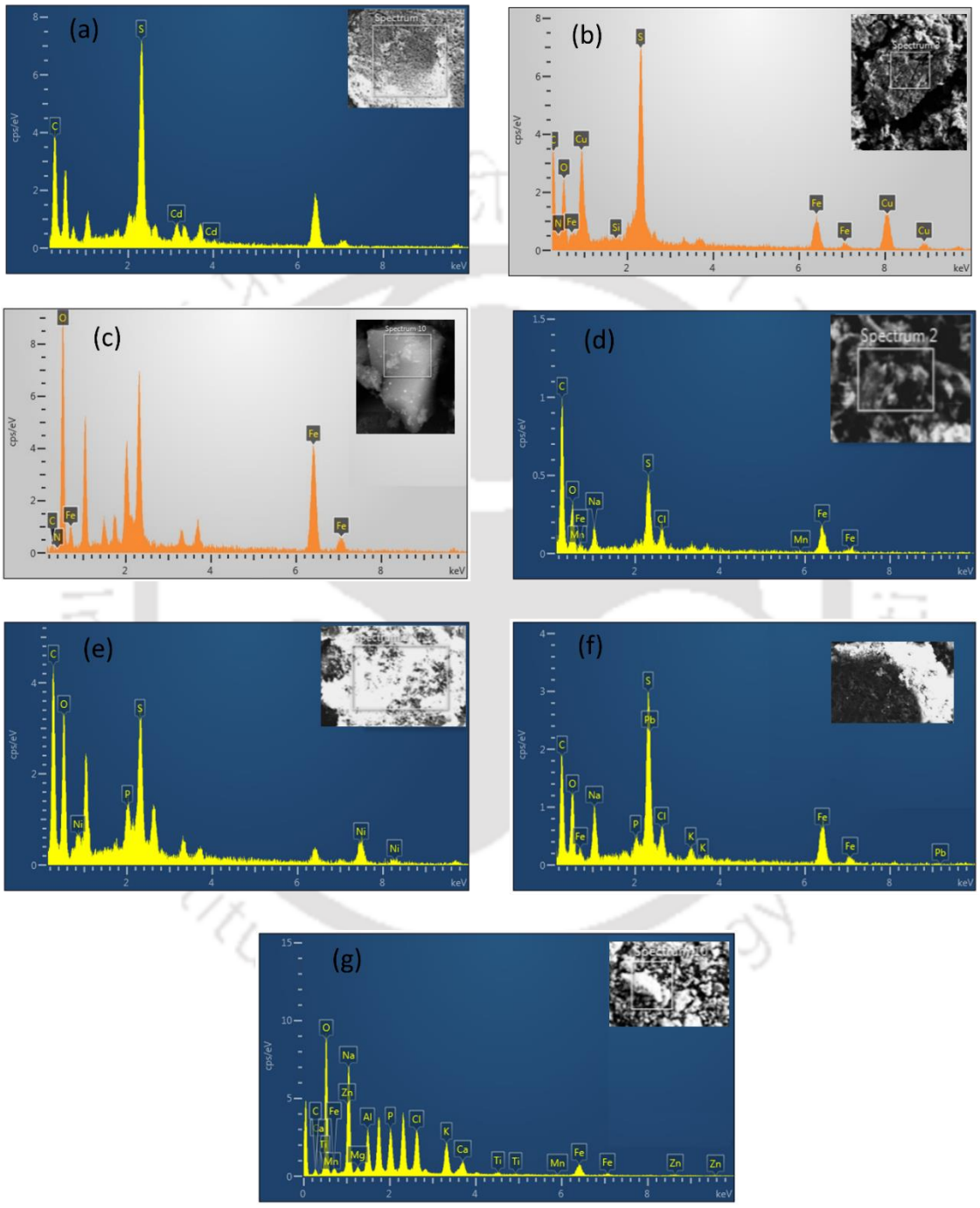

Fig. 3.9 EDX of the different metal bioprecipitates obtained in this study: (a) cadmium, (b) copper, (c) iron, (d) manganese, (e) nickel, (f) lead, and (g) zinc.

Structure and crystallographic orientation of the metal sulfide precipitates were determined from their XRD spectra obtained in the range of 10°-70° of diffraction angle (2θ) which are shown in Fig. 3.10. For CdS NPs, the peaks observed in the XRD spectra at the diffraction angles of 26.6°, 28.3°, 36.8°, 43.9°, 48.1°, 54.9°, 67.1° and 75.9° closely match with the (002), (101), (102), (110), (103), (004), (203) and (105) planes confirming the polycrystalline nature of the hexagonal structure of CdS in the reference pattern of ICDD PDF 80-0006 (Soltani et al., 2012). The spectrum for CuS NPs shows diffraction peaks at 2θ values of 26°, 31.75°, 45.46°, and 55.4° which correspond to the diffraction lines formed by (111), (200), (220) and (311) planes of the face-centered cubic structure of CuS (JCPDS card No. 5-0592). This result confirms the polycrystalline nature of the CuS nanoparticle and is in accordance with that reported in the literature by Nezamifar et al. (2015).

The diffraction peaks for FeS appear at 2θ values of approximately 29°, 33.20° and 35.6º corresponding to (311), (200), (400) planes attributed to hexagonal FeS (JCPDS: 65-9124). This result as well confirmed the polycrystalline nature of the FeS NPs (Akhtar et al., 2013). The spectrum for MnS shows diffraction peaks at 2θ values of 27°, 38.6°, 45.4°, and 55.33° which correspond to the diffraction lines formed by (100), (102), (110) and (112) planes of the face-centered cubic structure of MnS (JCPDS card No. 40-1289). This result confirms the polycrystalline nature of the MnS NPs as reported by Dhandayuthapani et al. (2017).

The diffraction peaks for NiS appear at 2θ values of approximately 19.6°, 26.1°, 32°, 33.1, 38.9°, and 50.11ºcorresponding to (200), (221), (300), (041), (241), (410) planes, match well with orthorhombic geometry of NiS NPs (JCPDS card No. 22-1193). The diffraction pattern reveals that the NiS NPs formed were polycrystalline in nature (Shajudheen et al., 2016).The diffraction peaks for PbS appear at 2θ values of 25.85°, 29.8°, 41°, 50.48°, 53.36° and 70.74° corresponding

to (111), (200), (220), (311), (222) and (420) planes which matched well with cubic form of PbS NPs nanoparticles (JCPDS card No. 78-1901) (Lee et al., 2015). Fig. 3.10(g) shows the diffraction peaks observed at 2θ values of 28.50°, 33.12°, 47.45°, 56.30°, 69.41° and 76.70° corresponding to (111), (200), (220), (311), (400) and (331) crystalline planes well-matched with face centered cubic structure of ZnS (ICDD PDF 65-1691) (Soltani at al., 2012; Ye et al., 2017).

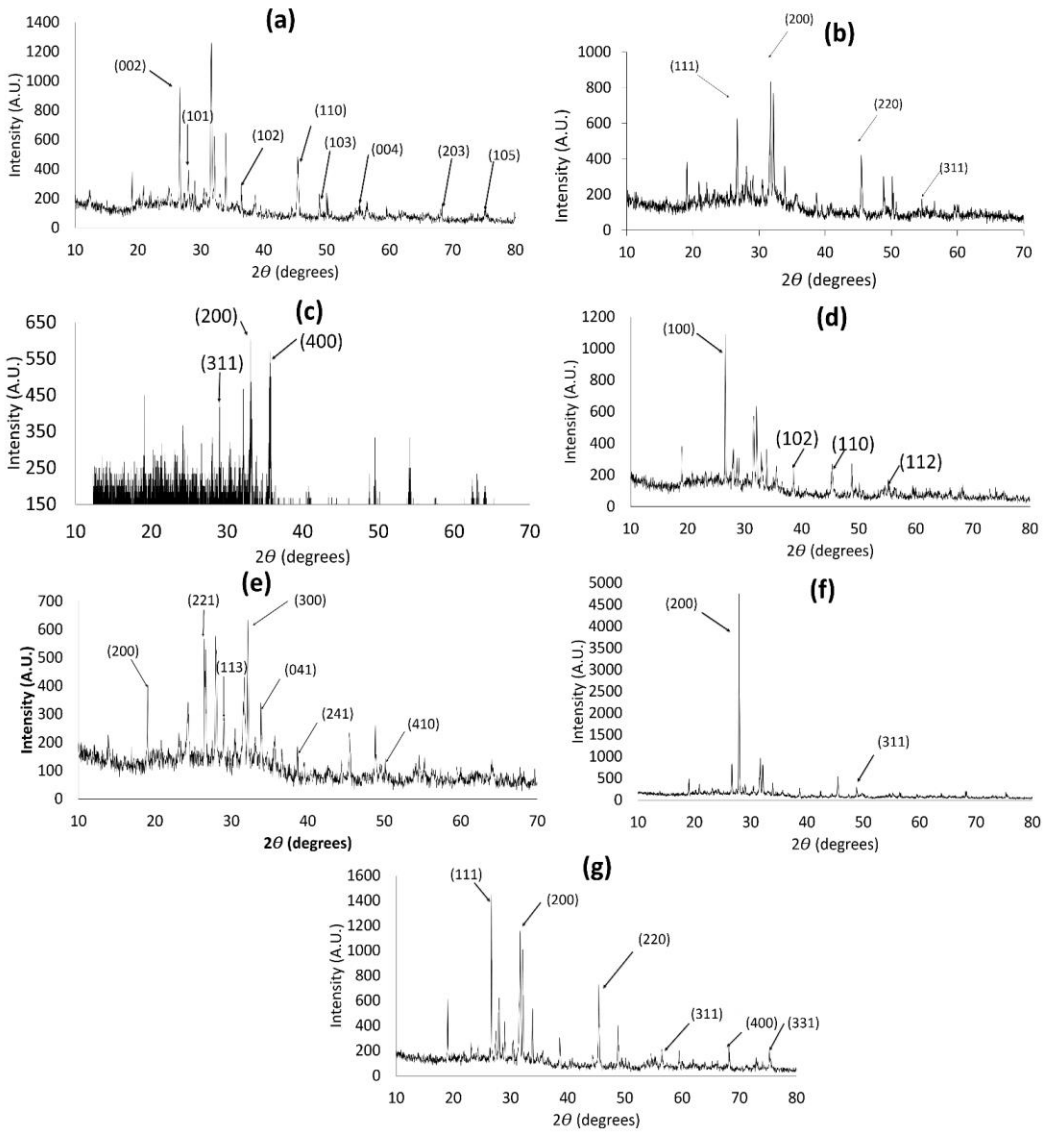

Fig. 3.10 XRD pattern of the different metal bioprecipitates obtained in this study (a) cadmium, (b) copper, (c) iron, (d) manganese, (e) nickel, (f) lead, and (g) zinc.

3.3.6 Mechanism of sulfate reduction and heavy metal removal

Anaerobic biomass samples from three different sources were screened based on their metal removal, sulfate reduction, and COD removal, and the results showed that all the three biomass were capable of heavy metal removal by sulfate reduction. These results correlate well with the solubility product values of the respective metal sulfides.

Heavy metal removal at a low initial concentration was better than at a high initial metal concentration due to metal inhibition on the biomass activity. Among the three biomass sources, the biomass obtained from An-RBC reactor showed the best result in terms of heavy metal removal as it was previously acclimatized to treat heavy metal containing wastewater (Kiran et al., 2017). Even at a low initial metal concentration (1-5 mg/L), the metals could not be completely removed (100%) from solution. One probable reason could be the formation of small particles (<0.45 µm) known as fines or hydrated colloidal particles, which do not settle at the bottom and remain suspended. These fines and colloidal particles can contribute to the residual metals in the effluent (Villa-Gomez et al., 2011).

The differences in COD and sulfate removal values due to an increase in the initial metal concentration could be explained based on metal to sulfide (M/S^{2-}) ratio as reported by Mothe et al. (2015). At a low initial metal concentration and a fixed concentration of sulfate, the sulfide produced by SRB is sufficient such that the M/S^{2-} is low (less than 1) for precipitating the metals, thereby avoiding any toxic effect on SRB. On the other hand, at a high initial metal concentration, the M/S^{2-} is high (more than 1) with a high residual metal concentration in solution that may be inhibitory to SRB for achieving a high efficiency of COD or sulfate removal.

The unutilized COD observed at the end of the experiment (Fig. 3.3) is mainly due to the incomplete metabolism of lactate and production of organic byproducts (e.g., acetate and bicarbonate) by SRB which correlate well with the results of VFA production shown in Fig. 3.6. A similar observation on acetate production was made by Luptakova et al. (2015) for treating AMD using SRB with lactate as the sole carbon source. Gallegos-Garcia et al. (2008) observed acetate accumulation while treating heavy metal (Fe, Zn, and Cd) containing wastewater using sulfidogenic down-flow fluidized bed reactor (DFFBR). Similarly, Nagpal et al. (2000) reported acetate accumulation using ethanol as the sole carbon source in a fluidized bed reactor for treating wastewater. However, no acetate consumers were found to be present in the biomass.

Biochemical reaction carried out by *Desulfovibrio* species as the predominant SRB present in the An-RBC reactor biomass can be written as follows (Kiran et al., 2018):

$$\text{Lactate} + \frac{1}{2}SO_4^{2-} \rightarrow \text{Acetate} + HCO_3^- + \frac{1}{2}HS^- + H^+ \qquad (3.5)$$

It is often observed that acetate produced as a byproduct of lactate metabolism serves as a secondary carbon source for sulfate reduction by SRB (Zhou et al., 2011). Some SRB such as *Desulfotomaculum* species utilize acetate as the sole carbon source for sulfate reduction, which can be represented by the following reaction (Liamleam et al., 2007; Sousa et al., 2018):

$$\text{Acetate} + SO_4^{2-} \rightarrow 2HCO_3^- + HS^- \qquad (3.6)$$

In this study, acetate was utilized by the biomass for sulfate reduction (Fig. 3.6), suggesting it to be a secondary carbon source for the SRB present in the biomass. Yildiz et al. (2019) used acetate as the sole carbon source for AMD treatment using a laboratory-scale anaerobic up-flow reactor, and observed that in the absence of a primary carbon substrate, acetate serves as a very good substrate for sulfate reduction in the bioreactor system.

In order to verify acetate conversion to bicarbonate in this study, the wastewater pH was monitored during the experiments (Fig. 3.11).

The pH of the metal containing synthetic media was 7.0, which dropped up to 6.5 within the first 24 h (Fig. 3.12). During the later period, the pH gradually increased due to the formation of bicarbonate ions as represented by Eq. (3.5), i.e., one mole each of acetate and bicarbonate were formed as a result of incomplete oxidation of lactate. The pH of the medium further increased when the acetate produced was converted to 2 moles of bicarbonate by SRB present in the biomass (see Eq. (3.6)). Finally, after five days of incubation, the media pH stabilized at different values for the metals tested in this study. In case of zinc and copper, the media pH reached up to a maximum value of 7.0, whereas with the other metals the final pH was slightly low but the value was near neutral (Fig. 3.11).

These results of stabilization of pH of the wastewater thus suggest potential application of this technique for treating acidic wastewater such as AMD. Besides, the alkalinity produced due to lactate/acetate metabolism by the SRB present in the biomass may contribute to the heavy metal removal (Goncalves et al., 2007; Neculita et al., 2007). However, heavy metal removal in this study was primarily due to sulfide precipitation, and other mechanisms seem to play only a minor role during the removal process (Radhika et al., 2006). FTIR spectra of metal precipitate revealed the presence of sulfate species, which further confirms the role of biological metal sulfide precipitation for removing the metals from solution (Feio Maria et al., 2004; Kiran et al., 2015).

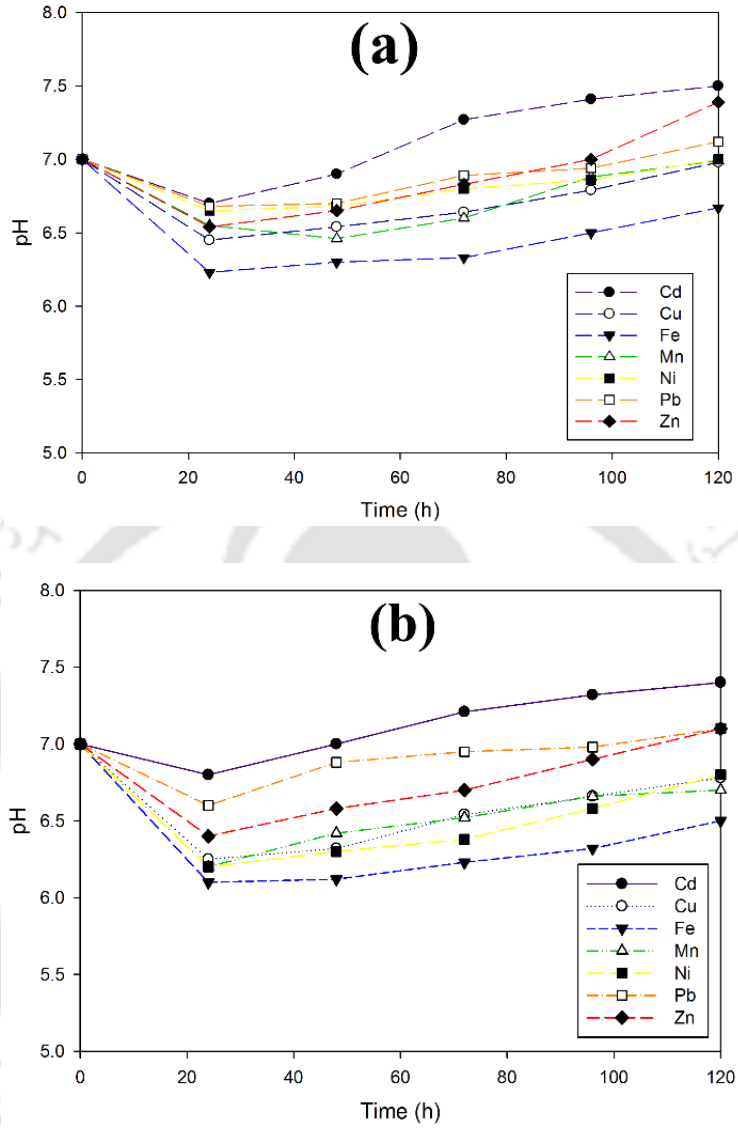

Fig. 3.11 Change in pH at (a) low and (b) high initial metal concentration.

3.3.7 Mechanism of metal recovery as nanopowders

FETEM images (Fig. 3.12a) showed the presence of curved rods and cylindrical shaped bacteria, which was typical of *Desulfovibrio sp.* morphology in the anaerobic biomass. FETEM images also showed that the shape and size of the metal sulfide nanoparticles formed varied depending upon the heavy metals. The nanoparticle formation was mainly extracellular as the metal nanoparticles

were found both freely suspended in the media as well as on the cell wall of the bacteria. The FETEM images further revealed a polymeric layer around the bacterial cell wall that contributed to the exopolysaccharides (EPS) (Fig. 3.12) (Kiran et al., 2015).

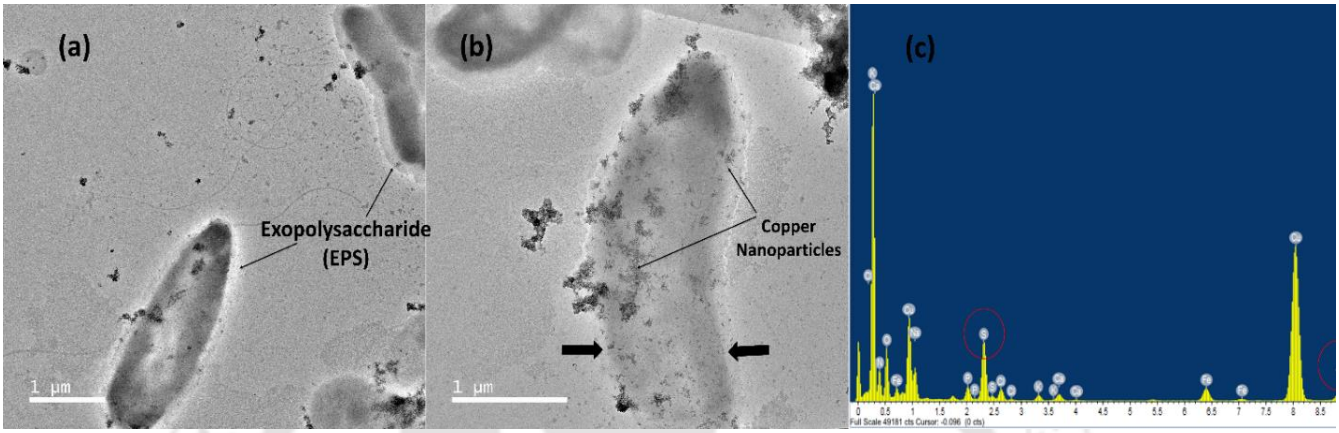

Fig. 3.12 TEM images of SRB present in An-RBC biomass loaded with copper: (a) bacterial EPS layer on the cell surface; (b) bacterial cell with CuS NPs deposited on its surface and (c) EDS spectrum of a spot on the bacterial cell wall indicated by the arrows.

EPS is generally secreted by such bacteria in order to avoid toxicity due to heavy metals and other compounds (Gupta el al., 2017), and it mainly contains proteins, carbohydrates and enzymes (Sardar et al., 2018). These compounds also help heavy metal sequestration on the bacterial cell surface. Metal ions which are freely suspended in the media bind with compound containing anionic groups present in the EPS present, around the cell wall of the bacteria. Vijayaraghavan et al. (2008) proposed a two-step mechanism for bacterial mediated metal sulfide nanoparticles formation: (1) binding of metal ions with the active anionic groups present on the cell wall (2) such bound metal ions serve as nucleation site for more ions to get deposited. Hence, bacterial cell wall serves as a nucleation site for metal deposition and metal sulfide formation. SRBs use lactate for sulfate reduction and produce sulfide which binds with metals present outside the bacterial cell

and forms metal sulfide nanoparticles. In this study, the formation of these metal sulfide on the outer surface of the bacterial cell wall was confirmed by the EDS peaks (Fig. 3.12c).

Moreover, the presence of individual metal and sulfide peaks in the EDX spectra and XRD patterns of the bioprecipitates confirmed the presence of metal sulfide in the bioprecipitates (Fig. 3.9, 3.10). Based on the results, a schematic of the detailed mechanism involved in metal sulfide nanoparticle formation by SRB is depicted in Fig. 3.13.

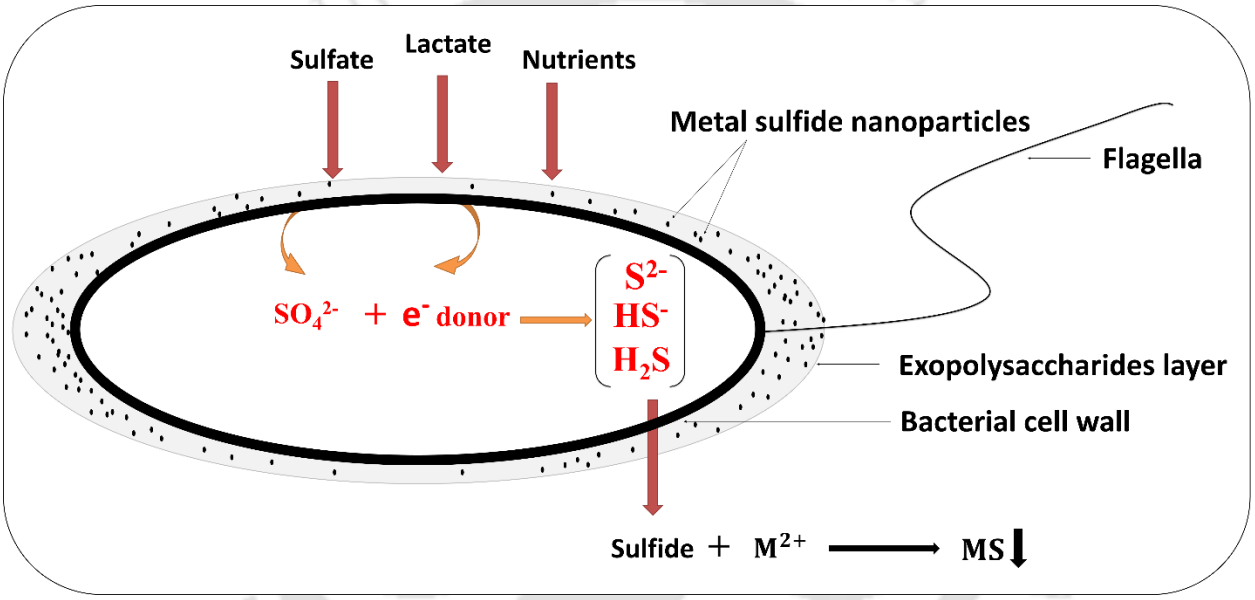

Fig. 3.13 Mechanism of metal sulfide nanoparticle formation.

3.4 Significant findings

This study demonstrated successful removal and recovery of different heavy metals in the form of nanopowders from simulated wastewater by anaerobic biomass containing SRB. The major mechanism of metal sulfide formation involved the binding of metals to sulfide produced outside bacterial cell surface due to sulfate reduction by the bacteria. The metal bioprecipitates formed external to the bacterial cell surface were thus easily recovered for reuse application. However, a

high initial metal concentration was detrimental to its own removal due to its inhibitory effect on the biomass. Detailed characterization of the recovered nanopowders indicates its potential use in the environment sector.

Chapter 4

Performance evaluation of sulfidogenic inverse fluidized bed reactor system for removal and recovery of heavy metal

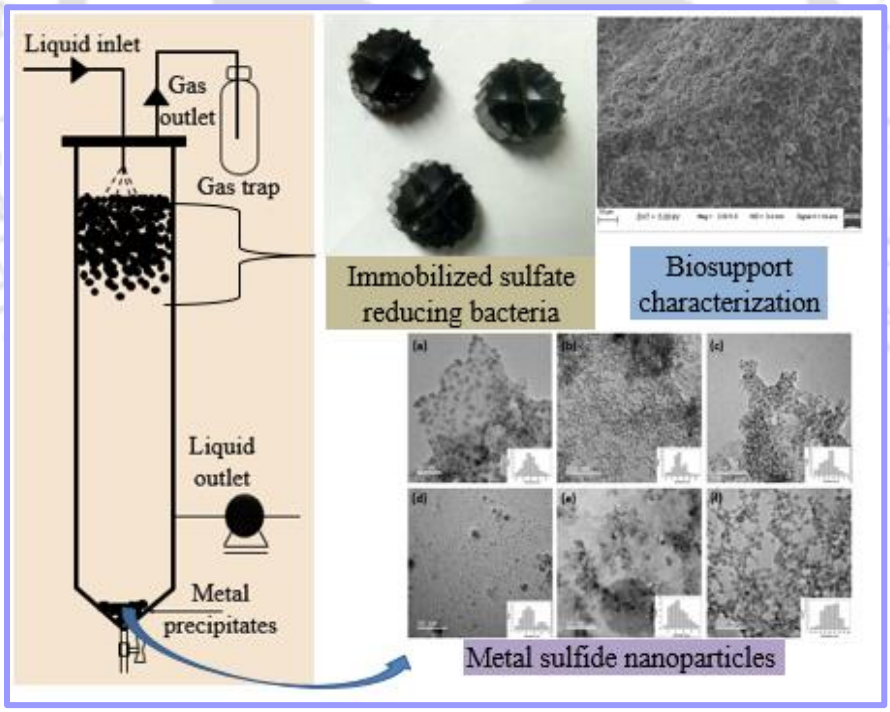

ABSTRACT

Acid mine drainage (AMD) is a serious environmental hazard in many countries with historic or ongoing mining industries. Biological sulfide precipitation is an emerging technique for both removal and recovery of heavy metals from such wastewater. This study demonstrated heavy metal removal and recovery from synthetic wastewater containing Cd^{2+}, $Cu^{2+,}$ Fe^{3+}, Ni^{2+}, Pb^{2+} and Zn^{2+} using two continuously operated sulfidogenic anaerobic inverse fluidized bed reactors (referred as R1 and R2) supplied with an influent pH of 7.0 and 3.0, respectively. In case of R1, more than 95% metal removal efficiency was achieved for all the metals except for Fe^{3+} (90%) and Ni^{2+} (85%), and in case of R2 the removal was more than 90% for all the metals except with Fe^{3+} (88%) and Ni^{2+} (82%). The metals were subsequently recovered in the form of metal nanopowder from the reactor bottom and equalizer, and the metal recovery was in the order: Cu > Pb > Cd > Zn > Ni > Fe. However R1 yielded a good recovery percentage (50-65%) of the metals in comparison with the reactor supplied with influent pH 3.0 (46-55%). Metal sulfides were recovered from the conical bottom and equalizer of the IFB bioreactor. The presence of immobilized sulfate reducing bacteria onto the support material in the bioreactors were identified using field emission scanning electron microscopy. The size and shape of the biometal nanoparticles were confirmed using field emission transmission electron microscopy, which revealed an excellent potential for industrial application. This paper demonstrates successful recovery of metal sulfides in the form of nanoparticles using IFBR.

4.1 Introduction

Metal containing wastewater from industries such as mining, metallurgy, electroplating, alloy manufacturing, etc. is characterized by low pH and high concentrations of sulfate and heavy metals (Reddy et al., 2010; Kiran et al., 2018). Besides, chemical oxygen demand (COD) concentration varies from few to 100 mg/L in such wastewaters (Sarti and Zaiat et al., 2011; Bai et al., 2013). Heavy metals, including copper (Cu^{2+}), iron (Fe^{3+}), zinc (Zn^{2+}), nickel (Ni^{2+}), lead (Pb^{2+}), and cadmium (Cd^{2+}), found in such wastewaters are toxic and pose several adverse health effects even at a low concentration (Oyekanmi et al., 2017; Adeleke et al., 2017; Oyekanmi et al., 2019). On the other hand, these heavy metals need to be recovered for industrial reuse applications (Kiran et al., 2018). Therefore, the treatment of heavy metal containing wastewater is mandatory prior to its release into the environment.

Biological heavy metal removal by bioprecipitation using sulfate reducing bacteria is gaining importance over conventional chemical neutralization and hydroxide precipitation methods, and this is attributed to the many drawbacks of chemical precipitation such as: (1) production of bulky sludge, (2) metal recovery is difficult and (3) high cost of chemical reagents (Villa-Gomez et al., 2011). In this context, biological sulfide precipitation proves useful for metal recovery in addition to metal removal. In this process, sulfate reducing bacteria (SRB) utilize organic matter or electron donor to reduce sulfate to sulfide, which combines with metals and forms highly insoluble metal sulfide precipitate, thereby facilitating the recovery of metals in the form of nanobioprecipitate (Kiran et al., 2017).

Different reactor configurations have been studied for biological metal sulfide precipitation, which include anaerobic filter (Jong and Parry et al., 2003), up-flow anaerobic sludge bed reactor (Kaksonen et al., 2003), expanded granular sludge bed reactor (Sierra-Alvarez et al., 2007), and

fluidized bed reactor (Kaksonen et al., 2003). However, these reactors are well known for sulfate and metal removal but fail in terms of metal recovery. Compared with these reactor configurations, the inverse fluidized bed reactor (IFBR) is an excellent alternative not only for metal precipitation but also for metal recovery. Compared with other conventional sulfidogenic reactor systems, the IFBR is based on floatable carrier materials, which are fluidized downwards due to liquid recirculation from the top. Following inoculation of the reactor with SRB, biofilm develops over the support materials. In contrast, metal sulfide formed due to the SRB activity gets precipitated at the bottom of the reactor, thus facilitating the easy recovery of the metal sulfide (Gallegos-Garcia et al., 2009).

The IFBR has been used for removal and recovery of heavy metals such as Cu^{2+}, Pb^{2+}, Zn^{2+} and Cd^{2+} but only low recovery efficiency of 40-50% has been reported thus far at pH 7.0 (Villa-Gomez et al., 2011). Hence, there is a need to intensify the process to achieve maximum recovery of metals from wastewater. This is mainly important also considering the fact that acidic wastewater such as acid mine drainage (AMD) has a low pH (Kiran et al., 2017). The low pH of the wastewater directly affects the recovery of heavy metals in adverse manner by solubilizing the metal sulfide (Zhang et al., 2018). Not only pH but also other factors, including hydraulic retention time (HRT), metal loading rate and sulfide concentration can affect metal recovery in the IFBR system (Villa-Gomez et al., 2011). Although a few studies on metal recovery using sulfidogenic reactors have been reported in the literature, the influence of certain critical process parameters, including influent with low pH, hydraulic retention time, low/high metal loading, etc. on metal recovery using reactors, in particular IFBR, have not been reported thus far. Moreover, detailed characterization of metal bioprecipitates obtained from sulfidogenic reactors treating wastewaters for potential industrial application has not been reported.

Therefore, the aim of this study was to evaluate the IFBR for metal removal and recovery from acidic wastewater using an IFBR. The effect of different hydraulic retention time (HRT) (12 h, 24 h, and 48 h) on metal removal was further evaluated. In order to gain insight into the mechanism involved in the process, biofilm was characterized through field emission scanning electron microscopy (FESEM), Metal bioprecipitates formed at the bottom of the reactor after each experimental run were characterized by FESEM-EDX and field emission transmission electron microscopy (FETEM).

4.2 Materials and methods

4.2.1 Sulfate reducing biomass

Biomass used as inoculum and as a source of SRB was acquired from a laboratory scale sulfidogenic anaerobic rotating biological contactor (An-RBC) reactor treating metallic wastewater, as previously described in Chapter 3. The attached biomass from An-RBC reactor regrown in Postgate medium (Postgate, 1984) and later used to inoculate the IFBR.

4.2.2 Synthetic wastewater composition

Composition of the synthetic wastewater used in the study was as follows (g/L): NH_4Cl (1.0), sodium citrate (0.3), KH_2PO_4 (0.5), SO_4^{2-} (1.47), yeast extract (1.0), $CaCl_2 \cdot 2H_2O$ (0.1), ethylenediaminetetraacetic acid (0.3) and $FeSO_4 \cdot 7H_2O$ (0.28) (Postgate, 1984). Sodium citrate was added in the media to prevent the precipitation of metals in solution prior to the experiments. Sodium lactate (60% v/v) was used as electron donor and the influent sulfate concentration was 1.47 g/L, and for which an equivalent amount of sodium sulfate was added at COD/SO_4^{2-} ratio of 0.67. The pH of the media was adjusted to 7.0 using NaOH and 3.0 using HCl. Individual metal stock solutions (10,000 mg/L concentration each) of Cd^{2+}, Cu^{2+}, Fe^{3+}, Ni^{2+}, Pb^{2+} and Zn^{2+} were

prepared using $Cd(NO_3)_2 \cdot 4H_2O$, $CuCl_2 \cdot 2H_2O$, $FeCl_3 \cdot 6H_2O$, $NiCl_2 \cdot 7H_2O$, $Pb(NO_3)_2$, and $ZnCl_2$, respectively. Desired concentrations of the individual metals in the experiments were achieved by adding a known volume of the respective stock solution in the media. All reagents used in this study were of analytical grade. All these experiments were conducted in triplicate, and the results were represented in the mean ± standard deviation format.

4.2.3 IFBR and start up

Two laboratory scale IFBRs (8 cm diameter, 60 cm height) (R1 and R2) with a total operational volume of 3 L each were fabricated using polymethyl methacrylate (PMMA) material. The bed expansion (30% of the reactor volume) was maintained by recirculating the liquid flow inside the reactor at 600 mL/min. The IFBR was added with 500 mL of low-density polyethylene rings of 1 cm mean diameter and 340 kg/m^3 density as the carrier support material. The IFBRs consisted of columns with conical bottom, and the gas outlet and flow distributor were mounted on the top of the reactors. The influent was pumped from the top of the reactor using a peristaltic pump connected to the influent tank, whereas one of the reactor received influent at pH 3.0, other reactor influent pH was maintained neutral (7.0) in order to compare their performances. Equalizer connected to the reactors were used to avoid overflow and keep the liquid level constant inside the reactors (Fig. 4.1).

Before operating the reactors under different process conditions, biofilm was grown on the support material using biomass obtained from An-RBC reactor, for which Postgate medium without any added metal solution was used. Nitrogen gas was purged to maintain anaerobic environment inside the reactors. During initial startup of the reactors, freshly prepared Postgate medium was supplied under semi-continuous mode every seven days for a total of 60 days. The reactors were operated at an ambient temperature in the range 25-27 °C. Following the startup phase and biofilm

formation on the support material, the IFBRs were operated under continuous mode with heavy metal containing wastewater at the influent pH 7.0 and 3.0, respectively. Samples were collected from effluent port at constant time intervals to analyze the sulfate, metal, COD and acetate concentrations.

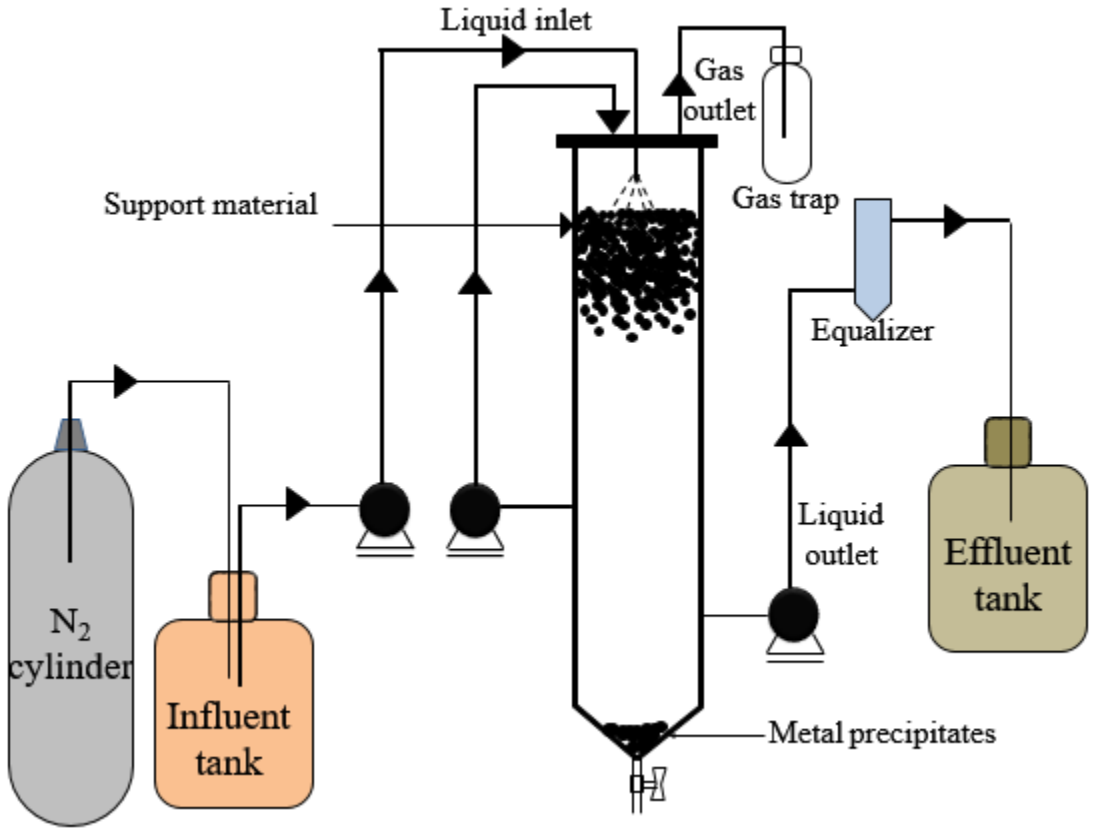

Fig. 4.1 Schematic of inverse fluidized bed reactor.

4.2.4 Effect of HRT

The effect of different HRT (48 h, 24 h and 12 h) on metal removal in the IFBRs was examined using an inlet copper concentration of 10 mg/L, influent pH of 7.0 and 3.0 and COD/SO_4^{2-} ratio of 0.67.

4.2.5 Experimental procedure for metal removal and recovery

The two reactors (R1 and R2) were operated for 150 days, respectively, at two different influent pH values keeping all other parameters constant. Whereas the R1 was operated at influent pH 7.0, R2 was operated at influent pH 3.0, both at HRT of 24 h for studying the heavy metal removal and recovery. The inlet concentration for Cd^{2+}, Ni^{2+}, Pb^{2+}, Zn^{2+} were selected as 5, and 10 mg/L and in case of Cu^{2+} it was 25 and 50 mg/L. The concentration in case of Fe^{3+} were 50 and 150 mg/L (Table 4.1).

Table 4.1 Operation time and other conditions followed for continuous metal removal and recovery using R1 and R2

Operating conditions	**Start up**	**Effect of HRT**	**Metal removal and recovery experiment**
Operation time (days)	0-60	61-90	91-150
HRT (h)	24	48, 24, 12	24
COD/sulfate ratio	0.67	0.67	0.67
Individual metal added in influent (mg/L)	No metal added	Cu^{2+} (10)	Cd^{2+} (5-10), Cu^{2+} (25-50), Fe^{3+} (50 – 150), Ni^{2+} (5-10), Pb^{2+} (5-10), Zn^{2+} (5-10)

Individual metal containing solutions of Cd^{2+}, Cu^{2+}, Fe^{3+}, Ni^{2+}, Pb^{2+} and Zn^{2+} were supplied as influent to the continuously operated IFBRs for studying the removal and recovery of these metals from the respective solutions. After completion of each metal removal experiment performed using single metal containing solution as the influent, the corresponding metal precipitate was removed

from the bottom and equalizer section of the reactors followed by washing of the reactor content inside with Postgate media devoid of any added metals. For recovering the metal bioprocipitates settled at the bottom and equalizer section of the reactors, both influent and the recirculation pump to the reactors were momentarily suspended for a few minutes. However, small-sized (<0.45 µm) metal precipitates, known as fines, which do not settle at the bottom and escaped through the reactor effluent, were not accounted for calculating the recovery efficiency in this study. The low and high inlet heavy metal concentration values were selected based on the composition of acid mine drainage.

4.2.6 Characterization of immobilized biomass and metal nanopowders

Characterization of support material used for immobilization of bacteria was carried out by FESEM. Sample containing SRB immobilized support material was first fixed using 3% glutaraldehyde and later dehydrated using ethanol for its characterization using FESEM (Sigma 300, Germany) (Kiran et al., 2017).

To verify potential application of metal nanoparticles recovered in this study, its composition analysis and detailed characterization were carried out using techniques such as FESEM-EDX and FETEM. The details of all these methods were provided in section 3.2.3 of Chapter 3.

4.2.7 Analytical methods

Biomass added for biofilm growth in the IFBR was determined as mixed liquor volatile suspended solids (MLVSS) according to standard methods defined in American Public Health Association (APHA) (APHA, 2005). COD of influent and effluent samples were determined using closed reflux method (APHA, 2005). Sulfate was measured using standard barium chloride based turbidimetric method (APHA, 2005). Dissolved sulfide in the effluent was determined using

colorimetric method described by Cord-Ruwish (1985). Acetate concentration in the samples was determined by HPLC with Aminex HPX-87H column (Bio-Rad Laboratories, USA).

Concentration of different metals in solution was determined by microwave plasma atomic emission spectroscopy (Varian, 4210 MP-AES, Agilent Technologies) (Sungur et al., 2015). For estimating the amount of metals recovered in the reactors, metal bioprecipitates settled at the bottom and equalizer section of the reactors were collected and solubilized by acidification with 20% HNO_3 (Villa-Gomez et al., 2011). All the reagents used were of analytical grade. The details of all these methods were provided in section 3.2.4 of Chapter 3.

4.2.8 Calculations

The metal removal efficiency was calculated based on the difference in the metal concentration in influent and effluent from R1 and R2, as represented in the equation (Eq. (4.1)) below:

$$\text{Metal removal efficiency (\%)} = \frac{M_{in} - M_{out}}{M_{in}} \times 100 \qquad (4.1)$$

Where M_{in} and M_{out} are metal concentrations (mg/L) in the influent and effluent to the reactors, respectively (Villa-Gomez et al., 2011).

The bioprecipitate obtained from conical bottom of the IFBRs and the equalizer was utilized to calculate the recovery percentage using the following Eq. (4.2):

$$\text{Metal recovery (\%)} = \frac{M_{total} - (M_{eq} + M_b)}{M_{total}} \times 100 \qquad (4.2)$$

Where M_b and M_{eq} are metal concentrations (mg/L) in the bioprecipitates collected from bottom and equalizer section of the reactors and M_{total} is the total metal concentration (mg/L) in the influent (Villa-Gomez et al., 2011).

4.3 Results and discussion

4.3.1 Characterization of immobilized biomass

Fig. 4.2 shows the low-density polyethylene support material before and after biofilm formation in the IFBRs during the startup phase. A gradual increase in the sulfate removal efficiency (~50%) along with change in color of the support material from white to black and that of liquid inside the reactor from brown to black confirmed formation of sulfate reducing biofilm onto the support material and anaerobic condition in the reactor, respectively. Startup phase with the reactor was carried out using Postgate medium devoid of any added heavy metals for biofilm growth and development. Fig. 4.3 shows FESEM images confirm the SRB biomass immobilized onto the support material.

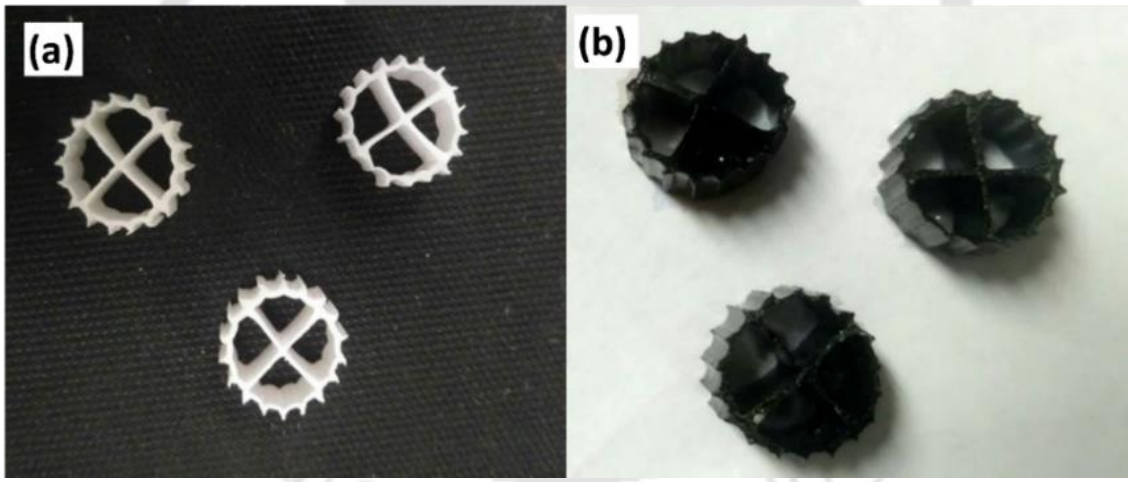

Fig. 4.2 Image showing polyethylene support (a) before and (b) after biofilm formation.

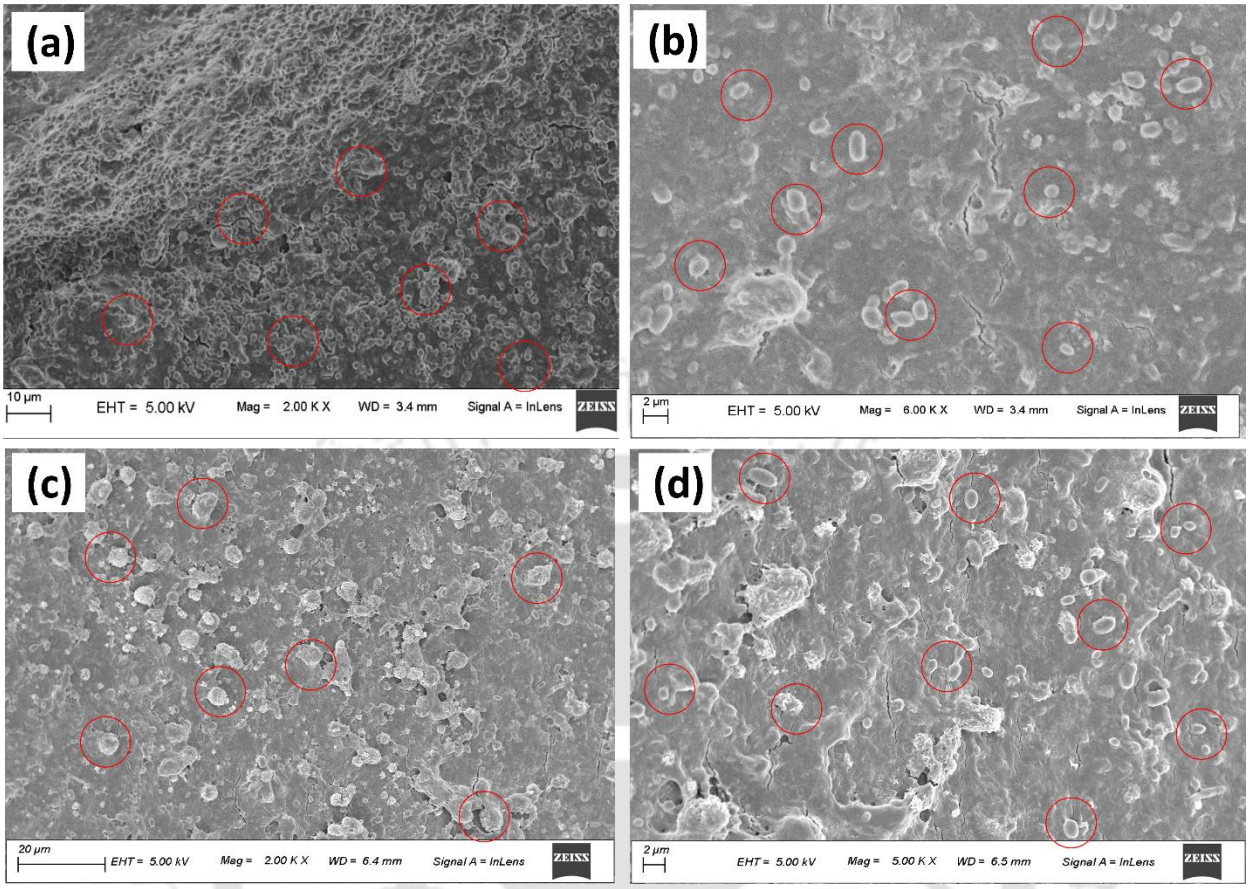

Fig. 4.3 FESEM images of biofilm on the support material in R1 (a-b) and R2 (c-d).

4.3.2 Effect of HRT for metal removal

The effect of different HRT on copper removal was first examined using the reactors. The results showed that at 48 h HRT, 99% copper removal efficiency was obtained, whereas at 24 h HRT, the value slightly reduced to 97.8%. The metal removal efficiency dropped to a very low value of 70% at 12 h HRT. Similar results of copper removal were obtained in the IFBR operated with influent pH 3.0, COD/SO_4^{2-} ratio 0.67 and copper concentration 10 mg/L. Hence, 24 h HRT was selected for carrying out further experiments on metal removal and recovery using the two IFBRs (Fig. 4.4).

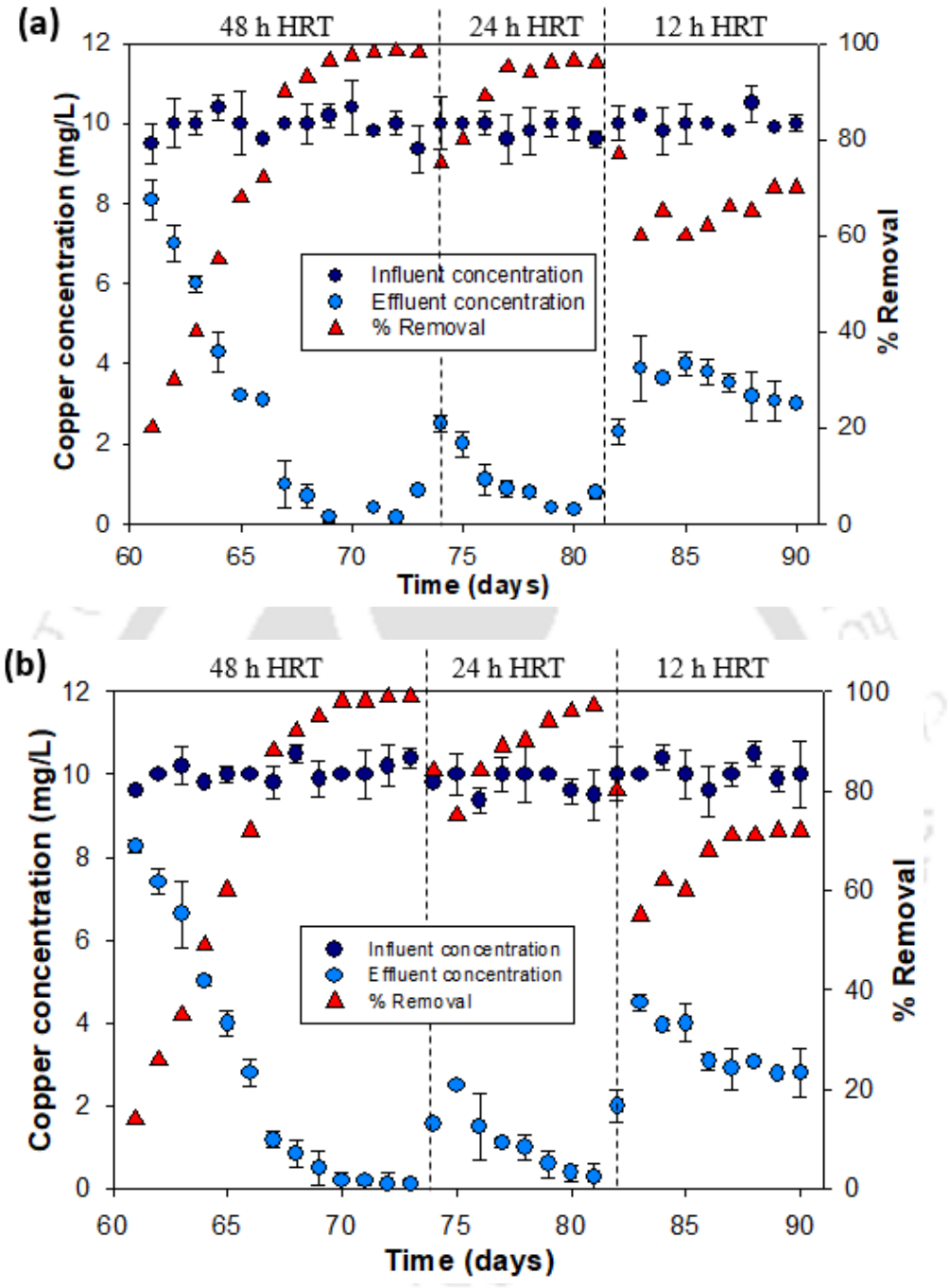

Fig. 4.4 Effect of different HRT on copper removal using (a) R1 and (b) R2.

4.3.3 Heavy metal removal

Fig. 4.5 shows the time profile of inlet and outlet metal concentration and percentage metal removal obtained using R1 and R2.

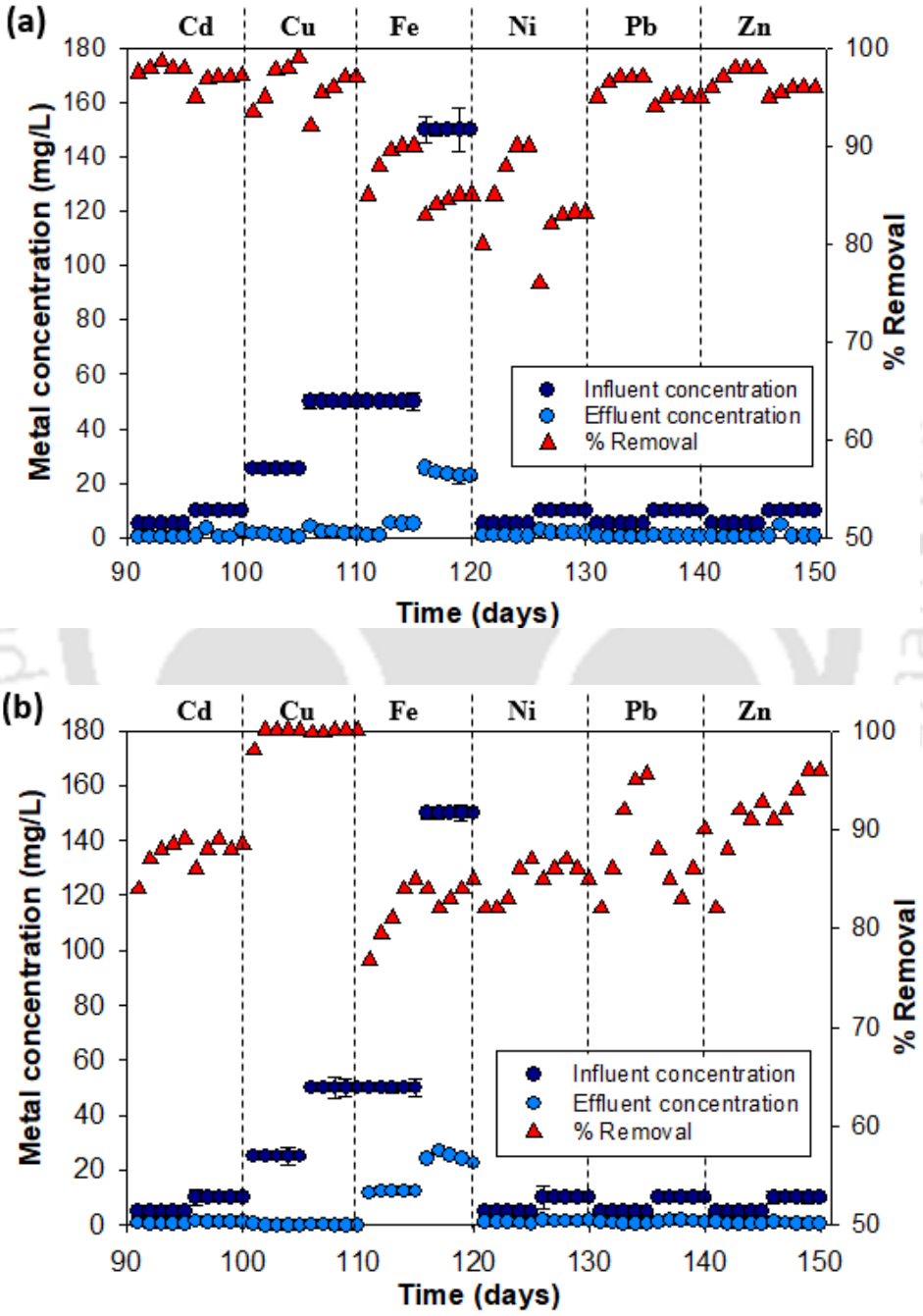

Fig. 4.5 Removal of different heavy metals using (a) R1 and (b) R2.

At all the low and high inlet metal concentrations, more than 95% metal removal was obtained in case of Cd^{2+}, Cu^{2+}, Pb^{2+} and Zn^{2+} using R1, except for Ni^{2+} and Fe^{3+} (85% and 90%, respectively).

These heavy metal removal values were, however, slightly higher than the values obtained with R2 for all the metals, but for copper the percentage removal value remained the same (Fig. 4.5). In case of R2, more than 90% metal removal was obtained in case of Cd^{2+}, Cu^{2+}, Pb^{2+} and Zn^{2+} at all the low and high metal concentrations, except in the case of Ni^{2+} and Fe^{3+} (82% and 88%, respectively).

4.3.4 Effect of heavy metals on sulfate reduction and COD removal

Fig. 4.6 and 4.7 show the sulfate reduction and COD removal profiles in the presence of different metal. At a low inlet metal loading in R1, sulfate reduction efficiency was 54-65%, and the value was slightly low (52-58%) in case of R2. Fig. 4.7 shows the COD removal profile in the presence of different metals. In case of R1, 68% to 80% COD removal was obtained at low inlet metal loading. Whereas, in case of R2, the COD removal was in the range 66-76%. The pH of the effluent from R1 was in the range 6.5-7.5 and in case of R2 it was more than 6.2-7.0 for all the metals used (Fig. 4.11). Fig. 4.10 shows the results of acetate and sulfide produced in R1 and R2, which matched well with afore-mentioned COD removal and sulfate reduction values.

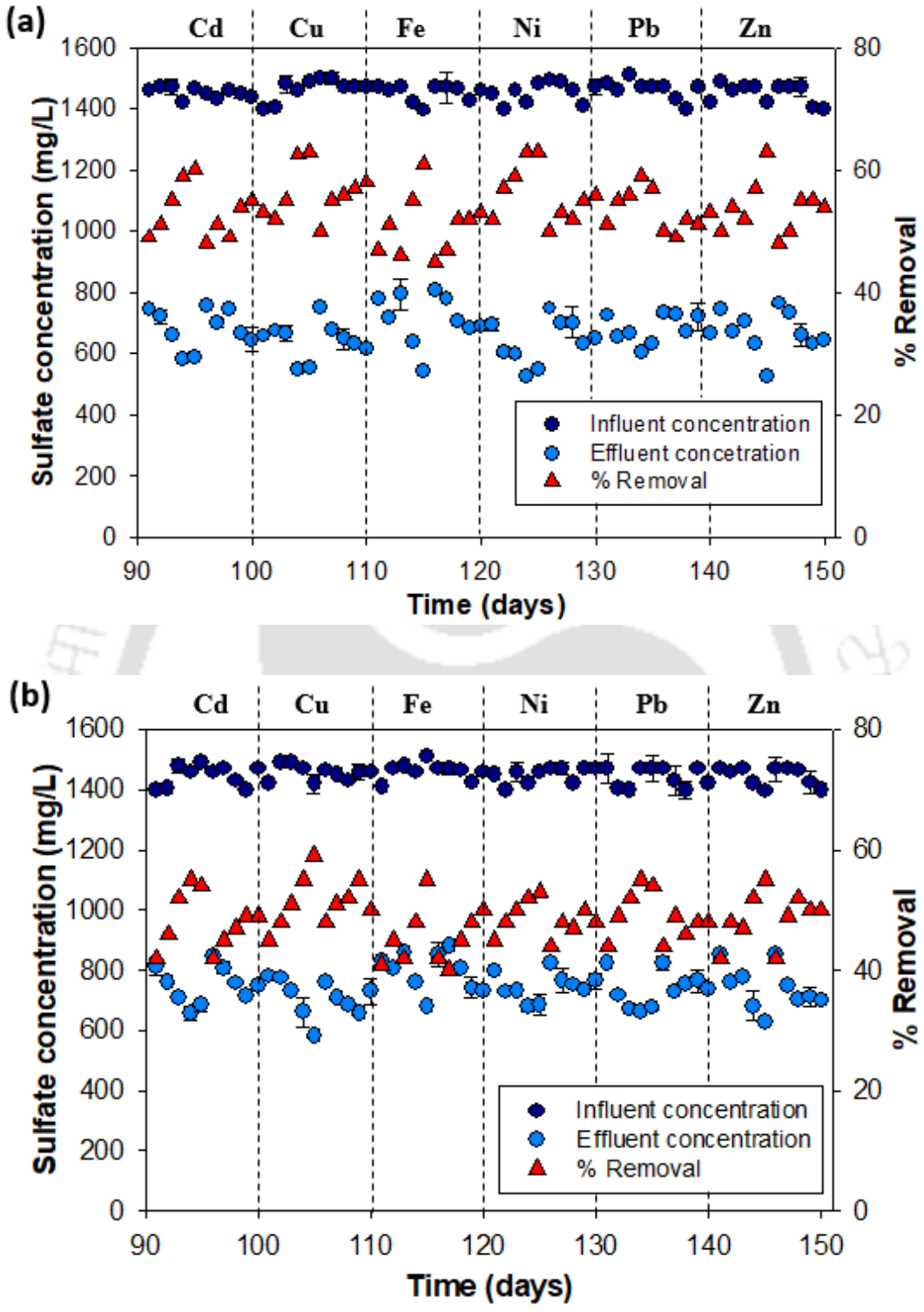

Fig. 4.6 Performance of IFBR for sulfate removal in the presence of different metals in (a) R1 and (b) R2.

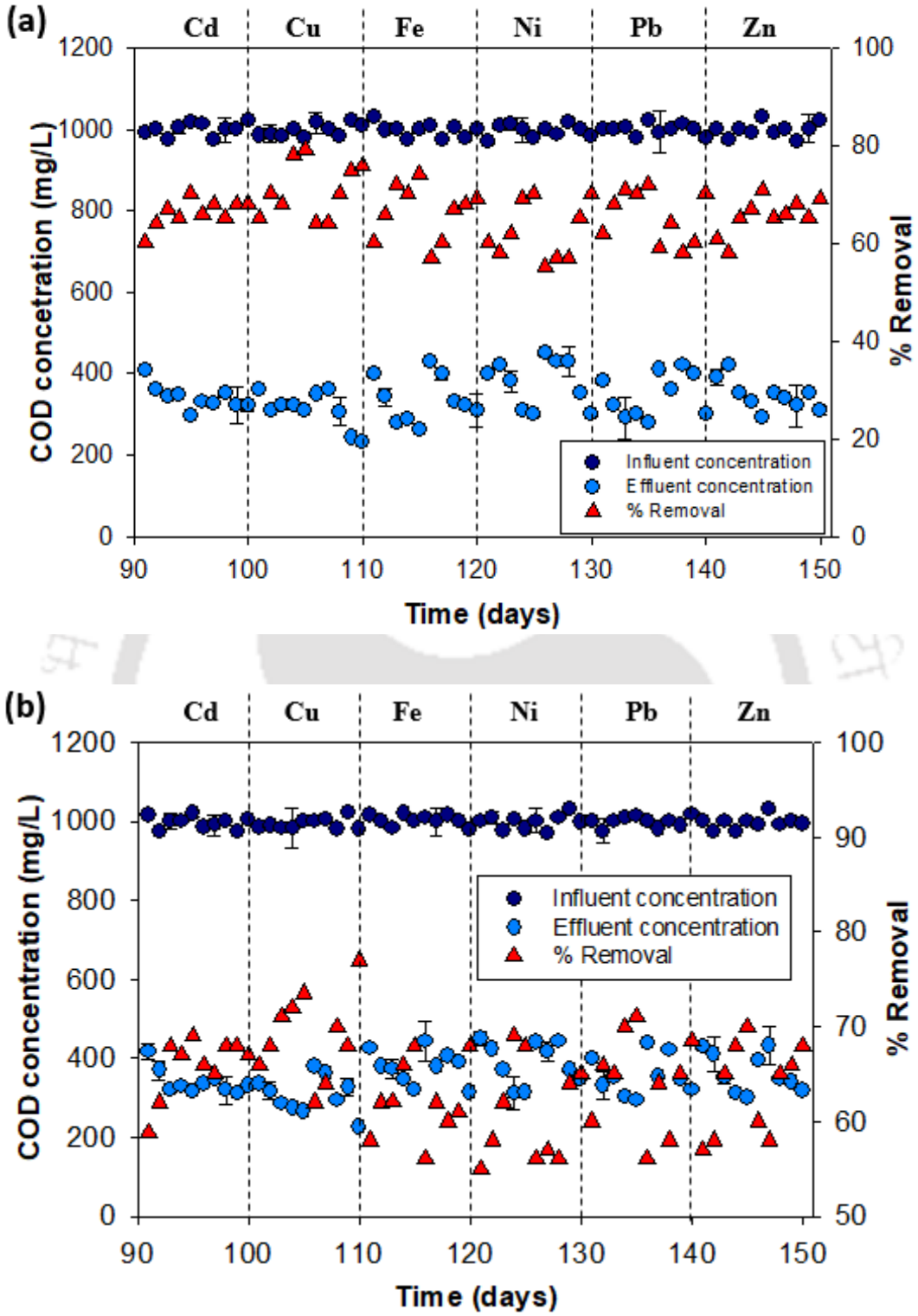

Fig. 4.7 COD removal profile in the presence of different metals in (a) R1 and (b) R2.

4.3.5 Metal recovery

Table 4.2 presents the metal recovery percentage from bioprecipitate obtained from bottom and the equalizer of R1 and R2. As described previously, the accumulated bioprecipitate was removed from conical bottom and the equalizer of the reactors, and the metal recovery values were calculated after every experimental run for each metal. Metal recovery percentage using R1 was in the range 50-65% and in case of R2 these values were slightly low (46-55%).

Table 4.2 Heavy metal recovery values obtained using R1 and R2

Metal	Metal recovery (%) using R1	Metal recovery (%) using R2
Cd^{2+}	61.5	53.2
Cu^{2+}	65.2	55.9
Fe^{3+}	50.1	48.5
Ni^{2+}	51.2	46.2
Pb^{2+}	64.8	53.4
Zn^{2+}	58.2	51.6

4.3.6 Bioprecipitate characterization

In order to understand the morphology and elemental composition of the metal bioprecipitates formed, FETEM and FESEM-EDX analyses were carried out with the individual metal bioprecipitates collected from the conical bottom of IFBR R1. FETEM images of the bioprecipiates are shown in the Fig. 4.8.

Size of the metal nanoparticles were different, and it ranged between 14 and 18 nm in case of copper and cadmium, in the case of lead and nickel nanoparticles it was in the range 8-10 nm. Size

of FeS NPs ranged between 10-12 nm and in case of ZnS NPs the size was 15-20 nm (Fig. 4.8). These results of metal nanoparticle size were further confirmed by particle distribution analysis.

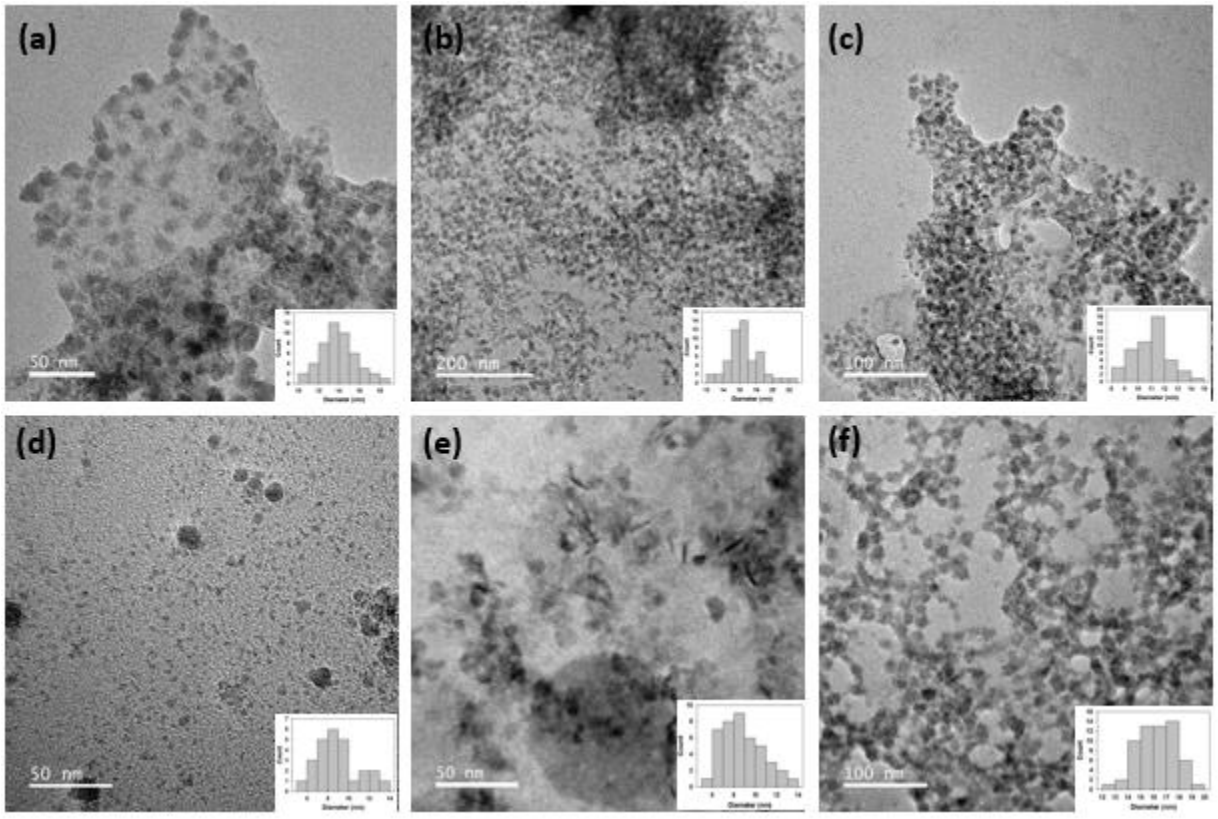

Fig. 4.8 FETEM images of bioprecipiates showing (a) cadmium, (b) copper, (c) iron, (d) nickel, (e) lead and (f) zinc nanoparticles. Particle size distribution of the different metal nanoparticles are shown as insert to these figures.

FESEM-EDX analysis of the bioprecipitates was performed for determining their elemental composition and morphology. Fig. 4.9 shows morphology and composition of bioprecipitate obtained from the conical bottom of the IFBR. EDX indicated presence of individual metals and sulfide, which signifies that nanoparticles formed were of different metal sulfides. EDX images also show small peaks due to carbon, sodium, potassium etc. initially present in the Postgate medium.

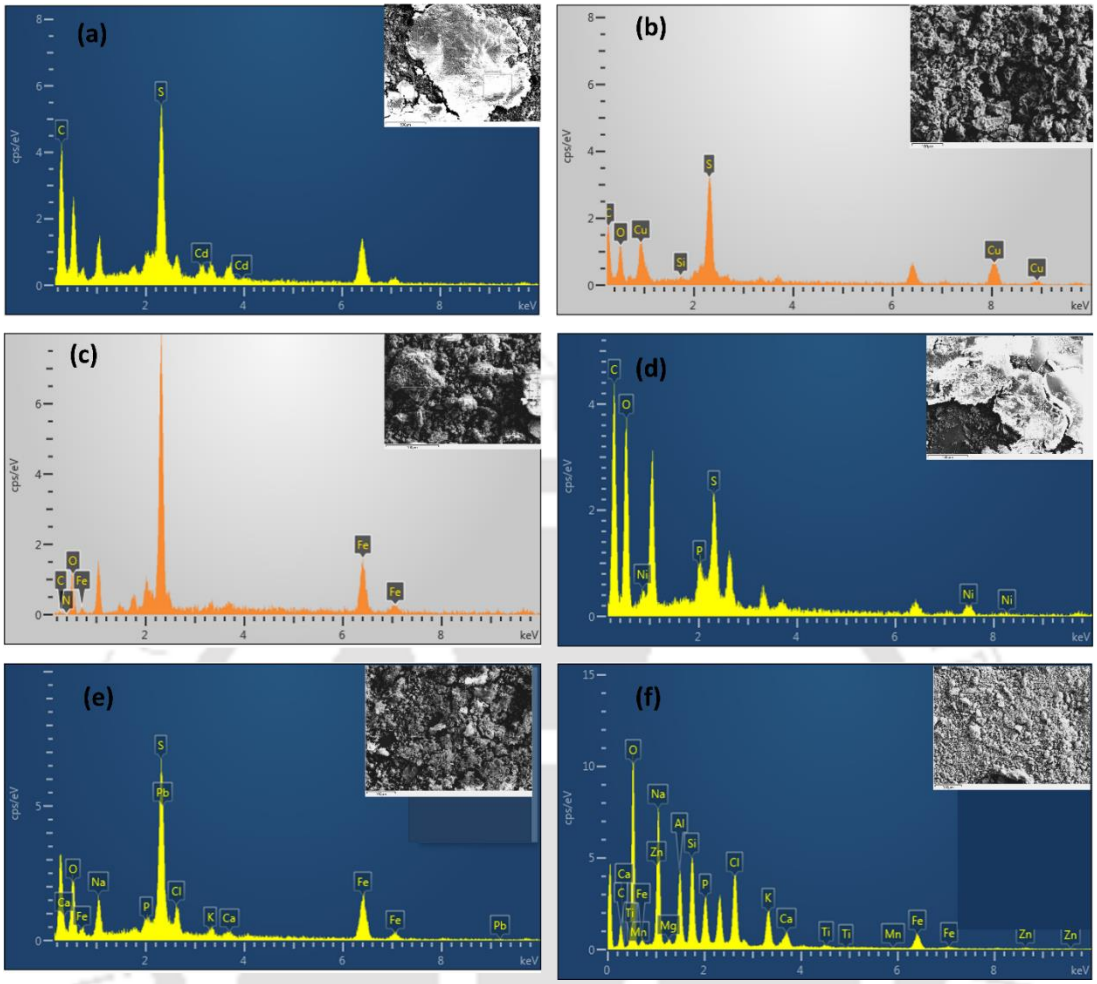

Fig. 4.9 FESEM-EDX of bioprecipiates showing (a) cadmium, (b) copper, (c) iron, (d) nickel, (e) lead and (f) zinc nanoparticles.

4.3.7 Heavy metal removal, sulfate reduction, COD removal and sulfide production

Numerous reactor configurations have been employed for metal, COD and sulfate removal by bioprecipitation but there are very limited reports on recovery of heavy metals from wastewater at a low pH using IFBR (Gallegos-Garcia et al., 2009; Villa-Gomez et al., 2011). The main aim of this study was to evaluate the metal recovery from wastewater at influent pH 3.0 using IFBR and compare its performance with another reactor receiving wastewater at influent pH 7.0.

The metal removal values were high at a low inlet metal concentration (more than 95% for all the metals in R1 and R2) suggesting that IFBR is highly suited to treat wastewater at low initial metal concentration despite the pH condition. Concentrations at which different metals exert toxic effect on SRB are as follows: 5-50 mg/L for Cu, >60 mg/L for Fe, 25-40 mg/L for Zn, 75-80 mg/L for Pb, 5-20 mg/L for Cd and 10-20 mg/L for Ni (Cabrera et al., 2006). In this study, toxic effect of the metals on SRB activity was not observed as the inlet metal concentrations were lower than the aforementioned values for the respective metals. Villa-Gomez et al. (2011) reported very high removal of Cd^{2+} (96.5%), Cu^{2+} (99.1%), Pb^{2+} (92.4%) and Zn^{2+} (91.3%) at 5 mg/L inlet concentration using IFBR at influent pH 7.0. The results of low value of metal removal efficiency obtained at a high inlet metal concentration in both R1 and R2 can be attributed to one or more factors, including formation of soluble metal polysulfide complexes, complexation with metabolites formed in the reactor and the production of fines that can pass through the filters (Lewis et al., 2010; Villa-Gomez et al., 2015).

Major mechanism of heavy metal removal by SRB involves metal precipitation as metal sulfide by sulfate reduction using SRB. Fig. 4.5 shows the removal of different metals at low and high inlet metal concentrations in R1 and R2. The metal removal efficiency is slightly low in both the reactors at a high inlet metal concentration. Metal to sulfide (M/S^{2-}) ratio is known to play an important role in the SRB mediated metal removal process (Kiran et al., 2017). High efficiency of metal removal is achieved at low M/S^{2-} ratio (<1) due to high concentration of sulfide available for precipitating the metals. Whereas, at a high M/S^{2-} ratio (>1), residual metal ions present in solution exerts toxic effect on the SRB, thus reducing the sulfate reduction efficiency and, therefore, its own removal (Villa-Gomez et al., 2015; Kiran et al., 2017). The results of low metal

removal efficiency correlated well with the sulfate reduction and COD removal values. As per the equation (Eq. (4.3)), acetate formed also served as an electron donor for sulfate reduction by SRB.

A high sulfate reduction efficiency (~65%) is observed at a low inlet metal concentration in both R1 and R2, which yielded a high sulfide concentration (~250 mg/L) for precipitating the metals (Fig. 4.6). A decrease in sulfate reduction efficiency (~50%) due to an increase in inlet metal concentration is observed due to inhibitory effect on SRB. R2 showed lower sulfate reduction efficiency in comparison with R1 at low as well as high inlet metal concentrations. It is reported that a low pH (<5) of wastewater inhibits the activity of SRB irrespective of the carbon source used and its concentration (Lopes et al., 2007). The reduced activity of SRB due to low pH is also ascribed to a low metal removal efficiency, sulfide concentration and metal recovery in R2.

Sulfide production results obtained (250 ± 30 mg/L in R1 and 200 ± 35 mg/L in R2) in this study were same as that previously reported by Gallegos-Garcia et al. (2009). An increase in the sulfide concentration thus indicated sulfate reduction to sulfide by SRB and a decrease in the sulfide concentration indicates its utilization for metal precipitation (Fig. 4.6 and Fig. 4.10a).

The results of COD removal (68-80% in R1 and 65-76% in R2) and production of organic byproducts matched well with the acetate concentration values (50-450 mg/L in R1 and 90-400 mg/L in R2) (Fig. 4.10b). Gallegos-Garcia et al. (2009) also observed that COD in their study was not utilized completely due to incomplete breakdown of lactate to acetate and bicarbonate as the byproducts by SRB. Zhou et al. (2011) reported that during lactate breakdown by SRB, acetate was produced as a byproduct and it was utilized as a secondary carbon source by some acetate utilizing SRB. Some SRB (e.g. *Desulfotomaculum* species) use acetate as carbon source for sulfide precipitation process as shown in the equation (Eq. (4.3)) below (Liamleam et al., 2007; Sousa et al., 2018):

$$\text{Acetate} + SO_4^{2-} \rightarrow 2HCO_3^- + HS^- \qquad (4.3)$$

In this study, the consumption of acetate as electron donor by SRB for sulfate reduction is observed from Fig. 4.10b. Fig. 4.10b clearly reveals that lactate was only partially converted to acetate. Fig. 4.10b also shows that in the presence of Cu and Fe, acetate was completely utilized, whereas, in the case of nickel and lead, the acetate was not completely utilized indicating inhibitory action of these metals on acetate-consuming bacteria for sulfate reduction.

The influent pH of the synthetic wastewater used in this study was 7.0 and 3.0 in R1 and R2; in the case of R1, the pH dropped within the first 24 h, whereas in case of R2 it slowly increased (Fig. 4.11). An abrupt change in pH of R2 fed with influent containing iron is due to a high added initial concentration of the metal (150 mg/L) which utilized all the available sulfide to form insoluble iron sulfide precipitates. A similar observation on drastic change in pH of R2 fed with nickel can be made. The pH slowly increased in both the reactors (R1 and R2) after the formation of bicarbonate due to incomplete oxidation of lactate as shown in equation (Eq. (4.4)).

In both the reactors, increase in the influent pH was observed due to bicarbonate ions produced and acetate consumption for sulfate reduction by SRB (Eq. (4.3)). Finally, after 4 days the effluent pH become stable at various values in both the reactors (Fig. 4.11). Similar observation were made in a previous study treating acidic wastewater at inlet pH of 5 or even 2.5 and effluent pH in the reactor was restored up to 7.0 due to alkalinity produced in the system (Jong and Parry et al., 2006; Gallegos-Garcia et al., 2009). In both the reactor systems (R1 and R2), the effluent pH was found to be around 6.5, which is well within the permissible limit for safe discharge of wastewaters into the environment (Kumar et al., 2012).

$$\text{Lactate} + \frac{1}{2}SO_4^{2-} \rightarrow \text{Acetate} + HCO_3^- + \frac{1}{2}HS^- + H^+ \qquad (4.4)$$

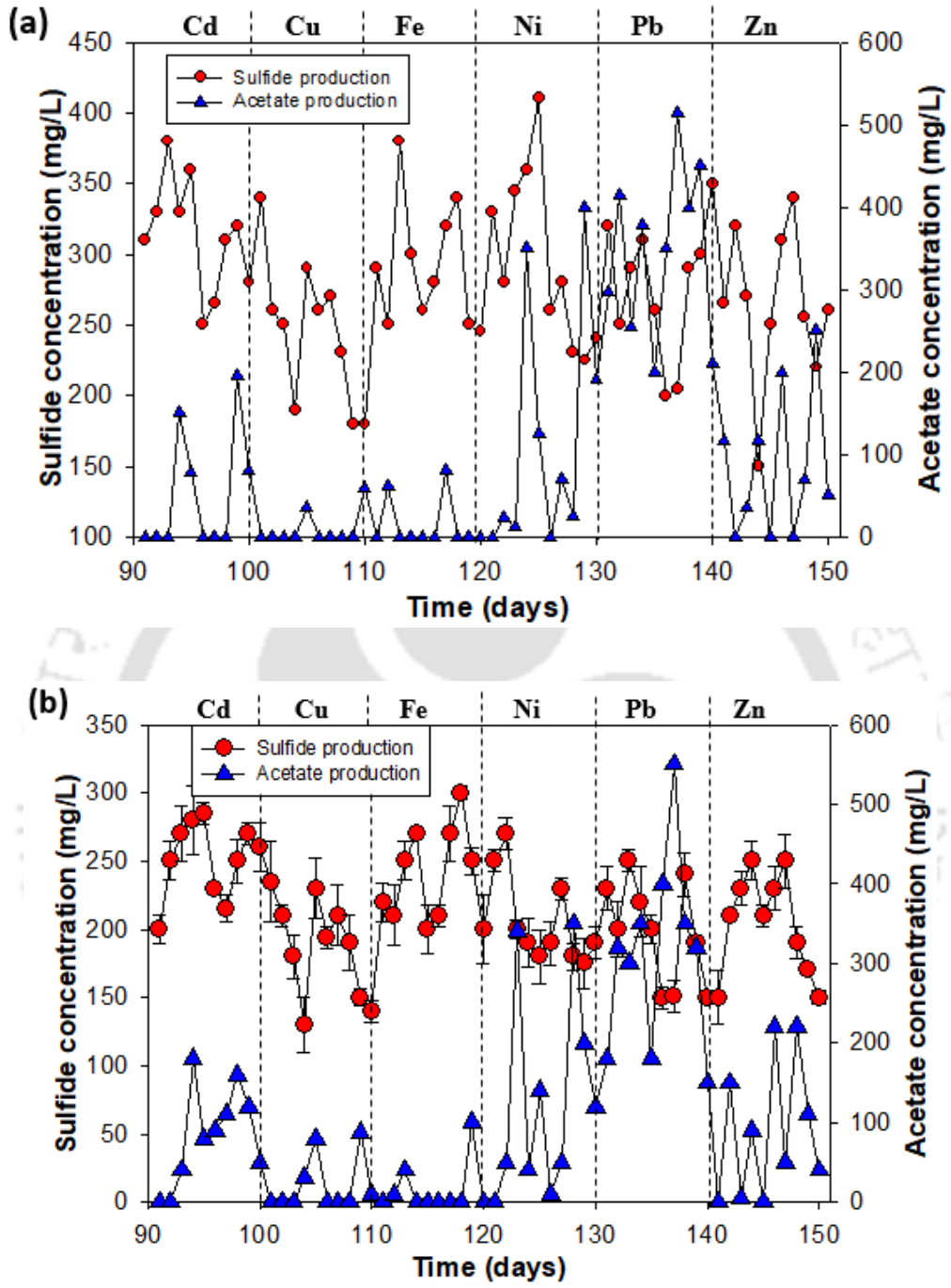

Fig. 4.10 Sulfide and acetate production profile in presence of different metals with (a) R1 and (b) R2.

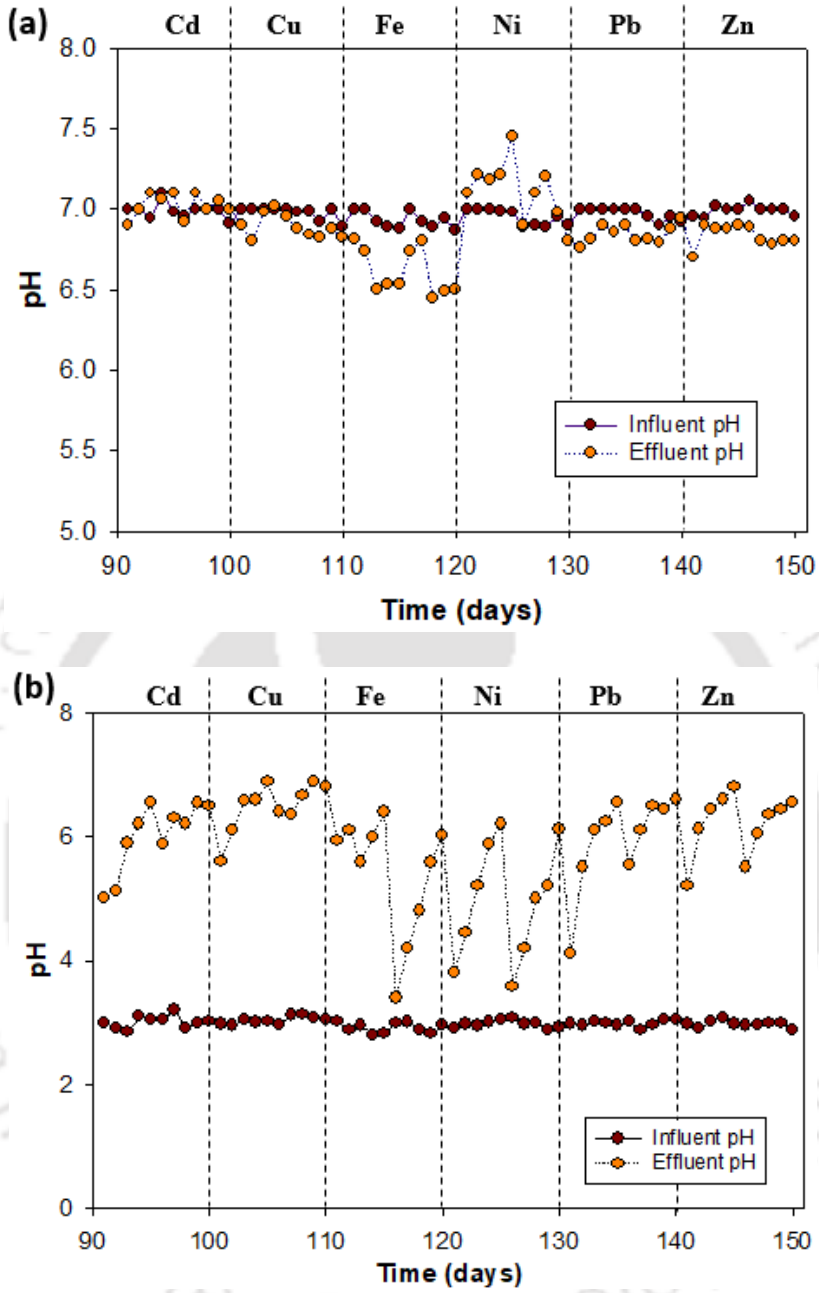

Fig. 4.11 Changes in pH value of the effluent from (a) R1 and (b) R2.

4.3.8 Metal removal mechanism

The mechanism of heavy metal removal can be defined as follows (1) sulfide production from sulfate by SRB and (2) formation of highly insoluble metal sulfide precipitate. In comparison to other reactor systems, IFBR system used in this study offers advantage of heavy metal recovery

as metal sulfide nanoparticles (Villa-Gomez et al., 2011). The formed metal sulfides precipitate accumulates in the conical bottom and the equalizer of the IFBR in this study (Gallegos-Garcia et al., 2009).

At all the initial metal concentration, copper removal efficiency was highest among all the different metals examined in both the reactors. The reason behind its maximum removal is because CuS has that least solubility product value among all the metal sulfides. Accordingly, the different metal removal efficiencies correlated with the solubility product value of the different metal sulfides. In the literature, it is reported that copper sulfide has the least solubility product of 8×10^{-37} (Yildiz et al., 2019). Nickel and iron showed low removal percentage among the different heavy metals owing to its high solubility product value with sulfide; hence, due to its high solubility product value, iron recovery was also low compared with the other metals. In addition to solubility product of the metal sulfides, formation of settleable solid is important in heavy metal removal. The formation of settleable solids mainly depends on pH of the solution. In case of iron, the pH value was lowest in comparison to other metals. Villa-Gomez et al. (2014) observed increase in the settleable solids amount from 5.1 to 9.4 mL/L due to an increase in the solution pH from 3 to 7.

4.3.9 Metal sulfide recovery as nanopowders

The present study successfully demonstrated metal sulfide precipitation and recovery from wastewater in the form of nanopowder at influent pH 7.0 and 3.0 using IFBR. Villa-Gomez et al. (2011) reported less than 50% recovery of Cu, Zn, Cd and Pb using IFBR by direct measurement of the metals following acidification of the recovered solids. In another study, Sinharoy et al. (2019) used IFBR and obtained 58% selenium recovery from synthetic wastewater at pH 7.0 by following the same acidification method. Gallegos-Garcia et al. (2009) used IFBR for Cd, Fe and Zn recovery and reported a very high recovery efficiency in the range 75-97%, which was,

however, attributed to the total suspended solids (TSS) present in the sample. In this TSS method, for estimating metal recovery, the suspended solids present in the samples were considered to be the same as metal sulfide present, but in reality TSS also contains salts from media which significantly contributed to its total weight (Villa-Gomez et al., 2011). Therefore, in this study direct measurement of metals following acidification of the recovered solids was followed for determining the metal recovery. More than 50% recovery was obtained for all the metals tested at influent pH 7.0 (R1) and a maximum recovery of 65% was obtained in case of Cu and Pb which is very high compared to results reported in the literature on metal recovery using IFBR with influent pH 7.0. In the case of R2, with low influent pH (3.0) slightly low recovery percentages of Cu (55.9%) and Pb (53.4%) were obtained. The low recovery efficiency with R2 is probably due to formation of fine particles with poor settling properties and formation of colloidal precipitates at low pH (Gallegos-Garcia et al., 2009).

As the metal removal efficiency values in R2 with influent pH of 3.0 were low in comparison with those in R1, the metal recovery values were also relatively low in R2. The low metal recovery with R2 is also possible due to formation of fine particles with poor settling properties or formation of the colloidal precipitates (Gallegos-Garcia et al., 2009). It is reported that low pH can solubilize these metals and affect their recovery (Gallegos-Garcia et al., 2009). Esposito et al. (2006) observed that the efficiency of ZnS precipitate formation decreased due to low pH (5.0) in a chemostat fed with Na_2S. Solution pH is known to affect the characteristics of metal precipitates by inducing the effect due to macronutrients and dissolved organic matter (DOM) present in the reactor. At low pH, binding of metals with DOM hampers agglomeration of metal sulfide particles and induces crystallization. On the other hand, at a neutral pH value, metal sulfide particles tend to aggregate and show high settling rates along with a high concentration of settleable solids in the

precipitate. The precipitate thus formed at pH 7.0 exhibit better solid-liquid separation as compared with precipitate formed at a low pH (Djedidi et al., 2009).

Metal precipitates formed at pH 7.0 settle quickly forming highly settleable solids and also show good dewatering characteristics as compared with the precipitates formed at other pH values. Villa-Gomez et al. (2014) observed similar result of increase in settleable solids concentration from 5.1 to 9.4 mL/L with an increase in solution pH from 3.0 to 7.0.

The formation of CdS, CuS, FeS, NiS, PbS and ZnS nanoparticles in the bioprecipiates was confirmed by FESEM-EDX analysis, which as well revealed that the precipitates were devoid of any metal hydroxide or carbonate. Overall, IFBR showed good potential for heavy metal removal as well as recovery through sulfate reduction process from both neutral and acidic metallic wastewater.

4.3.10 Role of SRB in metal sulfide nanoparticle recovery

From the FESEM images shown in Fig. 4.3, the presence of immobilized SRB biomass onto the support material can be clearly seen. These FESEM images also reveal the presence of cylindrical and curved rod shaped bacteria (typically *Desulfovibrio* species) attached to the support material, which is further confirmed from the FETEM images shown in Fig. 4.12. Hence, SRB biofilm formation around the support material in R1 and R2 was achieved during the startup phase. The well grown bacterial biofilm on the support material further resulted in a high removal and recovery efficiency of metals in R2 even at a low influent pH of 3.0.

SRB play an important role in both sulfide precipitation and metal recovery from wastewater. SRB first use sulfate to produce sulfide and sulfide combines with metals outside the bacterial cell wall. It can be clearly seen from FETEM images (Fig. 4.12) that nanoparticles are accumulated outside

as well as on the cell wall of the bacteria. The images also exhibited EPS kind of layer surrounding the bacteria. It has been reported that EPS layer is bind with bacterial cell by both physically as well as electrostatic interaction. The bacteria secrete EPS in defense against toxicity due to heavy metals (Fig. 4.12) (Kiran et al., 2015).

The nanoparticles formed were due to metal sulfides as previously confirmed by EDX spectra of the bioprecipiates (Fig. 4.9). Gallegos-Garcia et al. (2009) also reported that iron, zinc and cadmium were precipitated as their corresponding sulfide salts in a sulfidogenic down-flow fluidized bed reactor and no metal hydroxide or carbonates were present in the precipitates.

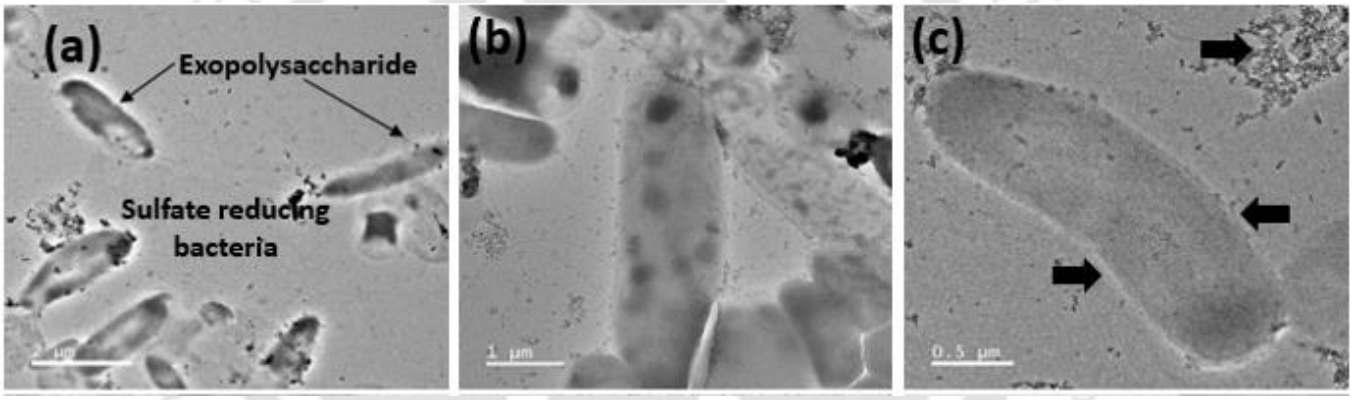

Fig. 4.12 FETEM images of bioprecipiate loaded with CuS NPs showing: (a-c) sulfate reducing bacteria with EPS outside the cell surface. CuS NPs are also seen in both free form as well as attached to the bacterial EPS around the cell wall.

Compared with the previous reports on metal recovery using IFBR with influent pH 7.0, the present study achieved significantly high (65%) recovery efficiency of Cu and Pb. This study further stablished that metals can be recovered from the AMD even at very low influent pH 3.0. In addition recovered metals in the form of metal sulfide nanopowder showed excellent characteristics for potential reuse application in industries.

4.4 Significant findings

IFBR with influent pH 7.0 (R1) performed better than R2 with influent pH 3.0 in terms of metal recovery from wastewaters. Maximum recovery of Cu was obtained followed by that of Pb and Cd. The overall order of metal recovery was Cu > Pb > Cd > Zn > Ni > Fe. In both R1 and R2, the effluent pH was ~6.5, thereby demonstrating that enough alkalinity was produced in the bioreactors to neutralize the acidic wastewater and the effluent could be safely reused or discharged into the environment. IFBR has the potential not only to treat heavy metal laden acidic wastewater but also the ability to recover heavy metals in the form of nanopowder. However, more research is warranted to purify the recovered metal sulfide nanopowder and check its potential applications. Results obtained in this study will be useful to scale up the technology for metal recovery from AMD. However, the results need to incorporate risks such as excess sulfide generation which may cause residual pollution problems and necessitate a post-treatment step for removing the excess sulfide from the effluent.

Chapter 5

Recovery and purification of copper sulfide nanoparticles from acid mine drainage by biological sulfate reduction and microfiltration using low-cost ceramic membrane

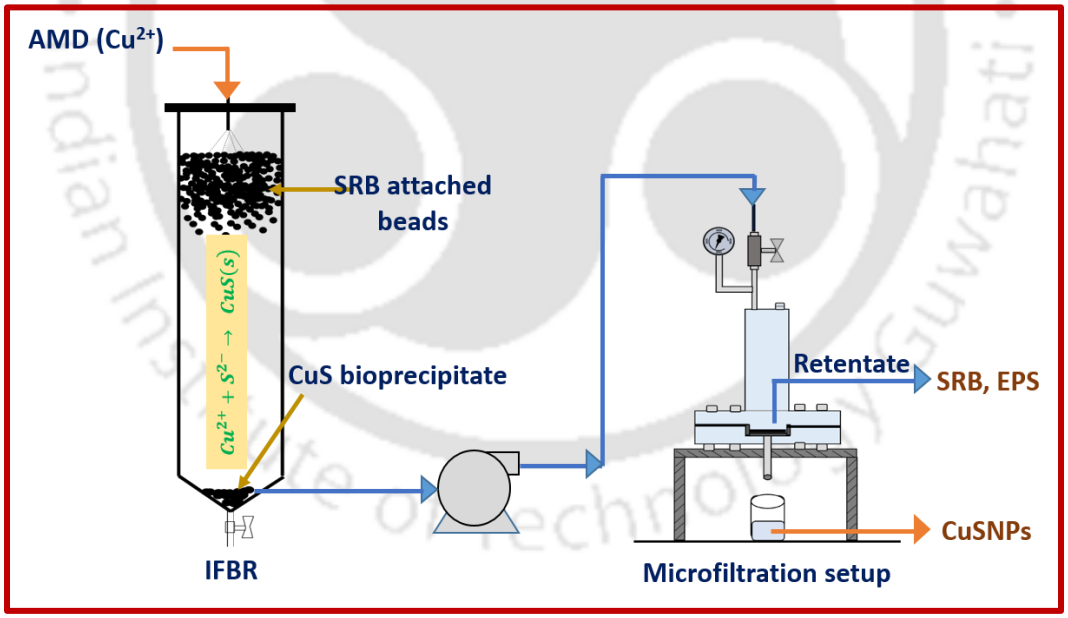

ABSTRACT

Acid mine drainage (AMD) is a severe threat to the environment, human communities, and water sources. On the other hand, AMD typically has a high amount of copper that can be recovered in pure form for different industrial applications. Biological metal sulfide precipitation is an emerging technique to both treat AMD and recover valuable metals. However, the problem with the metal sulfide precipitation process is with the purity of metals. This study combined metal bioprecipitation and microfiltration using an indigenously developed ceramic membrane for recovering copper from AMD in a highly pure form. Different pretreatment methods were also evaluated to obtain CuS nanoparticles (CuS NPs) in pure form, and probe sonication proved the most effective. Microfiltration using the ceramic membrane showed 92% purification efficiency of the CuS NPs with a flux of 77×10^{-4} m^3/m^2s. Following its purification, the nanoparticles were characterized using different techniques such as Fourier transform infrared spectroscopy (FTIR) and field emission transmission electron microscopy (FETEM). The pure CuS NPs were polycrystalline in nature with a size in the range 5-10 nm. The size, shape, and crystallinity of the CuS NPs revealed its excellent industrial reuse and application potential. Furthermore, based on the cost of the raw materials used to prepare the membrane, the membrane cost was estimated to be $\$160/m^2$.

5.1 Introduction

Metallic wastewater such as acid mine drainage (AMD) generated from coal mines and mining related operations is characterized by a low pH and contains a high concentration of metals, sulfate, and low COD (chemical oxygen demand) (Kiran et al., 2017; Singh et al., 2020). Discharge of the metallic wastewater into the environment is a serious problem if not treated properly. On the other hand, heavy metal recovery from AMD is interesting from both economic and environmental perspectives. Different methods have been used to treat the wastewater, including chemical precipitation, ion exchange, adsorption, ultrafiltration, nanofiltration, coagulation, floatation, etc. However, these methods have several drawbacks, e.g., high reagent cost, unpredictable metal removal efficiency, generation of toxic sludge, metal recovery problems, etc. (Kiran et al., 2017).

To treat such sulfate rich, heavy metal containing wastewater, sulfide precipitation using sulfate reducing bacteria (SRB) is a proven technique. It has many advantages over the chemical precipitation method in terms of efficiency and treatment cost. In this method, sulfide is produced by SRB, which combines with metals present to form insoluble metal sulfide precipitate. The single-stage sulfidogenic inverse fluidized bed reactor (IFBR) system can be used to efficiently recover the bioprecipitate (Paul et al., 2020). However, metal sulfide nanoparticles in the bioprecipitate are found attached to exopolysaccharide (EPS) secreted by SRB around the cell wall (Kiran et al., 2017). Hence, further processing of the bioprecipitate is required to extract the metal sulfide nanoparticles in pure form for its potential application in industries.

Conventional methods followed to separate metal sulfide precipitate are mainly sedimentation or filtration based. These methods require large equipment for operation and their separation performance is also poor due to presence of fine and colloidal particles in suspension. To overcome the limitations of the conventional processes, membrane separation processes viz. microfiltration

(MF) and ultrafiltration (UF) are a valid alternative. These techniques offer many advantages such as high yield, minimum separation steps, low working time, no requirement of clarifying agents, easy cleaning and maintenance of equipment, and waste product reduction. In addition, membrane processes are characterized by their high efficiency, simple equipment, and low energy consumption.

Ceramic membranes offer excellent chemical, thermal, and mechanical stability as compared with polymeric membranes and are, therefore, highly suited for industrial application (Kumar et al., 2016; Saja et al., 2018). Important applications of the ceramic membrane in chemical and biochemical processes are also due to its easy availability and high permeate flux. However, there is still a need for low-cost raw materials and simple process for ceramic membrane preparation. For instance, the commonly used alumina-based ceramic membranes are high-priced and involve high sintering temperatures for preparation (Goswami et al., 2020). In order to keep the membrane cost low, the focus has been shifted towards locally available natural clay materials for the fabrication of ceramic membranes.

Different clay materials are available for membrane preparation, including kaoline (Zou et al., 2021), natural raw clay (Kumar et al., 2019), tunisian clay (Kamoun et al., 2020), dolomite (Bessa et al., 2017), and fly ash (Goswami et al., 2020). Among these materials, kaoline is both inexpensive and suitable for preparing ceramic membranes with stable microfiltration performance. Kaolin can be used as a starting material and mixed with other additives to prepare a ceramic membrane. Monash et al. (2011) also provided the optimal formulation containing (dry basis) kaolin, ball clay, quartz, feldspar, calcium carbonate, and pyrophyllite to fabricate microfiltration ceramic membrane.

Hence, this study focused on developing an indigenous, low-cost ceramic membrane for microfiltration of bioprecipitate obtained by sulfide precipitation of synthetic AMD using SRB, to get pure metal sulfide nanoparticles. The pure nanoparticles were characterized using various techniques such as field emission transmission electron microscopy (FETEM), Fourier-transform infrared spectroscopy (FTIR), particle size analyzer, Raman spectroscopy, and X-ray diffraction (XRD) for the analysis of its shape, size, and crystallinity.

5. 2 Materials and methods

5.2.1 Raw materials

Kaolin (14.45 wt.%), quartz (26.59 wt.%), ball clay (17.58 wt.%), pyrophyllite (14.73 wt.%), and feldspar (5.6 wt.%) were used as the starting materials in fabricating the ceramic membrane. These materials were obtained from Kanpur, India. Calcium carbonate was purchased from Merck, India. Kaolin delivers low plasticity and refractory property, quartz provides physical strength and makes the support thermally strong, ball clay provides malleability and solidity to the green support, calcium carbonate ($CaCO_3$) is used to make the membrane porous, and feldspar provides hardness, strength, and resistance against chemical corrosion (Goswami et al., 2020).

5.2.2 Synthesis and pretreatment of copper sulfide nanoparticles (CuS NPs)

A laboratory scale anaerobic sulfidogenic inverse fluidized bed reactor (IFBR) was used to synthesize copper sulfide nanoparticles (CuS NPs) from synthetic AMD by sulfide precipitation. The synthetic AMD was supplemented with anaerobic medium composed of (g/L): NH_4Cl (1.0), yeast extract (1.0), KH_2PO_4 (0.5), Na_2SO_4 (1.47), $CaCl_2{\cdot}2H_2O$ (0.1), $FeSO_4{\cdot}6H_2O$ (0.289), $Na_3C_6H_5O_7$ (0.3) and EDTA (0.3) (Postgate, 1984). 60% (*v/v*) lactate was used as the electron donor (carbon source) for sulfate reduction, and the influent pH was adjusted to 7.0 using sodium hydroxide. The initial copper concentration in the feed was 50 mg/L. The crude bioprecipitate

obtained was washed twice by centrifuging at 7000 × g for 15 min each to remove the minerals and salts present. The washed bioprecipitate containing CuS NPs attached to the EPS and SRB biomass was suspended in Millipore water and its pretreatment was evaluated by different techniques, viz. centrifugation and heating, cell lysis using a French press, tip sonication, and bath sonication to detach the nanoparticles from EPS and SRB biomass for further purification by microfiltration. The different pretreatments followed are briefly mentioned as follows.

Pretreatment by centrifuge and heating was first carried by centrifuging the bioprecipitate at 12000 × g for 10, 20, and 30 min, followed by heating the mixture at 60 ºC for 30 min (Mal et al., 2017).

Similarly, bath sonication was carried out using an Ultrasonic cleaner (LMUC-2A, Labman Scientific Instruments, India) for different time periods (5, 10, 20 min), and cell lysis was performed using a French Press (Constant Systems CF1, Constant systems limited, UK) at different applied pressures of 200 and 400 MPa (Desaunay et al., 2014). For pretreatment by probe sonication, a tip sonicator (VC 505 Ultrasonic Processor, Sonics & Materials Inc., USA) was employed (Han et al., 2013). All these experiments were conducted in triplicate, and the results were represented in the mean ± standard deviation format.

5.2.3 Membrane fabrication and characterization

The membrane preparation process started with mixing the Kaolin (14.45 wt.%), quartz (26.59 wt.%), ball clay (17.58 wt.%), pyrophyllite (14.73 wt.%), and feldspar (5.6 wt.%) with 4 mL (2 wt. %) of aqueous polyvinyl alcohol (PVA) in a mixer grinder. After mixing, a desired amount of the powder mix was pressed uniaxially in a hydraulic press at a pressure of 50 MPa, which yielded a circular disk-shaped membrane. The freshly prepared membrane was first dried at room temperature and then in a hot air oven at 200 °C for 24 h to remove moisture. The dried membrane was subsequently sintered in a muffle furnace at 950 ºC for 6 h with a heating rate of 2 ºC per min,

followed by polishing the membrane with silicon carbide abrasive paper to get a flat shape. After polishing, the membrane was sonicated in an ultrasonic bath for 15 min to remove any loose particles attached to the membrane (Zou et al., 2021). Fig. 5.1 shows a schematic of the steps followed in fabricating the ceramic membrane.

Fig. 5.1 Schematic showing membrane fabrication steps followed in this study.

The ceramic membrane was then characterized by different methods as follows: the Archimedes method was first used to determine the porosity of the fabricated membrane, and for which dry weight (W_1) of the membrane was estimated after drying at 110 °C for 6 h in a hot air oven to remove moisture in the membrane. Following this drying step, the membrane was submerged in water at room temperature for about 24 h, and its wet weight (W_2) was determined after wiping it with tissue paper to remove excess water from the surface.

The membrane porosity (ε) was thus calculated using the following equation (Purnima et al., 2020).

$$\varepsilon\,(\%) = \frac{W_2 - W_1}{V \times \rho_w} \times 100 \qquad (5.1)$$

where V is the volume of the membrane and ρ_w is the water density.

In order to determine chemical stability of the membrane, it was immersed in hydrochloric acid (HCl) (pH 1) and sodium hydroxide (NaOH) (pH 14) solutions and, after one week, weight loss in the membrane was calculated. Morphology of the sintered membrane was investigated using Energy Dispersive X-ray integrated Field emission scanning electron microscopy (FESEM-EDX) (Zeiss, Sigma, Germany).

A dead-end filtration setup (400 mL capacity) was used to conduct the pure water permeation test of the membrane (Fig. 5.2). The filtration setup was made of stainless steel with cylindrical top and bottom parts. The membrane was placed in the bottom part, and a neoprene "O" ring was squeezed on top of the membrane to prevent any leakage. Filtration was affected by purging with N_2 gas at the desired pressure on top of the membrane. Prior to the test, Millipore water was passed under high pressure to clean the membrane and remove any loose particles attached to the membrane pores.

For calculating the membrane permeate flux, 300 mL Millipore water was filled from the feed inlet to the top cylindrical compartment of the setup and pressurized with N_2 gas. Finally, the time required to collect 100 mL water in the permeate stream was noted. The water flux was thus calculated as per the following equation:

$$J_w = \frac{Q}{A\Delta T} \qquad (5.2)$$

where J_w is the pure water flux ($m^3/m^2/s$), Q is the volume of water permeated (m^3), A is the effective membrane area (m^2), and ΔT is the sampling time (s).

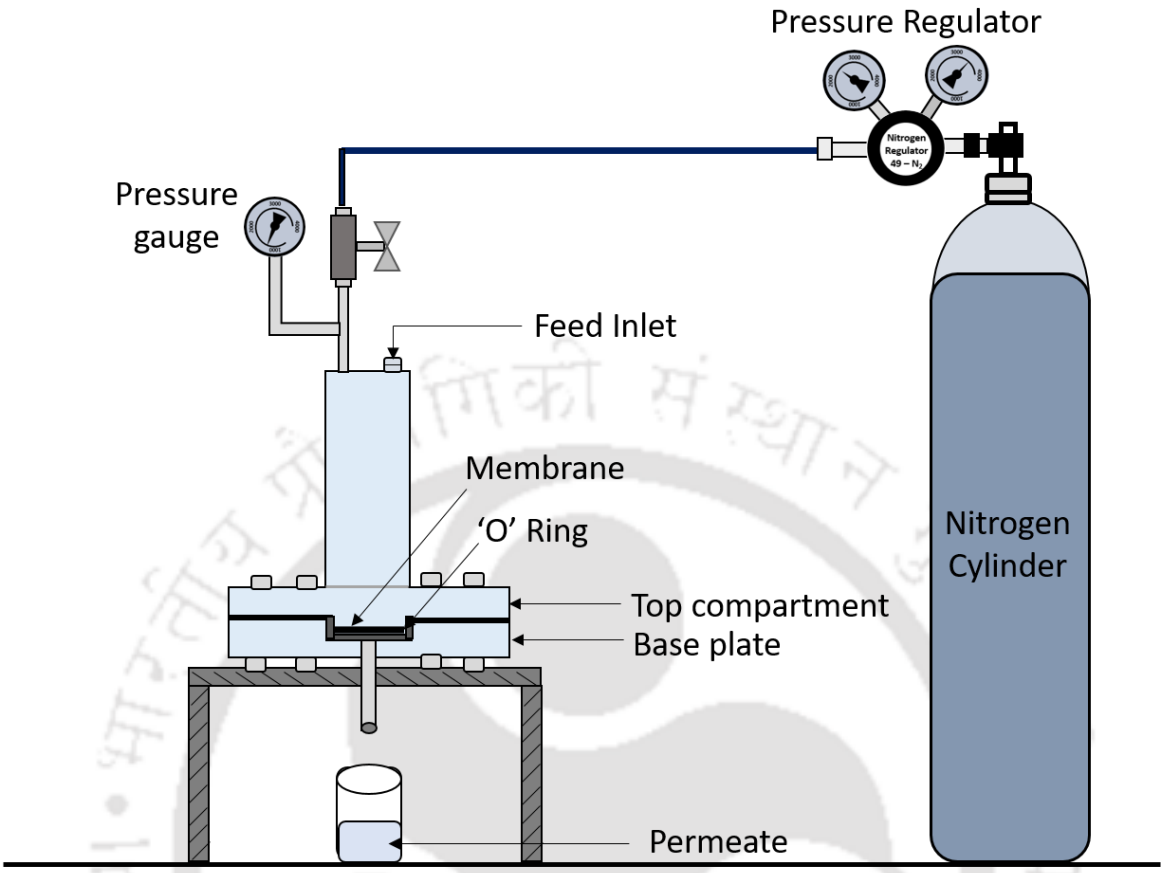

Fig. 5.2 Dead-end filtration setup used in this study.

5.2.4 Purification of CuS NPs by microfiltration

Microfiltration to obtain pure CuS NPs from the pretreated bioprecipitated was carried out at a fixed applied pressure and ambient room temperature (24 ± 2 °C). Prior to microfiltration, both the membrane and dead-end filtration setup used were sanitized using sodium hypochlorite solution (200 mg/L). The filtration setup and membrane were then washed using double distilled water. In order to measure the permeate flux, the time required to collect 10 mL of permeate was determined. At the end of the microfiltration experiment, the membrane was cleaned using sterile water at a high pressure until the original water flux was restored. The following equation was used to calculate the purification efficiency of the membrane:

$$\text{Purification efficiency (\%)} = \frac{M_i - M_f}{M_i} \times 100 \qquad (5.3)$$

where M_i and M_f are copper concentrations (mg/L) before and after microfiltration of the pretreated bioprecipitate.

In order to verify the purity and potential application of CuS NPs obtained in this study, its composition analysis and detailed characterization were performed by field emission transmission electron microscopy-energy dispersive spectroscopy (FETEM-EDS), Raman spectroscopy, and X-ray diffraction (XRD).

5.2.5 Characterization of CuS NPs

FETEM images and selected area diffraction (SAED) patterns of CuS NPs were obtained by EDS integrated FETEM (JEOL JEM2100, Japan) by casting a sample of it onto 200 mesh size copper grid followed by air-drying to remove excess water from the sample. For XRD analysis, the CuS NPs obtained was freeze-dried, grinded, and then dried in an oven at 120 ºC to remove any extra moisture from the sample.

The chemical bond and groups present in the CuS NPs were analyzed by FTIR (IR affinity-1S, Shimadzu, Japan). Vibrational properties, crystal phase, and crystallinity of the CuS NPs were examined by micro Raman spectroscopy. For this analysis, the sample was freeze-dried and finely ground before analysis using a Laser micro Raman spectrometer (Horiba JobinVyon, Model LabRam HR, France) with argon (Ar) ion laser at 515 nm and an incident power of 50 mW for excitation. The details of all these methods were provided earlier in Chapter 3.

5.2.6 Determination of biomass and copper concentration

Biomass (SRB) concentration in the bioprecipitate was determined as mixed liquor volatile suspended solids (MLVSS) as per the standard method detailed in the American Public Health Association (APHA) (APHA, 2005). Copper concentration in the bioprecipitate, before and after purification, was determined by microwave plasma atomic emission spectroscopy (Varian, 4210 MP-AES, Agilent Technologies, USA) following filtration of the samples through a 0.45 μm nitrocellulose filter (Millipore) (Sungur et al., 2015). Reagents used in the study were of analytical grade, and all sample analyses were done in triplicate.

5.3 Results and discussion

5.3.1 Membrane characterization

Fig. 5.3 illustrates FESEM images of the ceramic membrane prepared in this study, which reveal that the membrane surface is devoid of without any pinhole cracks or defects. It is reported that ceramic membrane sintered at a low temperature exhibits a porous structure, whereas, at a high sintering temperature, the particles tend to agglomerate, resulting in a highly consolidated ceramic body (Kumar et al., 2019). It is worth mentioning here that in the process of sintering, firstly, the contact between the particles increases and bridging of particle takes place through neck formation and grain growth (Diana et al., 2020). When the sintering temperature raises from 800 to 950 °C, the contact between particles increases further, causing a shrinkage and densification of the membrane. The entire process of necking, shrinkage and densification during the process of membrane sintering improves the membrane strength (Zou et al., 2019). In this study, a sintering temperature of 950 °C is thus found suitable for fabricating the membrane with good surface properties. EDX image of the membrane shown in Fig. 5.3c reveals the presence of different

elements present in the membrane, which are derived from the inorganic clay materials used as raw materials in preparing the membrane.

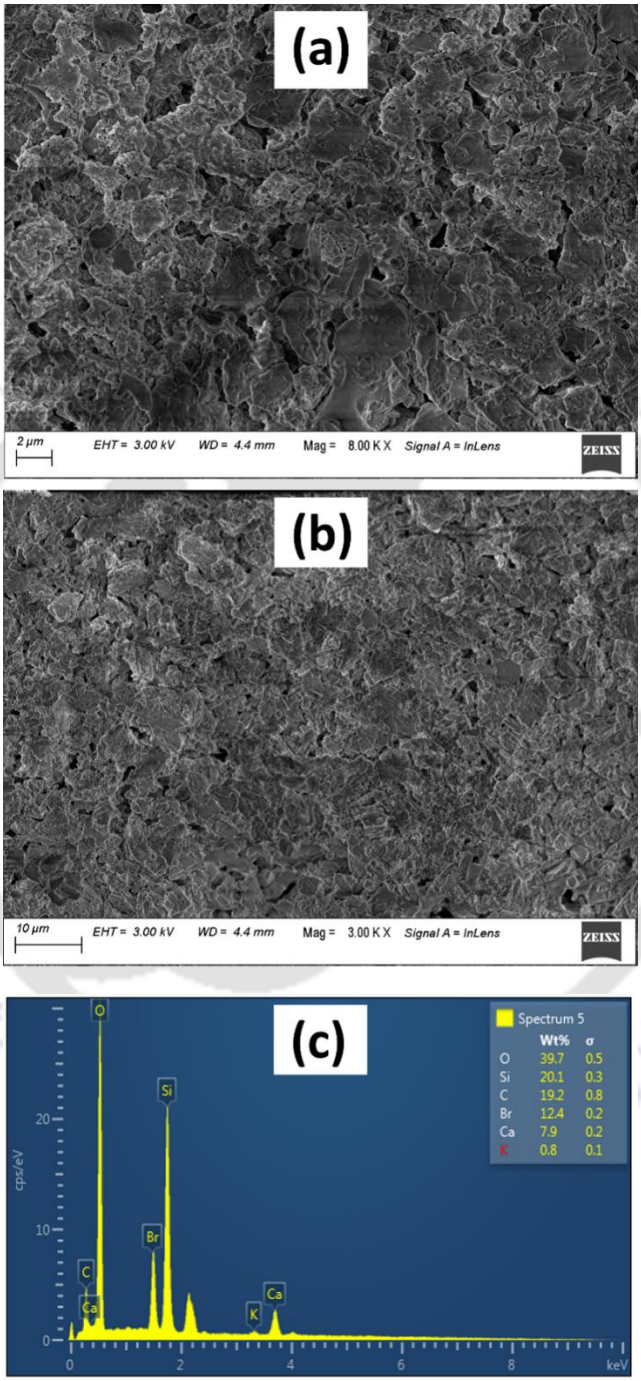

Fig. 5.3 (a-b) FESEM images showing the surface morphology of the membrane at different magnifications (8 K and 3 K), and (c) EDX image showing elements present in the membrane.

The FESEM images were further analyzed for pore size distribution and average pore diameter of the membrane using ImageJ™ software (open source software provided by the National Institute of Health (NIH), weblink: http://rsbweb.nih.gov/ij/download.html) (Fig. 5.3). A similar pore size distribution as reported by Vasanth et al. (2011) was obtained in this work, which confirms monodisperse nature of the prepared membrane; and a maximum number of pores (60–75%) were in size range 0.5 - 0.8 μm. The average pore size of the membrane was found to be 1.01 μm.

The chemical stability of the membrane was determined based on weight loss due to immersion in an acidic or alkaline solution. Two major observations were noticed from the results of this chemical stability test: the acidic solution resulted in a weight loss of around 5%, whereas the value was negligible in the alkali solution. These chemical stability results reveal that the membrane is highly resistant against both acidic and alkaline agents (Vasanth et al., 2011).

5.3.2 Pure water permeation test

From the results of the pure water permeation test, permeability (L_h) and average pore size of the membrane were determined using the following expression:

$$J_w = \frac{\varepsilon r^2 \Delta P}{8\mu\tau l} = L_h \Delta P \qquad (5.4)$$

where J_w represents liquid flux (m^3/m^2s), ΔP represents a change in trans-membrane pressure across the membrane (kPa), L_h represents hydraulic permeability, μ is viscosity of water (sPa), τ represents tortuosity factor, l represents pore length (m), which is taken as thickness of the membrane, ε is porosity of the membrane.

The pure water permeability, porosity, and the average pore diameter of the membrane were thus found to be 3.758 $\times 10^{-6}$ m/skPa, 40%, and 1 μm, respectively. Fig. 5.4 shows that water flux linearly correlates with the applied pressure, which is in accordance with the Darcy's rule. The

average pore diameter of the membrane calculated in this test also matches with the pore diameter obtained previously by FESEM analysis (Fig. 5.3).

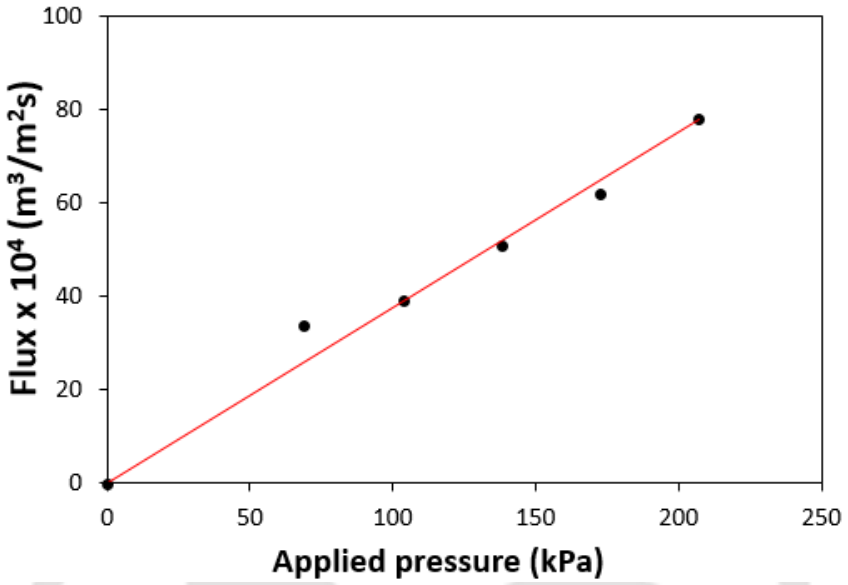

Fig. 5.4 Results of pure water permeability test with the membrane.

5.3.3 CuS NPs purification by microfiltration

Microfiltration to obtain pure CuS NPs from the bioprecipitate was carried out at a constant applied pressure of 172 kPa, which was found effective in avoiding blockage of pores and retention of EPS and bacteria on the membrane due to their large size as compared with the CuS NPs. SRBs are curved rod, cylindrical, or vibrio-shaped bacteria with a diameter of 2-3 µm (Kushkevych et al., 2019), and it is larger than the average pore size (1 µm) of the ceramic membrane used in this study. A similar result on the complete removal of *E. coli* from lysate solution is reported to be achieved by microfiltration, but using a polysulfone membrane (Karim et al., 2008).

Prior to the microfiltration experiment, the effect of different pretreatment methods was examined. Fig. 5.5 shows the effect of centrifugation and heating, bath sonication, and cell lysis using a French press on microfiltration to obtain pure CuS NPs.

A maximum CuS NPs purification efficiency of 32% was achieved by centrifugation at 12000 × g and subsequent heating at 60 °C. No significant change in the purification efficiency was observed beyond 20 min of centrifugation time followed by heating and microfiltration, whereas 21% pure CuS NPs were obtained by bath sonication for 20 min. In the case of cell lysis using a French press, purity of CuS NPs was 39% (Fig. 5.5).

Probe sonication as a pretreatment of the bioprecipitate was carried out for different time period, and the results are shown in Fig. 5.5. Very high purification efficiency of 92% is obtained for a sonication time of 90 min, and beyond which the value remained the same.

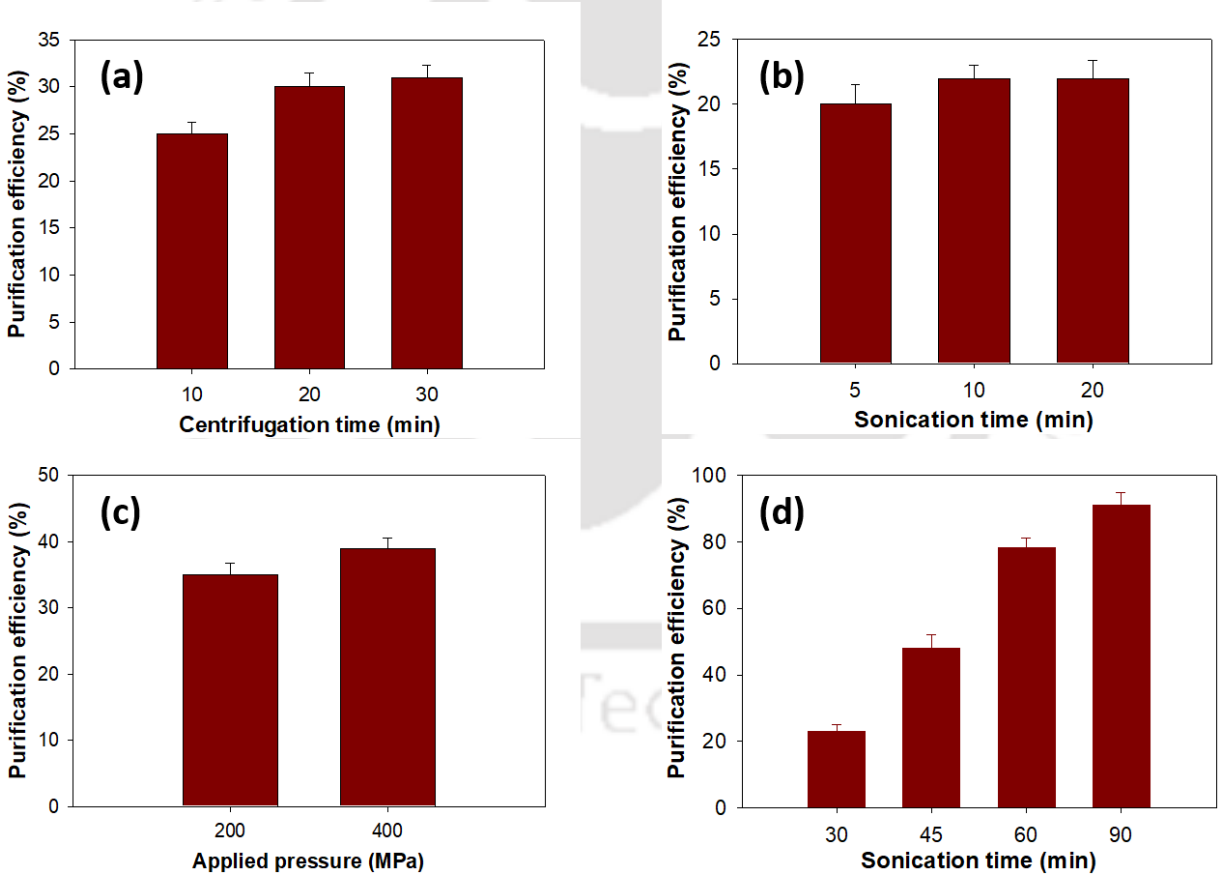

Fig. 5.5 Effect of different pretreatment techniques on CuS NPs purification: (a) centrifugation and heating, (b) bath sonication, (c) cell lysis and (d) probe sonication.

Hence, the best results were observed in the case of probe sonication, which was followed by cell lysis using a French press, centrifugation and heating, and bath sonication. Probe sonication involves high power ultrasound in a liquid medium and causes cavitation, which resulted in the release of CuS NPs from SRB and EPS for easy separation by microfiltration (Yang et al., 2019). Compared with probe sonication, bath sonication uses low power ultrasound, which did not yield a high separation efficiency of the CuS NPs.

In a recent study by Estay et al. (2021), a monotubular ceramic membrane was used for purifying chemically synthesized CuS NPs. As the chemically synthesized nanoparticles were free from biomass or any other compressible solids as impurities, a very high purification efficiency (100%) reported in the study is likely. As compared with this report, pretreatment of the biologically synthesized CuS NPs is found to be essential in the present work for obtaining it in a pure form.

It is reported that for heavy metal removal by sulfide precipitation, SRB secretes EPS in the form of a layer around the bacterial cell wall and onto which CuS NPs attach (Kiran et al., 2016). EPS is characterized as a gum kind of layer around the bacteria and comprises protein, carbohydrate, and amino acids (Sardar et al., 2018). EPS is also secreted into the medium by the bacterium in defense against metal toxicity (Gupta et al., 2017). Fig. 5.6 shows FETEM images of the bioprecipitate before pretreatment by probe sonication, which clearly shows CuS NPs attached to EPS around the cell wall of SRB as well as some of the nanoparticles in free form. Based on the results obtained in this study, a schematic showing mechanism of CuS NPs purification by probe sonication and microfiltration is depicted in Fig. 5.7.

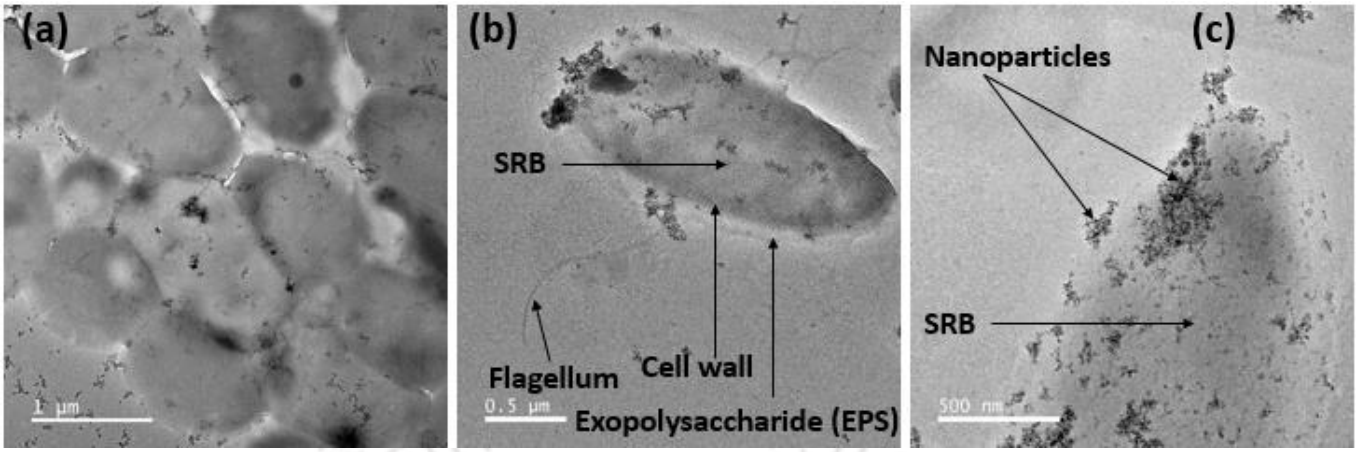

Fig. 5.6 FETEM images of the bioprecipitate showing: (a) SRB, (b) SRB with EPS around the cell surface and (c) CuS NPs attached to EPS.

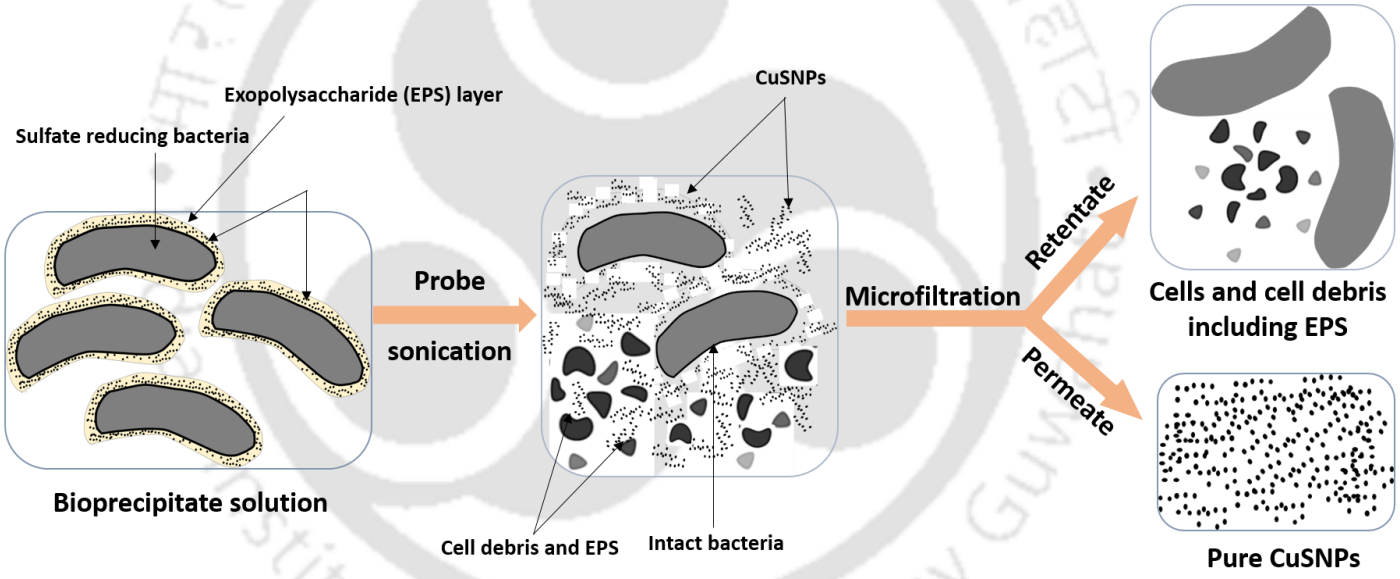

Fig. 5.7 Schematic showing the mechanism involved in CuS NPs purification by probe sonication and microfiltration.

Microfiltration of suspension containing bacteria and nanoparticles by using ceramic membrane is very limited. Table 5.1 compares microfiltration performance of different membranes reported in the literature with the membrane used in this study. *Escherichia coli* was successfully separated from water using a ceramic membrane (Vasanth et al., 2011). In another study, Karim et al. (2008)

used hollow fibre commercial polysulfone membrane and achieved 100% retention of bacteria cells. Similarly, Mwabi et al. (2012) used a commercially available ceramic filter to remove bacterial cells. Hence, it could be said that the indigenous ceramic membrane used in this work, which was prepared using cheap substrates, is competitive in term of its performance as compared with polymeric or other ceramic membranes reported in the literature.

Table 5.1 Comparison of performance of the indigenous ceramic membrane with those reported in the literature

Membrane type	**Pore size (µm)**	**Permeability (L/m^2sPa)**	**Separation/ Rejection (%)**	**Reference**
Kaolin, β-Quartz, $CaCO_3$ (flat membrane)	1.3	6.38×10^{-7}	85	Vasanth et al., 2011
Hollow fibre commercial poly sulfone membrane	0.1	NA (Not available)	100	Karim et al., 2008
Commercial ceramic filter (Headstream Water Holdings)	0.2	NA	99-100	Mwabi et al., 2012
Monotubular ceramic membrane	1.4	9.2×10^{-6}	99.9	Estay et al., 2021
Polypropylene, cellulose diacetate, and polycarbonate hollow fibre membranes	0.2 and 0.4	NA	100	Suchecka et al., 2003
Kaolin, ball clay, quartz, calcium carbonate, feldspar, and pyrophyllite (flat membrane)	1.0	3.758×10^{-6}	92	This study

5.3.4 Characterization of CuS NPs

FTIR spectra shown in Fig. 5.8 reveal the presence of hydroxyl group (-OH), represented by the band present at 3000-3600 cm^{-1} in the bioprecipitate (before microfiltration), and the peak was nearly absent in case of the pure CuS NPs. The band at 1050 cm^{-1} shows the presence of sulfate group (SO_4^{2-}) in the bioprecipitate, indicating that the CuS NPs were formed due to sulfate reduction by SRB (Kiran et al., 2016). The bands at 1500-1580 $cm^{-1,}$ and 1600-1700 cm^{-1} reveal the presence of amide (-NH) and carboxyl (-C=O) groups in the bioprecipitate, which were absent in the spectra of pure CuS NPs (Kiran et al., 2017). The bands at 1107 cm^{-1} and 618 cm^{-1} indicate the presence of Cu-S bond (Liang et al., 2018). These results of FTIR analysis confirms the purity of CuS NPs as compared with the crude bioprecipitate.

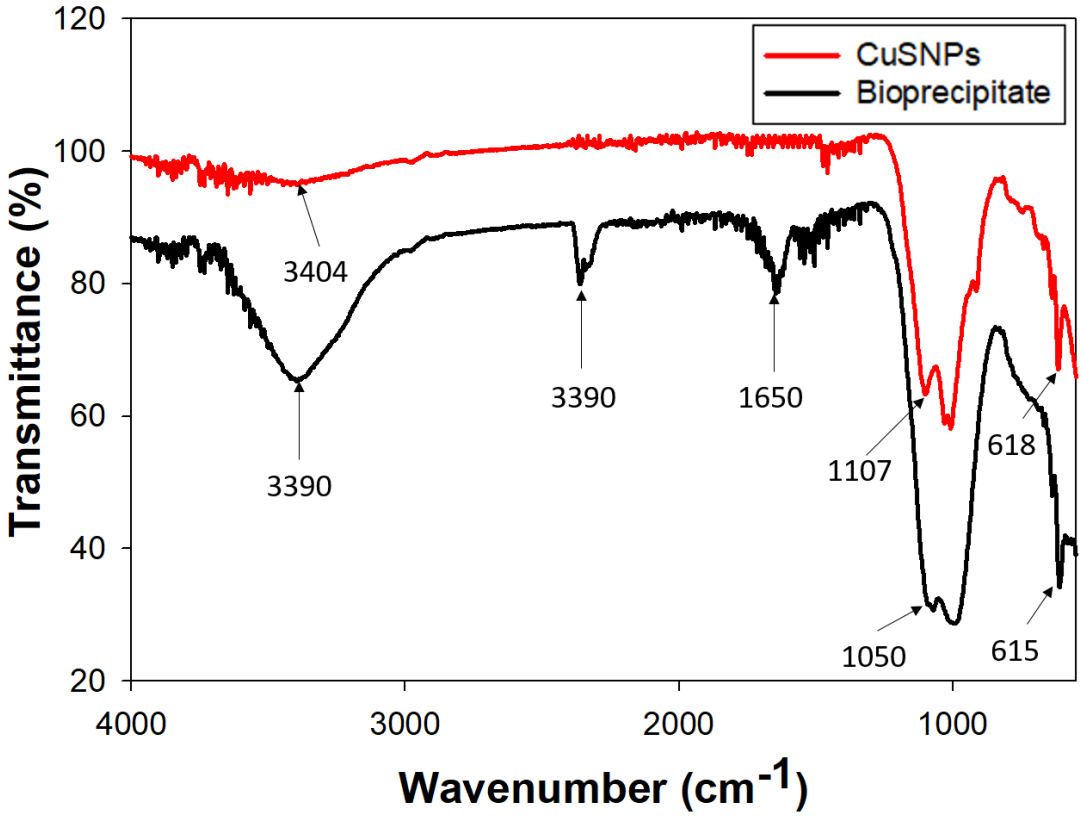

Fig. 5.8 FTIR spectra of crude bioprecipitate and pure CuS NPs.

Fig. 5.9 shows the FETEM images of CuS NPs obtained by microfiltration of the bioprecipitate, which confirm the spherical shape of the nanoparticles. Whereas the average size of the nanoparticles was determined to be 5-10 nm by size-distribution analysis, elemental analysis using EDS confirmed the presence of pure elemental copper in the nanoparticles (Fig. 5.9c). Polycrystalline nature of the nanoparticles present in the permeate was further verified by the selected area electron diffraction (SAED) pattern as depicted in Fig. 5.9a (right side top panel).

Furthermore, the FETEM and FESEM images confirmed the absence of any impurities such as debris in the CuS NPs.

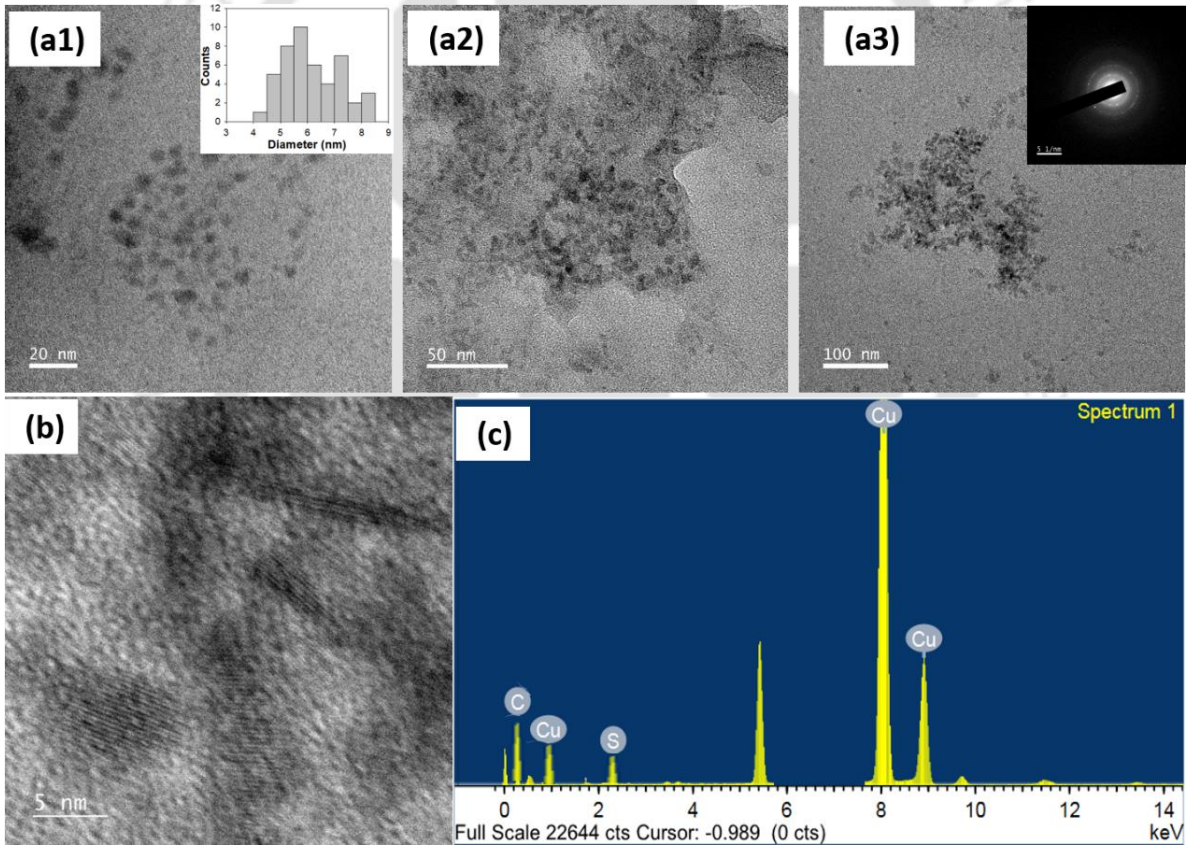

Fig. 5.9 (a) FETEM images at 20, 50 and 100 nm resolutions (particle size distribution and SAED pattern are shown as insert to a1 and a3) (b) high resolution TEM image and (c) EDS spectra of CuS NPs.

Crystallinity, surface condition, and homogeneity of CuS NPs were analyzed by Raman spectroscopy analysis. In general, crystallinity of a sample is identified by a sharp peak, whereas amorphous or polycrystalline samples yield broad Raman peaks. Raman spectrum presented in Fig. 5.10a shows a broad peak at 472.6 cm^{-1}, which characterizes the S-S stretching mode of S_2 ions at 4e sites of the CuS NPs (Chaki et al., 2014; Yadav et al., 2019).

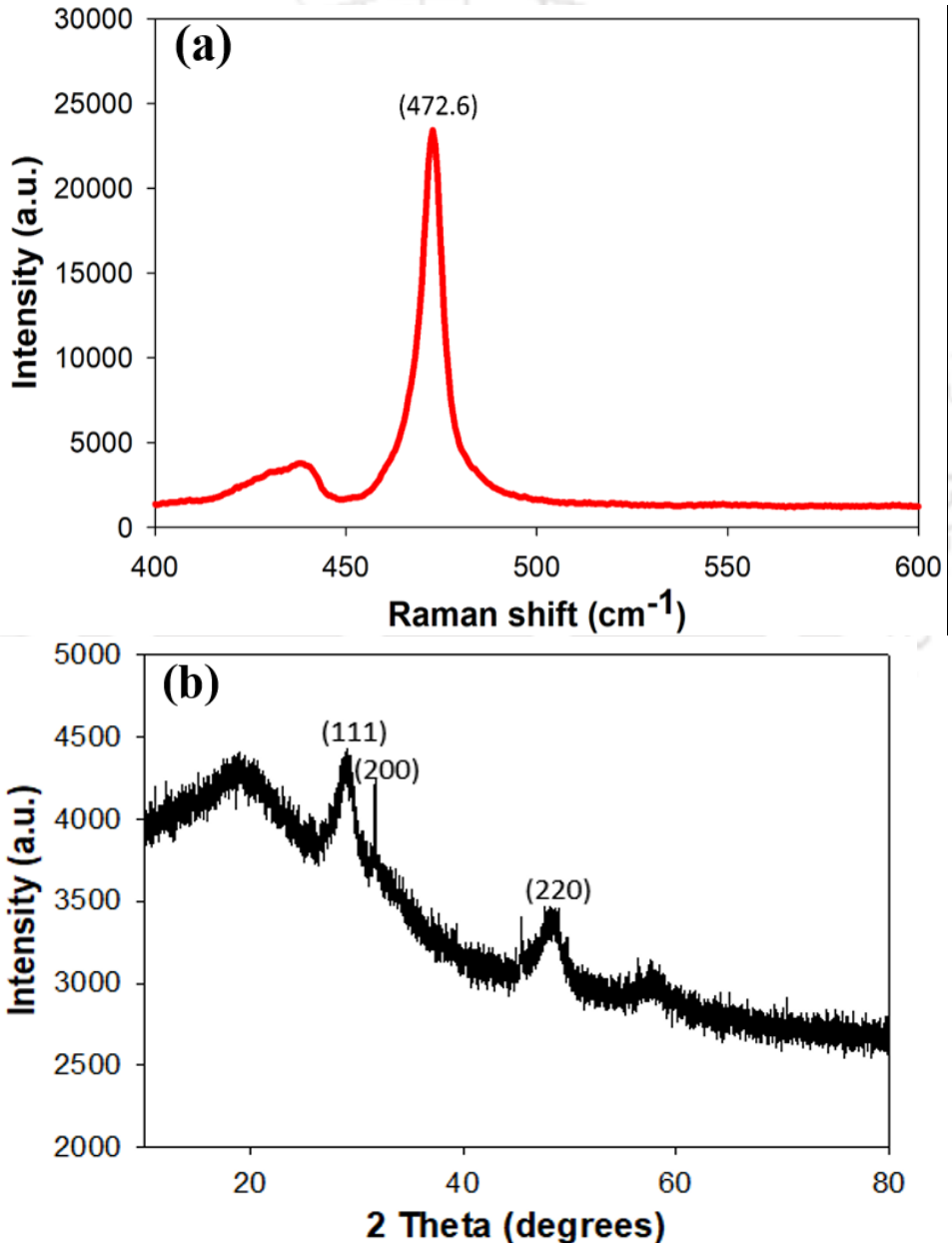

Fig. 5.10 (a) Raman spectrum and **(b)** XRD pattern of CuS NPs.

Fig. 5.10(b) shows X-ray diffraction (XRD) pattern of CuS NPs. The diffraction peaks at 2θ values of 26°, 31.7°, 45.6° correspond to different lines formed by (111), (200) and (220) planes and are ascribed to those of cubic CuS (JCPDS no. 04-0836). The diffraction peaks of the XRD pattern indicate the crystalline nature of CuS NPs (Nezamifar et al., 2015). All these results further confirm that the CuS NPs were obtained in pure polycrystalline form from AMD.

5.4 Analysis of membrane cost for CuS NPs purification

Table 5.2 presents the detailed manufacturing cost analysis of the ceramic membrane prepared in this study. The ceramic membrane manufacturing cost was assessed based on preliminary economic evaluation at the research level (Winter et al., 1969). The actual manufacturing cost can be calculated by adding all direct and indirect costs involved in manufacturing the membrane. The direct manufacturing costs include the cost of raw materials, electricity, labor, maintenance, and laboratory. The raw material cost is assessed by the sum of the costs due to different individual raw materials used to prepare the membrane. Labor cost is calculated based on the number of persons involved and man-hour per day. The maintenance cost is evaluated as 1% of the capital cost, and the laboratory cost is evaluated as 20% of the labor cost (Liang et al., 2018). The indirect manufacturing cost (capital cost), counting with the depreciation cost, is calculated using a straight-line method. Thus, the total manufacturing cost of the prepared ceramic membrane is estimated to be 1.0 \$/membrane (or 160 \$/m^2). As compared with this study, the cost of α-alumina membrane tubes (1–6 μm pore size) is \$500/$m^{2,}$ and that of stainless steel asymmetric membrane is \$3000/m^2 (Kumar et al., 2015). The reason for the high industrial cost of the symmetric tubular membrane is because of the highly expensive α-alumina and complex process involved in preparing the membrane.

Table 5.2 Manufacturing cost analysis of the fabricated ceramic membrane

Items	**Calculation for preparing hundred membranes**				**US$**
Direct manufacturing cost					
Raw materials	Raw materials	Unit price (US$/kg)	Amount of materials utilized (g)	Cost (US$)	
	Kaolin	0.096	216.7	0.020	
	Ball clay	0.055	263.7	0.014	
	Feldspar	0.069	84.0	0.006	
	Quartz	0.14	398.9	0.056	
	Calcium carbonate	3.43	257.1	0.882	
	Pyrophyllite	0.082	220.9	0.020	
			Total cost of raw materials:		1.0
Labor (including supervisory)	Labor cost = cost × total h = 6.8 × 8				54.4
Electricity	Furnace: 48 h × 4 kW = 192 kWh 192 × US$ 0.12		= 23.04		
	Mixer grinder: 0.17 h × 0.75 kW = 0.13 kWh 0.13 × US$ 0.12		= 0.02		
	Hot air oven: 24 h × 2.4 kW = 57.6 kWh 57.6 × US$ 0.12		= 6.91		
	Ultrasonicator: 0.25 h × 2 kW = 0.5 kWh 0.5 × US$ 0.12		= 0.06		

	Hydraulic press: 3.33 h × 1.49 kW = 4.96 kWh 4.96 × US$ 0.12 = 0.60 Total electricity cost:	30.63
Maintenance	Maintenance cost = (Capital cost × 1%)/day Mixer grinder = 34 Hydraulic press = 1364 Hot air oven = 546 Furnace = 2200 Ultrasonicator = 350 Capital cost = 4494 Total maintenance cost:	0.13
Laboratory	Laboratory cost = 20% of labor cost Laboratory cost:	10.88
Indirect manufacturing costs:		
Depreciation	Calculated by straight line method, $d = \frac{V - V_s}{n}$ where, d - annual depreciation cost, V - original cost, V_s - Salvage cost, n - service life.	0.50
Total manufacturing costs	Direct manufacturing costs + Indirect manufacturing costs	97.54
	Estimated manufacturing cost for one membrane	0.98
	Estimated manufacturing cost for one membrane (Round off value):	US$ 1

The presented values of the cost of the membrane prepared in this study are conceptual in nature and depend on factors such as (1) fouling characteristics, (2) working time period, and (3) durability of the ceramic membrane for industrial application. Hence, the ceramic membrane used in this study is not only less expensive in comparison with the alumina-based membranes but also offers excellent industrial application potential, as demonstrated in this study for the purification of biogenic CuS NPs.

5.5 Significant findings

Pure CuS NPs were prepared from synthetic AMD by biological sulfate reduction and microfiltration using indigenous low-cost ceramic membrane. Pretreatment using probe sonication was found effective in releasing the CuS NPs from contaminating impurities for an efficient purification of the nanoparticles. Excellent characteristics of the CuS NPs in terms of crystallinity, size, shape and purity established its potential industrial application. Porosity, pore size distribution, water permeability, resistance against acidic and alkaline solution as well as low-cost of the indigenously prepared ceramic membrane further established its application for potential use for large-scale purification of CuS NPs from AMD and for other industrial use.

Chapter 6

Synthesis and characterization of biogenic metal nanopowder from wastewater for dye removal application

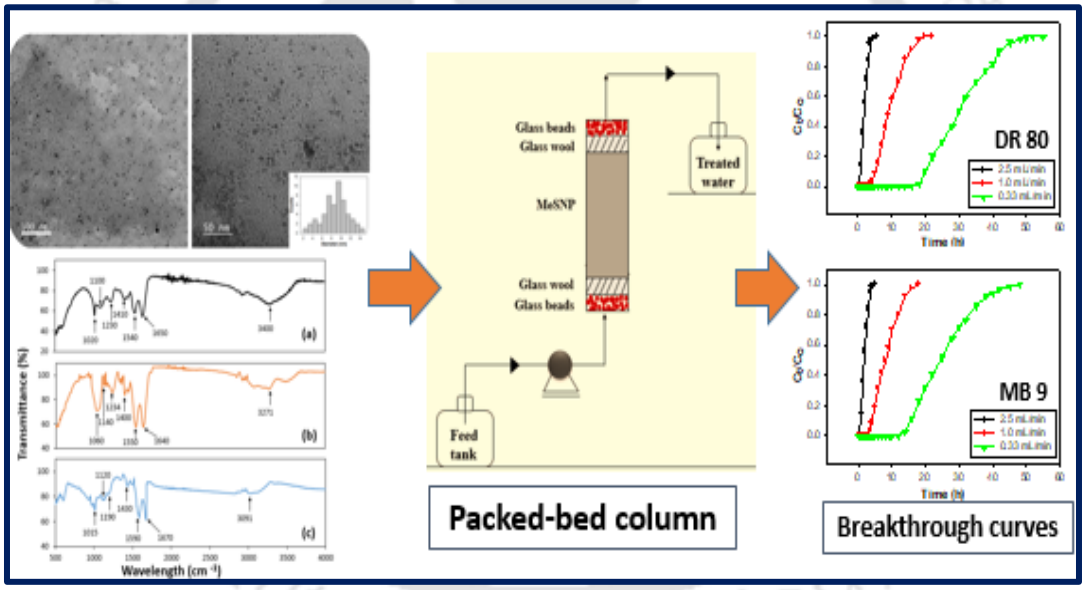

ABSTRACT

A novel adsorbent based on biogenic metal sulfide nanoparticles (MeSNPs) was synthesized from metallic wastewater and examined for azo dyes removal from aqueous solution in batch and continuous systems. The size of the MeSNPs was in the range of 8-10 nm, with an average specific surface area of 120.4 m^2/g. Batch adsorption study was initially carried out using Direct Red 80 and Mordant Blue 9 as the model azo dyes by varying MeSNPs dosage, contact time, pH, and initial dye concentration. More than 99% removal efficiency of both the dyes was achieved by using MeSNPs at the following optimum conditions: 200 mg dosage, pH 2, 6 min contact time, and 100 mg/L initial dye concentration. The batch sorption isotherm results were described using the non-linear Sips model, and the maximum predicted capacity values of 143.7 and 198.3 mg of dye per gram of adsorbent for DR 80 and MB 9, respectively were obtained using the model. Besides, the sorption kinetic data for both the dyes followed the pseudo-second-order rate model. Furthermore, maximum desorption efficiency values of 93% for DR 80 and 97% for MB 9 were achieved using an aqueous solution of pH 12, thus indicating that the adsorbent can be regenerated and reused further. Dynamic adsorption of the dyes was studied using a fixed-bed column with the MeSNPs and as a function of liquid flow rates. The results showed an increase in breakthrough time with a decline in the flow rates for both DR 80 and MB 9. The breakthrough behavior of the dyes was explained using Thomas, Clark, and Yoon-Nelson models.

6.1 Introduction

Around 700,000 – 800,000 tons of dyes of almost 10,000 different varieties are produced annually (Samsami et al., 2020). Classification of dyes is based on the origin of dye material used, type of chromophores present, and application method. Chromophores are the group of atoms responsible for color, and the most important chromophores present in dyes are azo, anthraquinone, indigo, nitro, nitroso, and triarylmethane. Chromophore strongly attaches to fiber through auxochorme via a chemical bond. Examples of the most significant chromophores are: carbonyls, nitrile, esters, ethylene, acetylene, and acids, and chromogen are the compounds which bear them (Kumar et al., 2018). Among the different chromophores, azo (70%) and anthraquinone (15%) are the largest classes of dyes. Azo dyes are organic compounds containing R-N=N-R′ linkage and are widely used in the textile, leather, and food industries. On the other hand, azo dyes are highly mutagenic and carcinogenic, and their presence in the environment can lead to various adverse effects on humans and other life forms (Dai et al., 2018). Moreover, industries involved in the manufacture of paper, dyestuffs, textile, plastic, etc., are known to discharge colored wastewater with a high content of chemical oxygen demand (COD). Color due to dyes present in the wastewater is unaffected by temperature, light, and other environmental conditions and therefore recalcitrant against treatment (Ghaedi et al., 2015; Kumar et al., 2018). Hence, proper choice of treatment of dye containing wastewater is essential before its release into the environment.

Various physicochemical and biological methods such as biodegradation, ion exchange, Fenton oxidation, adsorption, etc., have been examined to treat dye containing wastewater (Samsami et al., 2020). Among these methods, adsorption is used widely to treat colored wastewater because of its high efficiency and easy operation (Samsami et al., 2020). Different types of natural as well as synthetic adsorbents have been used to treat colored wastewater. Among the different

adsorbents, agricultural waste, fly ash, and activated carbon have been extensively studied and used to treat dye containing wastewater; in particular, activated carbon is the most thoroughly investigated adsorbent. However, these conventional adsorbents have one or more drawbacks, including high cost and difficulty to reuse, which restrict their use, particularly for large-scale applications (Yu et al., 2020). Hence, adsorbents that are both efficient and low cost are of recent interest. In this context, nano sized materials have emerged as the best alternative due to their several advantages, such as small diameter, large specific surface area, and high reactivity. Different nanomaterials have been reported to remove pollutants from various kinds of wastewater, including for dye removal (Singh et al., 2020). However, there is no study reported yet on biofabricated nano materials for dye removal. Moreover, preparation cost of such nano biosorbent can be kept low if waste residue or biomass can be used as the starting material. Hence, this study focused on biogenic metal sulfide nanoparticles (MeSNPs) obtained by biological sulfate reduction of metallic wastewater for dye removal application. Biological sulfide precipitation of metal produces highly insoluble bioprecipitate containing metal sulfide in nano form.

The MeSNPs used in this study comprised of six different metal sulfides, i.e., zinc sulfide (ZnS), iron sulfide (FeS), copper sulfide (CuS), lead sulfide (PbS), cadmium sulfide (CdS), and nickel sulfide (NiS), and synthesized by sulfide precipitation from wastewater using sulfate reducing bacteria. The azo dyes Direct Red 80 (DR 80) and Mordant Blue 9 (MB 9) were tested for their removal using the nanopowder as there is no report available on their removal using such biogenic MeSNPs (Table 6.1). Effect of different factors, e.g., initial dye concentration, contact time, solution pH, and nanoparticle dosage on the removal of DR 80 and MB 9 were studied, followed by the analysis of the dye sorption isotherm and kinetics. Dynamic removal of DR 80 and MB 9 by the MeSNPs was conducted using a fixed-bed column operated at different flow rates, and the

breakthrough curve behavior was described by suitable models reported in the literature for a better understanding of the process.

Table 6.1 Literature reports on removal of DR 80 and MB 9 by adsorption

Dye	Adsorbents	Condition	Adsorption capacity (q_{max}) (mg/g)	References
DR 80	Soy meal hull	20 ºC, pH 2	178.57	Arami et al., 2006
DR 80	Orange peel	25 ºC	21.05	Arami et al., 2005
DR 80	Mixture almond shell	20 ºC	22.42	Ardejani et al., 2007
DR 80	MeSNPs	25 ºC, pH 2	143.7	This work
MB 9	Activated carbon (Panreac-Ox)	30 ºC	93.00	Martins et al., 2015
MB 9	Fenton-activated persulfate	25 ºC	Not available (NA)	Pervez et al., 2019
MB 9	MeSNPs	25 ºC, pH 2	198.3	This work

6.2 Materials and methods

6.2.1 DR 80 and MB 9

The azo dyes DR 80 and MB 9 were procured from Sigma Chemicals (St. Louis, MO, USA); their chemical structure and other properties are presented in Table 6.2. Stock solutions of the dyes (1 g/L each) were prepared using double distilled water, and suitably diluted to a desired concentration in the sorption experiments. Initial pH of the dye solution was adjusted to a desired value using 1 N hydrochloride acid or 1 N sodium hydroxide solution.

Table 6.2 Molecular structure and properties of the azo dyes used in this study

Properties	**DR 80**	**MB 9**
Chemical formula	$C_{45}H_{26}N_{10}Na_6O_{21}S_6$	$C_{16}H_9ClN_2Na_2O_8S_2$
C.I number	35780	14855
Molecular mass	1373.07	502.81
λ_{max} (nm)	528	516
Molecular structure	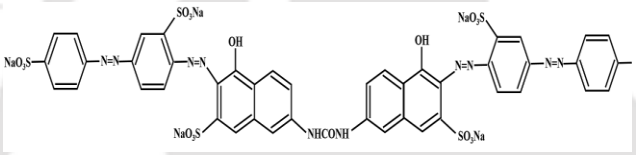	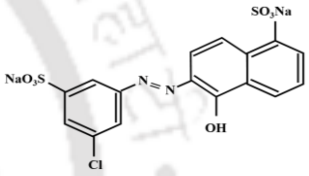

6.2.2 Synthesis and characterization of biogenic MeSNPs

The MeSNPs used in this study were obtained from synthetic sulfate rich, heavy metal containing wastewater by anaerobic sulfate reduction process as detailed earlier in Chapter 3. The synthetic wastewater consisted of six different metals, i.e. copper (Cu) (25 mg/L), cadmium (Cd) (5 mg/L), iron (Fe) (50 mg/L), nickel (Ni) (5 mg/L), lead (Pb) (5 mg/L) and zinc (Zn) (5 mg/L).

For MeSNPs formation, SRB secretes exopolysaccharide (EPS) around the cell wall, and metal ions in solution bind with anionic functional groups present in the EPS. Thus, the EPS functions as the nucleation site for metal ions to get deposited in forming the MeSNPs. After a certain incubation period, the bioprecipitate containing sulfide of different metals was centrifuged and

washed thrice to remove media salts and other impurities, which was followed by drying to remove excess water. The MeSNPs were further characterized before use in the dye removal experiments. Fig. 6.1 shows the various steps involved in the synthesis of MeSNPs.

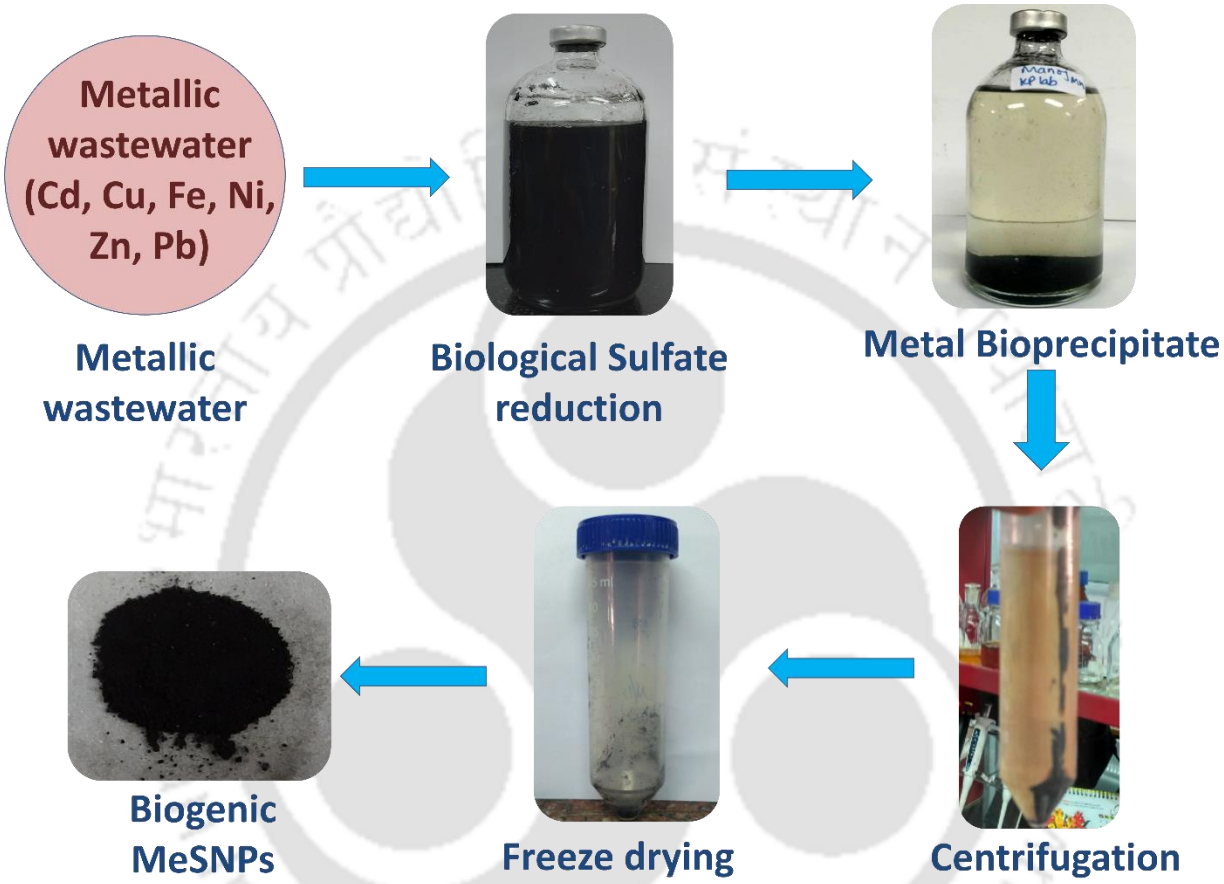

Fig. 6.1 Synthesis of biogenic MeSNPs by sulfide precipitation.

The biogenic MeSNPs were characterized by field emission scanning electron microscopy-energy dispersive X-ray (FESEM-EDX), Fourier-transform infrared spectroscopy (FTIR), field emission transmission electron microscopy (FETEM), zeta potential, X-ray diffraction (XRD) and Brunauer–Emmett–Teller (BET) surface area analysis.

The sample preparation and sample analysis details for FTIR and FETEM are the same as described earlier in Chapter 3. The Zeta potential of MeSNPs was measured by Litesizer-500

(Anton-Paar, Austria). The specific surface area of MeSNPs was measured using a Brunauer–Emmett–Teller (BET) surface area analyzer (Autosorb-IQ MP, Quantachrome) by nitrogen sorption method. XRD analysis was carried out by using a rotating anode based powder XRD (Rigaku TTRAX III, 18 kW, Japan) after drying the sample at 110 °C and then grinding it into powder form.

6.2.3 Batch adsorption experiments

The effect of different sorption parameters, viz. initial dye concentration, solution pH, incubation time, and MeSNPs dosage, was studied by varying the levels of the parameters one at a time and by keeping the other parameters at a constant level. All the batch adsorption tests were done in triplicate. The examined values of the different variables were as follows: contact time (1–30 min), initial dye concentration (50–300 mg/L), MeSNPs dosage (25–1000 mg), and solution pH (2–12).

Batch experiments on dye removal by adsorption using MeSNPs were conducted using 250 mL Erlenmeyer flasks. The test was conducted for each model dye by adding MeSNPs to 100 mL of dye containing solution, and the mixture was incubated at a constant temperature (25 ± 2 ºC) in an orbital shaker incubator maintained at 200 rpm. Following adsorption, the dye loaded MeSNPs were collected by centrifugation, and the supernatant obtained was analyzed for the residual dye concentration by using a UV–vis spectrophotometer (Antech, Ireland) at their respective $\boldsymbol{\lambda}_{max}$ values (Table 6.2). A standard graph plotted between absobance and dye concentration was used to determine the sample dye concentration in the experiments.

Dye removal percentage was calculated using the following expression:

$$\text{Dye removal (\%)} = \frac{C_0 - C_f}{C_0} \times 100 \qquad (6.1)$$

Where, C_0 and C_f are the initial and final dye concentrations (mg/L), respectively.

6.2.4 Adsorption isotherm

Utmost importance to any sorption process is the interaction of adsorbent and adsorbate, which can be explained by adsorption isotherm (Samsami et al., 2020). Isotherm relates equilibrium concentration of adsorbate in liquid phase and solid phase at a constant temperature. The three most commonly known isotherm models viz. Langmuir, Freundlich, and Sips models were applied to determine the dye sorption in this study.

For analyzing adsorption isotherm of DR 80 and MB 9, different concentration of the dyes in the range 50-300 mg/L in water (100 mL) were taken in Erlenmeyer flasks and then added with 200 mg MeSNPs. The flasks were incubated at constant room temperature (25-27 ºC) in an orbital shaker incubator for 48 h to attain equilibrium, and residual dye concentration at the end of the experiment was determined. The following equation was used to calculate the amount of dye adsorbed:

$$q_e = \frac{(C_0 - C_e)V}{m} \qquad (6.2)$$

where, q_e is the amount of dye adsorbed onto MeSNPs (mg/g), C_0 is the initial dye concentration (mg/L), V is the volume of dye solution (L), Ce is the equilibrium dye concentration (mg/L), and m is the mass (g) of dry MeSNPs added (Letterman et al., 1999).

Langmuir isotherm is based on a single solute system, and its adsorption is limited to a single molecular layer onto the outer surface of an adsorbent. It also assumes that adsorption occurs at specific sites on the adsorbent, and there is no interaction between the adsorbed molecules. Langmuir isotherm can be described using the following linearized expression (Langmuir et al., 1918):

$$\frac{C_e}{q_e} = \frac{1}{q_m K_L} + \frac{C_e}{q_m} \quad (6.3)$$

Where, q_m represents maximum quantity (mg/g) of dye that can be adsorbed on the monolayer surface of the adsorbent, K_L represents Langmuir adsorption constant (L/mg) which also defines the affinity of dye to the adsorbent.

The Freundlich model (Freundlich et al., 1906) can be expressed as follows:

$$\log q_e = \log K_F + \frac{1}{n} \log C_e \quad (6.4)$$

where, the exponent n refers to the sorption intensity; K_F is a constant (L/mg) and represents the adsorption affinity.

The Sips model is a combined form of the Langmuir and Freundlich models (Dotto et al., 2012):

$$q_e = \frac{q_m k_s C_e^{\frac{1}{n}}}{1 + k_s C_e^{\frac{1}{n}}} \quad (6.5)$$

where k_s is the Sips equilibrium constant (L/mg), q_m represents Sips maximum adsorption capacity (mg/g), and n is an exponent in the Sips model.

6.2.5 Adsorption kinetics

Dye sorption kinetics by MeSNPs in this study was examined by varying the contact time from 1 to 30 min, and keeping the initial dye concentration, pH and MeSNPs dosage in the experiments fixed at 100 mg/L, 2.0 and 200 mg, respectively.

Data obtained was fitted to pseudo first-order rate and pseudo second order rate kinetics models (Ho et al., 1999). The pseudo-first order rate is expressed as follows:

$$\frac{dq_t}{dt} = k_1(q_e - q_t) \quad (6.6)$$

Where, k_1 is the pseudo-first order rate constant (1/min), q_e is the adsorption capacity at equilibrium (mg/g), q_t is the adsorption capacity at time t (mg/g).

The above equation can be integrated after applying the following initial and boundary conditions

$t = 0$, $q_t = 0$; $t = t$, $q_t = q_t$

$$\log (q_e - q_t) = \log q_e - \frac{k_1}{2.303} t \qquad (6.7)$$

The pseudo-first order rate constant (k_1) can be determined from a plot of log ($q_e - q_t$) vs. t.

The pseudo-second order rate kinetics for dye removal involves physicochemical interaction between adsorbent and adsorbate, and it can be expressed as follows:

$$\frac{dq}{dt} = k_2(q_e - q_t)^2 \qquad (6.8)$$

Integration of the above equation between the boundary conditions, $t = 0$, $q_t = 0$; $t = t$, $q_t = q_t$, gives:

$$\frac{t}{q_t} = \frac{1}{k_2 q_e^2} + \frac{t}{q_e} \qquad (6.9)$$

Where q_e is the amount of sorbate on the adsorbent surface at equilibrium (mg/g), k_2 is the pseudo-second order rate constant (g/mg/min), q_t is the amount of sorbate on the adsorbent surface at time t (mg/g). The pseudo-second order rate constant (k_2) is determined from the intercept of a linear plot of t/q_t against t.

6.2.6 Dye desorption test

To test the potential reuse of MeSNPs following dye adsorption, dye loaded MeSNPs from a batch adsorption experiment, performed earlier with an initial dye concentration of 100 mg/L, was

separated from its mixture by centrifugation and then treated with water of different pH ranging from 2 to 12. The amount of dye desorbed was assessed as described earlier in Section 6.2.3.

6.2.7 Continuous dye removal experiments

Continuous removal of DR 80 and MB 9 by adsorption using MeSNPs was assessed using a glass column with an inner diameter of 10 mm and a column height of 120 mm, as shown in Fig. 6.2. A desired amount of MeSNPs were packed between glass wool and glass beads in the column to hold the adsorbent in place. Individual DR 80 and MB 9 dye containing solutions of certain initial concentration were fed through the fixed-bed column by means of a peristaltic pump operated at different speeds in order to study the influence of 0.33 mL/min, 1.0 mL/min and 2.5 mL/min flow rates on the dye adsorption process. The MeSNPs bed height (1 cm), inlet dye concentration (25 mg/L), and inlet solution pH 2.0 were the same in this column study for both DR 80 and MB 9.

The following expression was used to calculate the total quantity of dye (m_{total}) input to the column:

$$m_{total} = \frac{C_0 F t_{total}}{1000} \qquad (6.10)$$

Where C_0 represents inlet dye concentration (mg/L), F represents flow rate (mL/h), and t_{total} represents total time taken for the column to get saturated with the dye.

The following equation was used to estimate the amount of dye adsorbed into the column (Musah et al., 2020):

$$q_{total} = \frac{C_0 F}{1000} \times \left(t_{total} - \int_{t=0}^{t=t_{total}} \frac{C_t}{C_0} dt \right) \qquad (6.11)$$

where, t_{total} represents time for exhaustion of the adsorbent in the column. Dye removal percentage (Y) was calculated by dividing the total dye adsorbed (q_{total}) (mg) to the total quantity of dye loaded into the column (m_{total}) (mg) (Ravikumar et al., 2020):

$$Y\,(\%) = \frac{q_{total}}{m_{total}} \times 100 \qquad (6.12)$$

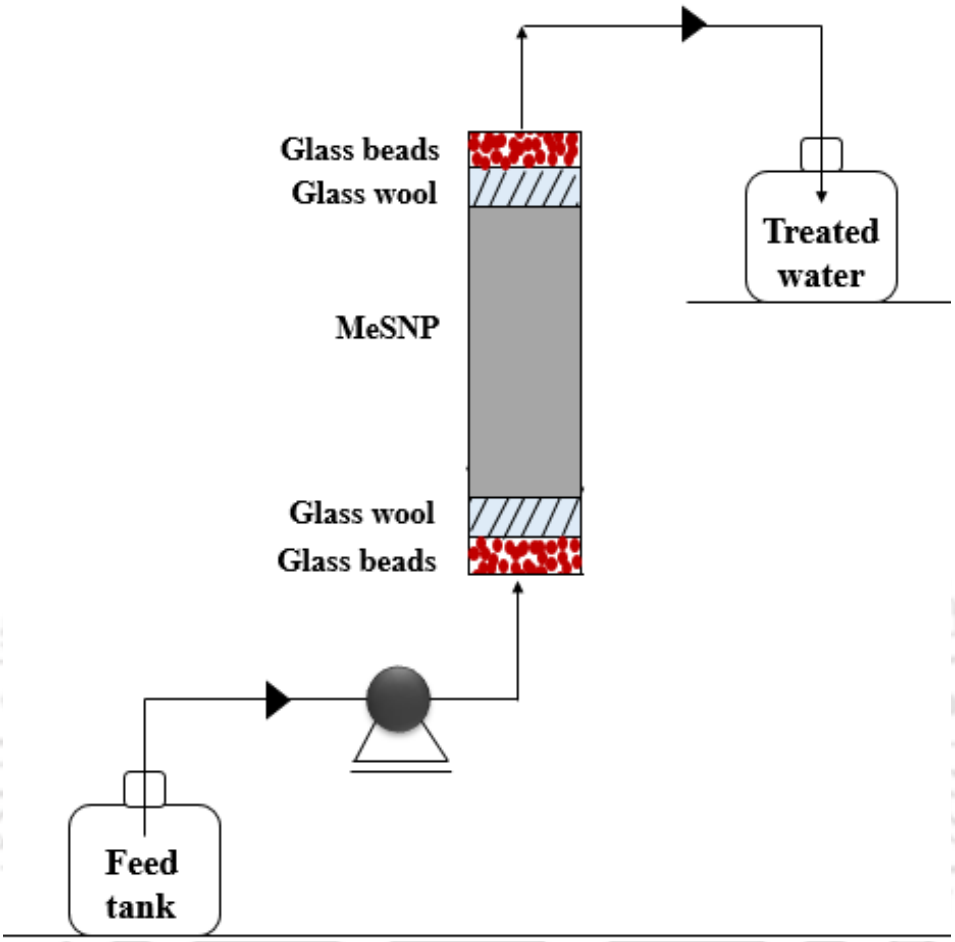

Fig. 6.2 Schematic of the fixed-bed column used for continuous dye adsorption by MeSNPs.

Maximum dye sorption capacity of the column ($q_{e(exp)}$) was calculated by the ratio of amount of dye adsorbed (q_{total}) (mg) to the amount of adsorbent used in the column (W) (g) (Ajmani et al., 2020).

$$q_{e(exp)} = \frac{q_{total}}{W} \qquad (6.13)$$

Regeneration of the dye loaded MeSNPs in the column was achieved by passing 2 M sodium hydroxide solution and analyzed for up to four continuous sorption-desorption cycles (Ajmani et al., 2020). The bed regeneration step in each cycle was performed by washing the bed with distilled

water until all the dye molecules were washed out of the column, and until the effluent pH reached 7.0. The following expression was used to calculate the regeneration efficiency (%) of the fixed-bed column in this study (Ajmani et al., 2020):

$$\text{Regeneration efficiency (\%)} = \frac{Q}{Q_0} \times 100 \qquad (6.14)$$

where, Q_0 and Q represent sorption efficiency (mg/g) of the adsorption column before and after each regeneration step.

6.3 Results and discussion

6.3.1 MeSNPs characterization

Surface morphology of the biogenic MeSNPs synthesized in this study was analyzed using FESEM and is shown in Fig. 6.3(a). EDX spectrum (Fig. 6.3b) of the biogenic MeSNPs reveals the presence of the different metals in the sample, whereas the sulfur peak shown in the EDX spectrum is attributed to the different metal sulfides present in the MeSNPs. Fig. 6.4 displays FETEM images of the MeSNPs, and its particle size distribution revealed that its size was in the range 8-10 nm.

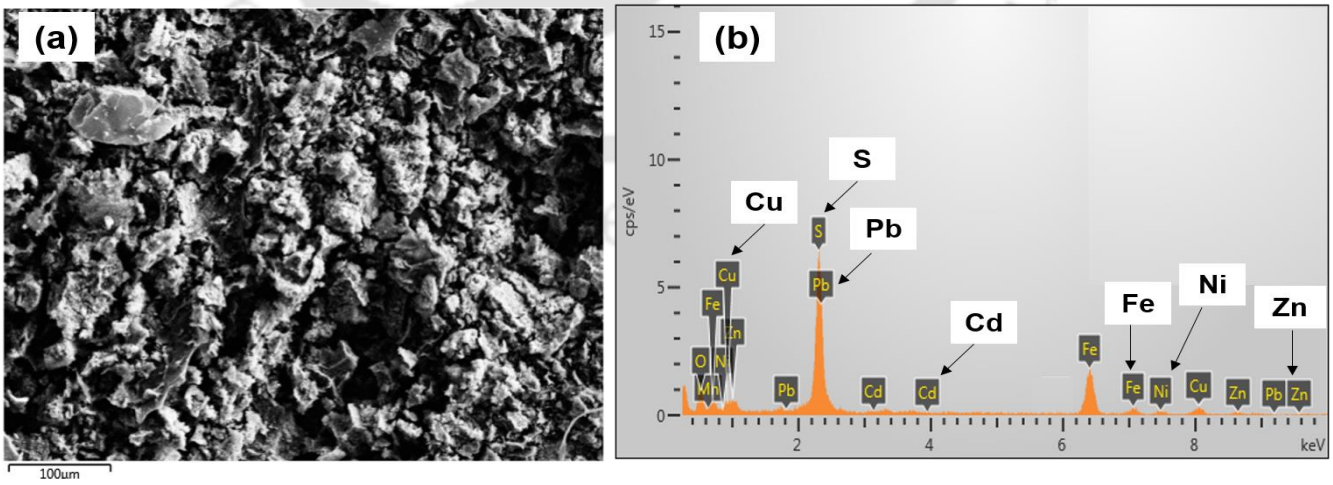

Fig. 6.3 (a) FESEM image and (b) FESEM-EDX spectra of MeSNPs.

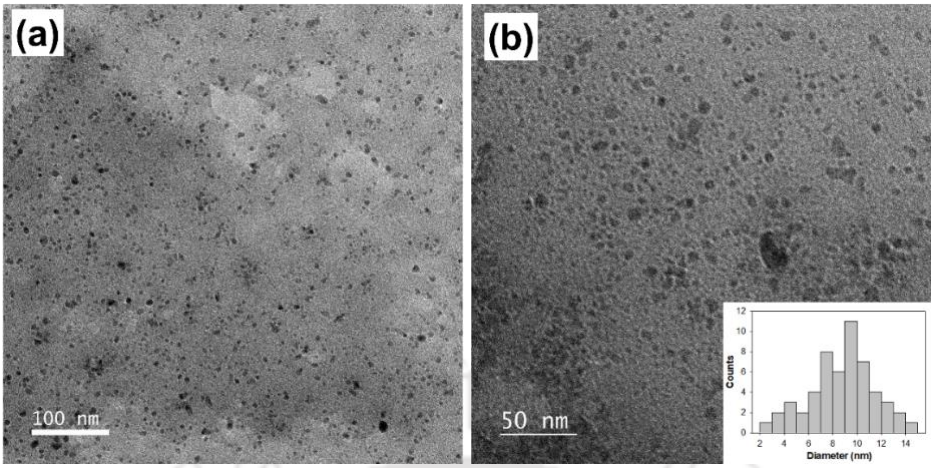

Fig. 6.4 FETEM images of MeSNPs at different resolutions (a) 100 nm (b) 50 nm. Particle size distribution is shown as an insert to Fig. 6.4(b).

Fig. 6.5(a) shows the FTIR spectrum of MeSNPs used for dye adsorption. For the FTIR analysis, the sample was scanned between 500 cm^{-1} and 4000 cm^{-1} wavelength to check the occurrence of different functional groups and diverse bonds responsible for the dye adsorption. The presence of hydroxyl group (-OH) can be confirmed by the band present at 3000-3600 cm^{-1}. The presence of sulfide group is indicated by the band present at 1020 cm^{-1} (Kiran et al., 2017). Bands stretched in the ranges 1500-1580 cm^{-1} and 1600 - 1700 cm^{-1} revealed the presence of amide group (-NH) and carboxyl group (-C=O), respectively (Arami et al., 2005). The peaks detected at 1410 cm^{-1}, 1230 cm^{-1}, and 1100 cm^{-1} revealed the possible presence of C-N stretching of aliphatic/ aromatic amines, C-C bond of the aromatic ring, N-O bond of the nitro group.

Figure 5b and c further show that the bands mentioned above were shifted to a new position following the adsorption of DR 80 and MB 9, which confirmed the involvement of these groups in the dye adsorption process. For instance, FTIR spectra of MeSNPs following DR 80 adsorption show bands stretched at 1060 cm^{-1}, 1550 cm^{-1}, 1640 cm^{-1} and 3271 cm^{-1}, and in case of MB 9 loaded MeSNPs new bands appeared at 1015 cm^{-1}, 1590 cm^{-1}, 1670 cm^{-1} and 3091 cm^{-1} (Fig. 6.4b

and c). The bands at 3271 cm^{-1} and 3091 cm^{-1} are due to the tensile frequencies of OH from alcohol and phenol groups involved in the dye adsorption process (Cipriani et al., 2016).

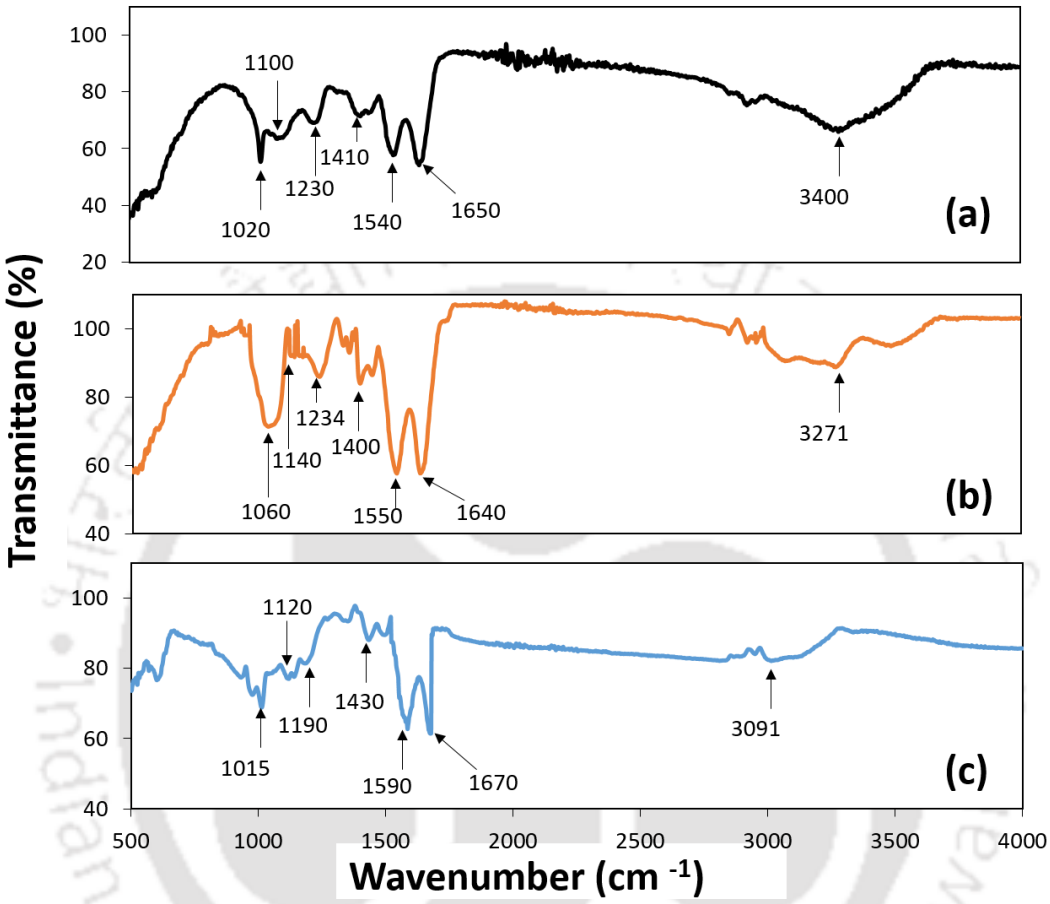

Fig. 6.5 FTIR spectra of MeSNPs (a) before dye adsorption and after (b) DR 80 adsorption and (c) MB 9 adsorption.

The zeta potential measurements revealed that the isoelectric point (IEP) of MeSNPs was in between 5 and 6, as shown in Fig. 6.6. Hence, in order to achieve maximum electrostatic interaction between the positively charged MeSNPs and the anionic dyes, a low pH value of 2, was chosen for their removal. The specific surface area of MeSNPs determined using the multiple BET equation was 120.4 m^2/g. XRD analysis further confirmed that the different metals were

present as their corresponding sulfides, i.e., CdS, FeS, CuS, NiS, PbS and ZnS, in the MeSNPs (Fig. 6.7).

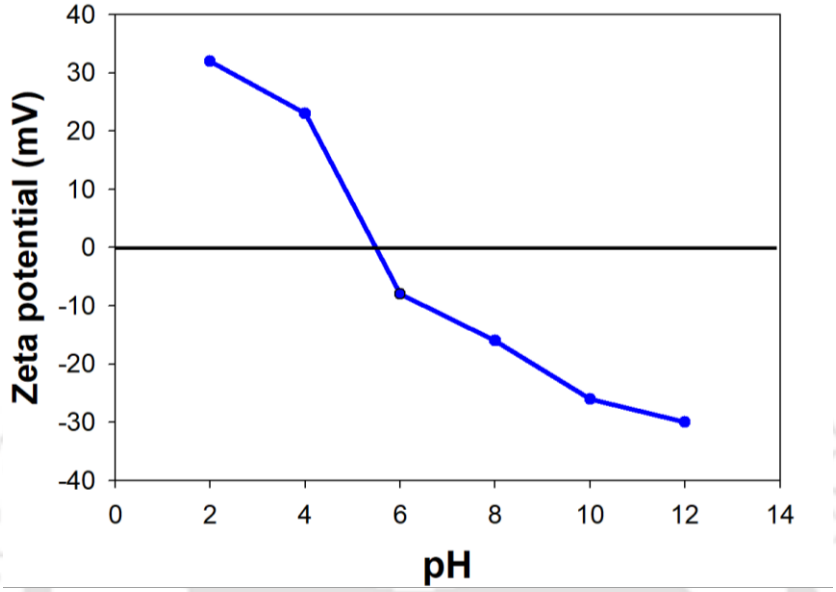

Fig. 6.6 Zeta potential analysis of MeSNPs.

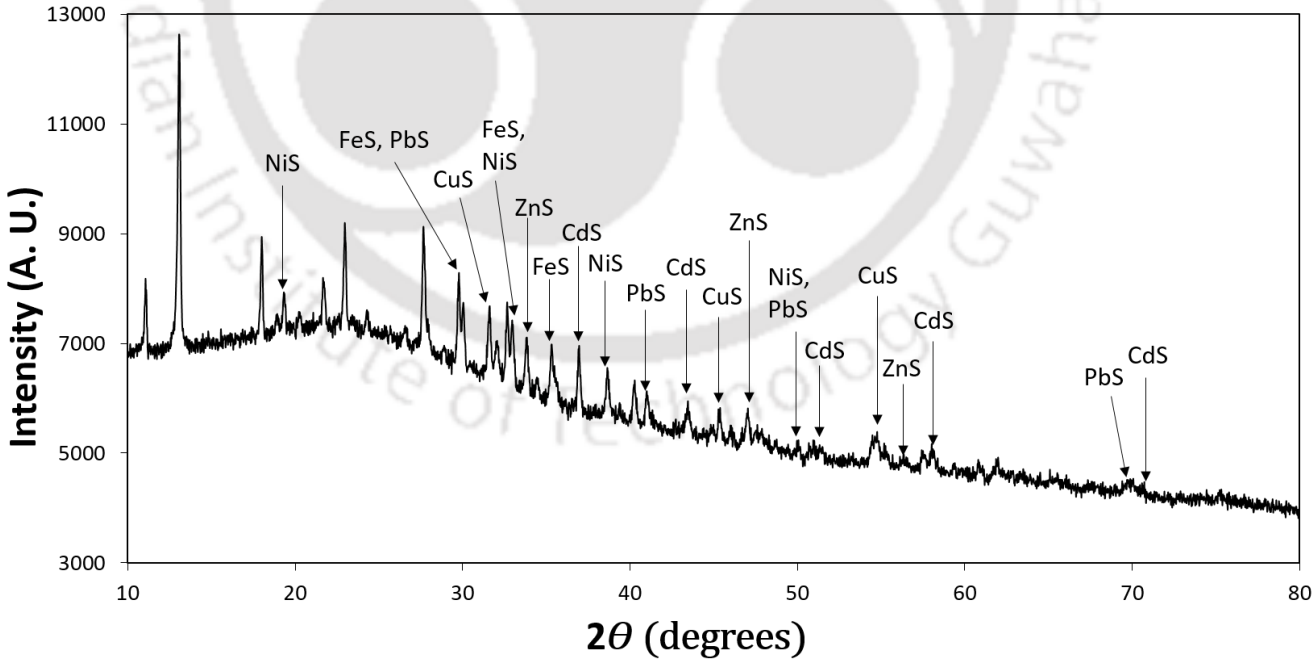

Fig. 6.7 XRD profile of MeSNPs.

6.3.2 Effect of different variables on dye removal

6.3.2.1 Contact time

From the results shown in Fig. 6.8(a) it is apparent that a very high removal efficiency (80%) of DR 80 is achieved in less than one minute of contact time, and the value quickly reached up to 100% without any further change. In the case of MB 9, the removal percentage was 50% in the first minute, and complete removal was obtained in 6 min. Thus, complete removal and equilibrium of both the dyes were obtained in 6 min. Such a short contact time is also preferred to keep the operating cost low for large-scale applications. Moreover, the short contact time for attaining equilibrium in this study with MeSNPs is less than the values reported for other adsorbents in the literature (Arami et al., 2005; Ardejani et al., 2008; Martins et al., 2015).

The experimental results obtained were fitted to pseudo-first and pseudo-second order reaction rate models in order to determine the rate and other kinetic parameters involved in the dye sorption process. Fig. 6.9 shows linear plots of these kinetic models on the experimental data, and Table 6.3 summarizes the estimated model parameters and coefficient of determination (R^2) values for DR 80 and MB 9. These results reveal that the R^2 value due to the second order kinetic model is greater than the R^2 value due to the first order rate kinetic model, signifying that the removal of DR 80 and MB 9 using MeSNPs is governed by physico-chemical interaction between the dyes and the adsorbent (Rebekah et al., 2020).

Table 6.3 Estimated kinetic model parameters on the removal of DR 80 and MB 9 by MeSNPs

Model	Parameters	Value	
		DR 80	**MB 9**
Pseudo-first order	k_1 (1/min)	0.734	0.348
	$q_{e,cal}$ (mg/g)	19.49	19.29
	R^2	0.98	0.94
Pseudo-second order	k_2 (g/mg/min)	0.062	0.048
	$q_{e,cal}$ (mg/g)	52.63	49.50
	R^2	0.99	0.99

6.3.2.2 Effect of MeSNPs dosage

The effect of different MeSNPs dosage was evaluated to find the optimum dosage required for dye removal. The values of the other parameters, i.e., initial dye concentration, pH and temperature, were 100 mg/L, 2.0, and 25 °C in this experiment, and an equilibrium time of 6 min, as determined earlier, was followed. As shown in Fig. 6.8(b), 25 mg/L dose of MeSNPs yielded 60% and 56% removal efficiency of DR 80 and MB 9, respectively. Upon increasing the dose of the nanoparticles, the removal efficiency of both the dyes also increased, and complete removal of both the azo dyes was achieved above 200 mg of MeSNPs (Fig. 6.8b). The increase in dye removal efficiency at a higher dose of MeSNPs is attributed to the availability of a large number of binding sites for dye adsorption onto the adsorbent than at a lower dosage.

3.3.2.3 Effect of solution pH

The effect of different pH values was evaluated on the adsorption efficiency of DR 80 and MB 9 by MeSNPs. The results shown in Fig. 6.8(c) reveal that the maximum removal efficiency of both

the dyes is obtained at pH 2, and the removal efficiency decreased with an increase in the solution pH. The maximum removal of the dyes at a very low pH is attributed to the electrostatic interaction between the negatively charged surface of the dyes (due to R-SO_3^- species) and the positively charged (due to H^+ ions) adsorbent surface. An increase in the solution pH reduces the number of positively charged species on the adsorbent surface, which in turn leads to reduced interaction between the adsorbent and the anionic dyes (Namasivayam et al., 2003). The low removal efficiency of both the dyes at a high pH is also due to competition between OH^- ions and the anionic dyes for binding with the positively charged adsorbent. In the literature, similar results on the effect of solution pH on the removal of Acid yellow 36 and Congo red dyes have been reported (Namasivayam et al., 2003; Malik et al., 2003).

6.3.2.4 Effect of initial dye concentration

The effect of different initial dye concentrations (50-300 mg/L) on the removal of DR 80 and MB 9 was investigated in this study by fixing the other parameters at their respective optimum levels. Fig. 6.8(d) displays a plot between dye removal efficiency and initial dye concentration, which revealed that complete removal of both the dyes is obtained for 50 and 100 mg/L initial dye concentrations. The removal efficiency of DR 80 and MB 9 decreased to 93% and 82%, respectively, with an increase in their initial concentration up to 300 mg/L. These results also show that the MeSNPs have more affinity towards DR 80 than MB 9, which can be explained based on the fact that DR80 has a higher molecular mass than MB 9. Moussavi et al. (2009) also obtained similar results on better removal of a high molecular mass dye compared to a low molecular mass dye by adsorption using MgO nanoparticles.

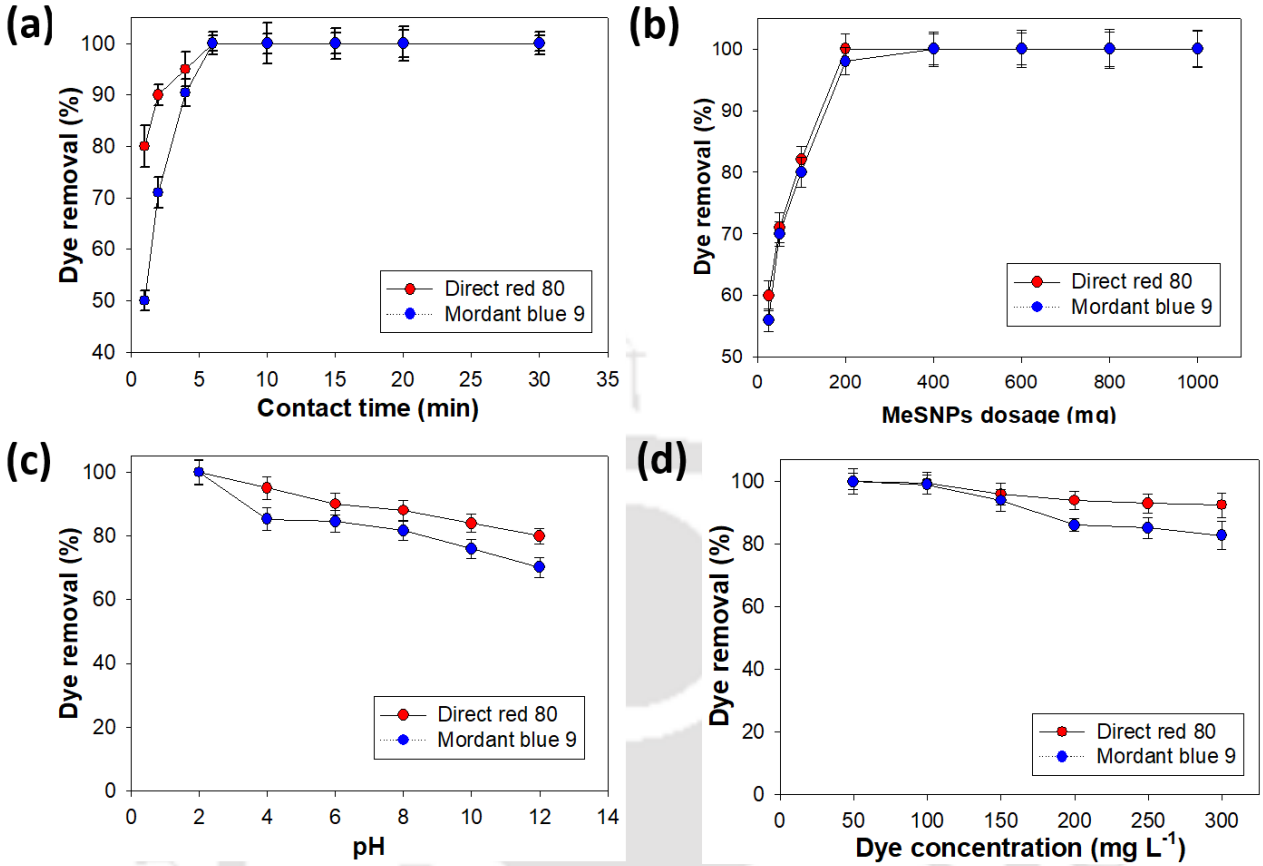

Fig. 6.8 Effect of (a) contact time (b) MeSNPs amount, (c) solution pH, and (d) initial dye concentration on the removal of DR 80 and MB 9.

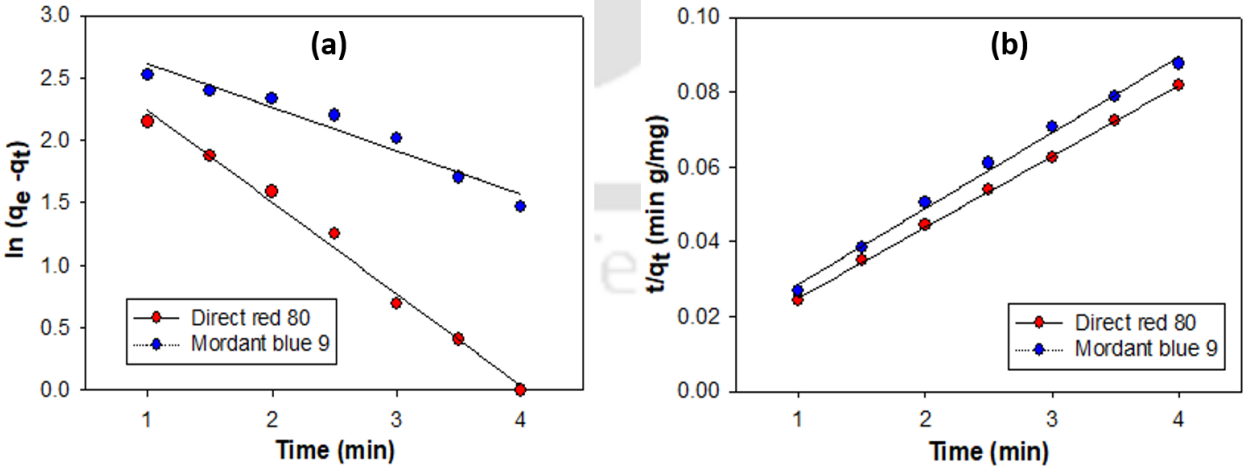

Fig. 6.9 Kinetic modeling of DR 80 and MB 9 removal by MeSNPs: (a) pseudo-first order and (b) pseudo-second order rate models.

Three commonly used isotherm models (Langmuir, Freundlich, and SIPs) were applied to define the batch adsorption of DR 80 and MB 9 by MeSNPs. The coefficient of determination (R^2) values of linear regression plot obtained using the isotherm models and the experimental data were estimated. The model constants and the R^2 values for both the dyes presented in Table 6.4, indicates that the dye adsorption follows SIPs isotherm, which is consistent with the literature on DR 80 and MB 9 dye removal by adsorption (Hayati et al., 2011; Tomic et al., 2014).

Table 6.4 Estimated isotherms model parameters on the removal of DR 80 and MB 9 by MeSNPs

Isotherm model	**Parameters**	**Value**	
		DR 80	**MB 9**
Langmuir	q_{max} (mg/g)	294.11	121.95
	K_L (L/mg)	0.063	0.23
	R^2	0.91	0.95
Freundlich	K_F (L/mg)	24	38.9
	n	1.9	3.73
	R^2	0.98	0.95
Sips	q_m (mg/g)	143.7	198.3
	k_s (L/mg)	0.039	1.509
	n	1.17	1.21
	R^2	0.999	0.997

From the Langmuir model, which fitted the experimental data with R^2 value >0.90 for both the dyes, the maximum adsorption capacity values were estimated to be 294.11 and 121.95 mg dye per gm MeSNPs for DR 80 and MB 9, respectively. The values further confirmed the very high

capacity of MeSNPs for dye adsorption (Table 6.4). The differences in DR 80 and MB 9 removal percentage and maximum adsorption capacity of the adsorbent are due to their different chemical structure, size, and properties (Table 6.2).

Comparison of MeSNPs with other adsorbents described in the literature for the removal of DR 80 and MB 9 reveals its better performance over the others (Table 6.1). In addition, a maximum adsorption efficiency of the dyes within a short time further indicates an easy and quick operation of the adsorption process.

6.3.3 Continuous dye sorption using fixed-bed column

The effect of different flow rates on dynamic sorption of DR 80 and MB 9 by MeSNPs was investigated at 0.33 mL/min, 1.0 mL/min, and 2.5 mL/min, and by keeping the adsorbent bed height and inlet dye concentration fixed at 1 cm and 25 mg/L fixed. Breakthrough behavior of the dyes (Fig. 6.10) reveal that increase in the flow rate reduced both the breakthrough time and exhaustion time for both the dyes.

Volume treated and removal efficiency of the dyes also decrease with an increase in the flow rate. The dye sorption capacity reduced from 18.31 mg/g to 16.87 mg/g in the case of DR 80 and from 16.83 mg/g to 14.25 mg/g in the case of MB 9 with an increase in flow rate from 0.33 mL/min to 2.5 mL/min (Table 6.5). The effect due to flow rate is due to less time available for interaction between the dye molecules and the adsorbent at a high flow rate.

The experimental breakthrough data was further analyzed using different models such as Thomas, Adams-Bohart, Clark, and Yoon-Nelson models for describing the breakthrough behavior of the dyes in the column.

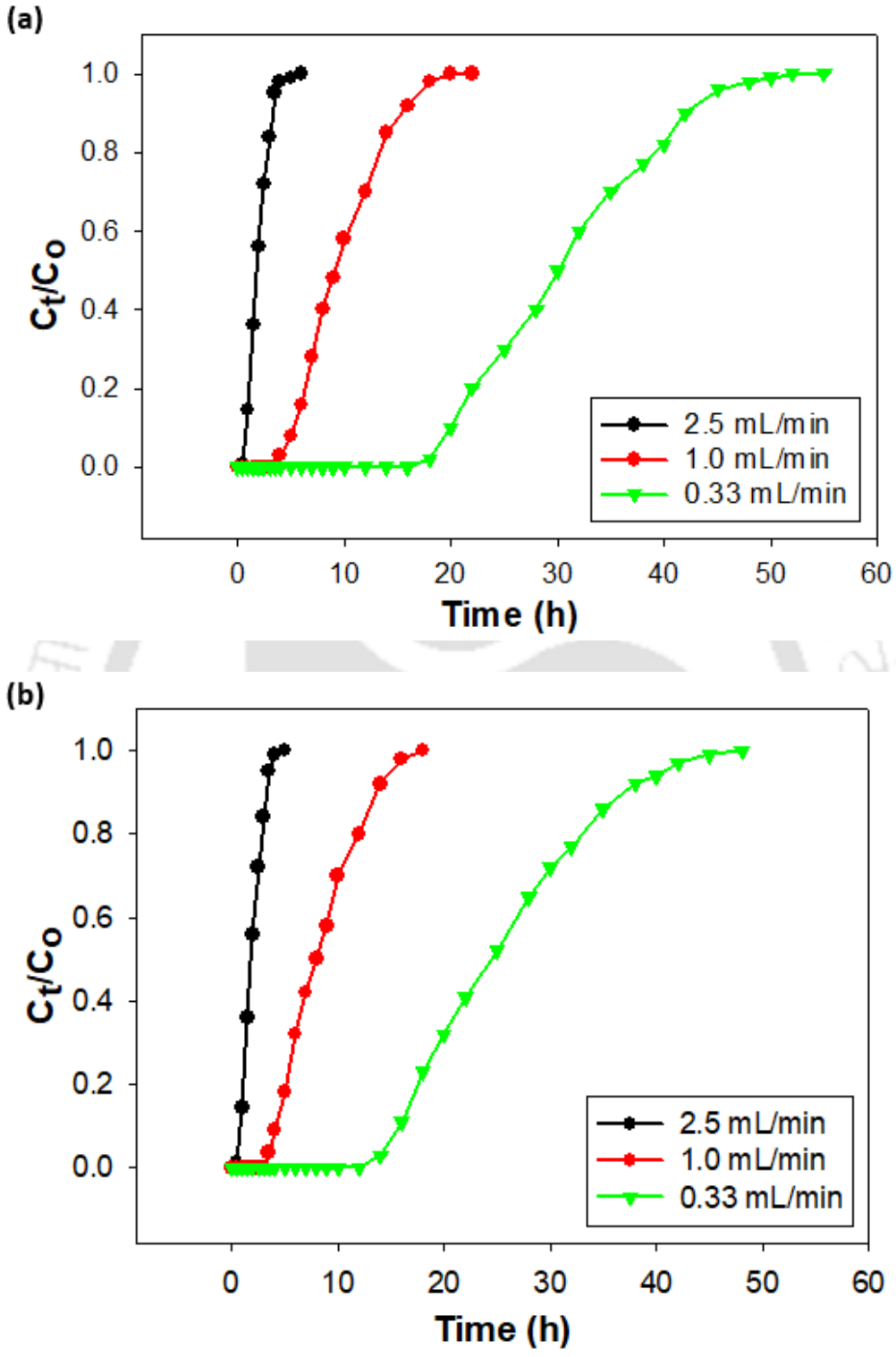

Fig. 6.10 Effect of different liquid flow rates on adsorption breakthrough behavior of (a) DR 80 and (b) MB 9 in the column study.

Table 6.5 Effect of different liquid flow rates on the column performance for removal of DR 80 and MB 9 by MeSNPs

U	F	DR 80						MB 9					
(cm/min)	(mL/min)	t_{total} (h)	m_{total} (mg)	q_{total} (mg)	$q_{e(exp)}$ (mg/g)	V_{eff} (L)	Y (%)	t_{total} (h)	m_{total} (mg)	q_{total} (mg)	$q_{e(exp)}$ (mg/g)	V_{eff} (L)	Y (%)
0.42	0.33	55	27.0	18.31	91.55	1.09	67.81	48	23.4	16.83	84.15	0.95	71.90
1.27	1.0	18	30.0	18.00	90.00	1.20	60.00	14	27.0	15.00	75.00	0.84	55.55
3.18	2.5	5	18.7	16.87	84.35	0.75	90.21	4.5	16.8	14.25	71.25	0.67	84.82

Thomas model is one of the most common and widely used models for experimental adsorption breakthrough behavior in column studies. This model is based on second-order rate kinetics and adsorption-desorption Langmuir isotherm (Thomas et al., 1944). This model is also used to estimate the maximum adsorption efficiency of an adsorbent in column studies.

The following equation represents the Thomas model (Eq. 6.15)

$$\ln\left(\frac{C_0}{C_t} - 1\right) = \frac{k_{Th} Q_0 W}{F} - k_{Th} C_0 t \qquad (6.15)$$

where k_{Th} is the sorption rate constant (mL/min/mg), and Q_0 is the maximum sorption capacity (mg/g). W refers to sorbent quantity (g) used in the column. C_0/C_t is the ratio of the inlet to effluent dye concentration. Dye adsorption capacity (Q_0) and rate constant (k_{Th}) were determined from a plot of $\ln(C_0/C_t - 1)$ vs. t, and their values are presented in Table 6.6. The Q_0 values for DR 80 and Mb 9 are 1273.04 mg/g and 1056.72 mg/g for a flow rate of 0.33 mL/min, and the values increased with an increase in the flow rate from 0.33 mL/min to 2.5 mL/min. A reverse trend is observed in the case of k_{Th} value with an increase in the flow rate.

Clark's model incorporates mass-transfer coefficient with Freundlich isotherm (Clark et al., 1987), and it is expressed in its linear form as follows (Eq. 6.16):

$$\ln\left[\left(\frac{C_t}{C_o}\right)^{n-1} - 1\right] = -rt + \ln A \qquad (6.16)$$

where n is the Freundlich constant; A (mg/L/min) and r (1/min) are the Clark model constants. As given in Table 6.6, the r value obtained in this study increased with an increase in the flow rate for both DR 80 and MB 9, which is due to the enhanced molecular diffusion and mass transfer rate at a high flow rate. Rout et al. (2017) reported a similar result on variation in mass-transfer rate for phosphate removal in a packed bed reactor operated under dynamic conditions.

Adams-Bohart model is mainly applied to define the initial part of the breakthrough curve. It is based on the assumption that the sorption rate depends on the solid residual capacity and dye concentration (Bohart et al., 1920). The model equation is given by Eq. (6.17):

$$\ln\left(\frac{C_0}{C_t}\right) = k_{AB}C_0t - k_{AB}N_{AB}\left(\frac{z}{u}\right) \qquad (6.17)$$

where k_{AB} (mL/mg/min) represents kinetic constant, N_{AB} (g/L) is the saturation concentration, Z (cm) represents bed height, u is the linear velocity of liquid flow inside the column (cm/min). From Table 6.6, increasing the flow rate from 0.33 mL/min to 2.5 mL/min, decreased the N_{AB} value from 3691.95 mg/L to 46.08 mg/L for DR 80 and in the case of MB 9 the values decreased from 3115.4 mg/L to 39.6 mg/L, k_{AB} value increased from 0.0029 mL/mg/min to 0.021 mL/mg/min for DR 80 and from 0.0033 mL/mg/min to 0.031 mL/mg/min MB 9, with an increase in the flow rate. However, among the different breakthrough models examined in this work, the Adams-Bohart model did not accurately describe the dye adsorption in the fixed-bed column, and its R^2 value was about 0.72 for both the dyes.

Yoon-Nelson model is another breakthrough model initially developed for the sorption of vapors or gases using activated charcoal. It is based on the assumption that the sorption rate depends on the sorbent adsorption capacity and the sorbate breakthrough (Yoon et al., 1984). Its linear form can be expressed as follows:

$$\ln\left(\frac{C_t}{C_0 - C_t}\right) = k_{YN}t - k_{YN}\tau \qquad (6.18)$$

where k_{YN} represents Yoon-Nelson rate constant (L/min), and τ represents the time to complete 50 % sorbate breakthrough (min).

Table 6.6 Estimated breakthrough model parameters for the removal of DR 80 and MB 9 by MeSNPs in the column study

Flow rate	Thomas model			Clark model			Adams-Bohart model			Yoon-Nelson model		
F (mL/min)	**Q_0 (mg/g)**	**k_{Th} (mL/mg/min)**	**R^2**	**r (1/min)**	**A (mg/L/min)**	**R^2**	**N_{AB} (mg/L)**	**k_{AB} (mL/mg/min)**	**R^2**	**k_{YN} (1/min)**	**τ (min)**	**R^2**
DR 80												
0.33	1273.04	0.0088	0.967	0.216	651.97	0.969	3691.95	0.003	0.680	0.222	30.80	0.967
1.0	1237.02	0.0185	0.970	0.449	70.10	0.974	559.21	0.006	0.685	0.464	9.86	0.970
2.5	648.51	0.0925	0.950	2.231	83.93	0.956	46.08	0.022	0.576	2.313	1.85	0.950
MB 9												
0.33	1056.72	0.0086	0.969	0.254	3294.46	0.990	3115.40	0.003	0.712	0.215	25.70	0.969
1.0	1061.55	0.0199	0.965	0.610	992.27	0.972	262.34	0.009	0.729	0.498	8.45	0.965
2.5	644.27	0.0908	0.955	2.69	1339.43	0.976	39.60	0.032	0.608	2.27	2.06	0.955

(bed depth = 1 cm and inlet dye concentration = 25 mg/L)

The values of the parameters can be calculated from a plot between $\ln(C_t/(C_0-C_t)$ and t. Increasing the flow rate from 0.33 mL/min to 2.5 mL/min resulted in an increase in k_{YN} and a decrease in τ values in the case of both DR 80 and MB 9, which could be reasoned based on the less time required to achieve a 50% breakthrough at a high liquid flow rate in the column (Table 6.6). R^2 values due to the Yoon-Nelson and Thomas models were the same as both these models are mathematically analogous.

6.3.4 Dye desorption

Dye desorption test was conducted to understand the dye adsorption mechanism invlolved and also to explore the possibility of recovering MeSNPs for reuse in the dye adsorption process. Dye desorption efficiency was maximum for both DR80 and MB 9 using the desorbing solution at pH 12 (Fig. 6.11), which is attributed to the excess negatively charged species on the adsorbent at an alkaline pH and the resulting in electrostatic repulsion between the dye and the adsorbent. Electrostatic interaction between the positively charged adsorbent surface and the anionic dyes was the significant at a low pH 2.0, as determined earlier in section 3.2.2.3 also.

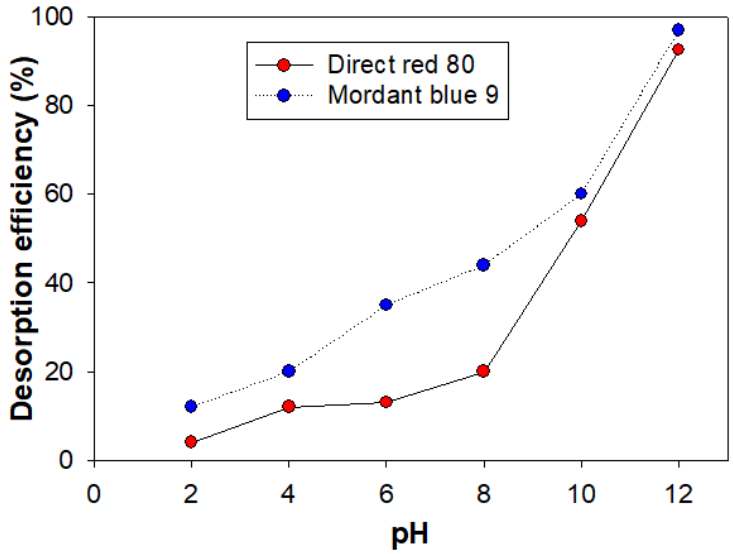

Fig. 6.11 Desorption efficiency of DR 80 and MB 9 from dye loaded MeSNPs using desorption solution of different pH (T = 25 ºC).

Following the batch desorption study, the sorption and desorption experiments were conducted with MeSNPs in the fixed-bed column for up to 4 sorption/desorption cycles by keeping the adsorbent bed height constant at 1 cm. Initially and during the first cycle, individual DR 80 and MB 9 solution of 25 mg/L concentration was passed through the adsorbent bed at a flow rate of 2.5 mL/min. Following the desorption step in each cycle, excess amount of the desorbing agent in the bed was washed off using distilled water.

Table 6.7 shows the results of breakthrough time and regeneration parameters obtained in the four sorption-desorption cycles carried out in the column study for DR 80 and MB 9. With every sorption-desorption cycle, the breakthrough time reduced from 300 min to 78 min for DR 80 and in case of MB 9 the value reduced from 290 min to 72 min.

Table 6.7 Breakthrough time and regeneration parameters of the fixed bed column operated for four sorption-desorption cycles

Cycle number	Breakthrough time (min)	Uptake capacity (mg/g)	Regeneration efficiency (%)
DR 80			
1	300	648.51	100
2	205	509.21	78.52
3	150	404.15	62.32
4	78	236.12	36.41
MB 9			
1	290	644.27	100
2	196	484.81	75.25
3	141	383.98	59.60
4	72	228.58	35.48

Similarly, the uptake capacity of the column reduced from 648.51 mg/g to 236.12 mg/g for DR 80 and also for MB 9 from 644.27 mg/g to 228.58 mg/g. These results reveal drastic reduction in adsorption capacity of the MeSNPs towards the end of the four sorption-desorption cycle, which could be due to the deactivation of binding sites present on the adsorbent as reported by Thabede et al. (2020).

6.4 Significant findings

Novel adsorbent based on biogenic synthesized MeSNPs from sulfate rich metallic wastewater revealed its excellent potential for treating dye containing wastewater. The MeSNPs showed a very high capacity to adsorb DR 80 and MB 9 from aqueous solution even at a high initial concentration and within a short time period. Mechanism of dye sorption onto MeSNPs was shown to involve electrostatic interaction between the dyes and the adsorbent. Dynamic dye sorption using a packed bed column with MeSNPs revealed that it can be used for upto 2-3 cycles of regeneration and reuse with minor loss in dye uptake capacity of the adsorbent bed. However, future studies on efficient regeneration of packed bed containing MeSNPs for prolonged reuse and recycle in dye removal from wastewater are necessary. In addition, application of MeSNPs in treating wastewater containing a mixture of dyes and other pollutants in order to further stablished its large-scale applications.

Chapter 7

Green synthesis and application of biogenic copper nanoparticles from metallic wastewater for click reaction

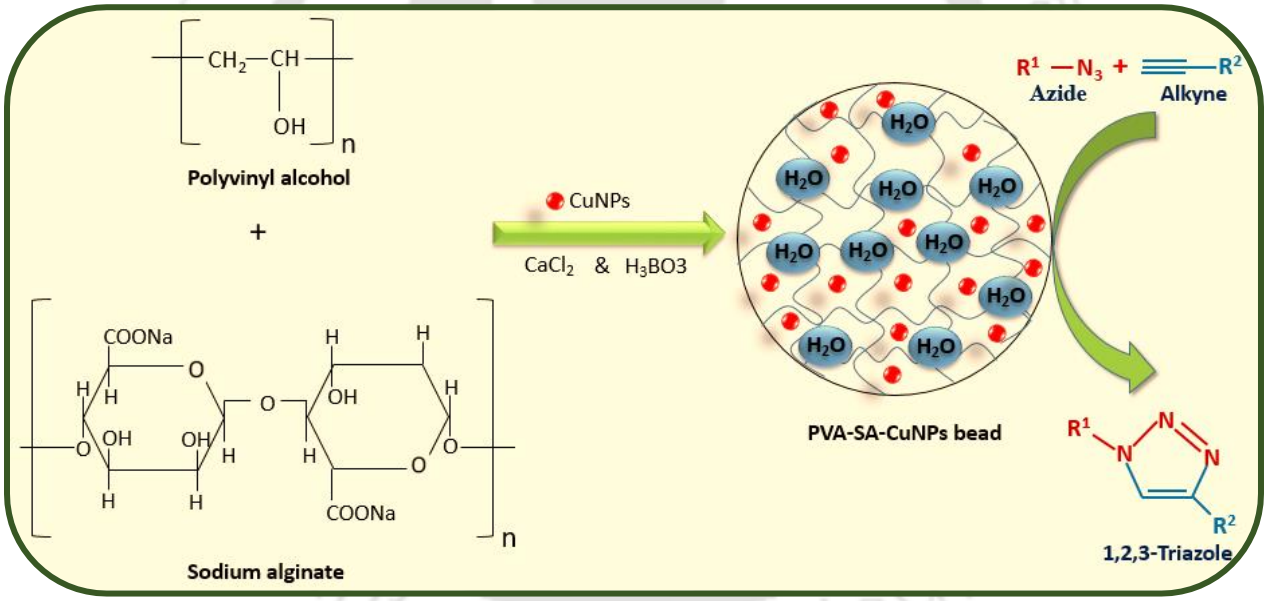

ABSTRACT

In the present investigation, biogenic copper sulfide nanoparticles from metallic wastewater were examined for triazoles formation. The size of the copper nanoparticles was in the range of 5-10 nm. Polyvinyl alcohol and sodium alginate supported copper nanoparticles (PVA-SA-CuNPs) were prepared by immobilizing copper sulfide on PVA-SA. The nanomaterial was characterized by field emission scanning electron microscopy (FESEM), energy dispersive X-ray spectroscopy (EDX), field emission transmission electron microscopy (FETEM), Thermogravimetric analysis (TGA), X-ray diffractometer (XRD), and UV−vis. The catalytic activity of PVA-SA-CuNPs was assessed in the three-component click synthesis of 1,2,3-triazoles in water under low catalyst loading and mild reaction conditions. The nanocatalysts can be recycled and reused several times without significant loss of their catalytic activity.

7.1 Introduction

1,2,3-Triazole is defined as an aromatic heterocycle, a five-membered ring of two carbon and three nitrogen atoms with the molecular formula $C_2H_3N_3$ (Sarkar et al., 2008; Kimber et al., 2020). Triazoles find many biomedical applications, such as activity against Gram-positive bacteria (Genin et al., 2000), a protein kinase inhibitor, and anti-HIV (Gholinejad et al., 2020). It also finds application as dyes, photostabilizers of polymers, agrochemicals, optical brighteners, photographic materials and corrosion inhibitors in industries (Fan et al., 1996). Various methods have been developed for the synthesis of 1,2,3-triazoles compounds. The Huisgen cycloaddition reaction comprising azides with terminal alkynes is widespread among the different techniques, called Cu-catalyzed azide-alkyne cycloaddition (CuAAC). A mixture of 1,4- and 1,5-disubstituted compounds are obtained as a result of the Huisgen cycloaddition reaction, which requires (1) high temperature, (2) long reaction time and (3) electron-withdrawing solid substituents (Gholinejad et al., 2020). Recent advancement shows the production of highly regioselective 1,4-disubstituted 1,2,3-triazoles using cycloaddition reaction of alkynes and azides catalyzed by copper complexes.

Due to raising interest towards environmentally sustainable processes for the synthesis of chemicals, development of cost-effective, recyclable catalysts and nontoxic solvents are top priorities. One such example is water as a solvent in chemical reactions instead of using expensive, flammable, and toxic organic chemicals that are harmful to the environment. One more advantage of conducting a reaction in an aqueous solution is that product separation is easy due to low solubility of organic compounds in water (Sheldon et al., 1994; Anastas et al., 2010).

Over the last few years, different copper catalysts have been used in click reaction of alkynes and azides (Liang et al., 2011; Harmand et al., 2012; Pathigoolla et al., 2013). However, despite achieving good efficiency, such processes find difficulty in separating the copper catalyst from the

final products. To overcome this problem, immobilization of copper nanoparticles onto other support is an interesting option. Examples of different immobilization supports are as follows: silica (Veerakumar et al., 2011), magnetite (Hudson et al., 2012; Kaboudin et al., 2013), polymers (Wang et al., 2010), coating of polyvinyl pyrrolidone (Zhang et al., 2010), surfactant-assisted hydrothermal-synthesis (Sharghi et al., 2008), and melamine-formaldehyde resin (Soltani et al., 2013).

In the recent years, biodegradable and eco-friendly polymers as recyclable heterogeneous catalysts are of interest (Dabbawala et al., 2012; Tokarek et al., 2013; Gholinejad et al., 2020). One such polymer is agarose, which was successfully used as a binding polymer in click reaction for the production of triazole (Gholinejad et al., 2020). Nasir Baig et al. (2014) reported an application of chitosan immobilized copper catalyst to synthesize 1,2,3-triazoles compounds. Similarly, Kal-Kashvandi et al. (2018) reported the use of polyvinyl alcohol (PVA) as a binding polymer in click reaction, which has many advantages such as (1) formation of intra and inter-chain hydrogen bonds in water, (2) crystalline nature and (3) small trailing hydroxyl group (Kal-Kashvandi et al., 2018). Moreover, PVA has higher mechanical strength than the other hydrogels. The other applications associated with PVA are in papermaking, textiles, bacterial immobilization, and as coating agent. However, its use as an immobilizing matrix for metal nanoparticles has been generally overlooked and only recently, successful efforts have been made to synthesize triazoles using click chemistry under heterogeneous catalysis and PVA as catalyst support.

PVA-based copper nanoparticles have been synthesized and used as nanoparticle stabilizers (Saez et al., 2009; Hammad et al., 2015). PVA-Cu nanocomposites were made and demonstrated by Hajipour et al. (2015). One more example of cheap, non-toxic, biodegradable polymer is sodium alginate (SA), extracted from brown algae. It has been widely used in different applications, e.g.,

as a carrier in drug release, removal of dye and heavy metals, etc. (Shalumon et al., 2011; Mohammadi et al., 2014).

It has been observed that an interpenetrating polymer network (IPN) structure, which is a mixture of two or more cross-linked polymers, shows excellent mechanical strength (Wang et al., 2016; Zhou et al., 2018). However, it is unknown whether embedding copper nanoparticles into PVA and sodium alginate (PVA-SA) hydrogel with IPN structure would have an excellent triazole yield. Furthermore, this kind of hydrogel for triazole production has not yet been studied to the best of our knowledge.

In our previous study, copper nanopowder was synthesized using sulfate-reducing bacteria (SRB) from acid mine drainage under anaerobic conditions. Synthesis of such copper catalysts recovered from wastewater has many benefits over the conventional chemical synthesis of nanoparticles. Disadvantages of the chemical route for the synthesis of the catalyst comprises of (1) use of toxic solvents, (2) high temperature, (3) stabilizers (4) harmful chemicals. On the other hand, microbial synthesis of catalyst can be advantageous in terms of (1) low-cost (2) simple process, (3) scalable and (4) mild reaction conditions.

This chapter presents the synthesis of a biogenic copper catalyst utilizing copper nanoparticles recovered from synthetic acid mine drainage. A mixture of PVA and sodium alginate were used as inexpensive, biodegradable, and stable polymers to support and stabilize the biogenic copper nanoparticles and its application as an efficient catalyst in click reaction in water.

7.2 Materials and methods

7.2.1 Chemicals

All reagents and chemicals used in this study were of analytical grade and were used without any further purification. All the alkynes and azides were procured from Sigma-Aldrich and used as received.

7.2.2 Synthesis of copper sulfide nanoparticles

Copper sulfide nanoparticles (CuS NPs) were synthesized through sulfide precipitation using sulfate-reducing bacteria (SRB). The anaerobic biomass was collected from a laboratory scale rotating biological contactor (RBC) reactor as detailed in Chapter 3. Synthetic media used for the biogenic CuNPs production was composed of (g/L): 1 ammonium chloride, 1.47 sodium sulfate, 0.2 trisodium citrate, 0.1 ascorbic acid, 0.1 calcium chloride dehydrate, 0.5 potassium dihydrogen phosphate, 0.2 ethylene diamine tetraacetic acid (EDTA), 0.2 bromo ethane sulfonic acid (BESA), 0.15 iron sulfate heptahydrate. Sodium lactate was used as the electron donor, and media pH was adjusted to 7.0. Recovery and purification of the CuNPs were described in the previous Chapter 5.

7.2.3 Immobilization of CuNPs

For immobilization of CuNPs, 8% (w/v) PVA was dissolved in 10 mL distilled water by mechanical shaking at 95 °C for 2 h and then cooled down to room temperature. Next, 1% (w/v) sodium alginate and CuNPs were added with mechanical stirring. All three solutions were stirred to form a homogeneous solution. The prepared homogenous solution was added dropwise into a 500 mL chilled 10% $CaCl_2$ and 3% boric acid crosslinking solution to form CuNPs immobilized beads using a 10 mL syringe. The spherical shaped PVA-SA beads with immobilized CuNPs were then soaked in the cross-linking solution for 10 h to for improving its stability. Finally, the beads

were rinsed using double distilled water to remove unreacted monomers and stored at 4 °C before further use.

7.2.4 Synthesis of 1,2,3-Triazoles

The standard procedure was followed to synthesize triazole using different alkynes and azides as detailed in Gholinejad et al. (2020). Assimilation of various alkynes and azides to the previously prepared PVA-SA-CuNPs beads resulted in the formation of triazoles. In one typical case, azidobenzene (0.25 mmol) and phenylacetylene (0.25 mmol) were added in a flask equipped with a magnetic stirring bar and containing 2 mL of water. The reaction mixture was then heated at 30 °C for 12 h. After completing the reaction, the mixture was cooled to room temperature, and the triazole product was separated using extraction with ethyl acetate. Finally, the ethyl acetate was evaporated to obtain the desired product in a highly pure form.

7.2.5 Recycling of catalyst

PVA-SA-CuNPs were tested for their recycle and reuse ability in a reaction of azidobenzene and phenylacetylene as model reactants. After the first run, the catalyst was separated, and ethyl acetate was used to extract the triazole. Next, the recovered PVA-SA-CuNPs catalyst was washed with diethyl ether for further use. Finally, the recovered PVA-SA-CuNPs beads were reused in a similar reaction. The exact process was repeated up to five consecutive cycles.

7.2.6 Characterization techniques

For FTIR, the PVA and PVA-SA-CuNPs beads were suitably dried to remove the excess water. Dried samples were used for FTIR analysis (IR affinity-1S, Shimadzu, Japan). Morphology of PVA-SA-CuNPs catalyst was checked using FESEM (Zeiss, Sigma, Germany). To check the presence of copper in the sample, Energy-dispersive X-ray spectroscopy (EDX) was carried out.

Copper content was determined by microwave plasma atomic emission spectroscopy (Varian, 4210 MP-AES, Agilent Technologies). For field emission transmission electron microscopy (FETEM) analysis using JOEL, JEM2100, Japan, operating at 200 kV, a drop of the sample was cast on a copper grid, and the grid was dried in an oven to remove moisture.

Thermo-gravimetric analysis (TGA) of immobilized CuNPs beads were carried out in a nitrogen atmosphere with a 40 mL/min flow rate, a heating rate of 10 °C/min, and a temperature range of 0–800 °C (TG 209 F1, Libra Analyser, Germany). The samples were placed in a 1 mL ceramic crucible for the analysis. Differential thermogravimetric analysis (DTG) was performed to obtain the maximum thermal degradation temperature of the samples. Nuclear magnetic resonance (NMR) analysis using was performed by dissolving the sample in deuterated chloroform ($CDCl_3$). The samples were then analyzed using nuclear magnetic resonance (NMR, ASCEND 600 model, Bruker 600 MHz).

7.3 Results and discussion

7.3.1 Characterization of CuNP immobilized PVA beads

The CuNPs in the PVA-SA-CuNPs matrix were analyzed using different techniques such as FESEM, EDX, FTIR, TGA, FETEM, and UV−vis. Amount of copper in the beads was determined to be 0.2 mmol/g by AES analysis Fig. 7.1 shows the FTIR spectra of PVA-SA and PVA-SA-CuNPs between the wavelengths 500 and 4000 cm^{-1}. The broad peak present at 3500 cm^{-1} signifies the hydroxyl (-OH) group in the PVA-SA, and a minor shift to 3450 cm^{-1} was observed in PVA-SA-CuNPs. The band due to hydroxyl group present in PVA-SA-CuNPs is stronger than for PVA-SA indicating that the hydroxyl unit of PVA-SA may have different H-bond interactions or coordination from that of the CuNPs immobilized beads.

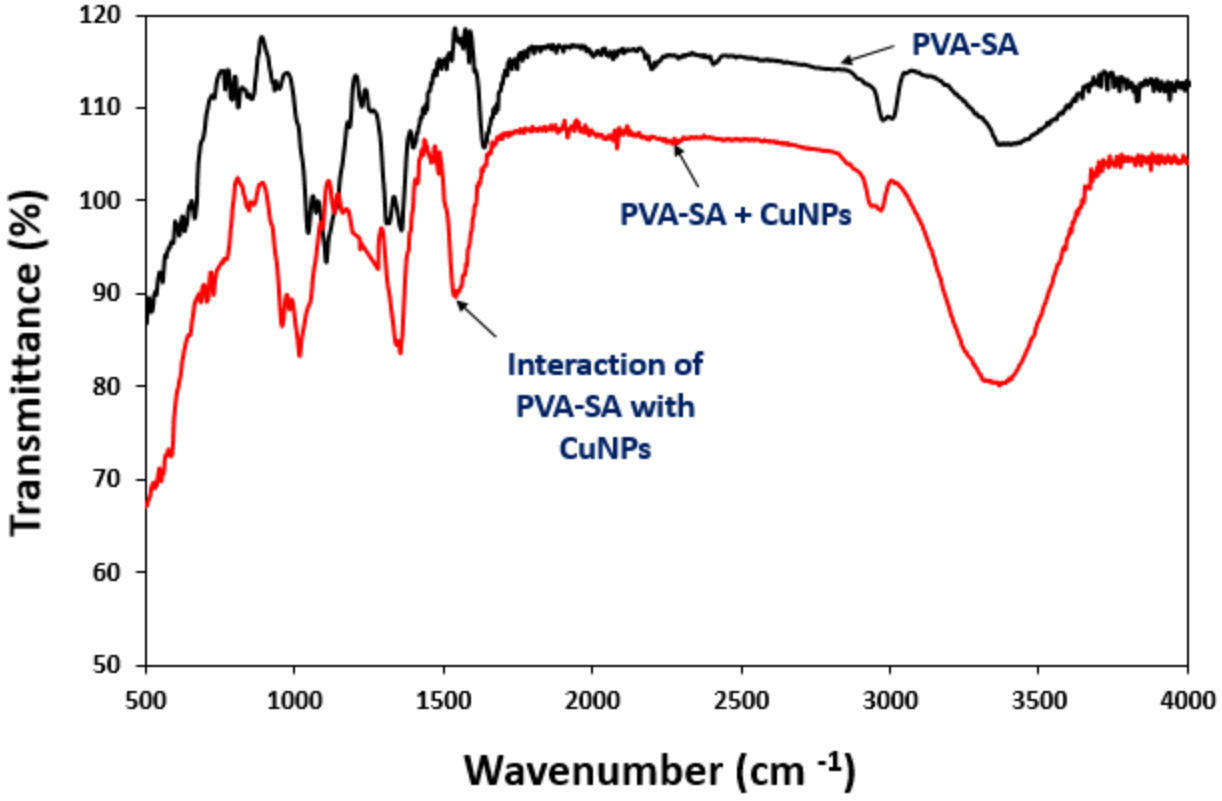

Fig. 7.1 FTIR spectra of PVA and PVA-SA-CuNPs.

The FTIR spectrum of PVA-SA-CuNPs shows prominent peak at 1500 cm^{-1}, which indicates the interaction of the PVA-SA matrix and the CuNPs present. The peak at 1500 cm^{-1} also denotes absorption due to asymmetric vibration of the carboxylate (COO^{-}) group. The aggregation of copper ions and carboxyl-containing polymers have been reported. A series of changes in the spectra of PVA-SA-CuNPs can be observed in the wavelength range 1000–2000 cm^{-1} due to the immobilization of CuNPs in the PVA-SA matrix (Fig. 7.1).

Fig. 7.2 displays FESEM images of the PVA-SA-CuNPs catalyst, which shows a dry gel-like structure. The FETEM images show the presence of uniform and monodispersed nanoparticles. Fig. 7.3 shows the FETEM images of CuNPs, which confirm the spherical shape and

polycrystalline nature of the nanoparticles. Fig. 7.3b shows the particle size distribution of the CuNPs, and the results show that the nanoparticles were in the range of 5-10 nm.

The thermal stability of the PVA-SA-CuNPs catalyst was checked using thermogravimetric analysis (TGA). It was confirmed from the TGA analysis that the prepared catalyst is thermally stable and negligible amount of PVA-SA leached up to 200 °C. Fig. 7.4 demonstrates the thermal decomposition behavior of the PVA-SA-CuNPs catalyst.

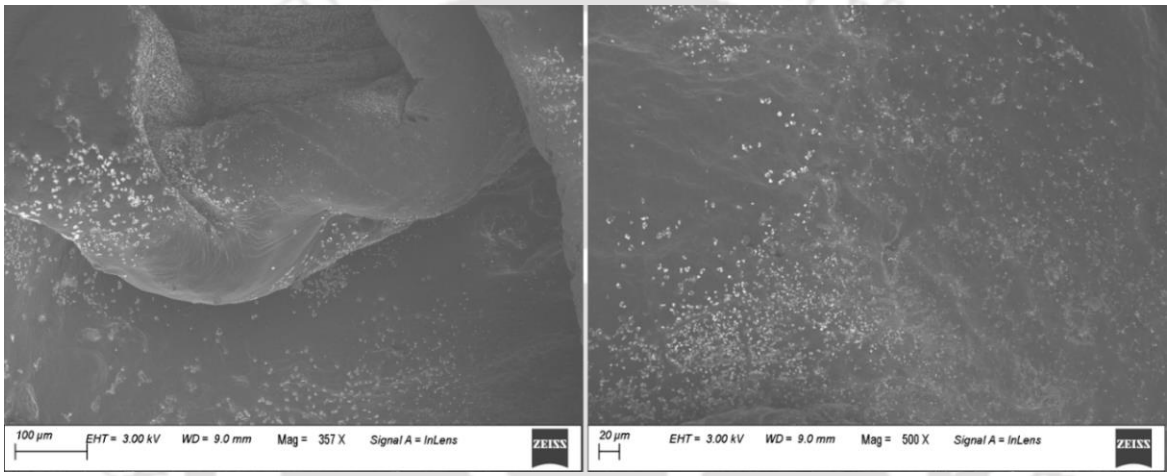

Fig. 7.2 FESEM images of CuNPs immobilized PVA-SA.

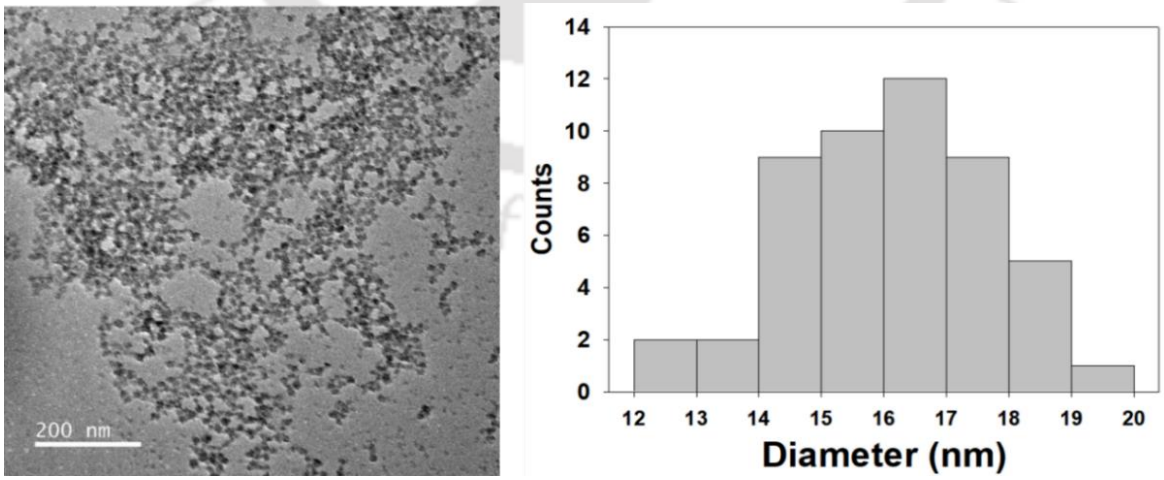

Fig. 7.3 FETEM image (a) and particle size distribution (b) of the CuNPs immobilized PVA-SA.

EDX spectra of CuNPs immobilized onto PVA-SA confirmed the presence of copper in the immobilized matrix (Fig. 7.6). Fig. 7.7 represents the UV–Vis spectrum of CuNPs and the band centered at 572 nm.

Structure and crystallographic orientation of the immobilized catalyst were analyzed based on its XRD spectrum in the range 10°–80° diffraction angle (2θ) (Fig. 7.8). The diffraction peaks at 2θ value of 26.2°, 28°, 46.5°, correspond to different lines formed by (111), (200) and (220) planes and are attributed to those of cubic shaped Cu (JCPDS no. 04-0836). The diffraction peaks in the XRD spectrum specify the crystalline nature of CuNPs in the sample (Lee et al., 2010; Kaboudin et al., 2013).

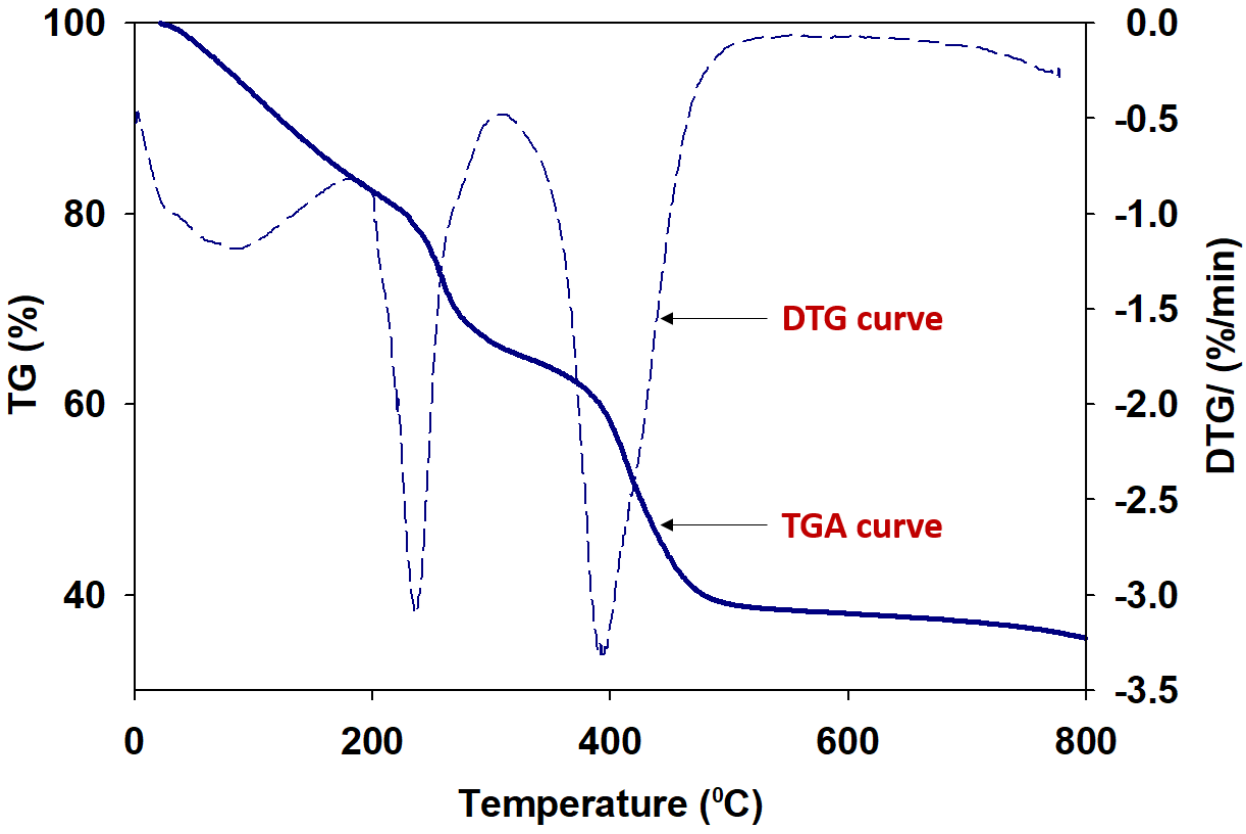

Fig. 7.4 Thermogravimetric analysis curve of CuNPs immobilized PVA-SA.

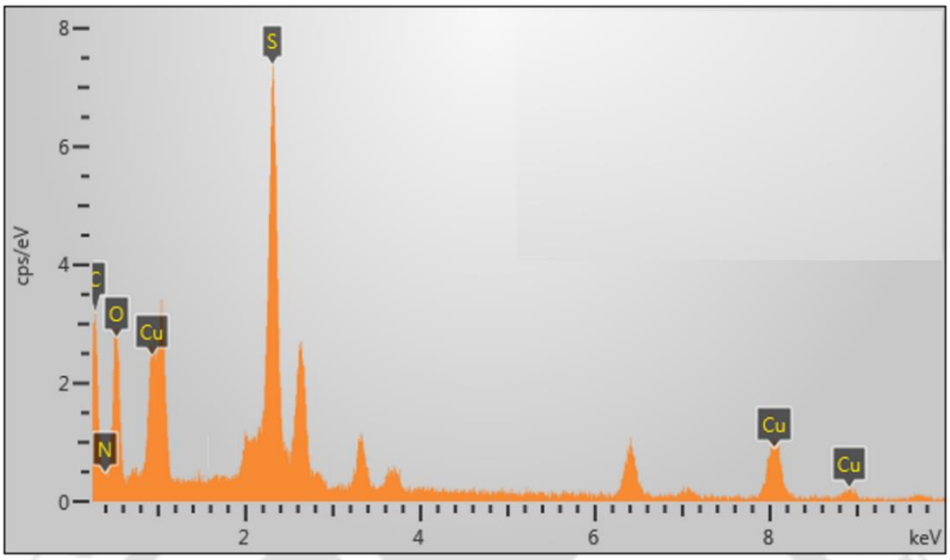

Fig. 7.5 EDX spectrum of CuNPs immobilized PVA-SA.

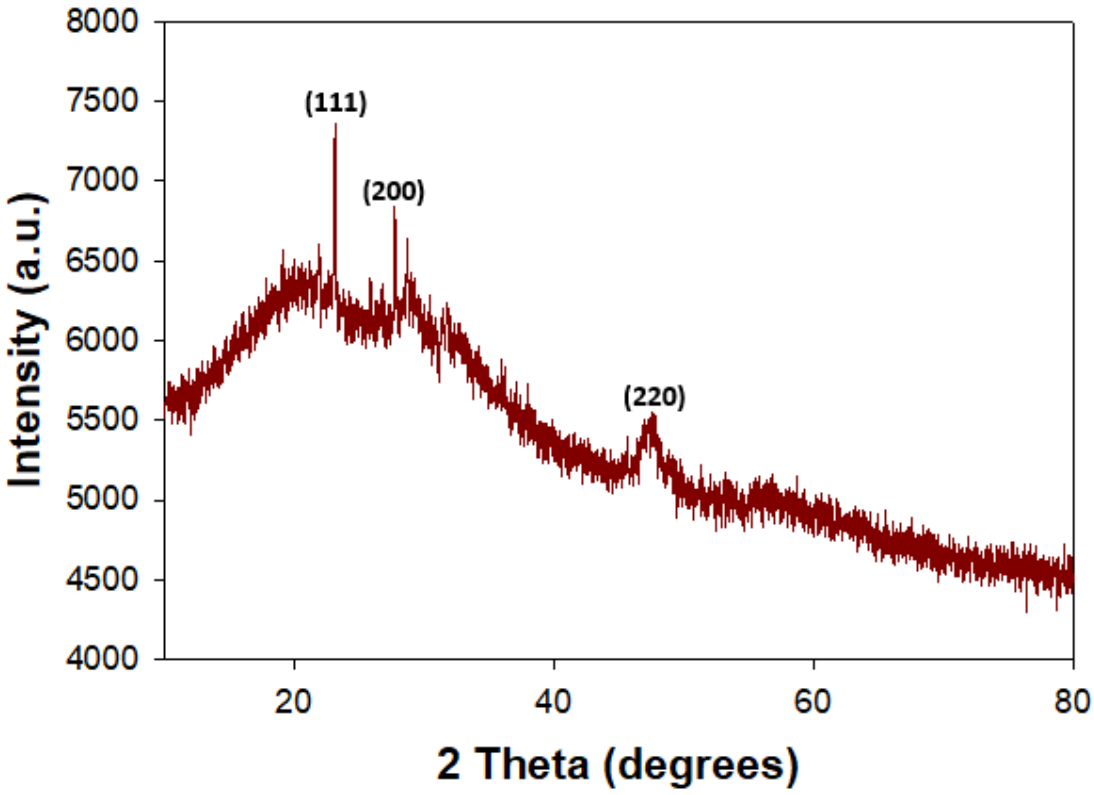

Fig. 7.6 XRD pattern of the CuNPs.

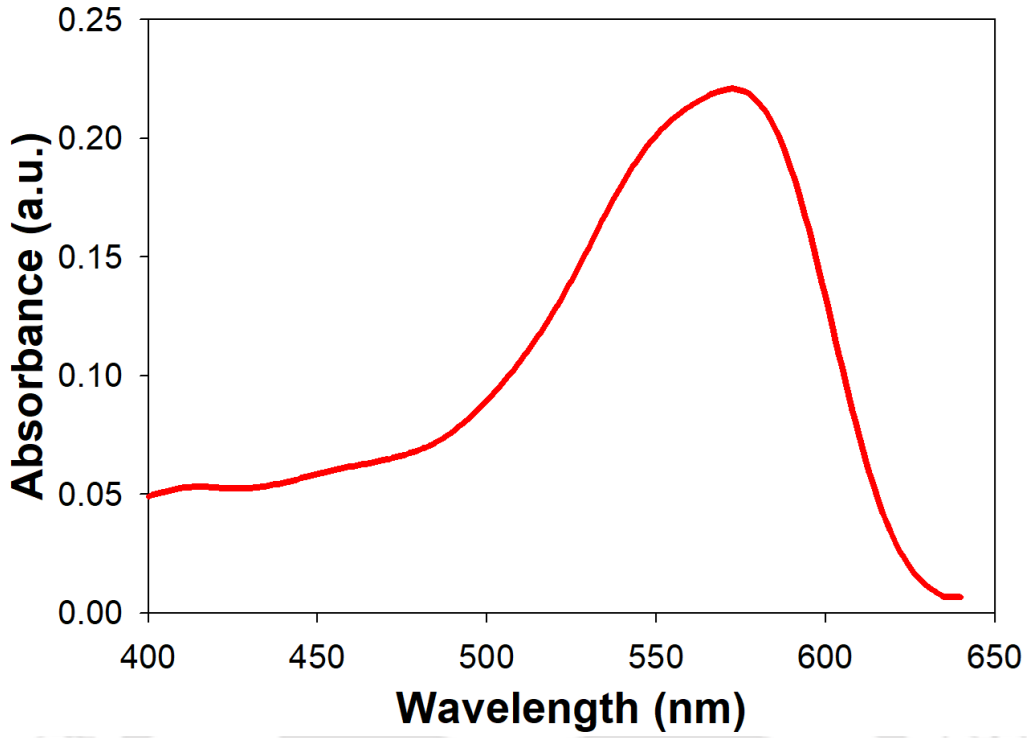

Fig. 7.7 UV–Vis spectrum of PVA-SA-CuNPs.

7.3.2 Selection of parameters for click reaction

The catalytic activity of PVA-SA-CuNPs was determined using a cycloaddition reaction of azide and alkyne using water as the solvent. Considering the reaction between azidobenzene and phenylacetylene was selected as a model reaction for this study, the effect of different reaction conditions, e.g., solvent, amount of catalyst, and reaction time, were examined. The results show that 0.10 mmol of the immobilized copper catalyst, using water as the solvent at 30 °C temperature and 12 h reaction time, is the best reaction condition (Table 7.2, Table 7.3, and Table 7.4). The reaction between azide and alkyne is presented as shown below (Reaction 1)

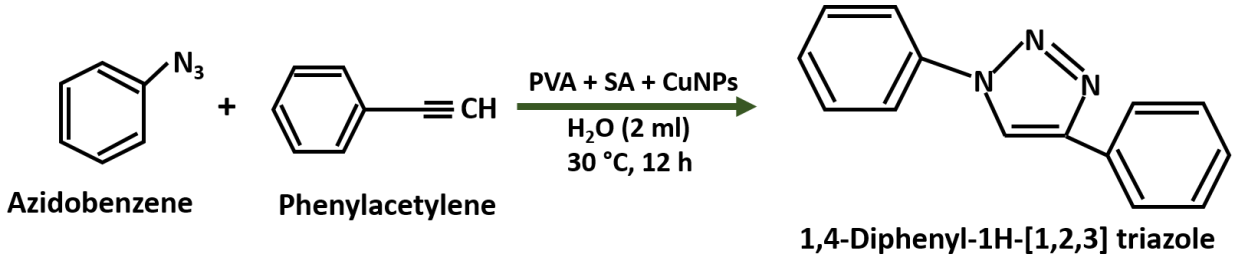

Table 7.1 Effect of different amounts of PVA-SA-CuNPs on the yield of 1,4-Diphenyl-1H-[1,2,3] triazole (other reaction conditions: 30 ºC temperature, water as solvent and 12 h reaction time)

S.No.	mole% CuNPs	Yield (%)
1	0.05	30
2	0.06	65
3	0.08	88
4	0.10	92

Table 7.2 Effect of different solvents on the yield of 1,4-Diphenyl-1H-[1,2,3] triazole (other reaction conditions: 30 ºC temperature, 0.10 mole% CuNPs and 12 h reaction time)

S.No.	Solvents	Yield (%)
1	Dichloromethane (CH_2Cl_2)	20
2	Tetrahydrofuran (THF)	20
3	Methanol (CH_3OH)	60
4	Water (H_2O)	92
5	Toluene (C_7H_8)	40

Table 7.3 Effect of reaction time on the yield of 1,4-Diphenyl-1H-[1,2,3] triazole (other reaction conditions: 30 ºC temperature, water as solvent and 0.10 mole% CuNPs)

S. No.	Reaction time (h)	Yield (%)
1	6	45
2	8	70
3	12	92
4	15	92

7.3.3 Synthesis of the Triazoles

In the case of nanoparticles, the reactivity of the particle's surface is more due to the free valencies of the surface atom. In addition, the surface area of the catalyst is very high in the case of nanosize particles.

Different alkynes and azides were used to produce a variety of triazole products using PVA-SA-CuNPs catalyst in copper catalyzed azide alkyne cycloaddition (CuAAC) reaction (Table 7.3). The cycloaddition reaction was conducted on a 2 mL scale using 0.25 mmol of each reagent and PVA-SA-CuNPs (0.10 mol%, 10 mg) as the catalyst at 30 °C for 12 h. The triazole product was separated by extraction with ethyl acetate. It was observed that the reactants were fully consumed in the reaction, and the final product obtained was white solid at ambient temperature. The PVA-SA-CuNPs catalyst used in this study showed excellent conversion efficiency, and a very high (82–93%) triazole yield was achieved. Compared with this value, slight lower yield of 1,2,3-triazoles yield (77-85%), were obtained using PVA-g-AA/Cu NPs catalyst via click reaction, as reported by Kal-Kashvandi et al. (2008). The high triazole yield obtained in the present study signifies the

high tolerance of the biogenic immobilized catalyst toward different functional groups, e.g., ketones, alcohols, ethers, esters, and heterocycles. Table 7.4 compares the performance of the biogenic CuNPs in this study with literature.

Table 7.4: Comparison of various protocols used for "Click" reaction

S. No.	Reaction time	Conditions	Reference
1	12 h	Copper catalyst from distillery wastewater, 25 °C	Kimber et al., 2019
2	8 h	Agarose-supported CuNPs, water as solvent	Gholinejad et al., 2020
3	25-50 min	Grafting of AA onto PVA involving MEK-peroxide during the sonication process	Kal-Kashvandi et al., 2018
4	10-15 min	PVP-protected CuNPs, aerated condition, room temperature	Sarkar et al., 2008
5	12 h	PVA-Sodium alginate as support material, 30 °C, water as solvent	This study

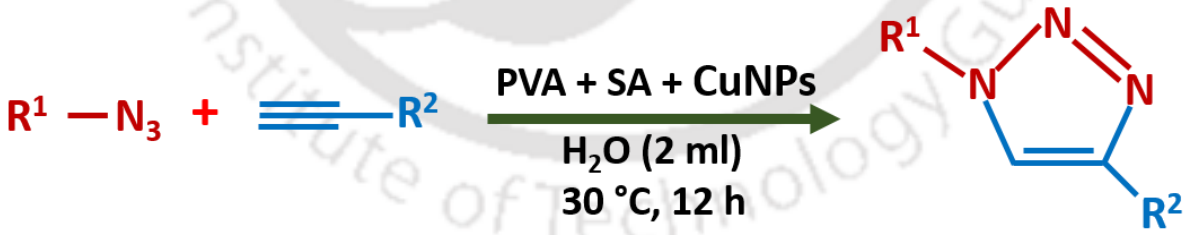

Fig. 7.8 Formation of 1,2,3-triazoles catalyzed by PVA-SA-CuNPs via click reaction.

Table 7.5 Yield of different products obtained in this study by reactions of different azides and alkynes in the presence of biogenic CuNPs in water

S.No.	Azide	Alkyne	Product	Yield (%)
1	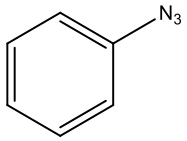 Azidobenzene	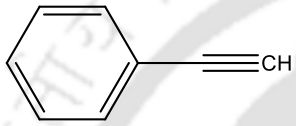 Phenylacetylene	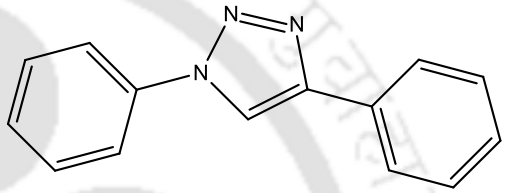 1,4-Diphenyl-1H-[1,2,3] triazole	92
2	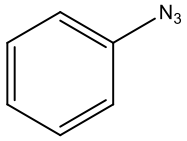 Azidobenzene	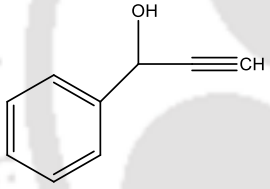 1-Phenyl-2-propyn-1-ol	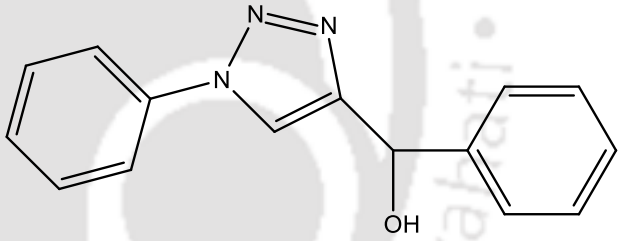 Phenyl (1-phenyl-1H-[1,2,3] -triazol-4-yl) methanol	90
3	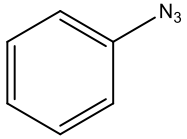 Azidobenzene	 Propargyl chloride	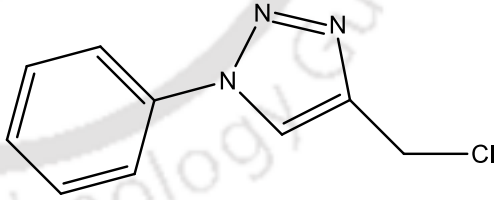 4-(chloromethyl)-1-pheny;-1H-[1,2,3] -triazole	94

4	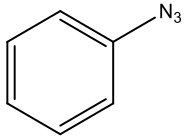 Azidobenzene	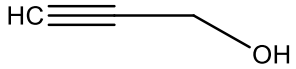 Propargyl alcohol	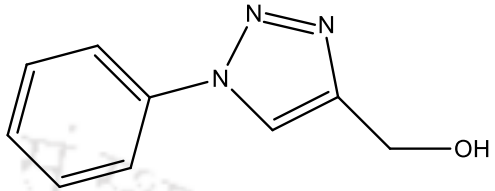 (1-phenyl-1H-[1,2,3] -triazol-4-yl) methanol	93
5	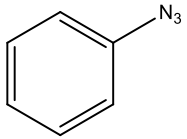 Azidobenzene	 Propargylamine	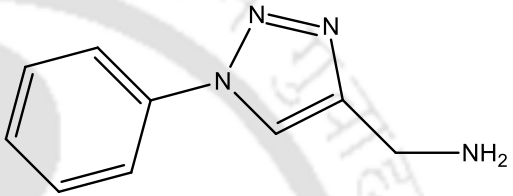 (1-phenyl-1H-[1,2,3] -triazol-4-yl) methanamine	92
6	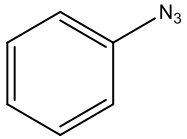 Azidobenzene	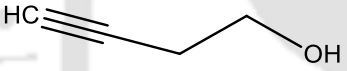 3-Butyn-1-ol	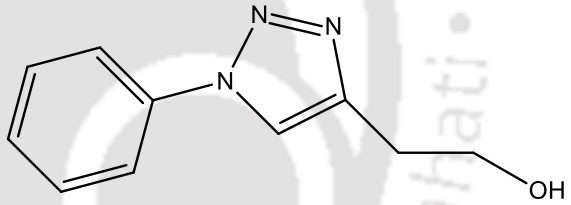 1-phenyl-4-hydroxyethane-1H-[1,2,3] triazole	93
7	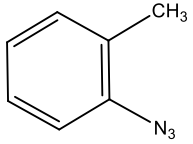 2-Azidotoluene	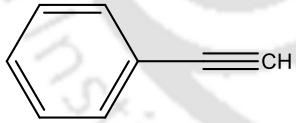 Phenylacetylene	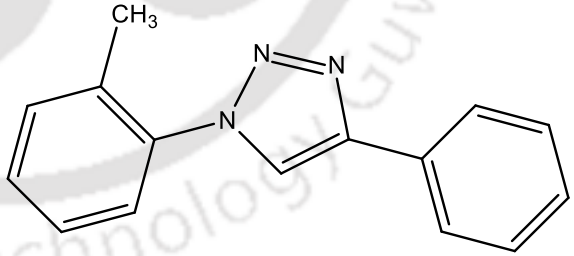 4-phenyl-1-(o-totyl)-1H-[1,2,3] -triazole	88

8	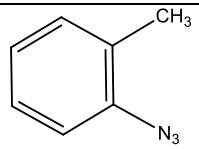 2-Azidotoluene	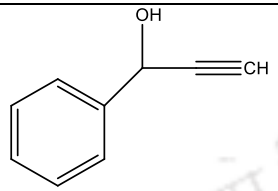 1-Phenyl-2-propyn-1-ol	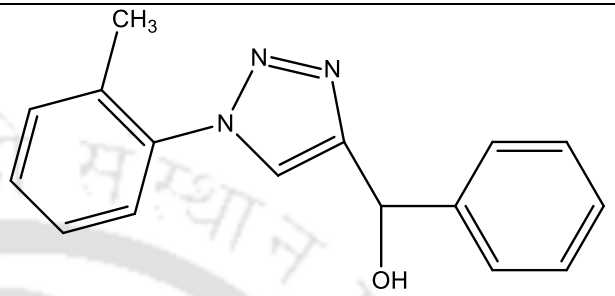 Phenyl(1-(o-totyl)-1H-[1,2,3] -triazol-4-yl) methanol	89
9	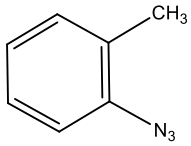 2-Azidotoluene	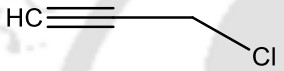 Propargyl chloride	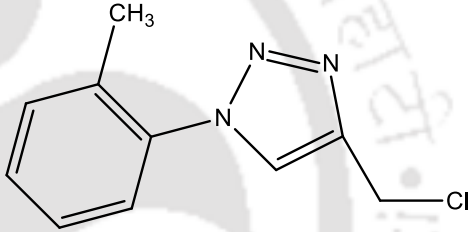 4-(chloromethyl)-1-(o-totyl)-1H-[1,2,3] -triazole	91
10	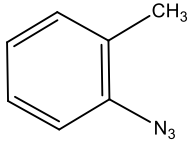 2-Azidotoluene	 Propargyl alcohol	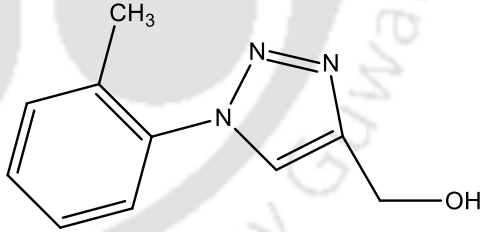 (1-(o-totyl)-1H-[1,2,3] -triazol-4-yl) methanol	85

11	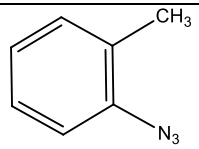 2-Azidotoluene	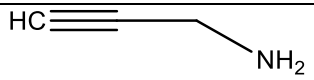 Propargylamine	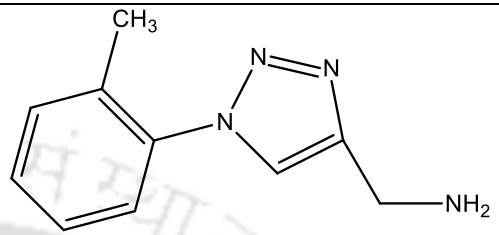 (1-(o-totyl)-1H-[1,2,3] -triazol-4-yl) methanamine	84
12	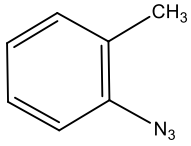 2-Azidotoluene	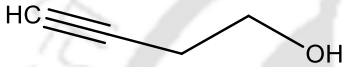 3-Butyn-1-ol	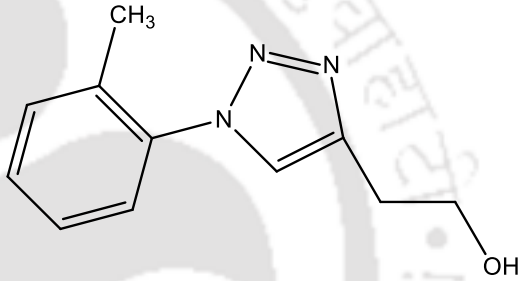 2-(1-(o-totyl)-1H-[1,2,3] -triazol-4yl) ethan-1-ol	82
13	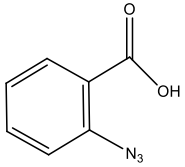 2-Azidobenzoic acid	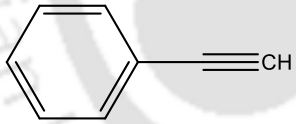 Phenylacetylene	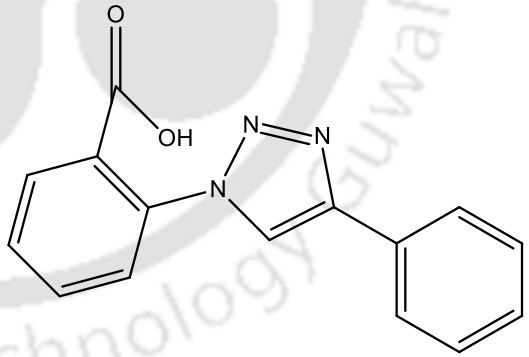 2-(4-phenyl-1H-[1,2,3] -triazol-1yl) benzoin acid	90

14	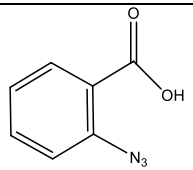 2-Azidobenzoic acid	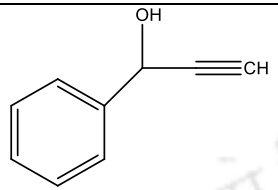 1-Phenyl-2-propyn-1-ol	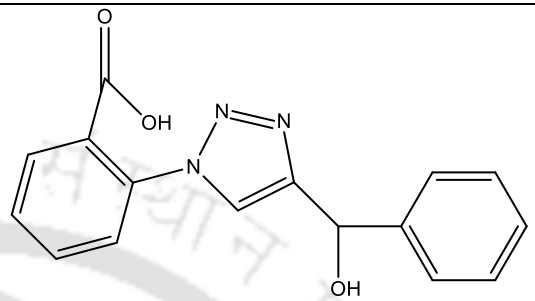 2-(4-(hydroxyl(phenyl)methyl)-1H-[1,2,3] -triazol-1-yl) benzoin acid	87
15	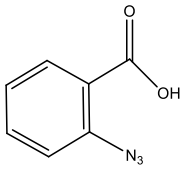 2-Azidobenzoic acid	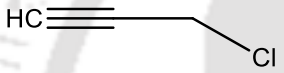 Propargyl chloride	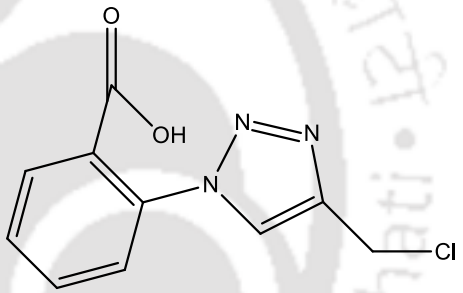 2-(4-(chloromethyl)-1H-[1,2,3] -triazol-1yl) benzoic acid	86
16	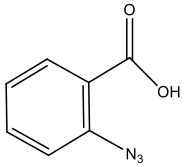 2-Azidobenzoic acid	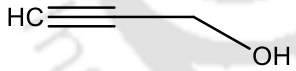 Propargyl alcohol	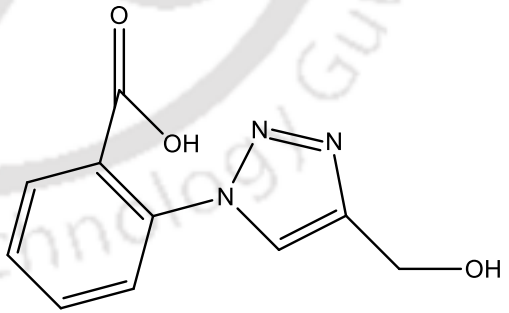 2-(4-(hydroxymethyl)-1H-[1,2,3] -triazol-1-yl) benzoic acid	88

17	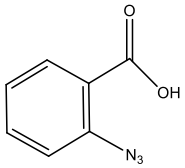 2-Azidobenzoic acid	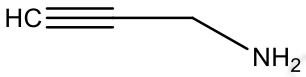 Propargylamine	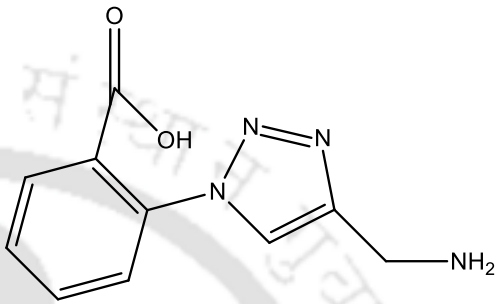 2-(4-(aminomethyl)-1H-[1,2,3] -triazol-1-yl) benzoic acid	92
18	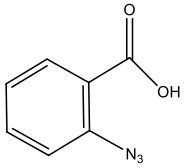 2-Azidobenzoic acid	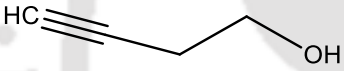 3-Butyn-1-ol	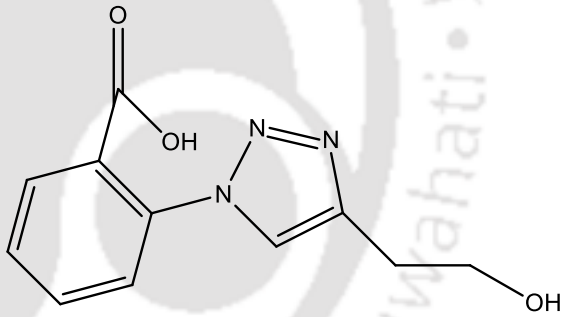 2-(4-(2-hydroxyethyl)-1H-[1,2,3] -triazol-1yl) benzoic acid	90

7.3.4 Mechanism

The proposed mechanism for the reaction between different alkynes and azides is the same as the mechanism reported in the literature for multicomponent click reactions (Gholinejad et al., 2020). A probable mechanism of the reaction is depicted in Fig. 7.8. The possible adsorption mechanism involved in immobilization of CuNPs onto PVA and sodium alginate is presented in Fig. 7.9.

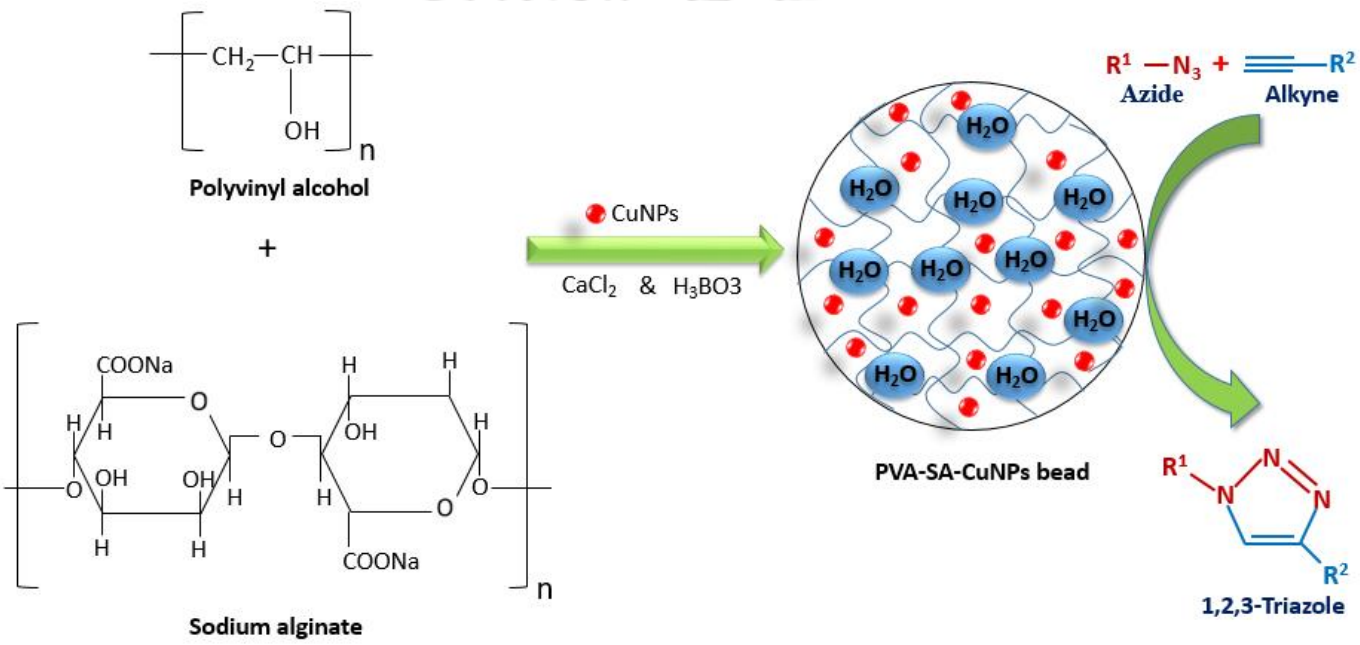

Fig. 7.9 Mechanism of synthesis of PVA-SA-CuNPs beads and triazoles.

7.3.5 Recycling of the catalyst

The regeneration capacity of the PVA-SA-CuNPs catalyst was investigated. The catalyst was separated from the product at the end of the reaction between azidobenzene and phenylacetylene, and after the product was extracted using ethyl acetate. The spent PVA-SA-CuNPs catalyst was then washed with water before use in next batch run. The same procedure was repeated for upto five cycles. Fig. 10 shows the results of the triazole yield, which shows that the catalytic activity of the biogenic CuNPs slightly decreased with every subsequent runs.

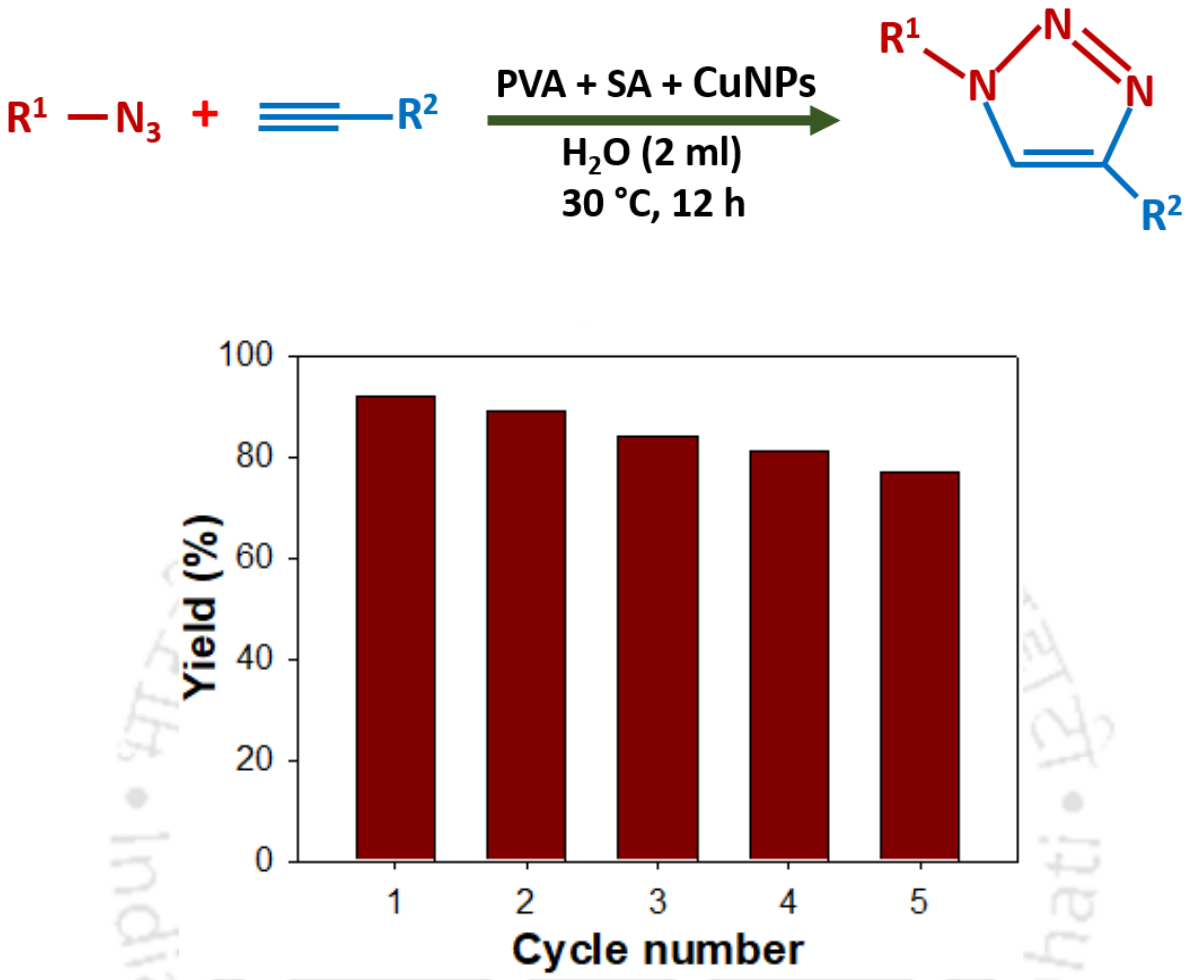

Fig. 7.10 Effect of recycle and reuse of PVA-SA-CuNPs catalyst on the product yield by reaction between azidobenzene and phenylacetylene.

7.4 Significant findings

In this study, biogenic CuNPs from acid mine drainage were synthesized and used in click reaction to produce triazoles. The biogenic catalyst used in this study showed excellent catalytic activity and triazole yield under mild reaction conditions. The catalyst was characterized using different techniques such as FESEM, EDX, FETEM, TGA, and XRD, revealed its potential for various industrial applications. Recycle and reuse of the spent PVA-SA-CuNPs catalyst in the study for upto five cycle resulted in a slight decrease in triazole yield with every subsequent run.

Chapter 8

Induced oxidative stress in *Rhodococcus opacus* due to biogenic and chemical nanoparticles of lead sulfide and cadmium sulfide

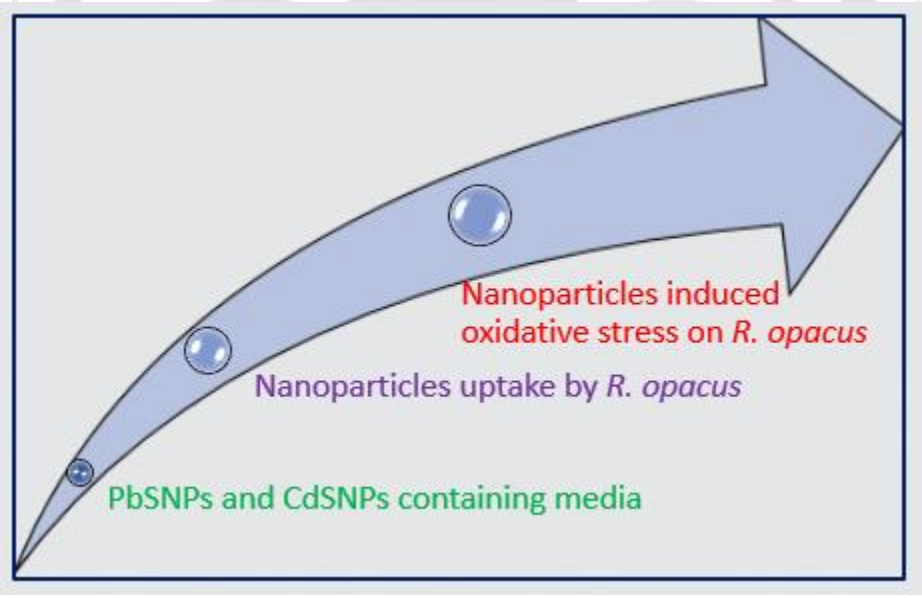

ABSTRACT

The occurrence of lead sulfide (PbS) and cadmium sulfide (CdS) nanoparticles in the effluents released from industries and wastewater treatment plants has raised concerns. The fate of these nanoparticles (NPs) and their potential impact on organisms from different ecosystems are widely investigated. In this work, the individual effect of biogenic and chemical PbS NPs and CdS NPs on the activity of the oleaginous bacterium *Rhodococcus opacus* PD630, which belongs to an ecologically important genus *Rhodococcus* was investigated. A dose-dependent increase in PbS NPs and CdS NPs uptake by the bacterium was observed upto a maximum of 16.4 and 15.6 mg/(g cell), corresponding to 98% and 95% uptake. In the case of chemical nanoparticles, the specific PbS NPs and CdS NPs uptake were slightly less (15.5 and 14.8 mg/(g cell)), corresponding to 93.2% and 88.4% uptake. Both biogenic and chemical PbS NPs and CdS NPs did not affect the bacterial viability. On the other hand, the triacylglycerol (biodiesel) content in the bacterium increased from 30% to a maximum of 75% and 73% CDW due to oxidative stress induced by biogenic PbS NPs and CdS NPS. The results of induced oxidative stress by biogenic metal nanoparticle were similar to that induced by chemical nanoparticle.

8.1 Introduction

The demand for nanoparticles has increased for different applications in energy, environment, catalysis, food, textile, biomedical, and material sciences (Singh et al., 2018). With the increasing use and application of diverse nanoparticles, there is an increasing need for a better understanding of the benefits and risks associated with the use of nanoparticles in different fields (Foulkes et al., 2020; Martinez et al., 2021). The increasing use of the engineered nanomaterials in consumer products necessitates the requirement for performing risk assessment on the environment and human health. Nanomaterials can be defined as materials with a single unit small-sized measuring 1-100 nm and having unique chemical and physical properties (Martinez et al., 2021).

With the rapid development of nanotechnology, metal sulfide nanoparticles have been widely detected in the environment, including water, soils, and sediments (Ubaid et al., 2020). Engineered metal sulfide nanoparticles such as cadmium sulfide nanoparticles (CdS NPS), CdS quantum dots (CdS-QDs), and lead sulfide nanoparticles (PbS NPS) have been intensively produced and used worldwide, resulting in their release into the environment (Ubaid et al., 2020). In recent years, metal sulfide nanoparticles, particularly CdS and PdS nanoparticles, have been observed in the sludge of wastewater treatment plants and sludge-amended soils, indicating their intensive occurrence in the environment (Garner et al., 2014; Ubaid et al., 2020).

Heavy metal removal by sulfate-reducing bacteria (SRB) is attributed to producing metal sulfide nanoparticles. Under anaerobic environment, SRB oxidizes simple organic compounds by utilizing sulfate as an electron acceptor and generates sulfide and alkalinity. The biogenic sulfide is capable of reacting with dissolved metals to form highly insoluble metal sulfide precipitates (Villa-Gomez et al., 2011). The problem with the sulfate reduction process for metal removal includes the generation of insoluble metal precipitates, which may leach out and adversely affect the

environment. Such metal nanoparticles are toxic to animals and other living organisms, thereby necessitating its further treatment and risk assessment on the ecosystem.

Several studies highlight the toxic effects of nanoparticles. However, their risk potential is uncertain and cannot be generalized as there are multiple factors such as size, shape, and surface area, among many others that govern nanoparticles behavior (Shang et al., 2014; Semenzin et al. 2015). A knowledge gap exists regarding PbS NPs and CdS NPs fate and hazard characterization, their uptake, and accumulation. Some techniques have been proposed to remove emerging contaminants (ECs) from the effluent of wastewater treatment plant (Lead et al., 2018; Bilal et al., 2019). Biodegradation of ECs is considered effective and involves the use of microbes and immobilized degradation enzymes (Men et al., 2017; Bilal et al., 2019). However, NPS such as PbS and CdS are nonbiodegradable. Meanwhile, the biological filtration process using a crustacean *Daphnia magna* was effective in removing ECs like pharmaceuticals from WTP effluent (Ahmed et al., 2017).

Different studies have shown high resistance and removal of lead and cadmium using *R. opacus* from wastewater (Bueno et al., 2008; Dobrowolski et al., 2017). However, the effect of PbS NPs and CdS NPs, on the *Rhodococcus* bacteria has not been thoroughly characterized. Further, since the genus *Rhodococcus* is a strong inhabitant of contaminated soil and water, and its plays a significant role in detoxification (Ivshina et al., 2019), studying their response to new environmental stressors like PbS NPs and CdS NPs is of importance. In general, *Rhodococci* accumulate triacylglycerols (TAG) as main storage compounds, whereas PHA and glycogen represent only minor components of cells (Urbano et al., 2014). Some strains can be considered oleaginous bacteria since they accumulate more than 20% of their biomass as lipids. *Rhodococcus opacus* PD630, the best known TAG-accumulating member of the *Rhodococcus* genus, can

accumulate very high TAG levels in cells by cultivation on gluconate and other substrates (Alvarez et al. 1996).

The accumulation of significant amounts of TAG by *Rhodococci* is a carbon-intensive and energy-demanding process, which competes with their cell growth. Thus, accumulation of such storage compounds in microorganisms under energy-poor environments must be an important feature in their physiology. Urbano et al. (2014) demonstrated that TAG metabolism is relevant for adapting and surviving the extremophile *Rhodococcus sp.* A5 under carbon starvation, osmotic stress, UV irradiation, and essential under desiccation conditions. The mobilization of TAG was also necessary for the survival of *R. opacus* PD630 cells under starvation, osmotic stress, and oxidative stress. Oxidative stress in cells causes overproduction of reactive oxygen species (ROS), resulting in significant damage to cell structures. However, as per literature reports, oxidative stress responses of *Rhodococcus* microorganisms have been less investigated previously. The selection of a suitable growth media is also necessary, which is a deciding factor for TAG accumulation.

Hence, in this study, the effects of different PbS NPs and CdS NPs, on the growth of *Rhodococcus opacus* bacterium as a model organism was studied. Owing to their high toxic effects, Cd and Pb nanoparticles were chosen for their induced oxidative stress study. In particular, the effect of PbS NPs and CdS NPs on their lipid (triacylglycerol or TAG) accumulation was studied as induced oxidative stress response to the nanoparticles.

8.2 Materials and methods

8.2.1 *Rhodococcus opacus* and seed culture cultivation

The oleaginous gram-positive bacterium *Rhodococcus opacus* PD630 was obtained from Microbial Type Culture Collection (MTCC), Chandigarh, India. For maintenance, the strain was grown on 1.8% (w/v) Nutrient Broth (NB) agar slants and was stored at 4 °C. The pure culture was

regularly sub-cultured every four weeks by growing at 30 °C for 48 h. The seed culture of *R. opacus* was cultivated in a 250 mL Erlenmeyer flask containing 50 mL of Luria Bertani (LB) broth. A full loop of the bacteria was inoculated into the autoclaved medium followed by incubation at 30 °C and 120 rpm until the absorbance of the culture reached 0.99, as measured at 660 nm using a UV–Vis Spectrophotometer (Agilent Technologies, Singapore). For biomass growth, and lipid production by *R. opacus*, nutrient broth (NB) media was used.

8.2.2 PbS NPs and CdS NPs

8.2.2.1 Biogenic nanoparticles

Biogenic PbS and CdS nanoparticles were synthesized from synthetic AMD by anaerobic sulfate reduction using sulfate reducing biomass in IFBR as described earlier in Chapter 4.

8.2.2.2 Chemical nanoparticles

Lead nitrate $Pb(NO)_3$ procured from Merck India was used for the synthesis of chemical PbS NPs. Lead nitrate was dissolved in double distilled water to make N/20 aqueous solution. NH_4OH solution was slowly added with constant stirring to obtain the required pH value (8.0). Then H_2S gas was then bubbled through the solution for a few seconds. The resulting black precipitate was collected and washed with distilled water several times and then centrifuged for 15 min. The nanoparticles were dried by heating for 30 min at 60 °C and then allowed to cool at room temperature. Finally, the black colored PbS NPs were obtained and stored room temperature for future use in the experiments.

Cadmium chloride ($CdCl_2$), sodium sulfide (Na_2S), and ascorbic acid purchased from Sigma for preparing chemical CdS NPs in this study. Double distilled water was used throughout the experiment. CdS NPs were prepared by stirring $CdCl_2$, Na_2S, and ascorbic acid in a 1: 1: 1 molar ratio. The yellow colored CdS NPs were washed with distilled water 10-15 times and subjected to

air drying. The as-prepared PbS NPs and CdS NPs were used without any further processing in all the experiments.

8.2.3 Effect of PbS and CdS nanoparticles on biomass growth and lipid accumulation by *R. opacus*

Different concentrations of biogenic and chemical PbS NPs and CdS NPs were used to study their effect on biomass growth and lipid accumulation by *R. opacus*. The different concentration chosen were 10 mg/L, 25 mg/L, 50 mg/L, and 100 mg/L of both biogenic and chemical PbS and CdS nanoparticles. The nanoparticle concentration was chosen based on the lead and cadmium concentration found in metallic wastewater such as acid mine drainage (AMD). The working concentrations of PbS NPs and CdS NPs mentioned earlier were obtained by adding required volume of respective PbS NPs and CdS NPs stock solutions to the NB medium. The media was inoculated with *R. opacus* PD 630 and maintained at 28 °C and 200 rpm on a shaker incubator. All the experiments were conducted using 250 mL Erlenmeyer flasks with 100 mL medium. Samples were taken at regular time intervals for the analysis of biomass, lipids and concentration of lead and cadmium.

8.2.4 Analytical methods

8.2.4.1 Characterization of *R. opacus* biomass and metal nanoparticles

Following the batch experiments to determine the effect of PbS NPs and CdS NPs on biomass growth and lipid accumulation by *R. opacus*, the metal-loaded biomass as well as biogenic PbS NPs and CdS NPs used in this study were characterized using various techniques, viz. Fourier-transform infrared spectroscopy (FTIR), field emission scanning electron microscopy-energy dispersive X-ray (FESEM-EDX), and field emission transmission electron microscopy (FETEM). For the FTIR analysis, control biomass (without any added metal) and metal laden biomass were

harvested by centrifugation of the respective culture at 12,000 × g for 15 min, followed by washing of pellet obtained with distilled water. The vacuum dried sample was analyzed using FTIR (IR affinity-1S, Shimadzu, Japan). Similar procedure for sample preparation was followed for FESEM-EDX (Zeiss, Sigma, Germany) analysis to check morphology of the biomass. For FETEM analysis, control and metal loaded biomass were obtained by centrifuging the respective culture at 8000 × g for 15 min followed by washing with distilled water. The obtained pellet was dissolved in distilled water, and a drop of the biomass suspension was cast in a copper grid and analyzed using FETEM (JOEL, JEM2100, Japan).

8.2.4.2 Lipid extraction and analysis

Standard Folch method with slight modifications was used to determine the total lipid content accumulated by *R. opacus* (Goswami et al., 2017). 5 mL of sample from the experiments was taken and centrifuged (1000 × g, 10 min) to collect the pellet, followed by hominization of the pellet in a solvent mixture comprised of chloroform and methanol (2:1). The homogenized mixture was shaken for 15-20 min in a shaker incubator at ambient room temperature and again centrifuged (3500 × g, 10 min) to recover the liquid solvent phase. The obtained liquid solvent phase was washed with 20% (v/v) of water or 0.9% (v/v) NaCl solution. The mixture was vortexed and then centrifuged (3500 × g, 10 min) for separating the two different phases. The upper phase was drawn off, and the lower chloroform phase containing the lipids was evaporated under vacuum using a rotary evaporator (Rotavapor R3, Buchi, Switzerland). The extracted lipids were finally quantified by gravimetric analysis.

8.2.4.3 Intracellular hydroxyl radical (oxidative stress) measurement

To measure the intracellular hydroxyl radical (˙OH) levels in *R. opacus* PD 630 as measure of oxidative stress, method based on the fluorescent dye p–aminophenyl fluorescein (APF) was used.

(Setsukinai et al., 2003). For this assay, sample of the bacteria culture harvested at 12th h was adjusted to OD 1, and APF was added to the cell suspension to yield a final concentration of 10 μM. A fluorimeter (LS55, PerkinElmer, Llantrisant, UK) was used for the fluorescence measurements at 490/515 nm excitation/emission in a 96-well plate.

8.2.4.4 Heavy metal analysis

Lead and cadmium concentrations were determined by microwave plasma atomic emission spectroscopy (Varian, 4210 MP-AES, Agilent Technologies, USA) following filtration of the samples through a 0.45 μm nitrocellulose filter (Millipore).

8.3 Results and discussion

8.3.1 Characterization of PbS NPs and CdS NPs

In order to check if the biogenic Cd and Pb nanoparticles were obtained in uniformly dispersed form in the solution, their particle size distribution analysis was performed, which revealed their particle size in the range 10-20 nm. In case of chemical PbS and CdS nanoparticles, their size were in the range of 30-40 nm. The zeta potential of biogenic PbS NPs and CdS NPs were – 30 ± 2.1 mV and – 31.5 ± 1.8 mV, respectively. In the case of chemical PbS NPs and CdS NPs, their zeta potential values were – 27 ± 2.7 mV and -28.4 ± 2 mV, which indicated that the metal nanoparticles synthesized in this study were stable and existed as colloidal aggregates. It is known that the zeta potential values greater than – 30 mV indicate highly stable colloidal aggregates (Ebaid et al., 2018).

Similarly, the size of PbS NPs and CdS NPs in NB to study their effect on biomass concentration and lipid accumulation by *R. opacus* was measured by DLS. The diameter of biogenic PbS NPs and CdS NPs at 10, 25, 50, and 100 mg/L concentration in NB was found to be 32 ± 3, 36 ± 4, 41 ± 5, and 50 ± 5 nm, respectively. In the case of chemical PbS NPs and CdS NPs, the diameter in

NB was 75 ± 6, 81 ± 9, 92 ± 10, and 100 ± 15 nm, respectively, for 10, 25, 50, and 100 mg/L initial concentration.

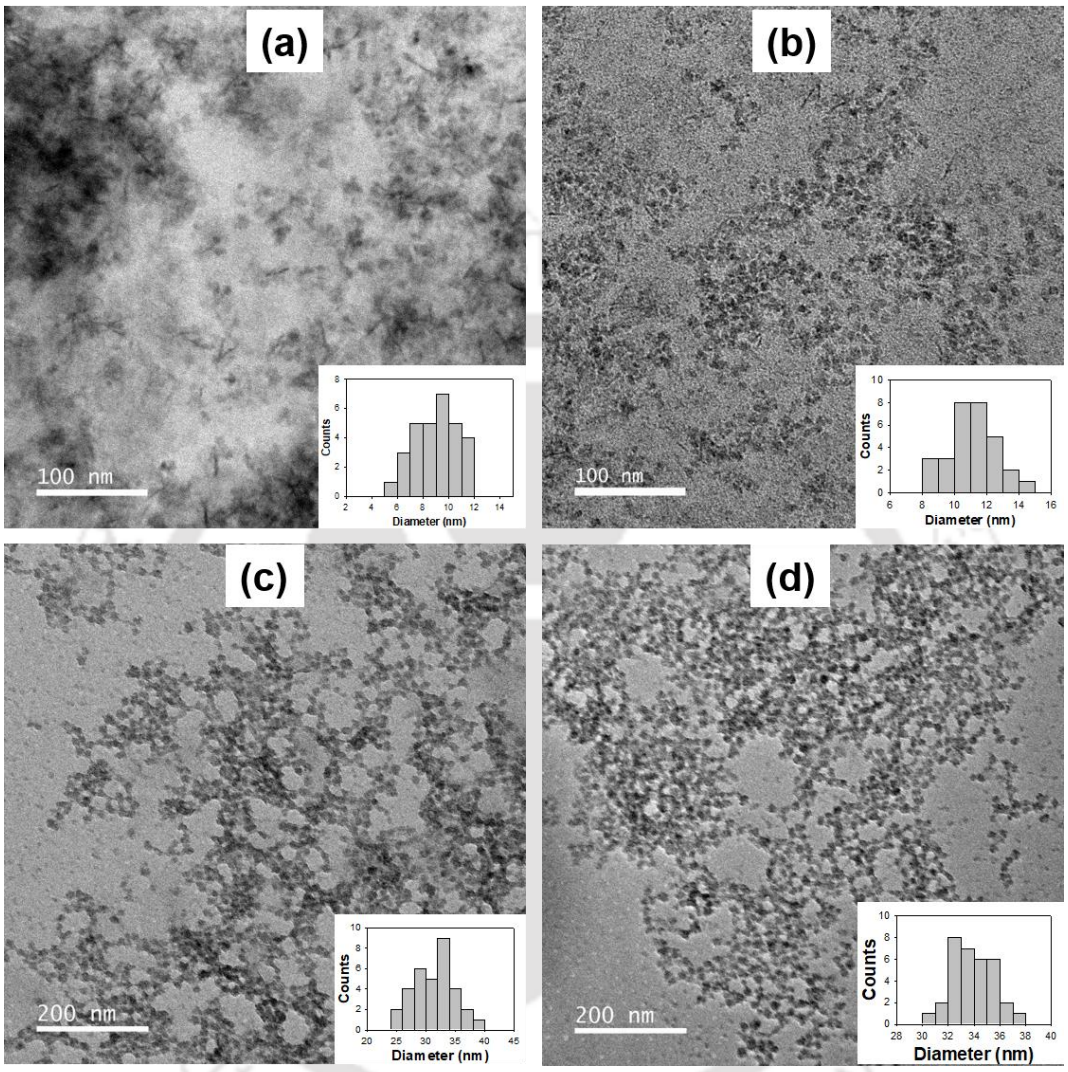

Fig. 8.1 FETEM images of biogenic (Mean size: 12.5 nm; Standard deviation: 1.2 nm) (a-b) and chemical (Mean size: 32.2 nm; Standard deviation: 1.5 nm) (c-d) PbS NPs and CdS NPs. Particle size distribution of each nanoparticle is shown as inset to these figures.

The size of both the biogenic and chemical PbS NPs and CdS NPs in NB are found to be large at a high initial concentration due to their aggregation in the liquid medium (Zong et al., 2018; Guerrini et al. 2018). The high ionic strength of the nutrient media can also lead to the nanoparticles aggregation (Guerrini et al., 2018). The nanoparticle aggregation in turn can lead to

particle sedimentation and reduction in reactive surface area of the nanoparticles. However, continuous shaking at a high speed can prevent nanoparticle aggregation and settling (Zhang et al., 2020), thus ensuring uniform dispersion of the metallic nanoparticles in the liquid media.

8.3.2 Binding and uptake of metal nanoparticles by *R. opacus* PD 630

For any study involving bacteria and nanoparticles, nanoparticle attachment on cell surface and internalization is common (Lai et al., 2018; Sundararaghavan et al., 2020). FTIR was used to confirm the attachment and internalization of Pb SNPs and CdS NPs onto *R. opacus* PD630.

For FTIR analysis, the control biomass sample was scanned from 500 cm^{-1} to 4000 cm^{-1} wavelengths to check the different functional groups present (Fig. 8.2). The hydroxyl group (-OH) presence can be confirmed by the band present in the range 3000-3600 cm^{-1} (Kiran et al., 2017). The presence of amide group (-NH) and a carboxyl group (-C=O) is indicated by the bands present at 1500-1580 cm^{-1} and 1600 - 1700 cm^{-1}, respectively (Kiran et al., 2017). The band present at 1050 cm^{-1} signifies the presence of the sulfide group.

Fig. 8.2 b, c, d, and e show that the bands mentioned above shifted to the new position in the spectra of metal laden biomass confirming internalization of the metal nanoparticles by *R. opacus* PD 630. For example, in case of biogenic PbS NPs, bands were stretched at 1065 cm^{-1}, 1642 cm^{-1} and 3288 cm^{-1} and in case of CdS NPs stretching of bands are observed at 1065 cm^{-1}, 1640 cm^{-1} and 3280 cm^{-1} in the spectra.

In case of chemical PbS NPs, shift in band is observed at 1074 cm^{-1}, 1645 cm^{-1} and 3286 cm^{-1} and in case of CdS NPs bands were shifter to 1073 cm^{-1}, 1631 cm^{-1} and 3298 cm^{-1}.

To better understand the nature of binding of metal nanoparticles onto bacterium the surface charge of both bacteria biomass and nanoparticles was measured. The mean zeta potential of *R. opacus* PD 630 was -9.2 mV, and in the case of biogenic PbS NPs and CdS NPs, it was -12.9 mV and -

11.5 mV. The values were -12.2 mV and -10.5 mV in the case of chemical PbS NPs and CdS NPs, respectively. The zeta potential results clearly suggest that the binding between the nanoparticles and *R. opacus* PD 630 did not involve electrostatic interaction.

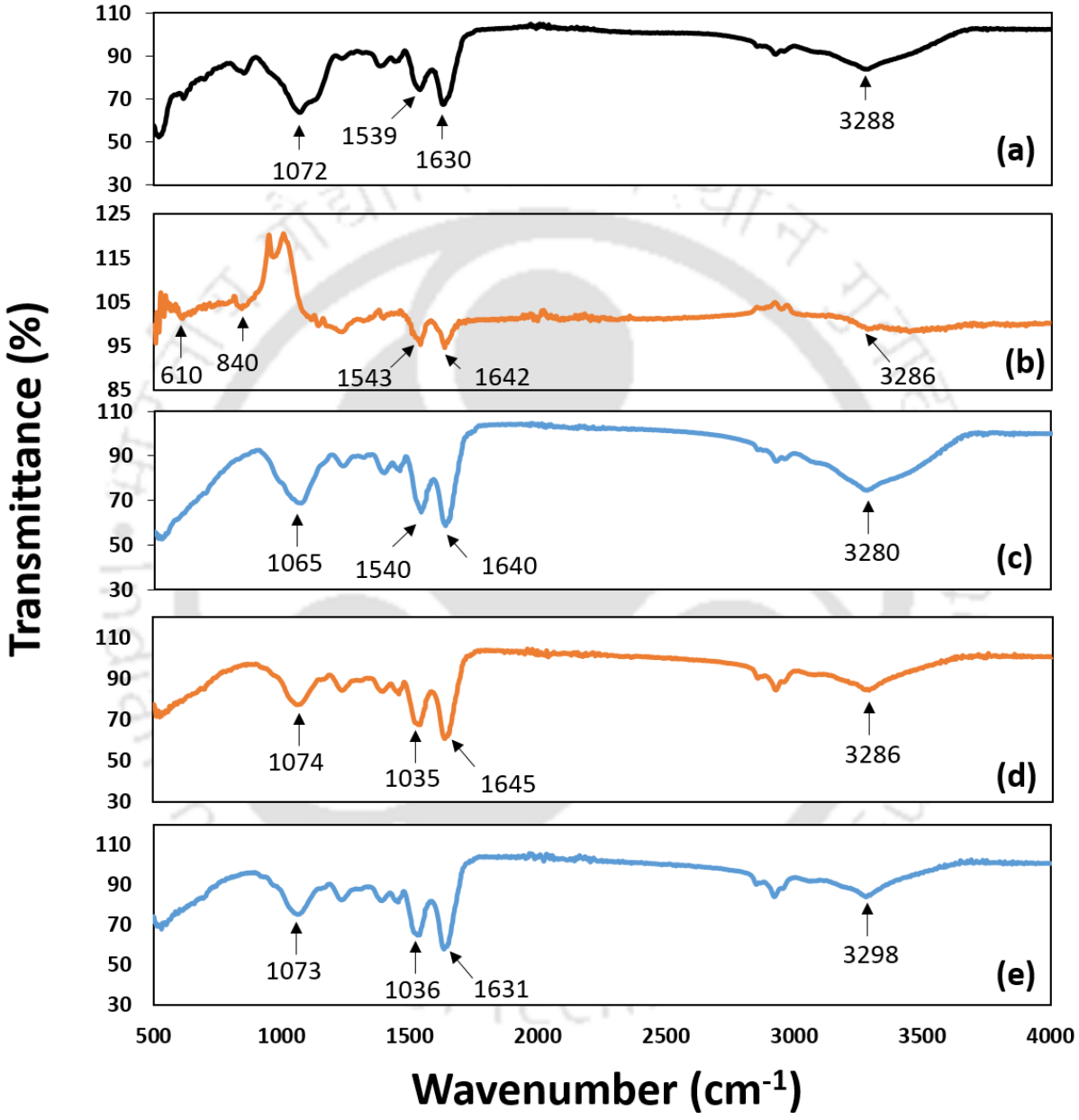

Fig. 8.2 FTIR spectra of (a) control biomass (b-c) biogenic PbS NPs and CdS NPs laden biomass and (d-e) chemical PbS NPs and CdS NPs laden biomass.

The metal uptake capacity of *R. opacus* PD 630 was checked by analyzing the concentration of nanoparticles both internalized and attached to bacterial surface. Fig. 8.2 shows the results of uptake capacity of *R. opacus* PD 630 for biogenic and chemical PbS NPs and CdS NPs. It is seen that the uptake capacity increased increase in initial concentration of the nanoparticles. The maximum uptake capacity was found with 100 mg/L initial concentration of the nanoparticles. Uptake values of biogenic PbS NPs and CdS NPs uptake were 16.4 and 15.6 mg/(g cell) for biologically synthesized nanoparticles, respectively. In the case of chemical nanoparticles, the specific PbS NPs and CdS NPs uptake values were 15.5 and 14.8 mg/(g cell), respectively (Fig. 8.3).

The high uptake capacity value of biogenic nanoparticles by the bacterium can be due to their less toxicity than the chemical nanoparticles.

The maximum uptake capacity values of 16.4 and 15.6 mg/(g cell) of the PbS NPs and CdS NPs correspond to the percentage uptake values of 98 and 95, respectively. In the case of chemical nanoparticles, the percentage uptake values are 93.2 and 88.4, which are slightly less than the percentage uptake of the biogenic PbS NPs and CdS NPs. Hence, it could be said that, the both biogenic and chemical metal nanoparticles showed similar results of metal uptake by the bacterium in a dose-dependent manner.

Similar results of increase in uptake percentage of titanium dioxide nanoparticles ($nTio_2$) by *R. opacus* PD 630 with an increase in their initial concentration were observed by Sundararaghavan et al. (2020).

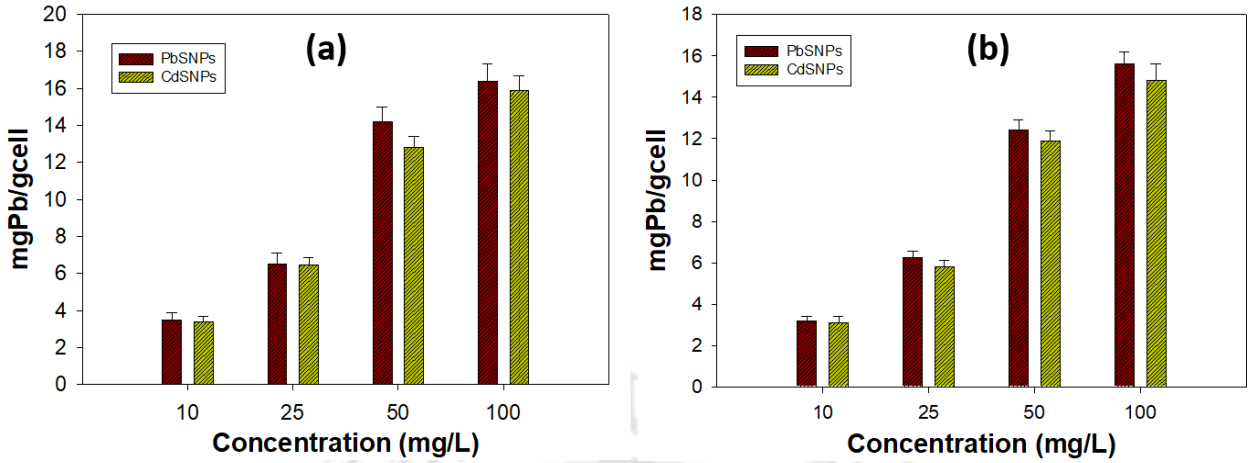

Fig. 8.3 Uptake capacity of (a) biogenic and (b) chemical PbS NPs and CdS NPs by *R. opacus* PD 630.

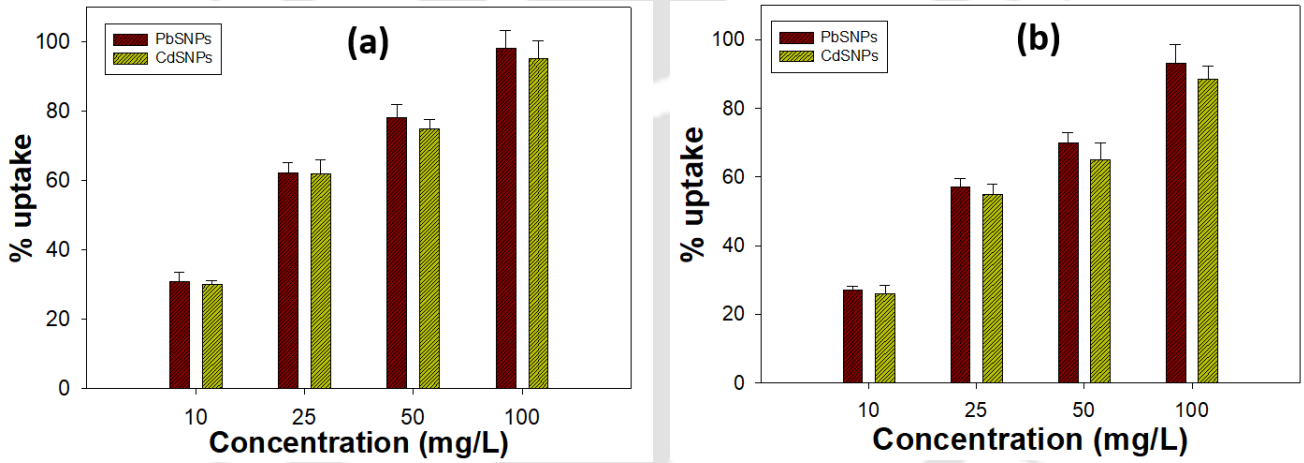

Fig. 8.4 Percentage removal of (a) biogenic and (b) chemical PbS NPs and CdS NPs by *R. opacus* PD 630.

8.3.3 Nanoparticle induced oxidative stress in *R. opacus* PD 630

One of the common responses of *R. opacus* PD 630, when exposed to any toxic compound such as heavy metals, is oxidative stress through the generation of reactive species (RS) (Sundararaghavan et al., 2020).). Thus, in this study, the induced oxidative stress in *R. opacus* PD 630 by PbS NPs and CdS NPs exposure was studied by determining the intracellular levels of hydroxyl radicals ($^{\bullet}OH$), which is the most reactive form of oxygen.

In the presence of biogenic PbS NPs and CdS NPs in the liquid medium, a dose-dependent increase in si–OH levels by *R. opacus* PD 630 were observed (Fig. 8.5). The increase in si–OH levels were 78, 115, 230, and 320% w.r.t control for initial PbS NPs concentrations of 10, 25, 50, and 100 mg/L, respectively. In the case of CdS NPs, the increase in si–OH levels were 30, 67, 95, and 108% w.r.t control for initial concentrations of 10, 25, 50, and 100 mg/L, respectively (Fig. 8.5). In case of chemical PbS NPs, the in si–OH levels were 75, 110, 220, and 310% w.r.t control for initial PbS NPs concentrations of 10, 25, 50, and 100 mg/L, respectively. However, in the case of CdS NPs, the si-levels were 70, 105, 204, and 300% w.r.t control for initial concentrations of 10, 25, 50, and 100 mg/L, respectively. Si-OH levels due to biogenic and chemical PbS NPs were nearly the same for different initial concentrations. But in case of chemical CdS NPs the values were higher than in the presence of biogenic CdS NPs.

The slightly higher values of si-OH levels on the case of chemical CdS NPs than the biogenic CdS NPs indicate their toxicity towards *R. opacus* PD 630. Hence, in order to confirm the relative toxicity effect of biogenic and chemical nanoparticles towards the bacterium, its cell morphology and lipid accumulation were examined.

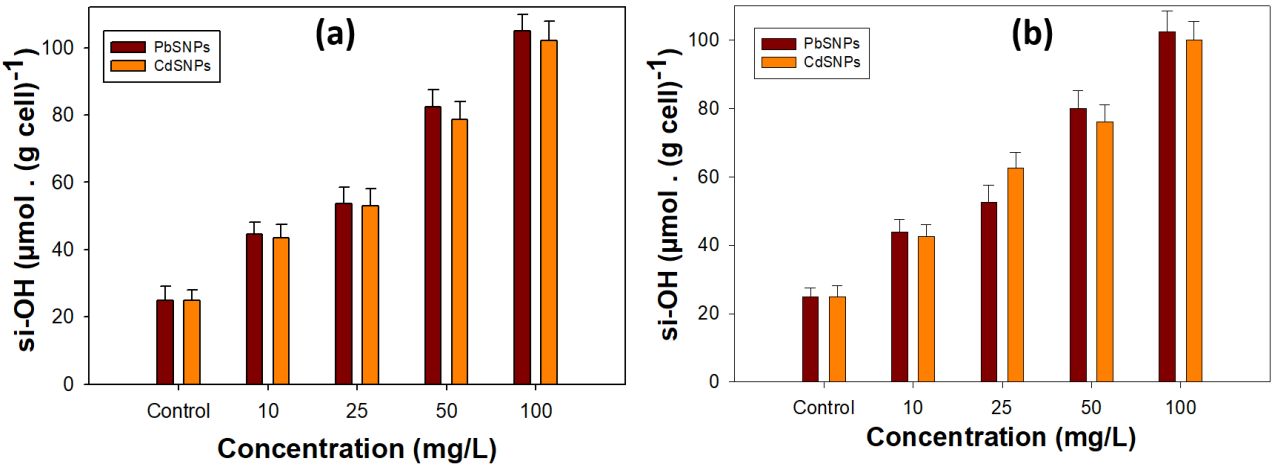

Fig. 8.5 Specific intracellular levels of hydroxyl radicals in *R. opacus* PD 630 in the presence of (a) biogenic (b) chemical PbS and CdS NPs.

The increase in RS generation in a cell due to toxicity of metal nanoparticles is a common phenomenon (Marslin et al., 2017; Chen et al., 2019). The oxidative stress induced by the nanoparticles can damage the cell membrane and viability of the cells (Sundararaghavan et al., 2020; Roy et al., 2018). The bacterium *R. opacus* is known to survive in very extreme and toxic conditions (Ivshina et al., 2019). Hence, in the current study, despite the high concentration of PbS NPs and CdS NPs in the bacterium growth media, no significant change in the growth of *R. opacus* PD 630 was observed with both biogenic and chemical nanoparticles.

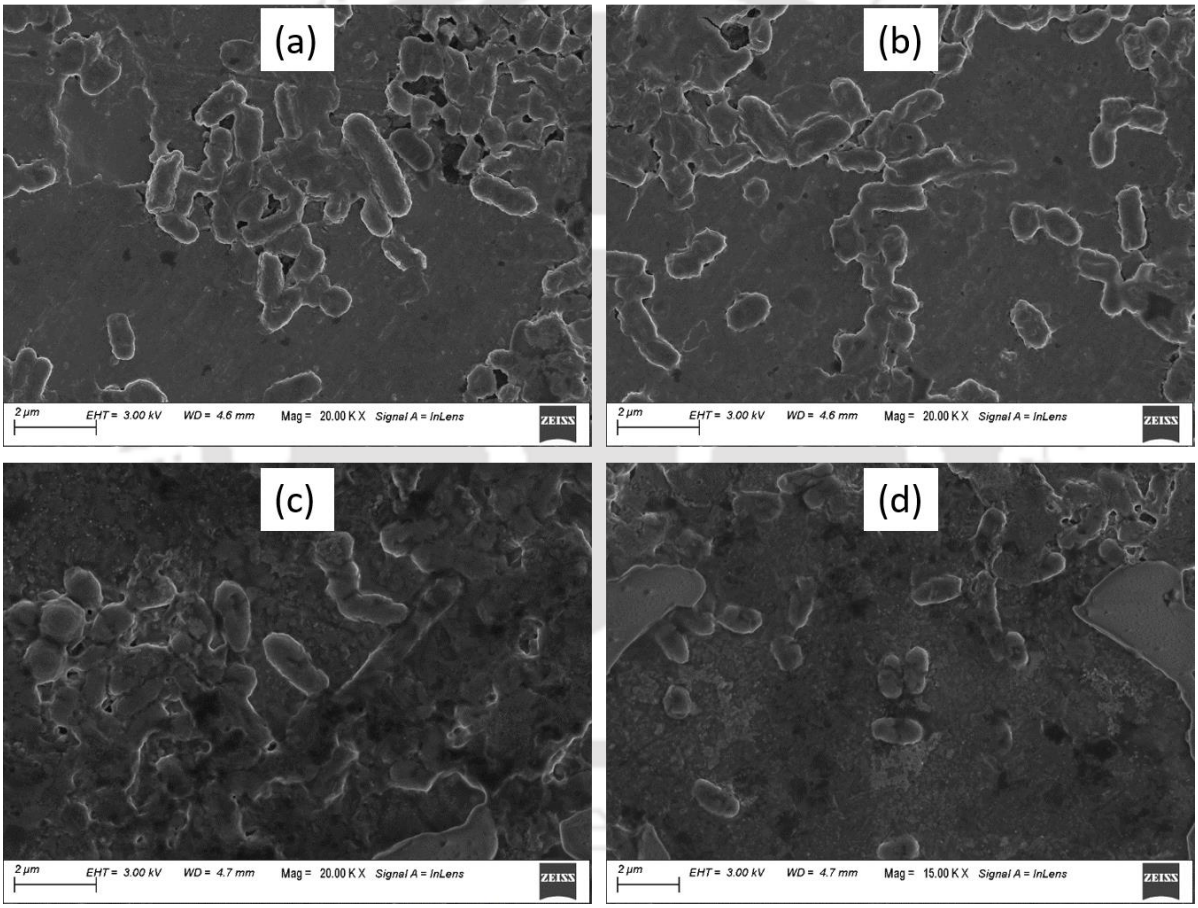

Fig. 8.6 FESEM images of *R. opacus* PD 630 cells in the presence of (a-b) biogenic (c-d) chemical PbS NPs and CdS NPs.

Moreover, from FESEM images of the bacterium shown in Fig. 8.6, no significant change in morphology of the cells are observed with both biogenic and chemical nanoparticles.

Oxidative stress caused by RS in oleaginous microorganisms is known to positively influence the lipid accumulation (Minhas et al., 2016; Bermejo et al., 2018). Hence, in this study, oxidative stress induced by PbS NPs and CdS NPs in *R. opacus* PD 630 improved the TAG production. In addition, dose-dependent increase in FAMEs content were observed in the presence of the nanoparticles.

In case of biogenic PbS NPs, the FAMEs content increased by 20, 36, 45, and 75% w.r.t control for initial PbS NPs concentration of 10, 25, 50, and 100 mg/L, respectively. Similarly, In the case of CdS NPs, the FAMEs content increased by 18, 35, 42, and 73% w.r.t control for initial CdS NPs concentration of 10, 25, 50, and 100 mg/L, respectively (Fig. 8.7).

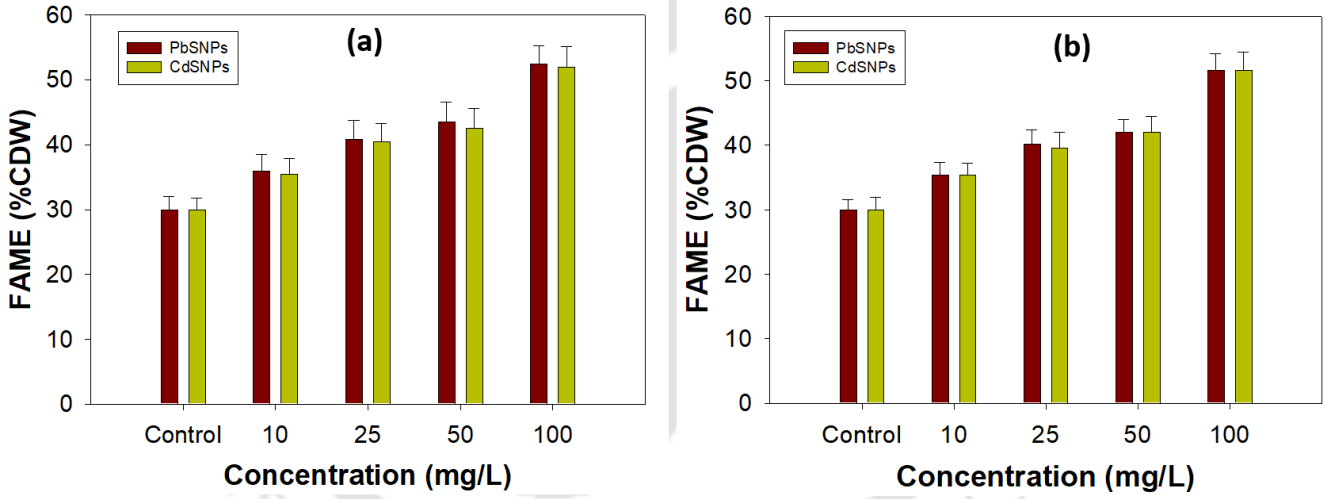

Fig. 8.7 FAME content of biodiesel from *R. opacus* PD 630 exposed to (a) biogenic (b) chemical PbS NPs and CdS NPs.

The values of FAME content were lower in the case of chemical nanoparticles. In the case of chemical PbS NPs the FAME content increased by 18, 34, 40, and 72% w.r.t control for initial PbS NPs concentration of 10, 25, 50, and 100 mg/L, respectively. These values were similar w.r.t control for initial CdS NPs concentration of 10, 25, 50, and 100 mg/L, respectively. The specific mechanism through which RS increased the lipid accumulation is not yet understood properly.

However, RS is an essential mediator in carbon partitioning and lipid accumulation (Shi et al., 2017).

All these results clearly reveal that both biogenic and chemical nanoparticles of PbS and CdS induced oxidative stress in the organism, but without any major change in morphology of the bacterial cells.

8.4 Significant findings

This study showed induced oxidative stress in *R. opacus* PD630 due to PbS NPs and CdS NPs. The bacterium revealed a very high uptake of the biogenic metal nanoparticles over the chemical nanoparticles. Besides, increase in TAG accumulation by *R. opacus* PD630 due to oxidative stress induced by biogenic/chemical PbS NPs and CdS NPs was observed. Hence, this study shows that both biogenic and chemical metal nanoparticles exert almost similar effect on the industrially relevant bacteria. Therefore, such metal nanoparticles, biogenic or chemical from wastewater, need to be reused and recycled for industrial application in order to avoid any environmental health hazard.

Chapter 9

Summary and conclusions

Metallic wastewater from industrial activities such as mining, metallurgy, galvanization of iron products, electroplating, and alloy manufacturing can serve as a potential source for recovering valuable metals. Biological sulfate reduction using sulfate reducing bacteria (SRB) is an emerging technique for both removal and recovery of valuable metals. Sulfide precipitation by SRB is advantageous over the conventional methods due to the following reasons: (i) formation of insoluble salts even in low pH (2.5-3.0) condition (ii) selective metal recovery is possible as metals differ by their solubility product with sulfide (iii) high settling rate, excellent thickening and dewaterability characteristics and (iv) low capital investment. Biological sulfate reduction is attractive for both removal and recovery of the metals in the form of nanosized insoluble metal sulfide precipitates from wastewater. Recovery of metal nanoparticles from wastewater by sulfide precipitation is interesting option from economic and environmental perspectives. Synthesis of metal nanopowders by sulfate reduction process is a new topic of research and has not been widely reported since earlier studies were focused on sulfate reduction and metal removal. It has been recognized recently that recovery of valuable metals such as Zn, Cu, Cd, Ni, etc. from wastewater can be achieved in nano-size range by precipitation as metal sulfide using SRB. Hence, this study focused on heavy metal recovery from wastewater and its potential application.

Initially, anaerobic biomass from three different sources were screened on the basis of their metal removal and sulfate reduction efficiencies. The results revealed that the biomass obtained from a laboratory scale anaerobic rotating biological contactor (An-RBC) reactor treating metallic wastewater showed a maximum metal removal, sulfate reduction and COD removal. The metal removal mechanism confirms that metal was precipitated due to the formation of metal sulfide precipitate, which was further confirmed using different techniques such as field emission scanning electron microscopes (FESEM), energy dispersive X-ray (EDX), field emission

transmission electron microscopy (FETEM), and X-ray diffractometer (XRD). The major mechanism of metal sulfide formation involved the binding of metals to sulfide produced outside the cell surface due to sulfate reduction. The metal bioprecipitates formed external to the bacterial cell surface showed easy recovery for potential application. A high initial metal concentration was detrimental to its own removal due to its inhibitory effect on activity of the SRB. Detailed characterization of the recovered nanopowders indicates its potential use in the environment sector.

Further, heavy metal removal and recovery from synthetic wastewater containing Cd^{2+}, $Cu^{2+,}$ Fe^{3+}, Ni^{2+}, Pb^{2+} and Zn^{2+} was investigated using two continuously operated sulfidogenic anaerobic inverse fluidized bed reactors (referred as R1 and R2) supplied with influent of pH 7.0 and 3.0, respectively. IFBR with influent pH 7.0 (R1) performed better than R2 with influent pH 3.0 in terms of metal recovery from wastewater. Maximum recovery of Cu was obtained followed by that of Pb and Cd. The overall order of the metal recovery was Cu > Pb > Cd > Zn > Ni > Fe. In both R1 and R2, the effluent pH was nearly neutral, thereby demonstrating that enough alkalinity was produced in the bioreactors to neutralize the acidic wastewater and the effluent could be safely reused or discharged into the environment. Hence, IFBR has the potential not only to treat heavy metal laden acidic wastewater but also the ability to recover heavy metals in the form of nanopowder.

Recovery of copper sulfide nanoparticles (CuS NPs) from synthetic wastewater by biological sulfate reduction and purification by microfiltration using an indigenous low-cost ceramic membrane were studied. Kaolin (14.45 wt.%), quartz (26.59 wt.%), ball clay (17.58 wt.%), pyrophyllite (14.73 wt.%), and feldspar (5.6 wt.%) were used as the starting materials in fabricating the ceramic membrane. Pretreatment using probe sonication was found effective for an efficient purification of the nanoparticles by releasing the CuS NPs from contaminating impurities.

Microfiltration using the ceramic membrane showed 92% purification efficiency of the CuS NPs with a flux of 77×10^{-4} m^3/m^2s. Excellent characteristics of the CuS NPs in terms of crystallinity, size, shape and purity established its potential industrial application. Porosity, pore size distribution, water permeability, resistance against acidic and alkaline solution as well as low-cost of the indigenously prepared ceramic membrane further established its potential application for large-scale purification of CuS NPs and for other industrial use.

Novel adsorbent based on biogenic metal sulfide nanoparticles (MeSNPs) from sulfate rich metallic wastewater was evaluated for treating dye containing wastewater. The MeSNPs showed a very high capacity to adsorb the azo dyes Direct Red 80 (DR 80) and Mordant Blue 9 (MB 9) from aqueous solution even at their high initial concentration and within a short contact time. More than 99% removal efficiency of both the dyes was achieved by using MeSNPs at the following optimum conditions. Mechanism of dye sorption onto MeSNPs was shown to involve electrostatic interaction between the dyes and the adsorbent. Dynamic adsorption of the dyes was studied using a fixed-bed column with the MeSNPs as a function of liquid flow rates. The MeSNPs bed height (1 cm), inlet dye concentration (25 mg/L), and inlet solution pH 2.0 were the same for both DR 80 and MB 9. The results showed an increase in breakthrough time with a decline in the flow rates for both DR 80 and MB 9 and the breakthrough behavior was explained using Thomas, Clark, and Yoon-Nelson models.

Biogenic CuS NPs from synthetic wastewater were synthesized and evaluated as a catalyst in click reaction to produce triazoles. The biogenic catalyst used in this study showed excellent catalytic activity and triazole yield under mild reaction conditions. The optimum condition for triazole formation was 0.1 mole% CuS NPs, water as a solvent, 12 h reaction time. Different azides and alkynes were used in this study for traizole production. The best triazole yield was obtained in a

reaction between azidobenzene and propargyl chloride. The catalyst was characterized using different techniques such as field emission scanning electron microscopes (FESEM), energy dispersive X-ray (EDX), field emission transmission electron microscopy (FETEM), Thermogravimetric analysis (TGA), and X-ray diffractometer (XRD), which revealed its potential industrial applications. Recycle and reuse of the spent PVA-SA-CuNPs catalyst in the study for upto five cycle resulted in a slight decrease in triazole yield with every subsequent run.

Induced oxidative stress in *R. opacus* PD 630 due to biogenic PbS NPs and CdS NPs was studied. A dose-dependent increase in PbS NPs and CdS NPs uptake by the bacterium was observed upto a maximum of 16.4 and 15.6 mg/(g cell), corresponding to 98% and 95% uptake. A dose-dependent increase in intracellular levels of hydroxyl radicals ($^{\bullet}$OH) were also observed. Besides, increase in TAG accumulation by *R. opacus* PD 630 due to oxidative stress induced by biogenic/chemical PbS NPs and CdS NPs was observed. Hence, this study shows that both biogenic and chemical metal sulfide nanoparticles exert almost similar effect on the industrially relevant bacteria.

In addition to the above findings, the following are the suggestions for future research based on this thesis:

(1) Application of biogenic metal sulfide nanoparticles in solar cells.

(2) Cost analysis of biogenic metal sulfide nanoparticles and comparison with chemical metal sulfide nanoparticles.

(3) Scale-up of the IFBR system for the treatment and recovery of heavy metals.

(4) Identification of specific genes and characterization of enzymes involved in the biosynthesis of nanoparticles.

(5) The currently followed methods to produce nanomaterials include precipitation, sol gel, atomic condensation, etc. However, these methods have not been demonstrated for the synthesis of metal nanoparticles from wastewater. Hence, future research aimed at large scale production of biogenic metal nanoparticles from wastewater can be explored for application in industries.

Bibliography

- Abbasi, M., Rafique, U., Murtaza, G. and Ashraf, M.A., 2018. Synthesis, characterisation and photocatalytic performance of ZnS coupled Ag_2S nanoparticles: A remediation model for environmental pollutants. Arabian journal of chemistry, 11(6), 827-837.
- Abdulrahman Oyekanmi, A., Abd Latiff, A.A., Daud, Z., Saphira Radin Mohamed, R.M., Ismail, N., Ab Aziz, A., Rafatullah, M., Hossain, K., Ahmad, A. and Kamoldeen Abiodun, A., 2019. Adsorption of cadmium and lead from palm oil mill effluent using bone-composite: optimisation and isotherm studies. International Journal of Environmental Analytical Chemistry, 99, 707-725.
- Adeleke, A.R.O., Abdul Latiff, A.A., Daud, Z., Mat Daud, N.F. and Aliyu, M.K., 2017. Heavy metal removal from wastewater of palm oil mill using developed activated carbon from coconut shell and cow bones. Key Engineering Materials, 737, 428-432.
- Ahmed, M.B., Zhou, J.L., Ngo, H.H., Guo, W., Thomaidis, N.S. and Xu, J., 2017. Progress in the biological and chemical treatment technologies for emerging contaminant removal from wastewater: a critical review. Journal of hazardous materials, 323, 274-298.
- Ajmani, A., Patra, C., Subbiah, S. and Narayanasamy, S., 2020. Packed bed column studies of hexavalent chromium adsorption by zinc chloride activated carbon synthesized from Phanera vahlii fruit biomass. Journal of Environmental Chemical Engineering, 8(4), 103825.
- Akcil, A., Koldas, S., 2006. Acid Mine Drainage (AMD): causes, treatment and case studies. Journal of Cleaner Production, 14, 1139-1145.
- Akhtar, M., Malik, M.A., Tuna, F. and O'Brien, P., 2013. The synthesis of iron sulfide nanocrystals from tris (O-alkylxanthato) iron (III) complexes. Journal of Materials Chemistry, 1, 8766-8774.
- Al-Tarazi, M., Heesink, A.B.M., Versteeg, G.F., Azzam, M.O. and Azzam, K., 2005. Precipitation of CuS and ZnS in a bubble column reactor. AIChE journal, 51(1), 235-246.
- Alvarez, H.M., Mayer, F., Fabritius, D. and Steinbüchel, A., 1996. Formation of intracytoplasmic lipid inclusions by Rhodococcus opacus strain PD630. Archives of microbiology, 165(6), 377-386.
- Amara, S., Seghezzi, N., Otani, H., Diaz-Salazar, C., Liu, J. and Eltis, L.D., 2016. Characterization of key triacylglycerol biosynthesis processes in rhodococci. Scientific reports, 6(1), 1-13.
- American Public Health Association, 2005. Standard methods for the examination of water and wastewater. American Public Health Association (APHA): Washington, DC, USA.
- Anastas, P. and Eghbali, N., 2010. Green chemistry: principles and practice. Chemical Society Reviews, 39(1), 301-312.
- Anderson, G.K., Ozturk, I. and Saw, C.B., 1990. Pilot-scale experiences on anaerobic fluidized-bed treatment of brewery wastes. Water Science and Technology, 22, 157-166.
- Arami, M., Limaee, N.Y., Mahmoodi, N.M. and Tabrizi, N.S., 2005. Removal of dyes from colored textile wastewater by orange peel adsorbent: equilibrium and kinetic studies. Journal of Colloid and interface Science, 288(2), 371-376.
- Ardejani, F.D., Badii, K., Limaee, N.Y., Shafaei, S.Z. and Mirhabibi, A.R., 2008. Adsorption of Direct Red 80 dye from aqueous solution onto almond shells: Effect of pH, initial concentration and shell type. Journal of hazardous materials, 151(2-3), 730-737.

- Arnaiz, C., Buffiere, P., Elmaleh, S., Lebrato, J. and Moletta, R., 2003. Anaerobic digestion of dairy wastewater by inverse fluidization: the inverse fluidized bed and the inverse turbulent bed reactors. Environmental technology, 24(11), 1431-1443.
- Aziz, H.A., Adlan, M.N. and Ariffin, K.S., 2008. Heavy metals (Cd, Pb, Zn, Ni, Cu and Cr(III)) removal from water in Malaysia: Post treatment by high quality limestone. Bioresource Technology, 99, 1578-1583.
- Bai, F., Huang, H., Hou, C. and Zhang, P., 2016. Porous carbon-coated cobalt sulfide nanocomposites derived from metal organic frameworks (MOFs) as an advanced oxygen reduction electrocatalyst. New Journal of Chemistry, 40(2), 1679-1684.
- Bai, H., Kang, Y., Quan, H., Han, Y., Sun, J. and Feng, Y., 2013. Treatment of acid mine drainage by sulfate reducing bacteria with iron in bench scale runs. Bioresource Technology, 128, 818-822.
- Bai, H., Kang, Y., Quan, H., Han, Y., Sun, J. and Feng, Y., 2013. Treatment of acid mine drainage by sulfate reducing bacteria with iron in bench scale runs. Bioresource Technology, 128, 818-822.
- Baig, R.N., Vaddula, B.R., Gonzalez, M.A. and Varma, R.S., 2014. N-Allylation of amines with allyl acetates using chitosan-immobilized palladium. RSC Advances, 4(18), 9103-9106.
- Barber, W.P. and Stuckey, D.C., 2000. Effect of sulfate reduction on chemical oxygen demand removal in an anaerobic baffled reactor. Water Environment Research, 72, 593-601.
- Barbosa, L.D.P., Costa, P.F., Bertolino, S.M., Silva, J.C.C.D., Guerra-Sá, R., Leão, V.A. and Teixeira, M.C., 2014. Nickel, manganese and copper removal by a mixed consortium of sulfate reducing bacteria at a high COD/sulfate ratio. World Journal of Microbiology and Biotechnology, 30(8), 2171-2180.
- Barman, J. and Sultana, F., 2016. Synthesis of mix Zinc Oxide and Cadmium Sulphide Nanoparticles, Optoelectronic and antimicrobial activity and application in Water treatment. IOSR-JAP, 8, 46-51.
- Barnes, L.J., Janssen, F.J., Sherren, J., Versteegh, J.H., Koch, R.O. and Scheeren, P.J.H., 1991. New process for the microbial removal of sulphate and heavy metals from contaminated waters extracted by a geohydrological control system. Chemical Engineering Research and Design, 69, 184-186.
- Bermejo, E., Ruiz-Domínguez, M.C., Cuaresma, M., Vaquero, I., Ramos-Merchante, A., Vega, J.M., Vílchez, C. and Garbayo, I., 2018. Production of lutein, and polyunsaturated fatty acids by the acidophilic eukaryotic microalga Coccomyxa onubensis under abiotic stress by salt or ultraviolet light. Journal of bioscience and bioengineering, 125(6), 669-675.
- Bertolino, S.M., Melgaço, L.A., Sá, R.G. and Leao, V.A., 2014. Comparing lactate and glycerol as a single-electron donor for sulfate reduction in fluidized bed reactors. Biodegradation, 25, 719-733.
- Bessa, L.P., Terra, N.M., Cardoso, V.L. and Reis, M.H.M., 2017. Macro-porous dolomite hollow fibers sintered at different temperatures toward widened applications. Ceramics International, 43, 16283-16291.
- Beyenal, H. and Lewandowski, Z., 2004. Dynamics of lead immobilization in sulfate reducing biofilms. Water Research, 38, 2726–2736.

- Bhagat, M., Burgess, J.E., Antunes, A.P.M., Whiteley, C.G. and Duncan, J.R., 2004. Precipitation of mixed metal residues from wastewater utilising biogenic sulphide. Minerals engineering, 17(7-8), 925-932.
- Bijmans, M.F., Dopson, M., Ennin, F., Lens, P.N. and Buisman, C.J., 2008. Effect of sulfide removal on sulfate reduction at pH 5 in a hydrogen fed gas-lift bioreactor. Journal of microbiology and biotechnology, 18(11), 1809-1818.
- Bijmans, M.F.M., Buisman, C.J.N., Meulepas, R.J.W. and Lens, P., 2019. Sulfate Reduction for Inorganic Waste and Process Water Treatment. Comprehensive Biotechnology second edition. Academic Press, Burlington, 435–446.
- Bijmans, M.F.M., van Helvoort, P-J., Buisman, C.J.N. and Lens, PNL., 2009. Effect of the sulfide concentration on zinc bio-precipitation in a single stage sulfidogenic bioreactor at pH 5.5. Separation and Purification Technology, 69, 243-248.
- Bilal, M., Adeel, M., Rasheed, T., Zhao, Y. and Iqbal, H.M., 2019. Emerging contaminants of high concern and their enzyme-assisted biodegradation–a review. Environment international, 124, 336-353.
- Bohart, G.S. and Adams, E.Q., 1920. Some aspects of the behavior of charcoal with respect to chlorine. Journal of the American Chemical Society, 42(3), 523-544.
- Borkow, G., Zatcoff, R.C. and Gabbay, J., 2009. Reducing the risk of skin pathologies in diabetics by using copper impregnated socks. Medical hypotheses, 73(6), 883-886.
- Breuer P. Dealing with copper in gold ores; implemented and future approaches. In: Proceedings of gold-PM conference, 20th anniversary event. Perth, Australia: ALTA; 2015. 23-30.
- Bueno, B.Y.M., Torem, M.L., Molina, F.A.L.M.S. and De Mesquita, L.M.S., 2008. Biosorption of lead (II), chromium (III) and copper (II) by R. opacus: Equilibrium and kinetic studies. Minerals engineering, 21(1), 65-75.
- Buffiere, P., Bergeon, J-P. and Moletta, R., 2000. The inverse turbulent bed: a novel bioreactor for anaerobic treatment. Water Research, 34, 673-677.
- Cabrera, G., Pérez, R., Gomez, J.M., Abalos, A. and Cantero, D., 2006. Toxic effects of dissolved heavy metals on *Desulfovibrio vulgaris* and *Desulfovibrio sp.* strains. Journal of Hazardous Materials, 135, 40-46.
- Cassano, A., Ruby-Figueroa, R. and Drioli, E., 2014. Membrane separation. In: Food eng. Fundam. Volume I handb. Food Process Engineering, 1-29.
- Castillo, J., Perez-Lopez, R., Caraballo, M.A., Nieto, J.M., Martins, M., Costa, M.C., Olias, M., Cerón, J.C. and Tucoulou, R., 2012. Biologically-induced precipitation of sphalerite–wurtzite nanoparticles by sulfate-reducing bacteria: Implications for acid mine drainage treatment. Science of the Total Environment, 423, 176-184.
- Chaki, S.H., Tailor, J.P. and Deshpande, M.P., 2014. Covellite CuS–Single crystal growth by chemical vapour transport (CVT) technique and characterization. Materials Science in Semiconductor Processing, 27, 577-585.
- Chang, I.S., Shin, P.K. and Kim, B.H., 2000. Biological treatment of acid mine drainage under sulphatereducing conditions with solid waste materials as substrate. Water Research, 34, 1269-1277.

- Chen, F., Xiao, Z., Yue, L., Wang, J., Feng, Y., Zhu, X., Wang, Z. and Xing, B., 2019. Algae response to engineered nanoparticles: current understanding, mechanisms and implications. Environmental Science: Nano, 6(4), 1026-1042.
- Chen, G., Yuan, C., Liu, J., Deng, Y., Jiang, G., Liu, W. and Zhu, C., 2014. Low cost preparation of Cu2ZnSnS4 and Cu_2ZnSn (SxSe1− x) 4 from binary sulfide nanoparticles for solar cell application. Journal of Power Sources, 262, 201-206.
- Chen, Q., Yao, Y., Li, X., Lu, J., Zhou, J. and Huang, Z., 2018. Comparison of heavy metal removals from aqueous solutions by chemical precipitation and characteristics of precipitates. Journal of Water Process Engineering, 26, 289-300.
- Chen, Y., Wang, D., Zhu, X., Zheng, X. and Feng, L., 2012. Long-term effects of copper nanoparticles on wastewater biological nutrient removal and N_2O generation in the activated sludge process. Environmental Science & Technology, 46, 12452-12458.
- Cipriani, E., Zanetti, M., Bracco, P., Brunella, V., Luda, M.P. and Costa, L., 2016. Crosslinking and carbonization processes in PAN films and nanofibers. Polymer Degradation and Stability, 123, 178-188.
- Clark, R.M., 1987. Evaluating the cost and performance of field-scale granular activated carbon systems. Environmental Science & Technology, 21(6), 573-580.
- Cord-Ruwisch, R., 1985. A quick method for the determination of dissolved and precipitated sulfides in cultures of sulfate-reducing bacteria. Journal of Microbiological Methods, 4, 33-36.
- Cotoras, D., Hurtado, C., Viedma, P., 2017. Integrated sulfate reduction and biosorption process for the treatment of mine drainages. Solid State Phenomena, 262, 582–586.
- Cui, Z.F. and Muralidhara, H.S., 2010. Membrane Technology, a Practical Guide to Membrane Technology and Applications in Food and Bioprocessing, Volume (1), Butterworth- Heinemann/IChemE.
- Dabbawala, A.A., Sudheesh, N. and Bajaj, H.C., 2012. Palladium supported on chitosan as a recyclable and selective catalyst for the synthesis of 2-phenyl ethanol. Dalton Transactions, 41(10), 2910-2917.
- Dai, Y., Sun, Q., Wang, W., Lu, L., Liu, M., Li, J., Yang, S., Sun, Y., Zhang, K., Xu, J. and Zheng, W., 2018. Utilizations of agricultural waste as adsorbent for the removal of contaminants: A review. Chemosphere, 211, 235-253.
- Deng, Z., Oraby, E.A. and Eksteen, J.J., 2020. Sulfide precipitation of copper from alkaline glycine-cyanide solutions: precipitate characterisation. Minerals Engineering, 145, 106102.
- Desaunay, A. and Martins, J.M., 2014. Comparison of chemical washing and physical cell-disruption approaches to assess the surface adsorption and internalization of cadmium by *Cupriavidus metallidurans* CH34. Journal of Hazardous Materials, 273, 231-238.
- Dhandayuthapani, T., Girish, M., Sivakumar, R., Sanjeeviraja, C., Gopalakrishnan, C., Nagarajan, R.S., Mathew, S., Jun, D., Venkatesan, T., Selvan, G.K. and Manikandan, K., 2018. γ-MnS films with 3D microarchitectures: comprehensive study of the synthesis, microstructural, optical and magnetic properties. CrystEngComm, 20(5), 578-589.
- Diana, S., Fauzan, R., Arahman, N., Razi, F. and Bilad, M.R., 2020. Synthesis and characterization of ceramic membrane from fly ash and clay prepared by sintering method at low temperature. Rasayan Journal of Chemistry, 13, 1335-1341.

- Dijkman, H., Buisman, C.J.N. and Bayer, H.G., 1999. Biotechnology in the mining and metallurgical industries: cost savings through selective precipitation of metal sulfides. In Copper 99, 113-126.
- Djedidi, Z., Médard, B., Cheikh, R.B., Mercier, G., Tyagi, R.D. and Blais, J.F., 2009. Comparative study of dewatering characteristics of metal precipitates generated during treatment synthetic polymetallic and AMD solutions. Hydrometallurgy, 98(3-4), 247-256.
- Dobrowolski, R., Szcześ, A., Czemierska, M. and Jarosz-Wikołazka, A., 2017. Studies of cadmium (II), lead (II), nickel (II), cobalt (II) and chromium (VI) sorption on extracellular polymeric substances produced by Rhodococcus opacus and Rhodococcus rhodochrous. Bioresource technology, 225, 113-120.
- Dotto, G.L., Lima, E.C. and Pinto, L.A.A., 2012. Biosorption of food dyes onto Spirulina platensis nanoparticles: equilibrium isotherm and thermodynamic analysis. Bioresource Technology, 103(1), 123-130.
- Dowland, S., 2013. Optoelectronic and spectroscopic characterisation of polymer-cadmium sulfide nanocomposite solar cells.
- Dries, J., De Smul, A., Goethals, L., Grootaerd, H. and Verstraete, W., 1998. High rate biological treatment of sulfate-rich wastewater in an acetate-fed EGSB reactor. Biodegradation, 9(2), 103-111.
- Drury, W.J., 1999. Treatment of acid mine drainage with anaerobic solid-substrate reactors. Water Environment Research, 71(6), 1244-1250.
- Dvorak, D. H., Hedin, R. S., Edenborn, H. M. and McIntire, P. E., 1992. Treatment of metal-contaminated water using bacterial sulphate reduction: Results from pilot-scale reactors, Biotechnology and Bioengineering, 40, 609–616.
- Ebaid, M.S., Ghrair, A.M. and Al-Busoul, M., 2018. Experimental investigation of cooling photovoltaic (PV) panels using (TiO2) nanofluid in water-polyethylene glycol mixture and (Al2O3) nanofluid in water-cetyltrimethylammonium bromide mixture. Energy Conversion and Management, 155, pp.324-343.
- El-Kemary, M., El-Shamy, H. and Mosaad, M.M., 2009. The role of capping agent on the interaction of cadmium sulphide nanoparticles with flufenamic acid drug. Materials Chemistry and Physics, 118(1), 81-85.
- Equeenuddin, S.M., Tripathy, S., Sahoo, P.K. and Panigrahi, M.K., 2010. Hydrogeochemical characteristics of acid mine drainage and water pollution at Makum Coalfield, India. Journal of Geochemical Exploration, 105, 75-82.
- Esposito, G., Veeken, A., Weijma, J. and Lens P.N.L., 2006. Use of biogenic sulfide for ZnS precipitation. Separation and Purification Technology, 51, 31–39.
- Estay, H., 2018. Designing the SART process–A review. Hydrometallurgy, 176, 147-165.
- Estay, H., Ruby-Figueroa, R., Gim-Krumm, M., Seriche, G., Quilaqueo, M., Díaz-Quezada, S., Cortés, I. and Barros, L., 2021. Changing the conventional clarification method in metal sulfide precipitation by a membrane-based filtration process. Journal of Materials Research and Technology, 11, 693-709.
- Fan, L.S., Muroyama, K. and Chern, S.H., 1982. Hydrodynamic characteristics of inverse fluidization in liquid solid and gas liquid solid systems. The Chemical Engineering Journal, 24(2), 143-150.

- Fan, W.Q., Katritzky, A. R. 1,2,3-Triazoles. In Comprehensive Heterocyclic Chemistry II; Katritzky, A. R., Rees, C. W., Scriven, E. F. V., Eds.; Elsevier Science: Oxford, U.K., 1996; Vol. 4, 1−126.
- Farmer, G.H., Updegraff, D.M., Radehaus, P.M. and Bates, E.R., 1995. Metal removal and sulfate reduction in low-sulfate mine drainage. In Bioremediation of inorganics.
- Feio, M.J., Zinkevich, V., Beech, I.B., Llobet-Brossa, E., Eaton, P., Schmitt, J. and Guezennec, J., 2004. Desulfovibrio alaskensis sp. nov., a sulphate-reducing bacterium from a soured oil reservoir. International Journal of Systematic and Evolutionary Microbiology, 54(5), 1747-1752.
- Flemming, H.C., 1995. Sorption sites in biofilms. Water Science and Technology, 32, 27–33.
- Foucher, S., Battaglia-Brunet, F., Ignatiadis, I. and Morin, D., 2001. Treatment by sulfate-reducing bacteria of Chessy acid-mine drainage and metals recovery. Chemical Engineering Science, 56, 1639-1645.
- Foulkes, R., Man, E., Thind, J., Yeung, S., Joy, A. and Hoskins, C., 2020. The regulation of nanomaterials and nanomedicines for clinical application: current and future perspectives. Biomaterials Science, 8(17), 4653-4664.
- Freundlich, H.M., 1996. Over the adsorption in solution. The Journal of Physical Chemistry, 57, 1100-7.
- Fu, Fenglian. and Wang, Qi., 2011. Removal of heavy metal ions from wastewaters: a review. Journal of Environmental Management, 92, 407–418.
- Gallegos-Garcia, M., Celis, LB., Rangel-Méndez, R. and Razo-Flores, E., 2009. Precipitation and recovery of metal sulfides from metal containing acidic wastewater in a sulfidogenic down-flow fluidized bed reactor. Biotechnology and Bioengineering, 102, 91-99.
- García-Calderón, D., Buffière, P., Moletta, R. and Elmaleh, S., 1998. Influence of biomass accumulation on bed expansion characteristics of a down-flow anaerobic fluidized-bed reactor. Biotechnology and bioengineering, 57(2), 136-144.
- Garner, K.L. and Keller, A.A., 2014. Emerging patterns for engineered nanomaterials in the environment: a review of fate and toxicity studies. Journal of Nanoparticle Research, 16(8), pp.1-28.
- Ghaedi, M., Hajjati, S., Mahmudi, Z., Tyagi, I., Agarwal, S., Maity, A. and Gupta, V.K., 2015. Modeling of competitive ultrasonic assisted removal of the dyes–Methylene blue and Safranin-O using Fe3O4 nanoparticles. Chemical Engineering Journal, 268, 28-37.
- Gharabaghi, M., Irannajad, M. and Azadmehr, A.R., 2012. Selective sulphide precipitation of heavy metals from acidic polymetallic aqueous solution by thioacetamide. Industrial & engineering chemistry research, 51(2), 954-963.
- Gholinejad, M. and Jeddi, N., 2014. Copper nanoparticles supported on agarose as a bioorganic and degradable polymer for multicomponent click synthesis of 1, 2, 3-triazoles under low copper loading in water. ACS Sustainable Chemistry & Engineering, 2(12), 2658-2665.
- Gibert, O., de Pablo, J., Luis Cortina, J. and Ayora C., 2004. Chemical characterization of natural organic substrates for biological mitigation of acid mine drainage. Water Research, 38, 4186-4196.

- Gim-Krumm, M., Quilaqueo, M., Rojas, V., Seriche, G., Ruby-Figueroa, R., Cortes-Arriagada, D., Romero, J., Troncoso, E. and Estay, H., 2019. Impact of precipitate characteristics and precipitation conditions on the settling performance of a sulfide precipitation process: An exhaustive characterization of the aggregation behavior. Hydrometallurgy, 189, 105150.
- Goel, S., Chen, F. and Cai, W., 2014. Synthesis and biomedical applications of copper sulfide nanoparticles: from sensors to theranostics. Small, 10(4), 631-645.
- Goncalves, M.M.M., Da Costa, A.C.A., Leite, S.G.F. and Sant'Anna Jr, G.L., 2007. Heavy metal removal from synthetic wastewaters in an anaerobic bioreactor using stillage from ethanol distilleries as a carbon source. Chemosphere, 69, 1815-1820.
- Gong, Y., Tang, J. and Zhao, D., 2016. Application of iron sulfide particles for groundwater and soil remediation: A review. Water research, 89, 309-320.
- Gopi Kiran, M., Pakshirajan, K. and Das, G., 2016. Heavy metal removal using sulfate-reducing biomass obtained from a lab-scale upflow anaerobic-packed bed reactor. Journal of Environmental Engineering, 142, C4015010.
- Goswami, K.P. and Pugazhenthi, G., 2020. Credibility of polymeric and ceramic membrane filtration in the removal of bacteria and virus from water: A review. Journal of Environmental Management, 268, 110583.
- Goswami, K.P. and Pugazhenthi, G., 2020. Treatment of poultry slaughterhouse wastewater using tubular microfiltration membrane with fly ash as key precursor. Journal of Water Process Engineering, 37, 101361.
- Goswami, L., Namboodiri, M.T., Kumar, R.V., Pakshirajan, K. and Pugazhenthi, G., 2017. Biodiesel production potential of oleaginous Rhodococcus opacus grown on biomass gasification wastewater. Renewable Energy, 105, 400-406.
- Gramp, J.P., Sasaki, K., Bigham, J.M., Karnachuk, O.V. and Tuovinen, O.H., 2006. Formation of covellite (CuS) under biological sulfate-reducing conditions. Geomicrobiology Journal, 23(8), 613-619.
- Grootscholten, T., Keesman, K.J. and Lens, P., 2008. Modelling and on-line estimation of zinc sulphide precipitation in a continuously stirred tank reactor. Separation and Purification Technology, 63 (3), 654-660
- Guerrini, L., Alvarez-Puebla, R.A. and Pazos-Perez, N., 2018. Surface modifications of nanoparticles for stability in biological fluids. Materials, 11(7), 1154.
- Gupta, P. and Diwan, B., 2017. Bacterial exopolysaccharide mediated heavy metal removal: a review on biosynthesis, mechanism and remediation strategies. Biotechnology Reports, 13, 58-71.
- Hajipour, A.R. and Mohammadsaleh, F., 2015. Polyvinyl alcohol-stabilized cuprous oxide particles: efficient and recyclable heterogeneous catalyst for azide–alkyne cycloaddition in water at room temperature. Journal of the Iranian Chemical Society, 12(8), 1339-1345.
- Hammack, R.W. and Edenborn, H.M., 1992. The removal of nickel from mine waters using bacterial sulfate reduction. Applied microbiology and biotechnology, 37(5), 674-678
- Hammack, R.W., Edenborn, H.M. and Dvorak, D.H., 1994. Treatment of water from an open-pit copper mine using biogenic sulfide and limestone: a feasibility study. Water Research, 28(11), 2321-2329.

- Hammad, T.M., Salem, J.K., Kuhn, S., Shanab, N.M.A. and Hempelmann, R., 2015. Surface morphology and optical properties of PVA/PbS nanoparticles. Journal of Luminescence, 157, 88-92.
- Han, X., Wang, Z., Zhu, C. and Wu, Z., 2013. Effect of ultrasonic power density on extracting loosely bound and tightly bound extracellular polymeric substances. Desalination. 329, 35-40.
- Hao, O.J., 2000. In: Lens, P.N.L., Hulshoff Pol, L. (Eds.), Metal Effects on Sulfur Cyclebacteria and Metal Removal by Sulfate Reducing Bacteria, Environmental Technologies to Treat Sulfur Pollution: Principles and Engineering. IWA Publishing, London (UK), 393–414
- Hariprasad, P., Durivadivel, P., Snigdha, M. and Venkateswaran, G., 2013. Natural occurrence of aflatoxin in green leafy vegetables. Food chemistry, 138, 1908-1913.
- Harmand, L., Lescure, M.H., Candelon, N., Duttine, M., Lastécouères, D. and Vincent, J.M., 2012. Huisgen click cycloadditions from a copper (II)-tren precatalyst without external sacrificial reductant. Tetrahedron Letters, 53(11), 1417-1420.
- Hayati, B., Mahmoodi, N.M., Arami, M. and Mazaheri, F., 2011. Dye removal from colored textile wastewater by poly (propylene imine) dendrimer: operational parameters and isotherm studies. Clean–Soil, Air, Water, 39(7), 673-679.
- Ho, Y.S. and McKay, G., 1999. Pseudo-second order model for sorption processes. Process Biochemistry, 34(5), 451-465.
- Hoa, T.T.H., Liamleam, W. and Annachhatre, A.P., 2007. Lead removal through biological sulfate reduction process. Bioresource Technology, 98, 2538-2548.
- Hongen, Q., Bai, H., Han, Y., Kong, Y. and Jiao, S. 2013. Removal of Cu(II) and Fe(III) from aqueous solutions by dead sulfate reducing bacteria. Frontiers of Chemical Science and Engineering, 7, 177–184.
- Huber, D.L., 2005. Synthesis, properties, and applications of iron nanoparticles. Small, 1(5), 482-501.
- Hudson, R., Li, C.J. and Moores, A., 2012. Magnetic copper–iron nanoparticles as simple heterogeneous catalysts for the azide–alkyne click reaction in water. Green chemistry, 14(3), 622-624.
- Ibrahim, R.K., Hayyan, M., AlSaadi, M.A., Hayyan, A. and Ibrahim, S., 2016. Environmental application of nanotechnology: air, soil, and water. Environmental Science and Pollution Research, 23(14), 13754-13788.
- Ibrahim, Y.A., Briens, C.L., Margaritis, A. and Bergongnou, M.A., 1996. Hydrodynamic characteristics of a three-phase inverse fluidized-bed column. AIChE journal, 42(7), 1889-1900.
- Ivshina, I.B., Tyumina, E.A., Kuzmina, M.V. and Vikhareva, E.V., 2019. Features of diclofenac biodegradation by Rhodococcus ruber IEGM 346. Scientific reports, 9(1), 1-13.
- Jayalakshmi, M. and Rao, M.M., 2006. Synthesis of zinc sulphide nanoparticles by thiourea hydrolysis and their characterization for electrochemical capacitor applications. Journal of Power sources, 157(1), 624-629.
- Jia, B., Mei, Y., Cheng, L., Zhou, J. and Zhang, L., 2012. Preparation of copper nanoparticles coated cellulose films with antibacterial properties through one-step reduction. ACS applied materials & interfaces, 4(6), 2897-2902.

- Jimenez-Rodriguez, A.M., Durán-Barrantes, M.M., Borja, R., Sánchez, E., Colmenarejo, M.F. and Raposo, F., 2009. Heavy metals removal from acid mine drainage water using biogenic hydrogen sulfide and effluent from anaerobic treatment: effect of pH. Journal of Hazardous Materials, 165, 759-765.
- Johnson, D.B. and Hallberg, K.B., 2005. Biogeochemistry of the compost bioreactor components of a composite acid mine drainage passive remediation system. Science of the Total Environment, 338, 81-93.
- Johnson, D.B., 2000. Biological removal of sulfurous compounds from inorganic wastewaters. In: Lens, P.N.L., Hulshoff Pol, L. (Eds.), Environmental Technologies to Treat Sulfur Pollution. Principles and Engineering. IWA Publishing, London, 175–205.
- Johnson, D.B., 2003. Chemical and microbiological characteristics of mineral spoils and drainage waters at abandoned coal and metal mines. Water, Air and Soil Pollution: Focus, 3, 47-66.
- Jong, T. and Parry, D.L., 2003. Removal of sulfate and heavy metals by sulfate reducing bacteria in short-term bench scale upflow anaerobic packed bed reactor runs. Water Research, 37, 3379-3389.
- Jong, T. and Parry, D.L., 2006. Microbial sulfate reduction under sequentially acidic conditions in an upflow anaerobic packed bed bioreactor. Water Research, 40, 2561-2571.
- Kaboudin, B., Mostafalu, R. and Yokomatsu, T., 2013. Fe_3O_4 nanoparticle-supported Cu (II)-β-cyclodextrin complex as a magnetically recoverable and reusable catalyst for the synthesis of symmetrical biaryls and 1, 2, 3-triazoles from aryl boronic acids. Green chemistry, 15(8), 2266-2274.
- Kaksonen, A.H. and Puhakka, J.A., 2007. Sulfate reduction based bioprocesses for the treatment of acid mine drainage and the recovery of metals. Engineering in Life Sciences, 7, 541-564.
- Kaksonen, A.H., Franzmann, P.D. and Puhakka J.A., 2004. Effects of hydraulic retention time and sulfide toxicity on ethanol and acetate oxidation in sulfate-reducing metal precipitating fluidized-bed reactor. Biotechnology and Bioengineering, 86, 332-343.
- Kaksonen, A.H., Riekkola-Vanhanen, M.L. and Puhakka, J.A., 2003. Optimization of metal sulphide precipitation in fluidized-bed treatment of acidic wastewater. Water Research, 37(2), 255-266.
- Kal-Kashvandi, A.T., Heravi, M.M., Ahmadi, S. and Hosseinnejad, T., 2018. Copper nanoparticles in polyvinyl alcohol–acrylic acid matrix: an efficient heterogeneous catalyst for the regioselective synthesis of 1, 4-disubstituted 1, 2, 3-triazoles via click reaction. Journal of Inorganic and Organometallic Polymers and Materials, 28(4), 1457-1467.
- Kamoun, N., Hajjeji, W., Abid, R., Rodríguez, M.A. and Jamoussi, F., 2020. Elaboration and properties of low-cost ceramic microfiltration membrane from local Tunisian clay for wastewater treatment. Ceramica, 66, 386-393.
- Karamanev, D.G. and Nikolov, L.N., 1992. Free rising spheres do not obey Newton's law for free settling. AIChE journal, 38(11), 1843-1846.
- Karami, H., Ghasemi, M. and Matini, S., 2013. Synthesis, characterization and application of lead sulfide nanostructures as ammonia gas sensing agent. International Journal of Electrochemical Science, 8(10), 11661-11679.
- Karim, M.N., Graham, H., Han, B. and Cibulskas, A., 2008. Flocculation enhanced microfiltration of Escherichia coli lysate. Biochemical engineering journal, 40(3), 512-519.

- Kastyuchik, A., Karam, A. and Aïder, M., 2016. Effectiveness of alkaline amendments in acid mine drainage remediation. Environmental Technology & Innovation, 6, 49-59.
- Kieu, H.T.Q., Müller, E. and Horn, H., 2011. Heavy metal removal in anaerobic semicontinuous stirred tank reactors by a consortium of sulfate-reducing bacteria. Water Research, 45, 3863–3870.
- Kimber, R.L., Parmeggiani, F., Joshi, N., Rakowski, A.M., Haigh, S.J., Turner, N.J. and Lloyd, J.R., 2019. Synthesis of copper catalysts for click chemistry from distillery wastewater using magnetically recoverable bionanoparticles. Green Chemistry, 21(15), 4020-4024.
- Kiran, M., Pakshirajan, K. and Das, G., 2015. Heavy metal removal using sulfate-reducing biomass obtained from a lab-scale upflow anaerobic-packed bed reactor. Journal of Environmental Engineering, 142, C4015010.
- Kiran, M.G., Pakshirajan, K. and Das, G., 2017. An overview of sulfidogenic biological reactors for the simultaneous treatment of sulfate and heavy metal rich wastewater. Chemical Engineering Science, 158, 606-620.
- Kiran, M.G., Pakshirajan, K. and Das, G., 2017. Heavy metal removal from multicomponent system by sulfate reducing bacteria: mechanism and cell surface characterization. Journal of hazardous materials, 324, 62-70.
- Kiran, M.G., Pakshirajan, K. and Das, G., 2018. Heavy metal removal from aqueous solution using sodium alginate immobilized sulfate reducing bacteria: mechanism and process optimization. Journal of environmental management, 218, 486-496.
- Kiran, M.G., Pakshirajan, K. and Das, G., 2018. Metallic wastewater treatment by sulfate reduction using anaerobic rotating biological contactor reactor under high metal loading conditions. Frontiers of Environmental Science & Engineering, 12(4), 1-11.
- Konhauser, K.O., Fyfe, W.S., Ferris, F.G. and Beveridge, T.J., 1993. Metal sorption and mineral precipitation by bacteria in two Amazonian river systems: Rio Solimoes and Rio Negro, Brazil. Geology, 21(12), pp.1103-1106. Flemming, H.C., 1995. Sorption sites in biofilms. Water Science and Technology, 32, 27–33.
- Kumar, C.M., Roshni, M. and Vasanth, D., 2019. Treatment of aqueous bacterial solution using ceramic membrane prepared from cheaper clays: A detailed investigation of fouling and cleaning. Journal of Water Process Engineering, 29, 100797.
- Kumar, M. and Puri, A., 2012. A review of permissible limits of drinking water. Indian journal of occupational and environmental medicine, 16(1), 40.
- Kumar, M.A., Poonam, S., Kumar, V.V., Baskar, G., Seenuvasan, M., Anuradha, D. and Sivanesan, S., 2017. Mineralization of aromatic amines liberated during the degradation of a sulfonated textile colorant using Klebsiella pneumoniae strain AHM. Process Biochemistry, 57, 181-189.
- Kumar, P.S., Varjani, S.J. and Suganya, S., 2018. Treatment of dye wastewater using an ultrasonic aided nanoparticle stacked activated carbon: kinetic and isotherm modelling. Bioresource Technology, 250, 716-722.
- Kumar, R.V., Ghoshal, A.K. and Pugazhenthi, G., 2015. Elaboration of novel tubular ceramic membrane from inexpensive raw materials by extrusion method and its performance in microfiltration of synthetic oily wastewater treatment. Journal of Membrane Science, 490, 92-102.

- Kumar, R.V., Goswami, L., Pakshirajan, K. and Pugazhenthi, G., 2016. Dairy wastewater treatment using a novel low cost tubular ceramic membrane and membrane fouling mechanism using pore blocking models. Journal of Water Process Engineering13, 168-175.
- Kushkevych, I., 2019. Isolation and Purification of Sulfate-Reducing Bacteria. In Microorganisms. IntechOpen.
- La, H-J., Kim, K-H., Quan, Z-X., Cho, Y-G. and Lee, S-T., 2003. Enhancement of sulfate reduction activity using granular sludge in anaerobic treatment of acid mine drainage. Biotechnology Letters, 25, 503-508.
- Lai, R.W., Yeung, K.W., Yung, M.M., Djurišić, A.B., Giesy, J.P. and Leung, K.M., 2018. Regulation of engineered nanomaterials: current challenges, insights and future directions. Environmental Science and Pollution Research, 25(4), 3060-3077.
- Langmuir, I., 1918. The adsorption of gases on plane surfaces of glass, mica and platinum. Journal of the American Chemical society, 40(9), 1361-1403.
- Lead, J.R., Batley, G.E., Alvarez, P.J., Croteau, M.N., Handy, R.D., McLaughlin, M.J., Judy, J.D. and Schirmer, K., 2018. Nanomaterials in the environment: behavior, fate, bioavailability, and effects—an updated review. Environmental toxicology and chemistry, 37(8), 2029-2063.
- Lebleu, N., Roques, C., Aimar, P. and Causserand, C., 2009. Role of the cell-wall structure in the retention of bacteria by microfiltration membranes. Journal of membrane science, 326(1), 178-185.
- Lee, B.S., Yi, M., Chu, S.Y., Lee, J.Y., Kwon, H.R., Lee, K.R., Kang, D., Kim, W.S., Lim, H.B., Lee, J. and Youn, H.J., 2010. Copper nitride nanoparticles supported on a superparamagnetic mesoporous microsphere for toxic-free click chemistry. Chemical communications, 46(22), 3935-3937.
- Lee, C.G., Jeon, J.W., Hwang, M.J., Ahn, K.H., Park, C., Choi, J.W. and Lee, S.H., 2015. Lead and copper removal from aqueous solutions using carbon foam derived from phenol resin. Chemosphere, 130, 59-65.
- Lefticariu, L., Walters, E.R., Pugh, C.W. and Bender, K.S., 2015. Sulfate reducing bioreactor dependence on organic substrates for remediation of coal-generated acid mine drainage: Field experiments. Applied Geochemistry, 63, 70-82.
- Legros, J. and Bolm, C., 2004. Highly enantioselective iron-catalyzed sulfide oxidation with aqueous hydrogen peroxide under simple reaction conditions. Angewandte Chemie International Edition, 43(32), 4225-4228.
- Lens, P.N.L., Vallero, M., Esposito G. and Zandvoort, M., 2002. Perspectives of sulfate reducing bioreactors in environmental biotechnology. Reviews Environmental Science & Bio/Technology, 1, 311-325.
- Lenz, M., Van Hullebusch, E.D., Hommes, G., Corvini, P.F. and Lens, P.N., 2008. Selenate removal in methanogenic and sulfate-reducing upflow anaerobic sludge bed reactors. Water Research, 42, 2184-2194.
- Letterman, R.D., 1999. Water Quality and Treatment, 5th edition, McGraw-Hill, Inc.
- Lettinga, G.A.F.M., Van Velsen, A.F.M., Hobma, S.W., De Zeeuw, W. and Klapwijk, A., 1980. Use of the upflow sludge blanket (USB) reactor concept for biological wastewater treatment, especially for anaerobic treatment. Biotechnology and Bioengineering, 22, 699-734.

- Lewis, A. and Swartbooi A., 2006. Factors Affecting Metal Removal in Mixed Sulfide Precipitation. Chemical Engineering & Technology, 29, 277-280
- Lewis, A.E., 2010. Review of metal sulphide precipitation. Hydrometallurgy, 104, 222-234.
- Li, J. and Chase, H.A., 2010. Applications of membrane techniques for purification of natural products. Biotechnology letters, 32(5), 601-608.
- Liamleam, W. and Annachhatre, A.P., 2007. Electron donors for biological sulfate reduction. Biotechnology Advances, 25, 452-463.
- Liang, L. and Astruc, D., 2011. The copper (I)-catalyzed alkyne-azide cycloaddition (CuAAC)"click" reaction and its applications. An overview. Coordination Chemistry Reviews, 255(23-24), 2933-2945.
- Liang, L., Peng, S., Yuan, Z., Wei, C., He, Y., Zheng, J., Gu, Y. and Chen, H., 2018. Biocompatible tumor-targeting nanocomposites based on CuS for tumor imaging and photothermal therapy. RSC Advances, 8, 6013-6026.
- Liu, Y., Xiao, W., Wang, J., Mirza, Z.A. and Wang, T., 2016. Optimized synthesis of FeS nanoparticles with a high Cr (VI) removal capability. Journal of Nanomaterials, 2016.
- Lopes, S.I.C., Sulistyawati I., Capela, M.I. and Lens, P.N.L., 2007. Low pH (6, 5 and 4) sulfate reduction during the acidification of sucrose under thermophilic (55°C) conditions. Process Biochemistry, 42, 580-591.
- Luptáková, A., Kotuličová, I., Bálintová, M. and Demčák, Š., 2015. Bacterial reduction of barium sulphate by sulphate-reducing bacteria. Nova Biotechnologica et Chimica, 14(2), 135-140.
- Ma, X., Hua, Y., Feng, J., Liu, J. and Ye, X., 1997. Cd super (2+) removal from wastewater by sulfate reducing bacteria with an anaerobic fluidized bed reactor. Journal of Environmental Sciences (China), 9(3), 366-371.
- Mack, C., Burgess, J.E. and Duncan, J.R., 2004. Membrane bioreactors for metal recovery from wastewater: A review. Water SA, 30, 521-532.
- Mal, J., Nancharaiah, Y.V., Maheshwari, N., van Hullebusch, E.D. and Lens, P.N., 2017. Continuous removal and recovery of tellurium in an upflow anaerobic granular sludge bed reactor. Journal of Hazardous Materials, 327, 79-88.
- Malik, P.K., 2003. Use of activated carbons prepared from sawdust and rice-husk for adsorption of acid dyes: a case study of Acid Yellow 36. Dyes and pigments, 56(3), 239-249.
- Manconi, I. and Lens, P.N.L., 2009. Removal of H_2S and volatile organic sulfur compounds by silicone membrane extraction. Journal of chemical technology and Biotechnology, 84, 69-77.
- Marin, P., Alkalay, D., Guerrero, L., Chamy, R. and Schiappacasse, M.C., 1999. Design and startup of an anaerobic fluidized bed reactor. Water Science and Technology, 40, 63-70.
- Marslin, G., Sheeba, C.J. and Franklin, G., 2017. Nanoparticles alter secondary metabolism in plants via ROS burst. Frontiers in plant science, 8, 832.
- Martínez, G., Merinero, M., Pérez-Aranda, M., Pérez-Soriano, E.M., Ortiz, T., Begines, B. and Alcudia, A., 2021. Environmental impact of nanoparticles' application as an emerging technology: A review. Materials, 14(1), 166.

- Martins, A. and Nunes, N., 2015. Adsorption of a textile dye on commercial activated carbon: a simple experiment to explore the role of surface chemistry and ionic strength. Journal of Chemical Education, 92(1), 143-147.
- Mavrov, V., Chmiel, H., Kluth, J., Meier, J., Heinrich, F., Ames, P., Backes, K. and Usner, P., 1998. Comparative study of different MF and UF membranes for drinking water production. Desalination, 117(1-3), 189-196.
- Melin, E.S., Ferguson, J.F. and Puhakka, J.A., 1997. Pentachlorophenol biodegradation kinetics of an oligotrophic fluidized-bed enrichment culture. Applied microbiology and Biotechnology, 47, 675-682.
- Men, Y., Achermann, S., Helbling, D.E., Johnson, D.R. and Fenner, K., 2017. Relative contribution of ammonia oxidizing bacteria and other members of nitrifying activated sludge communities to micropollutant biotransformation. Water research, 109, 217-226.
- Minhas, A.K., Hodgson, P., Barrow, C.J. and Adholeya, A., 2016. A review on the assessment of stress conditions for simultaneous production of microalgal lipids and carotenoids. Frontiers in microbiology, 7, 546.
- Mohammadi, A., Daemi, H. and Barikani, M., 2014. Fast removal of malachite green dye using novel superparamagnetic sodium alginate-coated Fe3O4 nanoparticles. International journal of biological macromolecules, 69, 447-455.
- Molla, A., Sahu, M. and Hussain, S., 2016. Synthesis of tunable band gap semiconductor nickel sulphide nanoparticles: Rapid and round the clock degradation of organic dyes. Scientific Reports, 6, 26034.
- Monash, P. and Pugazhenthi, G., 2011. Development of ceramic supports derived from low-cost raw materials for membrane applications and its optimization based on sintering temperature. International Journal of Applied Ceramic Technology, 8(1), 227-238.
- Moussavi, G. and Mahmoudi, M., 2009. Removal of azo and anthraquinone reactive dyes from industrial wastewaters using MgO nanoparticles. Journal of Hazardous Materials, 168(2-3), 806-812.
- Mulder, M., 1991. Basic Principles of Membrane Technology, Kluwer Academic Publishers, Dordrecht.
- Murray, A.J., Roussel, J., Rolley, J., Woodhall, F., Mikheenko, I.P., Johnson, D.B., Gomez-Bolivar, J., Merroun, M.L., Macaskie, L.E., 2017. Biosynthesis of zinc sulfide quantum dots using waste off-gas from a metal bioremediation process. RSC Advances, 7, 21484.
- Musah, B.I., Peng, L. and Xu, Y., 2021. Biosorption of Cr (VI) Using Bacillus licheniformis and Bacillus mucilaginosus Krassilnikov: Contrastive Investigation on Removal Performance, Kinetics, and Mechanisms. Environmental Engineering Science, 38(4), 231-244.
- Mwabi, J.K., Mamba, B.B. and Momba, M.N., 2012. Removal of Escherichia coli and faecal coliforms from surface water and groundwater by household water treatment devices/systems: a sustainable solution for improving water quality in rural communities of the Southern African development community region. International Journal of Environmental Research and Public Health, 9, 139-170.
- Nagaveena, S., Kumar, S.N. and Mahadevan, C.K., 2013. Synthesis by a novel method and application of image processing in characterization of nickel sulphide nanoparticles. International Journal of Engineering Research, 3, 1214-1218.

- Nagpal, S., Chuichulcherm, S., Peeva, L. and Livingston, A., 2000. Microbial sulfate reduction in a liquid–solid fluidized bed reactor. Biotechnology and Bioengineering, 70, 370-380.
- Namasivayam, C. and Kavitha, D., 2002. Removal of Congo Red from water by adsorption onto activated carbon prepared from coir pith, an agricultural solid waste. Dyes and pigments, 54(1), 47-58.
- Neculita, C.M., Zagury, G.J. and Bussière, B., 2007. Passive treatment of acid mine drainage in bioreactors using sulfate-reducing bacteria. Journal of Environmental Quality, 36, 1-16.
- Negi, B.B., Sinharoy, A. and Pakshirajan, K., 2020. Selenite removal from wastewater using fungal pelleted airlift bioreactor. Environmental Science and Pollution Research, 27(1), 992-1003.
- Nezamifar, J., Ghani, K. and Kiomarsipour, N., 2015. Solvothermal Synthesis of Cobalt and Copper Sulfides Nanoparticles with High Light Absorptance for New Solar Selective Coatings. Journal of Nanostructures, 5, 203-207.
- Nikolov, L. and Karamanev D., 1987. The inverse fluidization: a new approach to biofilm reactor design to aerobic wastewater treatment. Paper presented at the Studies in Environmental Science – Environmental Biotechnology.
- Omil, F., Lens, P., Pol, L.H. and Lettinga, G., 1996. Effect of upward velocity and sulfide concentration on volatile fatty acid degradation in a sulphidogenic granular sludge reactor. Process Biochemistry, 31, 699-710.
- Oyekanmi, A.A., Daud, Z., Daud, N.M. and Gani, P., 2017. Adsorption of Heavy Metal from Palm Oil Mill Effluent on the Mixed Media Used For the Preparation of Composite Adsorbent. MATEC Web Conf.103, 06020.
- Papirio, S., Villa-Gomez, D.K., Esposito, G., Pirozzi, F. and Lens, P.N.L., 2013. Acid mine drainage treatment in fluidized-bed bioreactors by sulfate-reducing bacteria: a critical review. Critical reviews in environmental science and technology, 43, 2545-2580.
- Pathigoolla, A., Pola, R.P. and Sureshan, K.M., 2013. A versatile solvent-free azide–alkyne click reaction catalyzed by in situ generated copper nanoparticles. Applied Catalysis A: General, 453, 151-158.
- Paul, S., Shakya, A.K. and Ghosh, P.K., 2020. Bacterially-assisted recovery of cadmium and nickel as their metal sulfide nanoparticles from spent Ni–Cd battery via hydrometallurgical route. Journal of Environmental Management261, 110113.
- Peng, X., Xia, Z., Kong, L., Hu, X. and Wang, X., 2019. UV light irradiation improves the aggregation and settling performance of metal sulfide particles in strongly acidic wastewater. Water research, 163, 114860.
- Pervez, M., Telegin, F.Y., Cai, Y., Xia, D., Zarra, T. and Naddeo, V., 2019. Efficient degradation of mordant blue 9 using the fenton-activated persulfate system. Water, 11(12), 2532.
- Postgate J.R, 1984. The Sulphate Reducing Bacteria, second ed. Cambridge University Press, New York.
- Purnima, M., Manikandan, N.A., Pakshirajan, K. and Pugazhenthi, G., 2020. Recovery of microalgae from its broth solution using kaolin based tubular ceramic membranes prepared with different binders. Separation and Purification Technology, 250, 117212.

- Quilaqueo, M., Gim-Krumm, M., Ruby-Figueroa, R., Troncoso, E. and Estay, H., 2019. Determination of size distribution of precipitation aggregates using non-invasive microscopy and semiautomated image processing and analysis. Minerals, 9(12), 724.
- Rad, M.N.S., Behrouz, S., Movahedian, A., Doroodmand, M.M., Ghasemi, Y., Rasoul-Amini, S., Gandomani, A.R.A. and Rezaie, R., 2013. Doped Nano-Sized Copper (I) Oxide (Cu_2O) on Melamine Formaldehyde Resin: a Highly Efficient Heterogeneous Nano Catalyst for 'Click'Synthesis of Some Novel 1H-1, 2, 3-Triazole Derivatives Having Antibacterial Activity. Helvetica Chimica Acta, 96(4), 688-701.
- Radhika, M. and Palanivelu, K., 2006. Adsorptive removal of chlorophenols from aqueous solution by low cost adsorbent-Kinetics and isotherm analysis. Journal of Hazardous Materials 138, 116-124.
- Ravikumar, K.V.G., Kubendiran, H., Ramesh, K., Rani, S., Mandal, T.K., Pulimi, M., Natarajan, C. and Mukherjee, A., 2020. Batch and column study on tetracycline removal using green synthesized NiFe nanoparticles immobilized alginate beads. Environmental Technology & Innovation, 17, 100520.
- Rebekah, A., Bharath, G., Naushad, M., Viswanathan, C. and Ponpandian, N., 2020. Magnetic graphene/chitosan nanocomposite: A promising nano-adsorbent for the removal of 2-naphthol from aqueous solution and their kinetic studies. International Journal of Biological Macromolecules, 159, 530-538.
- Reddy, D.H.K., Seshaiah, K., Reddy, A.V.R., Rao, M.M. and Wang, M.C., 2010. Biosorption of Pb^{2+} from aqueous solutions by Moringa oleifera bark: equilibrium and kinetic studies. Journal of Hazardous Materials, 174, 831-838.
- Rout, P.R., Bhunia, P. and Dash, R.R., 2017. Evaluation of kinetic and statistical models for predicting breakthrough curves of phosphate removal using dolochar-packed columns. Journal of Water Process Engineering, 17, 168-180.
- Rubilar, O., Rai, M., Tortella, G., Diez, M.C., Seabra, A.B. and Durán, N., 2013. Biogenic nanoparticles: copper, copper oxides, copper sulphides, complex copper nanostructures and their applications. Biotechnology Letters, 35(9), 1365-1375.
- Saad, M.A., 2004. Early discovery of RO membrane fouling and real-time monitoring of plant performance for optimizing cost of water. Desalination, 165, 183-191.
- Sáez, V. and Mason, T.J., 2009. Sonoelectrochemical synthesis of nanoparticles. Molecules, 14(10), 4284-4299.
- Sagadevan, S. and Sundaram, A.S., 2014. Dielectric properties of lead sulphide thin films for solar cell applications. Chalcogenide Letters, 11(3), 159-165.
- Sahinkaya, E. and Gungor, M., 2010. Comparison of sulfidogenic up-flow and down-flow fluidized-bed reactors for the biotreatment of acidic metal-containing wastewater. Bioresource Technology, 101, 9508-9514.
- Sahinkaya, E. and Yucesoy, Z., 2010. Biotreatment of acidic zinc-and copper-containing wastewater using ethanol-fed sulfidogenic anaerobic baffled reactor. Bioprocess and biosystems engineering, 33(8), 989-997.
- Sahinkaya, E., Gungor, M., Bayrakdar, A., Yucesoy, Z. and Uyanik, S., 2009. Separate recovery of copper and zinc from acid mine drainage using biogenic sulfide. Journal of Hazardous Materials, 171, 901-906.

- Sahinkaya, E., Özkaya, B., Kaksonen, A.H. and Puhakka, J.A., 2007. Sulfidogenic fluidized-bed treatment of metal-containing wastewater at low and high temperatures. Biotechnology and bioengineering, 96, 1064-1072.
- Saja, S., Bouazizi, A., Achiou, B., Ouammou, M., Albizane, A., Bennazha, J. and Younssi, S.A., 2018. Elaboration and characterization of low-cost ceramic membrane made from natural Moroccan perlite for treatment of industrial wastewater. Journal of environmental chemical engineering, 6(1), 451-458.
- Sampaio, R.M.M., Timmers, R.A., Xu, Y., Keesman, K.J. and Lens, P.N.L., 2009. Selective precipitation of Cu from Zn in a pS controlled continuously stirred tank reactor. Journal of Hazardous Materials, 165, 256-265.
- Samsami, S., Mohamadizaniani, M., Sarrafzadeh, M.H., Rene, E.R. and Firoozbahr, M., 2020. Recent advances in the treatment of dye-containing wastewater from textile industries: Overview and perspectives. Process safety and environmental protection, 143, 138-163.
- Sánchez-Andrea, I., Sanz, J.L., Bijmans, M.F. and Stams, A.J., 2014. Sulfate reduction at low pH to remediate acid mine drainage. Journal of Hazardous Materials 269, 98-109.
- Sardar, U.R., Bhargavi, E., Devi, I., Bhunia, B. and Tiwari, O.N., 2018. Advances in exopolysaccharides based bioremediation of heavy metals in soil and water: a critical review. Carbohydrate polymers, 199, 353-364.
- Sarkar, A., Chakraborty, A.K. and Bera, S., 2018. NiS/rGO nanohybrid: an excellent counter electrode for dye sensitized solar cell. Solar Energy Materials and Solar Cells, 182, 314-320.
- Sarkar, A., Mukherjee, T. and Kapoor, S., 2008. PVP-stabilized copper nanoparticles: a reusable catalyst for “Click” reaction between terminal alkynes and azides in nonaqueous solvents. The Journal of Physical Chemistry C, 112(9), 3334-3340.
- Sarti, A. and Zaiat, M., 2011. Anaerobic treatment of sulfate-rich wastewater in an anaerobic sequential batch reactor (AnSBR) using butanol as the carbon source. Journal of Environmental Management, 92, 1537-1541.
- Semenzin, E., Lanzellotto, E., Hristozov, D., Critto, A., Zabeo, A., Giubilato, E. and Marcomini, A., 2015. Species sensitivity weighted distribution for ecological risk assessment of engineered nanomaterials: The n-TiO_2 case study. Environmental toxicology and chemistry, 34(11), 2644-2659.
- Setsukinai, K.I., Urano, Y., Kakinuma, K., Majima, H.J. and Nagano, T., 2003. Development of Novel Fluorescence Probes That Can Reliably Detect Reactive Oxygen Species and Distinguish Specific Species* 210. Journal of Biological Chemistry, 278(5), 3170-3175.
- Shahabpour, J., Doorandish, M. and Abbasnejad, A., 2005. Mine-drainage water from coal mines of Kerman region, Iran. Environmental Geology, 47(7), 915-925.
- Shajudheen, V.M., Sivakumar, M. and Kumar, S.S., 2016. Synthesis and characterization of NiO nanoparticles by thermal oxidation of nickel sulfide nanoparticles. Materials Today: Proceedings, 3(6), 2450-2456.
- Shakil, M.A., Das, S., Rahman, M.A., Akther, U.S., Majumdar, M.K.H. and Rahman, M.K., 2018. A Review on zinc sulphide thin film fabrication for various applications based on doping elements. Materials Sciences and Applications, 9(9), 751-778.

- Shalumon, K.T., Anulekha, K.H., Nair, S.V., Nair, S.V., Chennazhi, K.P. and Jayakumar, R., 2011. Sodium alginate/poly (vinyl alcohol)/nano ZnO composite nanofibers for antibacterial wound dressings. International journal of biological macromolecules, 49(3), 247-254.
- Shamraiz, U., Hussain, R.A., Badshah, A., 2016. Fabrication and applications of copper sulfide (CuS) nanostructures. J. Solid State Chem. 238, 25–40.
- Shang, L., Nienhaus, K. and Nienhaus, G.U., 2014. Engineered nanoparticles interacting with cells: size matters. Journal of nanobiotechnology, 12(1), 1-11.
- Sharghi, H., Khalifeh, R. and Doroodmand, M.M., 2009. Copper nanoparticles on charcoal for multicomponent catalytic synthesis of 1, 2, 3-Triazole derivatives from benzyl halides or alkyl halides, terminal alkynes and sodium azide in water as a "Green" solvent. Advanced Synthesis & Catalysis, 351(1-2), 207-218.
- Sheldon, R.A., 2007. The E factor: fifteen years on. Green Chemistry, 9(12), 1273-1283.
- Shi, K., Gao, Z., Shi, T.Q., Song, P., Ren, L.J., Huang, H. and Ji, X.J., 2017. Reactive oxygen species-mediated cellular stress response and lipid accumulation in oleaginous microorganisms: the state of the art and future perspectives. Frontiers in microbiology, 8, 793.
- Shieh, W.K. and Hsu, Y., 1996. Biomass loss from an anaerobic fluidized bed reactor. Water Research, 30(5), 1253-1257.
- Sidhu, A., Barmota, H. and Bala, A., 2017. Antifungal evaluation studies of copper sulfide nano-aquaformulations and its impact on seed quality of rice (Oryzae sativa). Applied Nanoscience, 7(8), 681-689.
- Sierra-Alvarez, R., Karri, S., Freeman, S. and Field, JA., 2006. Biological treatment of heavy metals in acid mine drainage using sulfate reducing bioreactors. Water Science and Technology, 54, 179-185.
- Singh, A., Manivannan, R. and Victoria, S.N., 2019. Simple one-pot sonochemical synthesis of copper sulphide nanoparticles for solar cell applications. Arabian Journal of Chemistry, 12(8), 2439-2447.
- Singh, J., Dutta, T., Kim, K.H., Rawat, M., Samddar, P. and Kumar, P., 2018. 'Green'synthesis of metals and their oxide nanoparticles: applications for environmental remediation. Journal of nanobiotechnology, 16(1), 1-24.
- Singh, R., Behera, M. and Kumar, S., 2020. Nano-bioremediation: An innovative remediation technology for treatment and management of contaminated sites. In Bioremediation of industrial waste for environmental safety (165-182). Springer, Singapore.
- Singh, S. and Chakraborty, S., 2020. Performance of organic substrate amended constructed wetland treating acid mine drainage (AMD) of North-Eastern India. Journal of Hazardous Materials, 397, 122719.
- Sinharoy, A., Saikia, S. and Pakshirajan, K., 2019. Biological removal of selenite from wastewater and recovery as selenium nanoparticles using inverse fluidized bed bioreactor. Journal of Water Process Engineering, 32, 100988.
- Smet, P.F., Moreels, I., Hens, Z., Poelman, D., 2010. Luminescence in sulfides: a rich history and a bright future. Materials, 3 (4), 2834–2883.

- Smith, S.R., 2009. A critical review of the bioavailability and impacts of heavy metals in municipal solid waste composts compared to sewage sludge. Environment international, 35, 142-156.
- Soltani, N., Saion, E., Hussein, M.Z., Erfani, M., Abedini, A., Bahmanrokh, G., Navasery, M. and Vaziri, P., 2012. Visible light-induced degradation of methylene blue in the presence of photocatalytic ZnS and CdS nanoparticles. International journal of molecular sciences, 13(10), 12242-12258.
- Somlev, V., Banov, M., 1998. Three stage process for complex biotechnological treatment of industrial wastewater from uranium mining. Biotechnology Techniques, 12, 637–639.
- Sousa, D.Z., Visser, M., Van Gelder, A.H., Boeren, S., Pieterse, M.M., Pinkse, M.W., Verhaert, P.D., Vogt, C., Franke, S., Kümmel, S. and Stams, A.J., 2018. The deep-subsurface sulfate reducer Desulfotomaculum kuznetsovii employs two methanol-degrading pathways. Nature communications, 9(1), 1-9.
- Speece, R.E., 1983. Anaerobic biotechnology for industrial wastewater treatment. Environmental science & technology, 17(9), 416A-427A.
- Steed, V.S., Suidan, M.T., Gupta, M., Miyahara, T., Acheson, C.M., Sayles, G.D., 2000. Development of a sulfate-reducing biological process to remove heavy metals from acid mine drainage. Water Environment Research, 72, 530-535.
- Suchecka, T., Biernacka, E. and Piatkiewicz, W., 2003. Microorganism retention on microfiltration membranes. Filtration & separation, 40(8), 50-55.
- Sun, Y., Liu, C., Grauer, D.C., Yano, J., Long, J.R., Yang, P. and Chang, C.J., 2013. Electrodeposited cobalt-sulfide catalyst for electrochemical and photoelectrochemical hydrogen generation from water. Journal of the American Chemical Society, 135(47), 17699-17702.
- Sundararaghavan, A., Mukherjee, A. and Suraishkumar, G.K., 2020. Investigating the potential use of an oleaginous bacterium, *Rhodococcus opacus* PD630, for nano-TiO 2 remediation. Environmental Science and Pollution Research, 27(22), 27394-27406.
- Sungur, Ş. and Gülmez, F., 2015. Determination of metal contents of various fibers used in textile industry by MP-AES. Journal of Spectroscopy, 2015.
- Suteerapataranon, S., Bouby, M., Geckeis, H., Fanghänel, T. and Grudpan, K., 2006. Interaction of trace elements in acid mine drainage solution with humic acid. Water Research, 40(10), 2044-2054.
- Tabak, H.H., Scharp, R., Burckle, J., Kawahara, F.K. and Govind, R., 2003. Advances in biotreatment of acid mine drainage and biorecovery of metals: 1. Metal precipitation for recovery and recycle. Biodegradation, 14, 423-436.
- Taseidifar, M., Makavipour, F., Pashley, R.M. and Rahman, A.M., 2017. Removal of heavy metal ions from water using ion flotation. Environmental Technology & Innovation, 8, 182-190.
- Teitzel GM and Parsek MR, 2003. Heavy Metal Resistance of Biofilm and Planktonic Pseudomonas aeruginosa. Applied Environmental Microbiology 69, 2313–2320
- Thabede, P.M., Shooto, N.D., Xaba, T. and Naidoo, E.B., 2020. Adsorption studies of toxic cadmium (II) and chromium (VI) ions from aqueous solution by activated black cumin (Nigella sativa) seeds. Journal of Environmental Chemical Engineering, 8(4), 104045.

- Thangavel, S., Krishnamoorthy, K., Kim, S.J. and Venugopal, G., 2016. Designing ZnS decorated reduced graphene-oxide nanohybrid via microwave route and their application in photocatalysis. Journal of Alloys and Compounds, 683, 456-462.
- Thomas, H.C., 1944. Heterogeneous ion exchange in a flowing system. Journal of the American Chemical Society, 66(10), 1664-1666.
- Tokarek, K., Hueso, J.L., Kuśtrowski, P., Stochel, G. and Kyzioł, A., 2013. Green synthesis of chitosan-stabilized copper nanoparticles. European Journal of Inorganic Chemistry, 2013 (28), 4940-4947.
- Tomić, N.M., Dohcevic-Mitrovic, Z.D., Paunović, N.M., Mijin, D.Z., Radić, N.D., Grbić, B.V., Askrabic, S.M., Babić, B.M. and Bajuk-Bogdanovic, D.V., 2014. Nanocrystalline CeO^{2-} δ as effective adsorbent of azo dyes. Langmuir, 30(39), 11582-11590.
- Ubaid, K.A., Zhang, X., Sharma, V.K. and Li, L., 2020. Fate and risk of metal sulfide nanoparticles in the environment. Environmental Chemistry Letters, 18(1), pp.97-111.
- Urbano, S.B., Di Capua, C., Cortez, N., Farías, M.E. and Alvarez, H.M., 2014. Triacylglycerol accumulation and oxidative stress in Rhodococcus species: differential effects of pro-oxidants on lipid metabolism. Extremophiles, 18(2), 375-384.
- Vadapalli, V.K., Klink, M.J., Etchebers, O., Petrik, L.F., Gitari, W., White, R.A., Key, D. and Iwuoha, E., 2008. Neutralization of acid mine drainage using fly ash, and strength development of the resulting solid residues. South African Journal of Science, 104(7), 317-322.
- Vallero, M.V., Lettinga, G. and Lens, P.N., 2005. High rate sulfate reduction in a submerged anaerobic membrane bioreactor (SAMBaR) at high salinity. Journal of Membrane Science, 253, 217-232.
- Vallero, M.V.G., Trevino, R.H.M., Paulo, P.L., Lettinga, G., Lens, P.N.L., 2003. Effect of sulfate on methanol degradation in thermophilic (55 °C) methanogenic UASB reactors. Enzyme and Microbial Technology, 32, 676-687.
- van Hullebusch, Eric D., Zandvoort, Marcel H. and Lens, Piet N.L., 2003. Metal immobilisation by biofilms: mechanisms and analytical tools. Reviews in Environmental Science & Bio/Technology 2. Kluwer Academic Publishers, 9–33, (Printed in the Netherlands).
- Vasanth, D., Pugazhenthi, G. and Uppaluri, R., 2011. Fabrication and properties of low cost ceramic microfiltration membranes for separation of oil and bacteria from its solution. Journal of Membrane Science, 379, 154-163.
- Veerakumar, P., Velayudham, M., Lu, K.L. and Rajagopal, S., 2011. Highly dispersed silica-supported nanocopper as an efficient heterogeneous catalyst: application in the synthesis of 1, 2, 3-triazoles and thioethers. Catalysis Science & Technology, 1(8), 1512-1525.
- Velasco, A., Ramírez, M., Volke-Sepúlveda, T., González-Sánchez, A. and Revah, S., 2008. Evaluation of feed COD/sulfate ratio as a control criterion for the biological hydrogen sulfide production and lead precipitation. Journal of Hazardous Materials, 151, 407-413.
- Verma, R. and Dwivedi, P., 2013. Heavy metal water pollution-A case study. Recent research in science and technology, 5.
- Vijayaraghavan, K. and Yun, Y.S., 2008. Bacterial biosorbents and biosorption. Biotechnology Advances, 26, 266–291.

- Villa Gomez, D.K., Enright, A.M., Rini, E.L., Buttice, A., Kramer, H. and Lens, P., 2015. Effect of hydraulic retention time on metal precipitation in sulfate reducing inverse fluidized bed reactors. Journal of Chemical Technology & Biotechnology, 90(1), 120-129.
- Villa-Gomez, D., Ababneh, H., Papirio, S., Rousseau, D.P.L. and Lens, P.N.L., 2011. Effect of sulfide concentration on the location of the metal precipitates in inversed fluidized bed reactors. Journal of hazardous materials, 192, 200-207.
- Villa-Gomez, D.K., van Hullebusch, E.D., Maestro, R., Farges, F., Nikitenko, S., Kramer, H., Gonzalez-Gil, G. and Lens, P.N.L., 2014. Morphology, mineralogy, and solid–liquid phase separation characteristics of cu and Zn precipitates produced with biogenic sulfide. Environmental science & technology, 48(1), 664-673.
- Visser, A., Beeksma, I., Van der Zee, F., Stams, A.J.M. and Lettinga, G., 1993. Anaerobic degradation of volatile fatty acids at different sulphate concentrations. Applied Microbiology and Biotechnology, 40, 549-556.
- Wang, Z., Xing, M., Fang, W. and Wu, D., 2016. One-step synthesis of magnetite core/zirconia shell nanocomposite for high efficiency removal of phosphate from water. Applied Surface Science, 366, 67-77.
- Weber, F.A., Voegelin, A., Kretzschmar, R., 2009. Multi-metal contaminant dynamics in temporarily flooded soil under sulfate limitation. Geochem. Geochimica et Cosmochimica Acta, 73, 5513–5527.
- Winter, O., 1969. Preliminary economic evaluation of chemical processes at the research level. Industrial & Engineering Chemistry, 61(4), 45-52.
- Wrighton-Araneda, K., Ruby-Figueroa, R., Estay, H. and Cortés-Arriagada, D., 2019. Interaction of H_2O with $(CuS)_n$,$(Cu_2S)_n$, and $(ZnS)_n$ small clusters (n= 1–4, 6): relation to the aggregation characteristics of metal sulfides at aqueous solutions. Journal of molecular modeling, 25(9), 1-11.
- Yadav, S., Shrivas, K. and Bajpai, P.K., 2019. Role of precursors in controlling the size, shape and morphology in the synthesis of copper sulfide nanoparticles and their application for fluorescence detection. Journal of Alloys and Compounds, 772, 579-592.
- Yan, X., Chai, L., Li, Q., Ye, L., Yang, B. and Wang, Q., 2017. Abiological granular sludge formation benefit for heavy metal wastewater treatment using sulfide precipitation. CLEAN–Soil, Air, Water, 45(4), 1500730.
- Yang, G., Lin, J., Zeng, E.Y. and Zhuang, L., 2019. Extraction and characterization of stratified extracellular polymeric substances in *Geobacter* biofilms. Bioresource Technology, 276, 119-126.,
- Ye, M., Li, G., Yan, P., Ren, J., Zheng, L., Han, D., Sun, S., Huang, S. and Zhong, Y., 2017. Removal of metals from lead-zinc mine tailings using bioleaching and followed by sulfide precipitation. Chemosphere, 185, 1189-1196.
- Yildiz, M., Yilmaz, T., Arzum, C.S., Yurtsever, A., Kaksonen, A.H. and Ucar, D., 2019. Sulfate reduction in acetate-and ethanol-fed bioreactors: Acidic mine drainage treatment and selective metal recovery. Minerals Engineering, 133, 52-59.
- Yoda, M., Kitagawa, M. and Miyaji, Y., 1988. Granular sludge formation in the anaerobic expanded micro-carrier bed process. In Water Pollution Research and Control Brighton, 109-120.

- Yoon, Y.H. and NELSON, J.H., 1984. Application of gas adsorption kinetics I. A theoretical model for respirator cartridge service life. American Industrial Hygiene Association Journal, 45(8), 509-516.
- Yu Bi, Yongbo Yuan, Christopher L. Exstrom, Scott A. Darveau, and Jinsong Huang 2011. Air Stable, Photosensitive, Phase Pure Iron Pyrite Nanocrystal Thin Films for Photovoltaic Application. Nano Letters. 11, 4953-4957.
- Yu, J., Feng, H., Tang, L., Pang, Y., Zeng, G., Lu, Y., Dong, H., Wang, J., Liu, Y., Feng, C. and Wang, J., 2020. Metal-free carbon materials for persulfate-based advanced oxidation process: Microstructure, property and tailoring. Progress in Materials Science, 111, 100654.
- Yu, J.H., Kwon, S.H., Petrášek, Z., Park, O.K., Jun, S.W., Shin, K., Choi, M., Park, Y.I., Park, K., Na, H.B. and Lee, N., 2013. High-resolution three-photon biomedical imaging using doped ZnS nanocrystals. Nature materials, 12(4), 359-366.
- Yuebin Li, Wei Lu, Qian Huang, Chun Li and Wei Chen, 2010. Copper sulfide nanoparticles for photothermal ablation of tumor cells. Nanomedicine, 5, 8.
- Zagury, GJ., Kulnieks, VI. and Neculita, CM., 2006. Characterization and reactivity assessment of organic substrates for sulphate-reducing bacteria in acid mine drainage treatment. Chemosphere, 64, 944-954.
- Zaluski, M.H., Trudnowski, J.M., Harrington-Baker, M.A. and Bless, D.R., 2003. Post-mortem findings on the performance of engineered SRB field-bioreactors for acid mine drainage control. In Proceedings of the 6th International Conference on Acid Rock Drainage, Cairns, QLD 12-18.
- Zhang, M., Yi, K., Zhang, X., Han, P., Liu, W. and Tong, M., 2020. Modification of zero valent iron nanoparticles by sodium alginate and bentonite: Enhanced transport, effective hexavalent chromium removal and reduced bacterial toxicity. Journal of hazardous materials, 388, 121822.
- Zhang, Y., Zhang, H., Zhang, Z., Liu, C., Sun, C., Zhang, W. and Marhaba, T., 2018. pH effect on heavy metal release from a polluted sediment. Journal of Chemistry, 2018.
- Zhang, Z., Dong, C., Yang, C., Hu, D., Long, J., Wang, L., Li, H., Chen, Y. and Kong, D., 2010. Stabilized Copper (I) Oxide Nanoparticles Catalyze Azide-Alkyne Click Reactions in Water. Advanced Synthesis & Catalysis, 352(10), 1600-1604.
- Zhao, L. and Gao, L., 2004. Coating multi-walled carbon nanotubes with zinc sulfide. Journal of Materials Chemistry, 14(6), 1001-1004.
- Zhao, L., Tao, F., Quan, Z., Zhou, X., Yuan, Y. and Hu, J., 2012. Bubble template synthesis of copper sulfide hollow spheres and their applications in lithium ion battery. Materials Letters, 68, 28-31.
- Zhou, A., Zhu, C., Chen, W., Wan, J., Tao, T., Zhang, T.C. and Xie, P., 2018. Phosphorus recovery from water by lanthanum hydroxide embedded interpenetrating network poly (vinyl alcohol)/sodium alginate hydrogel beads. Colloids and Surfaces A: Physicochemical and Engineering Aspects, 554, 237-244.
- Zhou, Z., Meng, Q. and Yu, Z., 2011. Effects of methanogenic inhibitors on methane production and abundances of methanogens and cellulolytic bacteria in in vitro ruminal cultures. Applied and Environmental Microbiology, 77(8), 2634-2639.
- Zong, C., Xu, M., Xu, L.J., Wei, T., Ma, X., Zheng, X.S., Hu, R. and Ren, B., 2018. Surface-enhanced Raman spectroscopy for bioanalysis: reliability and challenges. Chemical reviews, 118(10), 4946-4980.

- Zou, D., Chen, X., Drioli, E., Qiu, M. and Fan, Y., 2019. Facile mixing process to fabricate fly-ash-enhanced alumina-based membrane supports for industrial microfiltration applications. Industrial & Engineering Chemistry Research, 58(20), 8712-8723.
- Zou, D., Fan, W., Xu, J., Drioli, E., Chen, X., Qiu, M. and Fan, Y., 2021. One-step engineering of low-cost kaolin/fly ash ceramic membranes for efficient separation of oil-water emulsions. Journal of Membrane Science, 621, 118954.

Appendix

Characterization of Products

^{1}H and ^{13}C NMR spectra were recorded on a ASCEND 600 (Bruker, USA) spectrometer in $CDCl_3$. All the reagents and solvents were purchased from Sigma-Aldrich, and used without further purification.

(1) 1,4-Diphenyl-1H-[1,2,3] triazole:

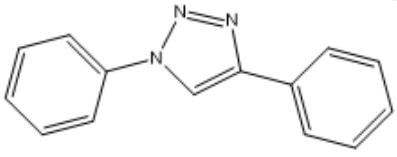

White solid, m.p. 168-172 °C; ^{1}H NMR (600 MHz, $CDCl_3$): δ 7.715, 7.712, 7.702, 7.700, 7.698, 7.592, 7.580, 7.536, 7.284, 7.280, 6.151, 4.159, 4.147, 4.135, 4.123, 2.072, 1.654, 1.639, 1.627, 1.625, 1.312, 1.301, 1.293, 1.281, 1.269, 1.211. ^{13}C NMR (151 MHz, $CDCl_3$): δ 117.55, 119.64, 120.96, 126.21, 128.65, 129.10, 130.55, 137.02, 148.61.

(2) 1-phenyl-4-hydroxy-5-phenyl-1H-[1,2,3] triazole:

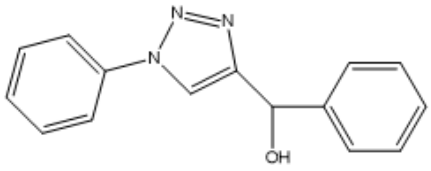

White solid, m.p. 175-178 °C; ^{1}H NMR (600 MHz, $CDCl_3$): δ 7.595, 7.592, 7.583, 7.580, 7.436, 7.434, 7.422, 7.412, 7.409, 7.386, 7.384, 7.381, 7.375, 7.371, 7.359, 7.286, 5.506, 5.502, 4.163, 4.151, 4.139, 4.127, 4.116, 2.701, 2.698, 2.382, 2.370, 2.364, 2.357, 2.352, 2.347, 2.200, 2.196, 2.069, 1.682, 1.636, 1.356, 1.308, 1.295. ^{13}C NMR (151 MHz, $CDCl_3$): δ 119.02, 120.70, 127.10, 127.98, 128.23, 128.84, 129.22, 132.54, 136.41, 142.78, 144.21.

(3) 1-phenyl-4-chloromethyl-1H-[1,2,3] triazole:

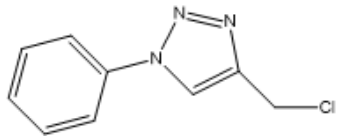

Yellow solid, m.p. 42-44 °C; ^{1}H NMR (600 MHz, $CDCl_3$): δ 7.284, 4.766, 4.756, 4.197, 4.180, 4.160, 4.148, 4.137, 4.125, 4.113, 4.104, 4.081, 4.070, 4.061, 4.051, 4.032, 4.022, 4.013, 3.511, 2.194, 2.066, 1.627, 1.280, 1.275. ^{13}C NMR (151 MHz, $CDCl_3$): δ 40.40, 119.11, 120.47, 121.91, 128.20, 129.45, 132.66, 133.65, 138.74.

(4) 1-phenyl-4-hydroxymethyl-1H-[1,2,3] triazole:

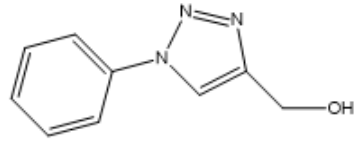

Yellow solid, m.p. 52-55 °C; ^{1}H NMR (600 MHz, $CDCl_3$): δ 7.586, 7.583, 7.574, 7.571, 7.428, 7.416, 7.404, 7.402, 7.379, 7.377, 7.368, 7.365, 7.285, 7.282, 5.493, 5.489, 4.813, 4.806, 4.801, 4.792, 4.784, 4.146, 4.144, 4.134, 4.132, 2.697, 2.694, 2.691, 2.190, 2.187, 2.064, 2.061, 1.291, 1.289, 1.279, 1.277, 1.267, 1.265. ^{13}C NMR (151 MHz, $CDCl_3$): δ 54.22, 118.44, 119.74, 120.04, 121.47, 128.62, 132.89, 139.47, 145.52.

(5) 1-phenyl-4-aminomethyl-1H-[1,2,3] triazole:

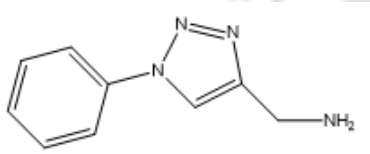

White solid, m.p. 60-64 °C; ^{1}H NMR (600 MHz, $CDCl_3$): δ 7.591, 7.574, 7.568, 7.565, 7.559, 7.556, 7.551, 7.547, 7.544, 7.541, 7.534, 7.521, 7.508, 7.286, 7.058, 7.044, 5.358, 3.508. ^{13}C NMR (151 MHz, $CDCl_3$): δ 40.88, 119.54, 120.07, 127.40, 128.74, 129.79, 132.28, 133.34, 138.99.

(6) 1-phenyl-4-hydroxyethane-1H-[1,2,3] triazole:

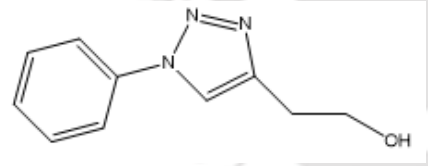

Pale yellow liquid; ^{1}H NMR (600 MHz, $CDCl_3$): δ 7.589, 7.587, 7.578, 7.574, 7.429, 7.417, 7.414, 7.407, 7.404, 7.379, 7.367, 7.284, 5.499, 5.495, 4.809, 4.800, 4.790, 4.787, 4.147, 4.135, 2.697, 2.693, 2.191, 1.291, 1.279, 1.267. ^{13}C NMR (151 MHz, $CDCl_3$): δ 29.10, 61.45, 119.87, 120.20, 120.07, 126.40, 127.44, 132.64, 136.57, 139.01.

(7) 1-(2-Methyl-phenyl)-4-phenyl-1H-[1,2,3] triazole:

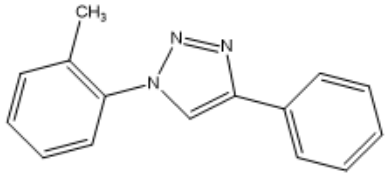

White solid, m.p. 73-75 °C; ^{1}H NMR (600 MHz, $CDCl_3$): δ 7.586, 7.574, 7.428, 7.416, 7.403, 7.378, 7.366, 7.354, 7.287, 5.496, 5.492, 4.159, 4.147, 4.135, 4.123, 2.931, 2.696, 2.693, 2.336, 2.212, 2.063, 1.292, 1.280, 1.268, 1.213, 0.027. ^{13}C NMR (151 MHz, $CDCl_3$): δ 17.33, 121.20, 125.54, 127.80, 128.21, 129.27, 130.31, 131.55, 132.07, 136.91, 142.42.

(8) 1-(2-Methyl- phenyl)-4-hydroxy-5-phenyl-1H-[1,2,3] triazole:

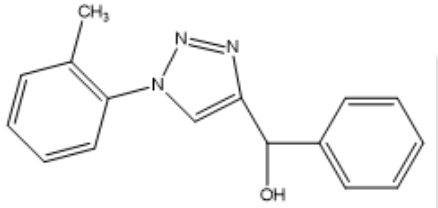

Yellow solid, m.p. 180-182 °C; ^{1}H NMR (600 MHz, $CDCl_3$): δ 7.986, 7.952, 7.939, 7.594, 7.581, 7.564, 7.550, 7.507, 7.494, 7.482, 7.466, 7.457, 7.452, 7.435, 7.432, 7.376, 7.373, 7.361, 4.164, 4.152, 4.108, 4.008, 2.385, 2.381, 2.374, 2.371, 2.366, 2.360, 2.353, 2.348, 2.342, 2.336, 2.309, 2.278, 2.070. ^{13}C NMR (151 MHz, $CDCl_3$): δ 17.20, 117.41, 119.01, 121.74, 127.32, 127.34, 129.01, 132.55, 132.28, 136.49, 140.58, 142.04.

(9) 1-(2-Methyl- phenyl)-4-chloromethyl-1H-[1,2,3] triazole:

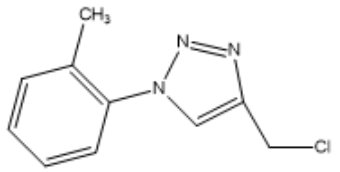

Yellow solid, m.p. 60-62 °C; ^{1}H NMR (600 MHz, $CDCl_3$): δ 7.617, 7.593, 7.590, 7.578, 7.553, 7.550, 7.538, 7.469, 7.438, 7.433, 7.420, 7.319, 7.316, 7.286, 4.786, 4.769, 4.757, 4.161, 4.149, 4.138, 4.126, 2.067, 1.651, 1.293, 1.281, 1.276, 1.269. ^{13}C NMR (151 MHz, $CDCl_3$): δ 17.74, 39.32, 119.21, 128.52, 128.87, 130.36, 132.43, 136.49, 142.87.

(10) 1-(2-Methyl- phenyl)-4-hydroxymethyl-1H-[1,2,3] triazole:

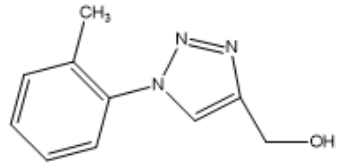

Yellow solid, m.p. 68-70 °C; ^{1}H NMR (600 MHz, $CDCl_3$): δ 7.745, 7.740, 7.736, 7.730, 7.559, 7.554, 7.550, 7.544, 7.286, 5.361, 4.329, 4.325, 4.313, 4.302, 4.150, 4.138, 3.936, 2.195, 2.068, 1.772, 1.769, 1.761, 1.749, 1.737, 1.671, 1.661, 1.659, 1.651, 0.913, 0.903, 0.891. ^{13}C NMR (151 MHz, $CDCl_3$): δ 17.10, 54.25, 117.74, 119.86, 125.50, 128.09, 128.44, 130.15, 132.28, 140.12, 142.02.

(11) 1-(2-Methyl- phenyl)-4-aminomethyl-1H-[1,2,3] triazole:

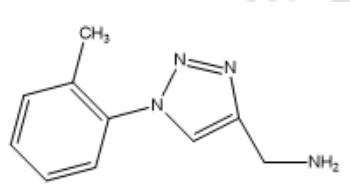

White solid, m.p. 70-74 °C; ^{1}H NMR (600 MHz, $CDCl_3$): δ 7.586, 7.574, 7.428, 7.416, 7.403, 7.378, 7.366, 7.354, 7.287, 5.496, 5.492, 4.159, 4.147, 4.135, 4.123, 2.696, 2.692, 1.292, 1.280, 1.268. ^{13}C NMR (151 MHz, $CDCl_3$): δ 17.21, 27.20, 119.25, 125.95, 128.46, 128.31, 132.41, 135.50, 140.07, 142.28.

(12) 1-(2-Methyl- phenyl)-4-hydroxyethane-1H-[1,2,3] triazole:

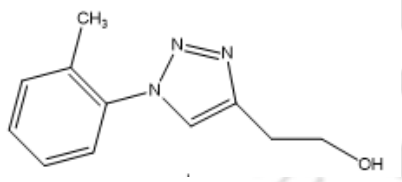

Yellow solid, m.p. 102-105 °C; ^{1}H NMR (600 MHz, $CDCl_3$): δ 7.766, 7.763, 7.759, 7.753, 7.749, 7.744, 7.739, 7.735, 7.729, 7.727, 7.576, 7.571, 7.567, 7.561, 7.559, 7.553, 7.549, 7.547, 7.544, 7.286, 7.284, 5.361, 4.324, 4.312, 4.301, 4.161, 4.149, 4.137, 4.125, 3.935, 2.067, 2.032, 1.736, 1.705. ^{13}C NMR (151 MHz, $CDCl_3$): δ 17.06, 30.19, 62.84, 119.61, 125.21, 127.50, 128.32, 129.82, 129.94, 132.66, 133.20, 136.48.

(13) 1-benzoic acid-4-phenyl-1H-[1,2,3] triazole:

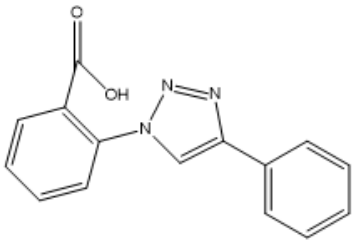

White solid, m.p. 165-170 °C; ^{1}H NMR (600 MHz, $CDCl_3$): δ 7.587, 7.584, 7.572, 7.425, 7.423, 7.421, 7.412, 7.409, 7.399, 7.375, 7.373, 7.370, 7.360, 7.284, 5.501, 5.497, 4.291, 4.289, 4.156, 4.144, 4.132, 4.121, 4.071, 4.067, 4.063, 4.058, 2.690, 2.687, 1.288, 1.276, 1.265. ^{13}C NMR (151 MHz, $CDCl_3$): δ 117.20, 119.45, 119.47, 125.21, 127.39, 127.46, 128.74, 128.40, 130.08, 132.11, 135.54, 142.63, 155.81.

(14) 1-benzoic acid-4-hydroxy-5-phenyl-1H-[1,2,3] triazole:

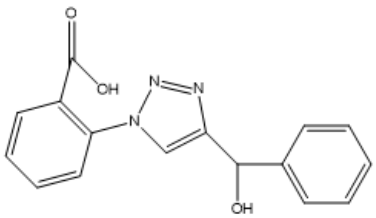

White solid, m.p. 170-175 °C; ^{1}H NMR (600 MHz, $CDCl_3$): δ 7.549, 7.546, 7.536, 7.533, 7.379, 7.370, 7.367, 7.365, 7.357, 7.355, 7.315, 5.453, 5.449, 4.106, 4.097, 4.094, 2.651, 2.647, 2.025, 2.022, 1.254, 1.245, 1.242, 1.230. ^{13}C NMR (151 MHz, $CDCl_3$): δ 74.30, 117.21, 117.91, 119.48, 122.50, 127.14, 129.64, 130.28, 130.62, 132.32, 133.82, 136.64, 142.92, 160.87.

(15) 1-benzoic acid-4-cheloromethyl-1H-[1,2,3] triazole:

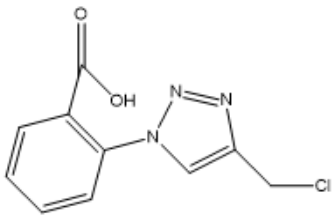

White solid, m.p. 74-78 °C; ^{1}H NMR (600 MHz, $CDCl_3$): δ 7.937, 7.935, 7.923, 7.921, 7.767, 7.761, 7.756, 7.752, 7.746, 7.741, 7.738, 7.732, 7.728, 7.723, 7.704, 7.331, 7.286, 6.704, 6.692, 6.689, 6.681, 6.679, 4.164, 4.152, 4.140, 4.128, 3.938, 1.295, 1.283, 1.272. ^{13}C NMR (151 MHz, $CDCl_3$): δ 38.20, 117.12, 119.17, 127.40, 128.49, 130.02, 132.93, 132.86, 136.54, 160.29.

(16) 1-benzoic acid-4-hydroxymethyl-1H-[1,2,3] triazole:

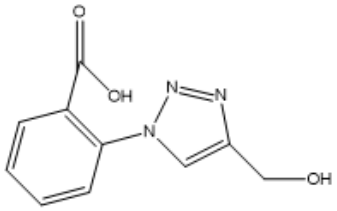

White solid, m.p. 90-95 °C; ^{1}H NMR (600 MHz, $CDCl_3$): δ 7.552, 7.286, 4.164, 4.152, 4.140, 4.128, 3.938, 2.197, 2.070, 1.596, 1.357, 1.309, 1.296, 1.284, 1.272, 0.904, 0.865, 0.024. ^{13}C NMR (151 MHz, $CDCl_3$): δ 55.20, 119.20, 128.46, 128.54, 130.58, 132.98, 133.18, 136.35, 140.48, 160.03.

(17) 1-benzoic acid-4-aminomethyl-1H-[1,2,3] triazole:

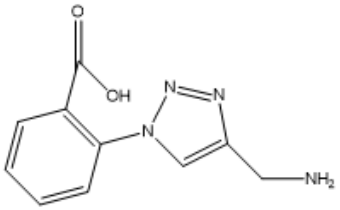

White solid, m.p. 94-99 °C; ^{1}H NMR (600 MHz, $CDCl_3$): δ 8.270, 8.216, 8.181, 8.165, 7.593, 7.580, 7.548, 7.421, 7.419, 7.409, 7.382, 7.371, 7.286, 5.608, 5.507, 5.503, 5.407, 5.380, 5.360, 4.151, 4.139, 4.128, 2.069, 1.724, 1.295, 1.283, 1.271. ^{13}C NMR (151 MHz, $CDCl_3$): δ 43.81, 117.21, 119.02, 126.48, 126.16, 130.30, 130.78, 132.54, 133.95, 159.20.

(18) 1-benzoic acid-4-hydroxyethane-1H-[1,2,3] triazole:

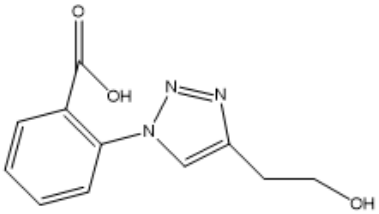

White solid, m.p. 110-112 °C; ^{1}H NMR (600 MHz, $CDCl_3$): δ 8.058, 8.013, 7.567, 7.562, 7.558, 7.553, 7.549, 7.543, 7.540, 7.538, 7.535, 7.283, 5.343, 5.314, 4.130, 4.118, 3.921, 2.076, 2.069, 2.055, 1.783, 1.768, 1.277, 1.265, 1.253. ^{13}C NMR (151 MHz, $CDCl_3$): δ 31.33, 62.51, 119.21, 122.87, 128.22, 130.80, 131.46, 132.32, 135.86, 142.18, 155.38, 164.08.

List of publications

- **Publications in international journals**

1. Kumar, M., and Pakshirajan, K. (2020). Novel insights into mechanism and applications of biometal nanopowder from wastewater. *Environmental Technology & Innovation*, *17*, 100542.
2. Kumar, M., Nandi, M. and Pakshirajan, K., 2021. Recent advances in heavy metal recovery from wastewater by biogenic sulfide precipitation. *Journal of Environmental Management*, *278*, 111555.
3. Kumar, M. and Pakshirajan, K., 2021. Continuous removal and recovery of metals from wastewater using inverse fluidized bed sulfidogenic bioreactor. *Journal of Cleaner Production*, *284*, 124769.
4. Kumar, M., Kumar, A. and Pakshirajan, K., 2022. Preparation, characterization and application of biometal nanopowders from metallic wastewater for azo dye removal from aqueous solution. *Environmental Science and Pollution Research*, 1-15.
5. Kumar, M., Kumar, A., Pugazhenthi, G. and Pakshirajan, K., 2022. Recovery and purification of copper sulfide nanoparticles from acid mine drainage by biological sulfate reduction and microfiltration using low-cost ceramic membrane. *Clean Technologies and Environmental Policy* (Under Revision) (Manuscript number: CTEP-D-21-01081).
6. Kumar, M. and Pakshirajan, K., 2022. Immobilized biogenic copper nanoparticles from metallic wastewater as catalyst for triazole synthesis by click reaction using water as solvent. *RSC Advances* (Under Review) (Manuscript number: RA-ART-02-2022-000808).

- **Presentations in international/national conferences**

1. M. Kumar and K. Pakshirajan. Biological removal and recovery of heavy metals from acid mine drainage. 6th Bioprocessing India Conference, December 16-18, 2018, IIT Delhi, New Delhi, India.
2. M. Kumar and K. Pakshirajan. Removal and recovery of heavy metals from acid mine drainage by bio-precipitation. International Conference on Biomass, Fuels and Chemicals, September 12-13, 2019, Annamalai University, India.
3. M. Kumar and K. Pakshirajan. Continuous removal and recovery of metals from wastewater using inverse fluidized bed sulfidogenic bioreactor. International

Conference on Environment, Agriculture, Human and Animal Health, June 5-6, 2021 (Virtual).

- **Manuscript under preparation**

1. Kumar, M. and Pakshirajan, K., 2022. Induced oxidative stress in *Rhodococcus opacus* due to biogenic and chemical nanoparticles of lead sulfide and cadmium sulfide.